

# **Self-assembled Molecular Templates for Conducting Polyaniline Nanomaterials**

THESIS SUBMITTED TO  
**THE UNIVERSITY OF KERALA**

FOR THE DEGREE OF  
**DOCTOR OF PHILOSOPHY**  
IN CHEMISTRY

**UNDER THE FACULTY OF SCIENCE**



BY  
**ANILKUMAR. P**

**CHEMICAL SCIENCES & TECHNOLOGY DIVISION  
NATIONAL INSTITUTE FOR INTERDISCIPLINARY  
SCIENCE & TECHNOLOGY (CSIR)  
(Formerly: Regional Research Laboratory)  
THIRUVANANTHAPURAM- 695019  
KERALA, INDIA.**

**AUGUST 2009**

*To*  
*My Beloved Parents*

## **DECLARATION**

I hereby declare that the matter embodied in the thesis entitled “**Self-assembled Molecular Templates for Conducting Polyaniline Nanomaterials**” are the results of the investigations carried out by me at the Chemical Sciences and Technology Division, National Institute for Interdisciplinary Science and Technology (CSIR), Thiruvananthapuram, under the supervision of Dr. M. Jayakannan and the same has not been submitted elsewhere for any other degree.

**Anilkumar.P**

Thiruvananthapuram

August 2009

# राष्ट्रीय अंतर्विषयी विज्ञान तथा प्रौद्योगिकी संस्थान

(वैज्ञानिक एवं प्रौद्योगिकी अनुसंधान परिषद्)

(पहले क्षेत्रीय अनुसंधान प्रयोगशाला)

## NATIONAL INSTITUTE FOR INTERDISCIPLINARY SCIENCE AND TECHNOLOGY

(Council of Scientific & Industrial Research)

(formerly Regional Research laboratory)

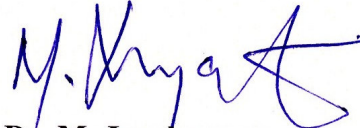
इन्डस्ट्रियल इस्टेट डाक घर, तिरुवनन्तपुरम 695 019, भारत  
Industrial Estate P.O., Thiruvananthapuram 695 019, India



### CERTIFICATE

This is to certify that the work embodied in the thesis entitled “**Self-assembled Molecular Templates for Conducting Polyaniline Nanomaterials**” has been carried out by **Mr. Anilkumar. P.** under my supervision at the Chemical Sciences and Technology Division of National Institute for Interdisciplinary Science and Technology (*Formerly Regional Research Laboratory*), Thiruvananthapuram and the same has not been submitted elsewhere for any other degree.

Thiruvananthapuram

  
**Dr. M. Jayakannan**  
(Thesis Supervisor)

## ACKNOWLEDGMENTS

I wish to express my deepest gratitude to my adviser, **Prof. M. Jayakannan** for suggesting me an interesting problem, intellectual support, encouragement, and enthusiasm throughout the course of this research.

I am highly thankful to Prof. T. K. Chandrashekar and Dr. B. C. Pai, Directors, NIIST, Trivandrum, for providing all the laboratory facilities for my research.

I thank Prof. K. N. Ganesh, Director, IISER, Pune, for giving me all the facilities at IISER during my stay there.

I wish to thank the heads of the Chemical Sciences and Technology Division, NIIST Dr. Suresh Das and Dr. C. K. S. Pillai, for their help extended towards me.

I owe a special note of gratitude to Dr. M. L. P. Reddy for all his generous help and advices to me.

I also express my sincere thanks to Dr. S. K. Asha and Dr. A. Srinivasan for their suggestions, advices and help.

I am very thankful to Dr. C. Pavithran, Dr. V. S. Prasad, Dr. J. D. Sudha, Dr. A. R. R. Menon and Mr. M. Brahmakumar for their help.

I would like to thank my unfailingly pleasant and interesting lab mates, Deepa, Amrutha, Jinish, Anish, Balamurugan, Resmi, Smitha, Jancy, Deepak, Rekha, Bindu, Bakare, Reena, Chameswary, Biju, Ambili Raj, Sivakala, Sasikala, Vinu and others for their help and warmly friendship.

I am very thankful to all my friends at NIIST especially at Photosciences and Photonics group for their good friendship. I also appreciate my friends at NCL and IISER, Pune, who made my stay at Pune very special one.

I am very much thankful to Dr. Peter Koshy, Mr. M. R. Chandran, Dr. V. S. Prasad, Mr. Naren Karthi, Mr. Robert Philip, Mr. Prasanth, Dr. U. Syamaprasad, Mr. P. Gurusamy, Mrs. Soumini, Mr. Adarsh and Mrs. Viji of NIIST for their help in SEM, TEM, AFM, WXR, NMR, CHN and Mass analysis. I also thank Dr. C. P. Sharma, Mr. Willi Paul and Dr. Annie John of SCTIMST, Thiruvananthapuram for DLS and TEM studies.

I fall short of words in expressing my gratitude to my parents for their selfless love and motivation throughout my education. I warmly acknowledge the love showed by my brother and my relatives.

Finally, financial assistance from University Grants Commission (UGC), New Delhi and KSCSTE, Trivandrum is gratefully acknowledged.

Anil

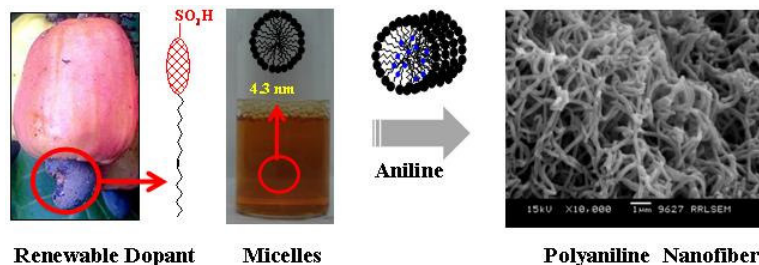
## PREFACE

Organic conducting nanomaterials have gained significant interest in recent times because of their potential applications in biological and chemical sensors, electronic and optical devices etc. Polyaniline nanomaterials are particularly important due to their facile synthesis, simple non-redox doping/dedoping chemistry based on acid/base reactions, and environmental stability. In this thesis we have developed a versatile renewable resource based amphiphilic molecular template for producing various types of polyaniline nanomaterials like fibers, tubes, spheres, rods and tapes.

The work consists of five important parts:

- (i) Design and development of novel amphiphilic azobenzene sulfonic acid molecule from renewable resource cardanol and employ it as structure-directing molecular templates for polyaniline nanofibers.
- (ii) Selective micellar template approach for divergent polyaniline nanostructures.
- (iii) Cylindrical and vesicular templates for polyaniline nanofibers and nanotapes.
- (iv) Amphiphilic dopant organogel template for polyaniline nanofibers.
- (v) Functionalized polyaniline nanospheres as a sensor material for vitamin C.

The thesis has been divided into seven chapters. First chapter gives a brief introduction to polyaniline nanostructures, synthetic methodology, properties associated with nano-domains and their application in electrical and opto-electronic industry.



The second chapter describes the design and synthesis of a unique amphiphilic dopant molecule, 4-[4-hydroxy-2 ((Z)-pentadec-8-enyl) phenylazo]-benzene sulfonic acid, from a renewable resource cardanol and its utilization as structure-directing agent for polyaniline nanomaterials. The micellar behavior and critical micelle concentration (CMC) of the dopant was analyzed by dye encapsulation, surface tension, fluorescence, conductance and dynamic light scattering (DLS) measurements.

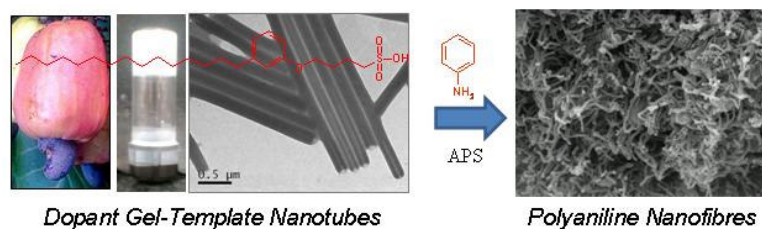
Dendritic and linear nanofibers were produced with length varying upto 8 -10  $\mu\text{M}$  having diameters of 130-180 nm. The approach is also successfully extended to bulk-scale synthesis of nanofibers up to 100 gram without losing the morphology.

Third chapter deals with the selective templating of nanomaterials like nanofibers, nanotubes, nanospheres and nanorods from identical reactant ingredients under emulsion, dilution and interfacial polymerizations. Dilution of thick emulsion produce uniform small micellar aggregates of 175 nm which template exclusively for the nanorods. On the other hand, the dopant micelles form spherical aggregates with oxidizing agent ammonium persulfate (APS) in water. In interfacial route, aniline molecules diffuse through organic/aqueous interface and absorbed at these spherical aggregates and the subsequent chemical oxidation resulted in the formation of polyaniline nanospheres. The mechanism of the polyaniline nanomaterials formation was investigated by DLS and transmission electron microscopy (TEM). The detail studies on the mechanistic aspects revealed that the dopant-aniline complex exist as either aggregated or isolated cylindrical or spherical micelles and upon oxidation of these templates produce polyaniline nanomaterials. The nanomaterials were highly dispersible in polar solvents, which enabled their characterization by NMR and UV-vis spectroscopic techniques. Wide angle X-ray diffraction patterns of the nanomaterials showed a sharp peak at  $2\theta = 6.4$  (d-spacing =13.6) corresponding to highly ordered polyaniline chains by the effective inter-digitations of dopant molecules.

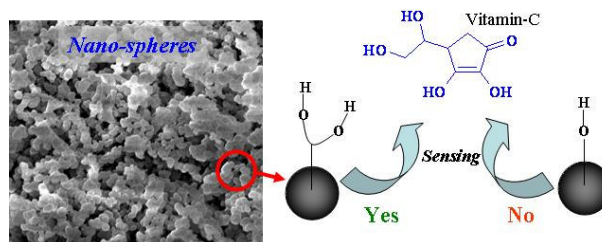


Fourth chapter is based on soft template approach of custom-designed novel surfactant-cum-dopant 4-(3-dodecyl-8-enylphenoxy) butane sulfonic acid. The new amphiphilic dopant was freely soluble in water and produced spherical micelles of 5.6 nm in water. In the emulsion route, the dopant was complexed with aniline to produce cylindrical micellar aggregates which template exclusively for polyaniline nanofibers.

The dispersion of aniline+dopant complex in water/toluene solvent mixtures produces vesicles which resulted in polyaniline nanotapes.



In the fifth chapter we have utilized the supramolecular gel templating nature of the 4-(3dodecylphenoxy) butane sulfonic acid dopant (saturated form) for fabricating polyaniline nanofibers. The self assembled nanotubular network morphology of the gel was confirmed by SEM, TEM and atomic force microscopy (AFM) studies. The aniline molecules preferentially fill in the nano-cavity inside the tubes due to the increased capillary action. Upon oxidation, these trapped aniline monomers inside the nano-gel oxidized to produce polyaniline nanofibers. Gel-assisted polymerization was also carried out at various temperatures to investigate the role of the physical state of the gel on the morphology of the final product.



Sixth chapter is focused on the synthesis of novel polyaniline nanospheres bearing mono and bis-hydroxyl functional groups to trace the molecular interactions at the nano-surfaces. Two new aniline monomers were synthesized via tailor-made approach and polymerized to produce soluble and uniform polyaniline nanospheres. Vitamin-C was employed as an analyte to trace the molecular interaction at the nanospheres surface and study the influence of nano-surface functionalization on the sensing ability of biomolecules. The bis-hydroxyl functionalized polyaniline nanospheres were found to show efficient molecular interactions towards vitamin C whereas nanospheres with mono-hydroxyl group or un-substituted nanofibers failed as sensing materials.

The last chapter summarizes the outcome of the research work carried out in this PhD thesis.



## CONTENTS

	<b>Page</b>
<b><i>Chapter 1: Introduction</i></b>	<b><i>1-33</i></b>
1.1. Introduction to Nanomaterials	2
1.2. Conducting Polymers	9
1.3. Polyanilines	11
1.3.1. Synthesis of Polyaniline	13
1.4. Polyaniline Nanomaterials	16
1.4.1. Electrospinning Method	17
1.4.2. Hard Template Synthesis	18
1.4.3. Soft Template synthesis	19
1.4.4. Interfacial Synthesis	21
1.5. Applications of Polyaniline Nanomaterials	24
1.5.1. Chemical Sensors	24
1.5.2. Actuators	25
1.5.3. Memory Devices	26
1.6. Aim of the Thesis	26
1.7. References	29
<b><i>Chapter 2: Development of Renewable Amphiphilic Molecular Template for Polyaniline Nanomaterials</i></b>	<b><i>34-75</i></b>
2.1. Introduction	35
2.2. Experimental Methods	39
2.2.1. Materials	39
2.2.2. General Procedures	39
2.2.3. Synthesis of Azobenzene Dopant	40
2.2.4. Synthesis of Polyaniline Nanomaterials	41
2.3. Results and Discussion	43
2.3.1. Synthesis of Azobenzene Dopant	43
2.3.2. DLS studies of Azobenzene Dopant	45
2.3.3. Determination of CMC of Azobenzene Dopant	47
2.3.4. Synthesis of Polyaniline Nanomaterials	50
2.3.5. Characterization of Polyaniline Nanomaterials	52
2.3.6. Morphology of Polyaniline Nanomaterials	54
2.3.7. Mechanism of Nanomaterial Formation	58
2.3.8. Properties of Polyaniline Nanomaterials	61
2.3.9. Effect of Experimental Conditions on Morphology	65
2.3.10. Property Reversibility of Nanofibers	70
2.4. Conclusion	72
2.5. References	73

<b>Chapter 3: Selective Micellar Templating for Divergent Polyaniline Nanostructures</b>	<b>76-110</b>
3.1. Introduction	77
3.2. Experimental Methods	79
3.2.1. Materials	79
3.2.2. General Procedures	80
3.2.3. Synthesis of Nanomaterials by Dilute Route	81
3.2.3. Synthesis of Nanomaterials by Interfacial Route	81
3.3. Results and Discussion	82
3.3.1. Dilute Route for Nanomaterials	82
3.3.2. Interfacial Route for Nanomaterials	84
3.3.3. Morphology of Nanomaterials	86
3.3.4. Mechanism of Nanomaterials Formation	90
3.3.5. Optical and Solid-state Properties	94
3.3.6. Luminescent Properties of Nanomaterials	102
3.4. Conclusion	108
3.5. References	109

**Chapter 4: Cylindrical and Vesicular Templates for Polyaniline Nanofibers and Nanotapes** **111-144**

4.1. Introduction	112
4.2. Experimental Methods	116
4.2.1. Materials	116
4.2.2. General Procedures	116
4.2.2. Synthesis of Amphiphilic Dopant	117
4.2.3. Synthesis of Polyaniline Nanomaterials	117
4.3. Results and Discussion	119
4.3.1. Synthesis and Characterization of Dopant	119
4.3.2. Study of Micellar Behaviour of Dopant	121
4.3.3. Synthesis of Polyaniline Nanomaterials	125
4.3.4. Morphology of Polyaniline Nanomaterials	130
4.3.5. Mechanism of Nanomaterials Formation	132
4.3.5. Properties of Polyaniline Nanomaterials	136
4.4. Conclusion	141
4.5. References	142

**Chapter 5: Amphiphilic Dopant Organogel Template for Polyaniline Nanofibers** **145-172**

5.1. Introduction	146
5.2. Experimental Methods	149
5.2.1. Materials	149

5.2.2. General Procedures	149
5.2.2. Synthesis of Amphiphilic Gelator Dopant	150
5.2.3. Synthesis of Polyaniline Nanofibers	150
5.3. Results and Discussion	151
5.3.1. Synthesis and Gelation Studies of Dopant 3	151
5.3.2. Synthesis and Morphology of Nanomaterials	156
5.3.3. Structural Characterization of Nanomaterials	160
5.3.4. Optical and Solid-state Properties of Nanofibers	161
5.3.5. Thermal Analysis by DSC	164
5.3.5. Four Probe Conductivity Measurements	166
5.4. Conclusion	170
5.5. References	171
<b><i>Chapter 6: Functionalized Polyaniline Nanospheres- Vitamin C Sensing</i></b>	<b>173-200</b>
6.1. Introduction	174
6.2. Experimental Methods	176
6.2.1. Materials	176
6.2.2. General Procedures	176
6.2.2. Synthesis of Monomers and Polymers	177
6.3. Results and Discussion	180
6.3.1. Synthesis and Characterization	180
6.3.2. Morphology of Nanomaterials by SEM and TEM	184
6.3.3. Mechanism of Nanomaterials Formation	187
6.3.4. Properties of Nanomaterials	190
6.3.5. Vitamin C Sensing	193
6.4. Conclusion	198
6.5. References	199
<b><i>Chapter 7: Summary and Conclusions</i></b>	<b>201-205</b>
<b><i>List of Publications</i></b>	<b>206-208</b>

***Chapter-1***

---

***Introduction***

### 1.1. Introduction to Nanomaterials

During the last twenty years, the term “Nano” is increasingly employed to describe the science and analytical techniques for materials with structural features in between those of atoms and bulk materials, with at least one dimension in the nanometre range<sup>1-5</sup>. Properties of materials of nano-dimensions are considerably different from those of atoms as well as of bulk materials<sup>6</sup>. Suitable control of the properties of nanometer-scale structures can lead to new science as well as new devices and technologies<sup>7</sup>. The first predictions of the enormous potential of miniaturization of materials was proposed by renowned physicist Richard Feynman during a talk titled "There's Plenty of Room at the Bottom," in 1959<sup>8</sup>. Feynman envisaged the changing magnitude of various physical phenomena if it can able to manipulate and arrange individual atoms and molecules down to a smaller needed scale. For a clear understanding of size ranges a comparison of various commonly encountered objects are given in figure 1.1.

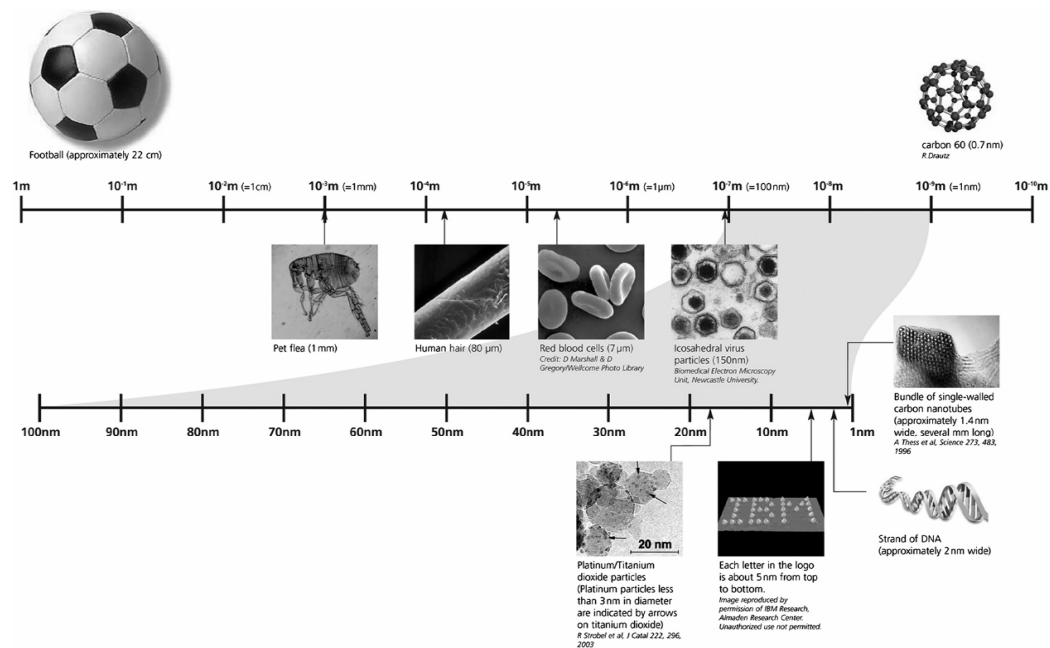


**Figure 1.1.** *The nano scale – A comparison of the size of some of the common objects with that of nanomaterials. (Adapted from reference 9)*

A number of physical phenomena become pronounced as the size of the system decreases. These include statistical mechanical effects, as well as quantum mechanical effects, for example the “quantum size effect” where the electronic

properties of solids are altered considerably with great reductions in particle size<sup>6-9</sup>. This effect does not come into play by going from macro to micro dimensions, but it becomes dominant only when the nanometer size range is reached. Besides these electronic effects there is a tremendous increase of surface area upon miniaturization as compared with that of corresponding bulk materials. It will dramatically improve the surface properties of the materials like adsorption, catalytic activity etc. For example a material such as gold, which is chemically inert at normal scales, can serve as a potent chemical catalyst at nano-scales. Currently nanoscience has grown up to a fully fledged fascinating interdisciplinary area of research because of the novel quantum and surface phenomena exhibited by these new classes of materials at the nano-scale enabled a wide range of applications in the field of physics, chemistry, biology, material science and engineering.

**Table.1.1.** *Examples of nanomaterials (Adapted from reference 8)*

<i>Type</i>	<i>Size</i>	<i>Materials</i>
Quantum dots	Diam. 1-10 nm	Metals, semiconductors
Other nanoparticles	Diam. 1–100 nm	Ceramic oxides
Nanowires	Diam. 1-100 nm	Metals, oxides, sulfides, nitrides
Nanotubes	Diam.1–100 nm	Carbon, metal chalcogenides
Nanoporous solids	Diam. 0.5–10 nm	Zeolites, phosphates etc.
2-Dimensional arrays	2 nm –2 μm	Metals, semiconductors, magnetic materials
Surfaces and thin films	1–1000 nm	A variety of materials (e.g., polymers)
3-D structures (super lattices)	Several nm in the three dimensions	Metals, semiconductors, magnetic materials

An important aspect of nanomaterials is the vastly increased ratio of surface area to volume present in many nano-scale materials which makes effects like the “quantum size effect” and improved surface activity. The synthesis, characterization and processing of nanostructured materials are part of an emerging and rapidly growing field. Research and development in this field emphasizes scientific

discoveries in the generation of materials with controlled micro structural characteristics, research on their processing into bulk materials with engineered properties and technological functions, and introduction of new device concepts and manufacturing methods<sup>8,9</sup>. Nanostructured materials may be grouped under nanoparticles, nano-intermediates, and nanocomposites (see table 1.1).

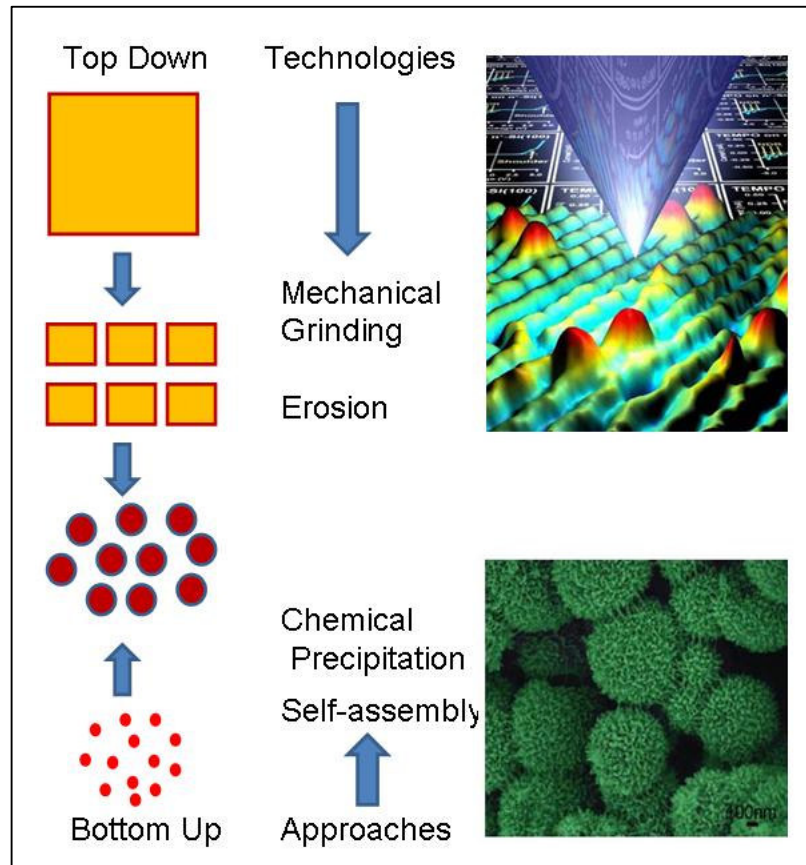


**Figure 1.2.** Schematic representation of top down and bottom up methods.

There are two important approaches for the synthesis of nanomaterials, that is, top down and bottom up synthesis. In Top down fabrication a piece of the bulk base material is gradually eroded until the desired nano-shape is achieved (see figure 1.2). The most important and widely used top down fabrication technique is nanolithography. In this process, required material is protected by a mask and the exposed material is etched away<sup>8,10</sup>. Depending upon the level of resolution required for features in the final product, etching of the base material can be done chemically using acids or mechanically using ultraviolet light, x-rays or electron beams. Other

important methods are atomic layer deposition (ALD) techniques and dip pen nanolithography- Atomic force microscope tips can be used as a nanoscale "write head" to deposit a chemical upon a surface in a desired pattern. Whereas in the case of bottom up fabrication a desired nano-object was constructed by placing atoms or molecules in an ordered way (see figure 1.2). The important tool used in this regard is self assembly<sup>7,12</sup> . For example, for the construction of DNA the specificity of Watson-Crick base pairing to construct well-defined structures out of DNA and other nucleic acids. Similarly molecular self-assembly seeks to use concepts of supramolecular chemistry, and molecular recognition in particular, to cause single-molecule components to automatically arrange themselves into some useful conformation. Up to date a variety of nanostructures like spheres, rods, fibers, tubes etc were fabricated from inorganic as well as organic materials.

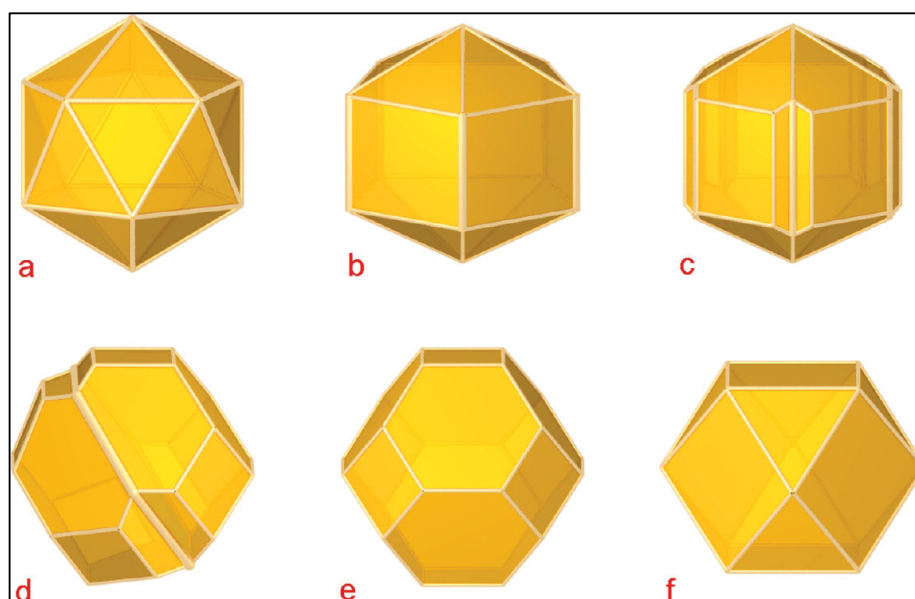


**Figure 1. 3.** Various shapes exhibited by gold nanoparticles: the Mackay icosahedron (a) the Ino (b) Marks (c) decahedra, the symmetrically twinned truncated octahedron (d), the ideal truncated octahedron (e), and the ideal cuboctahedron (f) (Adapted from reference 14).

Among this, nanomaterials derived from gold and carbon is particularly important and well studied<sup>12,13</sup>. The first report on colloidal gold by the famous English scientist Michel Faraday dates back 1857<sup>14</sup>. He deduced that the unexpected colour of the colloidal gold was due to the extremely small size of the gold particles. Last two decades a much effort has been paid to fabricate various structures like



spheres, rods, cubes, and prisms (see figure 1.3). Due to the unique optical, electronic, and molecular-recognition properties of gold nano-particles, they are the subject of substantial research<sup>13</sup>. These nano-particles can be functionalized with various organic ligands to create organic-inorganic hybrids with advanced functionality.

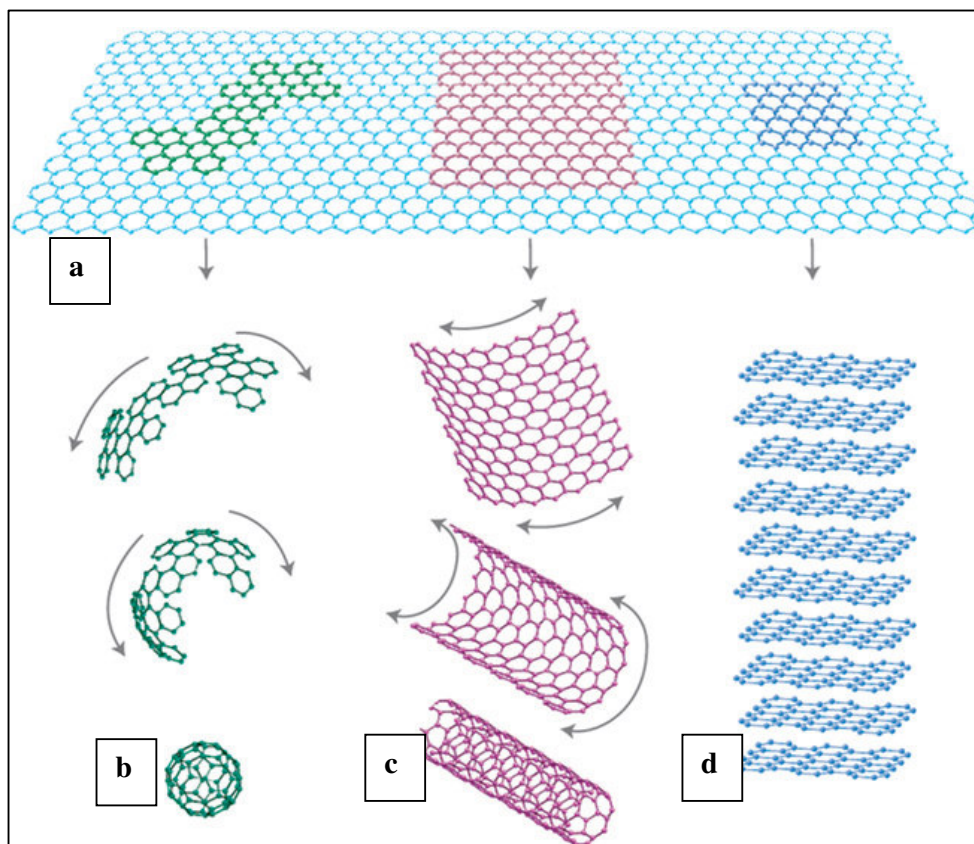


**Figure 1.4.** Various forms of carbon allotropes (a) graphene (b) fullerenes (c) carbon nanotube and (d) graphite ( adapted from reference 15)

Carbon exists in different allotropic forms and especially carbon nanotubes (CNTs) and fullerenes (bucky balls) are having nano-dimension (see figure 1.4)<sup>15</sup>. The CNTs are cylindrical carbon molecules have novel properties like extraordinary strength and unique electrical properties, and are efficient conductors of heat<sup>16</sup>. The ends of a nanotube might be capped with a hemisphere of the ball structure. Their name is derived from their size, since the diameter of a nanotube is on the order of a few nanometers, while they can be up to several millimeters in length. Nanotubes are categorized as single-walled nanotubes (SWNTs) and multi-walled nanotubes (MWNTs). Generally CNTs were synthesized by arc discharge, laser ablation, high

pressure carbon monoxide (HiPCO), and chemical vapor deposition (CVD) techniques. Very recently much interests is focused in synthesizing a new type of carbon based nanostructure namely graphene<sup>15</sup>. Graphene is the nano-dimensional layered form of graphite and scientists are successful synthesizing even single layered graphene. Graphene is considered to be the mother of all carbon based nanomaterials since all structures are basically made up of graphene layers (see figure1.4).

Similar to inorganic systems miniaturization of organic counterparts also will improve its properties like surface adsorption, catalytic activity etc due to the enormously increased surface area and highly ordered arrangement of molecules<sup>7</sup>. During the last two decades a number of approaches for several of organic nanostructures by using tools learned from supramolecular chemistry are developed. Molecular self-assembly is an important aspect of bottom-up approaches to organic nanostructures<sup>11</sup>. Using molecular self-assembly the desired structure is programmed in the shape and functional groups of the molecules. Among organic structures polymeric systems are particularly important since it combine the advantages of low-dimensional systems as well the properties associated with polymer like mechanical strength, processibility etc. In synthetic polymeric systems, the morphology control has been achieved via two important approaches: one using block copolymers and the other using surfactants<sup>17,18</sup>. Similar to any other multi-component polymer systems or multi-component solutions, phase separation is commonly encountered in block copolymers because of the difference in the physical and chemical properties between the different blocks<sup>18</sup>. However, unlike in ordinary polymers, in amphiphilic copolymers the different blocks in a single polymer chain are covalently bonded. The covalent linkage between the different blocks makes bulk macroscopic phase separation impossible. Instead, the phase separation occurs on the nanometre scale, as determined by the dimension of the blocks. If all the polymer chains have narrow size distribution, the phase separation will produce ordered nanostructures similar to surfactant systems. Because of the advance in the polymer chemistry to synthesize block copolymers with very narrow molecular weight distribution, and the flexibility to modify the compositions and molecular architecture, the rich phase behaviour in block copolymers far exceeds what is observed in surfactant systems<sup>19</sup> (see figure 1.5).

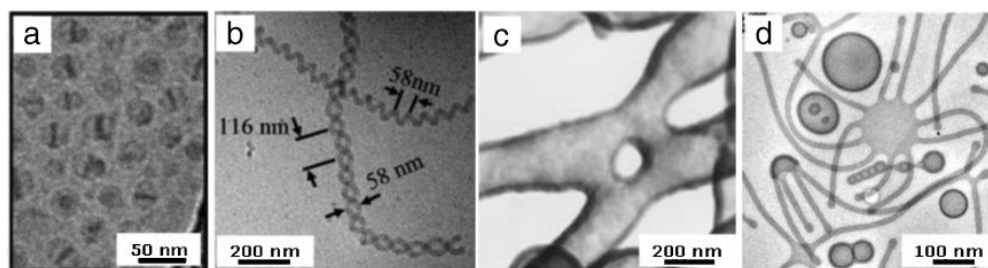


**Figure 1.5.** Transmission electron micrographs of various block-co-polymer structures: a) 'hamburger' micelles b) helical micelles c) bilayers tubules, and d) mixtures of polymer vesicles and 'octopi' structures. (Adapted from reference 19)

The surfactant induced approach can be useful for both homo-polymers and block-co-polymers<sup>20,22</sup>. In this approach the supramolecular interaction between polymer chain and amphiphile is utilized. The polymer-amphiphile complex is formed by the attractive physical interaction (e.g. hydrogen bonding, ionic interaction etc.) of the head group of amphiphile with the polymer backbone<sup>24</sup>. In the case of homo-polymers, these complexes can form comb-shaped supramolecular structures in the solid state. The self-assembly of polymer-amphiphile complexes can be combined with diblock copolymers also, which leads to hierarchy of structures, i.e. structure-within-structure<sup>25</sup>. In this case one block has an attraction with the amphiphile and the other block has not, so the self-assembly now takes place at two length scales (see figure 1.6). The morphology depends on several parameters such as the volume fraction of domains, the degree of complexation, the alkyl tail lengths of the amphiphiles, and temperature.

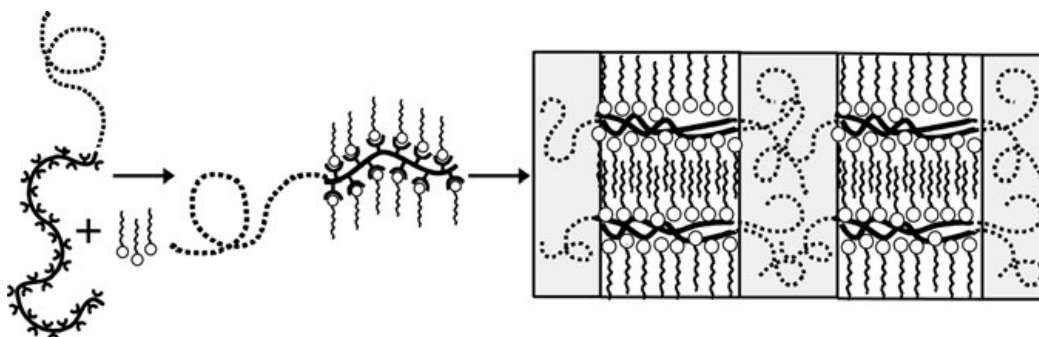


**Figure 1.6.** A schematic presentation for a hierarchical self-assembly of co-polymer-amphiphile complexes. (Adapted from reference 25)

Another interesting surfactant based approach is the synthesis of amphiphilic surfactant like monomers containing polymerizable group, either within the hydrocarbon tail or as a part of the hydrophilic head group<sup>17</sup>. Since amphiphilic

monomers have an inherent tendency to form nano - assemblies in solution and its subsequent polymerization will lead nanostructure formation.

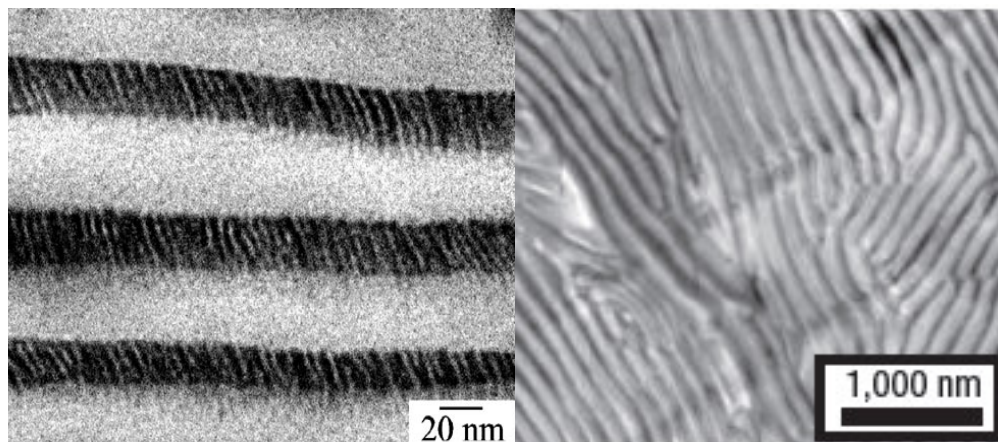


**Figure 1.7.** TEM images of the complex formed between poly [styrene-block-(4-vinyl pyridine) + nonadecylphenol (left) and polystyrene-block-poly (4-vinylpyridinium methane sulphonate) + 3-n-pentadecylphenol (right). (Adapted from references 23, 24)

## 1.2. Conducting Polymers

Conducting polymers are organic polymers that can conduct electricity. This class of polymers has a highly delocalized  $\pi$ -electron system with alternative single and double bonds (conjugated) in the polymer backbone. It was discovered in 1977 by Mac Diarmid, Heeger and Shirakawa that the conjugated polyacetylene conduct electricity upon exposure to iodine vapour<sup>25,26</sup>. This discovery initiated a substantial amount of effort in understanding these new classes of polymers and were recognized by 2000 Nobel Prize. In conducting polymers the  $\pi$ -conjugation of the polymer chain generates high energy occupied (HOMO) and low energy unoccupied molecular orbitals (LUMO) leading to a system that can be readily oxidized or reduced<sup>27</sup>. Their electronic conductivity is called intrinsic as it is caused by the presence of conjugated electrons in the polymer backbone which enable electric charges to move around without any added conducting materials (e.g. metals, graphite). In most of the cases, these polymers are insulators in their neutral state and they become conducting only after introduction of electron acceptors/donors by a process known as ‘doping’ (see figure 1.8). Conducting polymers can provide the conduction of electric charges through movement of electrons in unoccupied energy states or movement of holes in filled energy states. The creation of conductive holes in polymer by oxidation is called

p-type doping and the creation of free electrons by reduction is called n-type doping

28

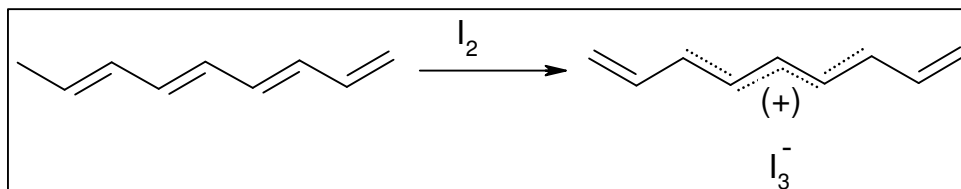


**Figure 1.8.** Doping in conducting polymer.

The first discovered conducting polymer polyacetylene has a high conductivity, but its poor environmental stability hampers practical applications. This has led to the discovery of a variety of other conducting polymers such as polypyrrole (PPy), polythiophene, poly-p-phenylene, poly-p-phenylenevinylene (PPV), polyaniline (PANI) etc<sup>26,29</sup>. The electrical behaviour of these polymers and their derivatives are similar to that of polyacetylene, but they showed higher stability and better processability. Figure 1.9 summarizes the structures of some of the commonly known conducting polymers.

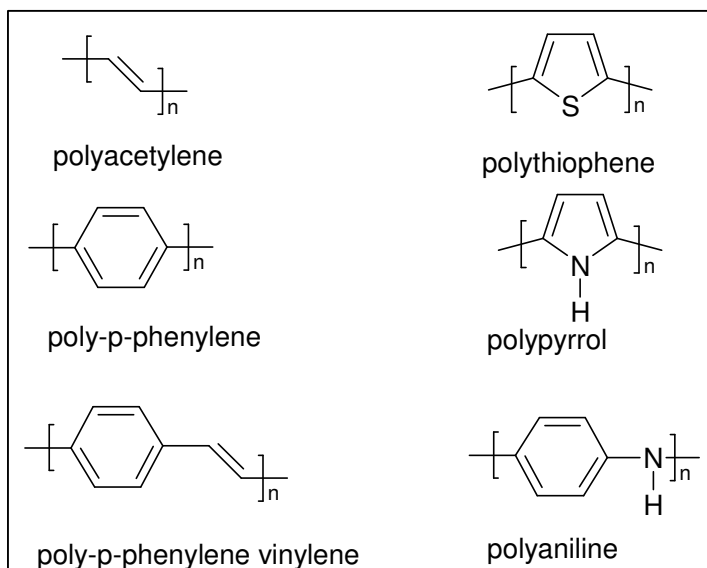


**Figure 1.9.** Various types of conducting polymers.

The doping of these materials results in rearrangements of polymer chains and induces ordered structure formation. Conductivity and other properties of the doped material can be varied and controlled by the amount and type of dopants used. Both n-type and p-type dopants have been utilized to induce an insulator to conductor

transition in electrically conducting polymers. Some common conducting polymers, their properties, doping materials used etc are given in table 1.2.

**Table 1.2.** Dopant used, conductivity, processibility, stability and cost details of some common conducting polymers.

Polymer	Dopants	Conductivity (S/cm)	Stability	Processibility	Cost
Polyacetylene	I <sub>2</sub> , Br <sub>2</sub> , Li, Na	10000	Poor	Limited	High
Polypyrrole	BF <sub>4</sub> <sup>-</sup> , ClO <sub>4</sub> <sup>-</sup>	500-7500	Good	Good	High
Polythiophene	BF <sub>4</sub> <sup>-</sup> , ClO <sub>4</sub> <sup>-</sup>	1000	Good	Excellent	High
Polyphenylene	AsF <sub>5</sub> , Li, Na	1000	Poor	Limited	High
Polyaniline	HCl, R-SO <sub>3</sub> H	200	Good	Good	Low

Conducting polymers emerged as potential candidates for various applications since they combine high electrical conductivity and processability. Among the two major groups of applications, one category considers the conductivity as the main property while the second group give importance to their electro-active properties<sup>30</sup>. The first set of applications includes diodes, transistors, aircraft structures, printed circuit boards, artificial nerves conducting adhesives, electromagnetic shielding etc. The second classification gave way to molecular electronics, displays, sensors, rechargeable batteries etc. where electro-optical properties of the polymers play the major role.

### 1.3. Polyaniline

Among the conducting polymers polyaniline (PANI) is unique due to its wide range of conductivity from insulating to metallic regime, redox tunability, good environmental stability, low cost, ease of synthesis, and promising applications in various fields, such as metallic corrosion protection, electromagnetic interference shielding, electrostatic discharge ,sensors , actuators , etc<sup>25,31</sup>. Polyaniline and its derivatives are generally synthesized by chemical or electrochemical oxidative polymerization of the aniline monomers in acidic aqueous media<sup>31,33</sup>. Polyaniline has three different oxidation states as shown in figure 1.10. They are fully reduced

colourless leucoemeraldine form; half oxidized blue coloured emeraldine base form and fully oxidized brown coloured pernigraniline form<sup>32,34</sup>. These oxidation states can be reversibly change from one to other by means of chemical or electrochemical means. All these three forms are found to be insulators of electricity in normal conditions<sup>35</sup>. But the emeraldine base form on protonation will yield green coloured emeraldine salt, which is a highly conducting material. When polyaniline is prepared by the conventional chemical oxidative polymerization from aniline monomer in acidic media, emeraldine salt (protonated form) can be obtained that can then be converted in to the emeraldine base form by treating with base.

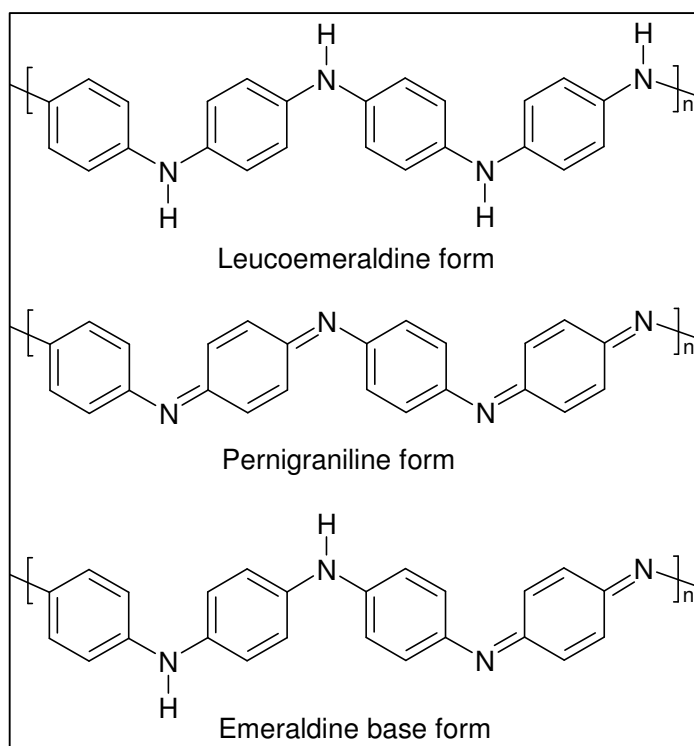


**Figure 1.10.** Various oxidation states of polyaniline.

The conductivity change between emeraldine salt ( $\sigma \geq 1 \text{ S cm}^{-1}$ ) and emeraldine base ( $\sigma \leq 10^{-10} \text{ Scm}^{-1}$ ) states can be greater than ten orders of magnitude. The optical, electrical, thermal, electrochemical and solid state properties of this interesting polymer were extensively studied and well documented by various groups around the world, especially by MacDiarmid and co-workers<sup>35-39</sup>.

### 1.3.1. Synthesis of Polyaniline

Polyaniline can be easily obtained as dark green powder (salt form) by polymerization of aniline in aqueous acidic media using oxidizing agents such as ammonium persulfate, potassium iodate, hydrogen peroxide, potassium dichromate etc<sup>31,35</sup>. The reaction scheme is given in figure 1.11. The polymerization start with the formation of radical cations, followed by coupling to form di-cation and the repetition leads to the polymer growth<sup>31,34</sup>. Since oxidative chemical polymerization is exothermic it is carried out at low temperatures (−15 to 5 °C) in order to obtain polyaniline with high molecular weight.

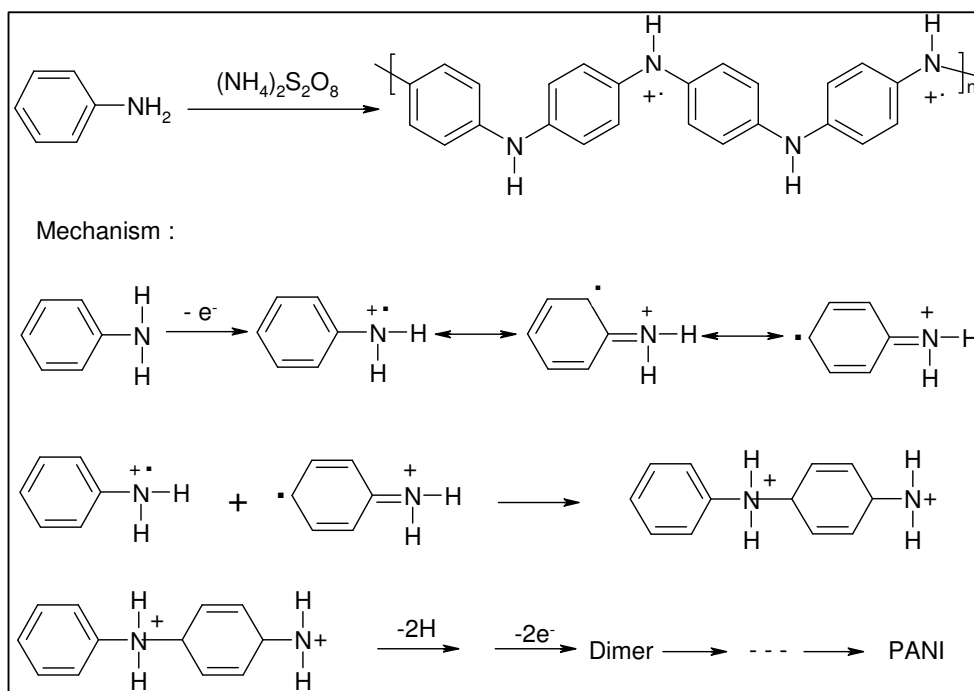


**Figure 1.11.** Chemical synthesis and plausible mechanism of polyaniline formation.

The dark green/blue-green precipitate (ES) formed was collected and purified by repeated washing. Polyaniline emeraldine base can be obtained by stirring the emeraldine salt powder in  $\text{NH}_4\text{OH}$  solution of for 10–12 h. One of the disadvantages of this method stems from the experimental observation that an excess of the oxidant and higher ionic strength of the medium leads to materials that are essentially intractable.



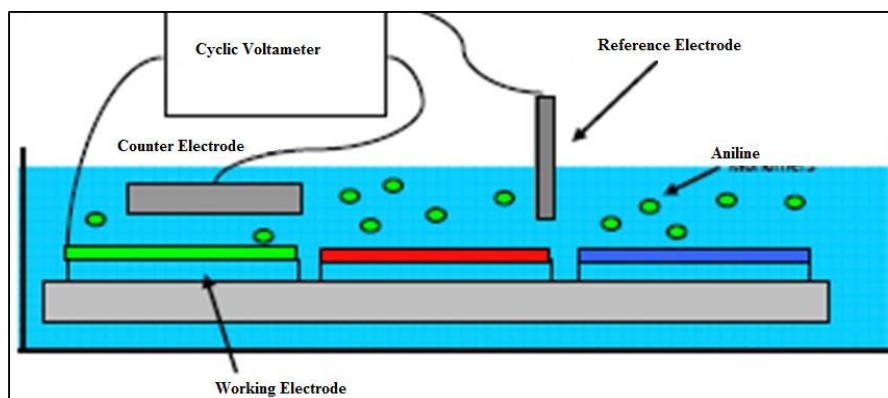


**Figure 1.12.** Scheme depicting the setup for electrochemical synthesis of polyaniline.

Polyaniline can be synthesised by electrochemical oxidation reaction also. The polymerization of aniline is carried out in a three electrode single cell compartment containing aqueous acidic solution of aniline (figure 1.12). Standard electrochemical techniques include a three-electrode cell which contains a working electrode (WE), a reference electrode (RE) and a counter electrode (CE) or an auxiliary electrode (AE) (*ref*). For many conceivable applications, deposition of the polymer film can be achieved using electrochemical polymerization.

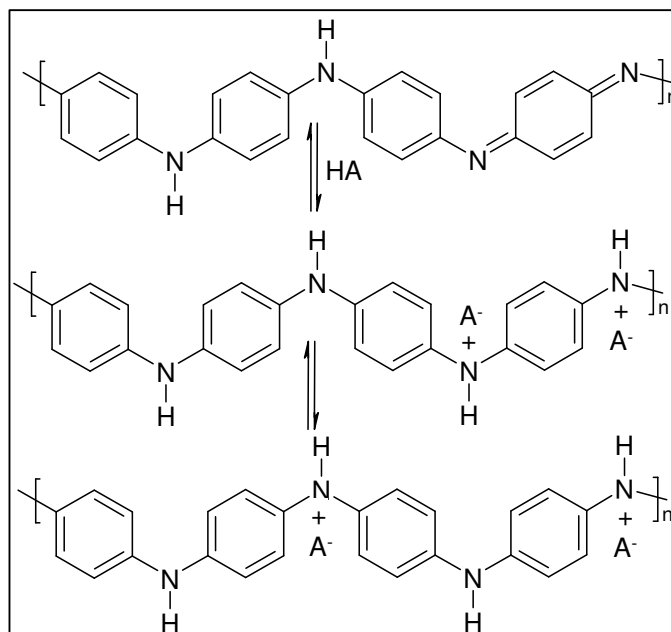


**Figure 1.13.** Doping in polyaniline-Acid-base chemistry.

In pristine state all conducting polymers are insulators and they are made conducting by partial oxidation or partial reduction of the  $\pi$ -system of the polymer

which leads to either increase or decrease in the number of electrons associated with it. But the uniqueness of polyaniline arises due to the high sensitivity of its emeraldine oxidation state (EM) towards the pH which yields emeraldine base (EB) and emeraldine salt (ES) forms of polyaniline<sup>34</sup>. So the non-conducting EB form of polyaniline can be doped to a highly conducting regime (ES) without changing the total number of electrons associated with it. Such a doping is achieved by a simple protonation of the –NH group of EB by mineral or organic protonic acids and is known as ‘acid doping’ (see figure 1.13). The acid doping process increases the conductivity of polyaniline by more than ten orders of magnitude. Emeraldine base (EB, undoped form) consists of alternating reduced and oxidized repeating units, i.e. benzoid (phenylene diamine) and quinoid (quinoid diimine) groups. Reversible switching between doped form and undoped form (i.e. emeraldine salt and base) can be achieved via protonation of imine nitrogen atoms of the quinoid group forming an acid-base complex and vice versa. This processing is called protonation since acids and bases neither reduce nor increase the number of electrons associated with the polymer chains as shown in figure 1.13 . Heavily doped polyaniline (often termed 50% protonation) corresponds to protonation of all imine nitrogen atoms of quinoid group resulting in the highest conductivity. Positive charges accumulated on the polymer backbone during protonation of polyaniline are neutralized by the negatively charged counter ions of the dopant. The protonation is also effects a dramatic change in the electronic structure, crystallinity, solubility, etc of the polymer<sup>34,37</sup>. Inorganic mineral acids such as hydrochloric acid (HCl), sulphuric acid (H<sub>2</sub>SO<sub>4</sub>), etc. are the most effective dopants to get highly conducting polyaniline, but the resulting polymer is completely insoluble in most of the solvents<sup>31</sup>. Therefore workers started using strong organic acids like sulfonic acid as dopants which will improve the conductivity as well as processability of the materials<sup>34,42</sup>. The most extensively used organic dopants are camphor sulfonic acid (CSA), p-toluene sulfonic acid (PTSA), and dodecyl benzene sulfonic acid (DBSA) etc.

Polyaniline is a promising material because of its easy synthesis from cheap starting materials, tunable redox properties by simple acid-base doping chemistry, high thermal stability etc<sup>25</sup>. But due to semi rigid back bone structure the material is not soluble in common solvents that make its processability very difficult which

hampers most its potential applications<sup>43</sup>. Historically the first attempt to solve this issue was the dispersion polymerization techniques in which steric stabilizers like amphiphilic water soluble polymers or inorganic colloidal particles were added in the polymerization media to prevent the bulk precipitation of the polyaniline chains<sup>44-46</sup>. This results the formation of polyaniline-stabilizer composite particles dispersion and easily transformed in to any substrates. Another important approach to solve the infusibility of polyaniline material was the use functional organic dopants. The use of functional dopants like CSA, DBSA etc. solved the issue of solubility considerably and enabled polyaniline to be casted in to film using solvents like m-cresol, chloroform etc<sup>42</sup>. This area of novel functional dopants was well explored and a number of novel sulfonic acids were developed and utilized as dopants for polyaniline<sup>47-48</sup>. Additional to solubility, these dopants were able to impart good solid state properties and morphologies to polyaniline and thereby improved the electrical properties of the material<sup>49</sup>.

Accordingly, the synthesis of nano-structured polyaniline is a new key step in preparing highly dispersible material. In comparison with the polyaniline particles, which are mainly synthesized by dispersion technique, one dimensional nano-structured polyaniline, including nanofibers, nanowires, nanorods, nanotubes, nanosphers, nanobelts and nanoribbons, have several advantages in fabricating nano-devices and in preparing nanoscale electrical connections<sup>43,50</sup>. Additional to this, the nanostructures are expected to exhibits some special physical and chemical properties differing from the bulk material and will render it for new applications such as chemical sensors, energy conversion and storage, light-emitting display, microelectronics, optical storage, and so on<sup>43,51</sup>.

#### **1.4. Polyaniline Nanomaterials**

In recent times there is a tremendous growth in the synthesis and applications of both inorganic and organic nanomaterials, parallel to this a handful of attempts have been carried out to confine polyaniline in nano-dimension and explore its novel properties<sup>52,53</sup>. The first developed and straight forward methods for the synthesis of nano polyaniline were physical routes like electro spinning and mechanical stretching<sup>25</sup>. But these techniques are not suitable for making nanostructures of <100

nm dimension. So the interest shifted in to develop in situ synthetic approaches for nano-dimensional polyaniline which is the modification of either chemical or electrochemical conventional oxidative route<sup>43</sup>. This chemical approach was again categorized namely the template synthesis and the no-template synthesis, with respect to whether template is used or not. The template based methods were subdivided into hard template (physical template) and soft template (chemical template) synthesis approach according to the solubility of the templates in the reaction media, while the no-template approaches includes interfacial, rapid mixing, dilute polymerisation etc<sup>43,53</sup>.

#### 1.4.1. Electrospinning Method

The electro spinning is an important physical method, in which a polymer solution is placed in a hypodermic syringe at a fixed distance from a metallic plate, which is acting as a cathode<sup>54</sup>. The anode is attached to the metal tip of the syringe and can be placed vertically over the cathode. When the voltage applied between the anode and cathode reaches a critical value the charge overcomes the surface tension of the deformed drop of the polymer solution on the tip of the syringe and a jet is produced. Since the polymer molecules all bear positive charge, they repel each other to get separated while traveling in air during a few milliseconds from the anode and the evaporation of the solvent molecules results nanofiber formation<sup>55</sup>. (see figure 1.14).

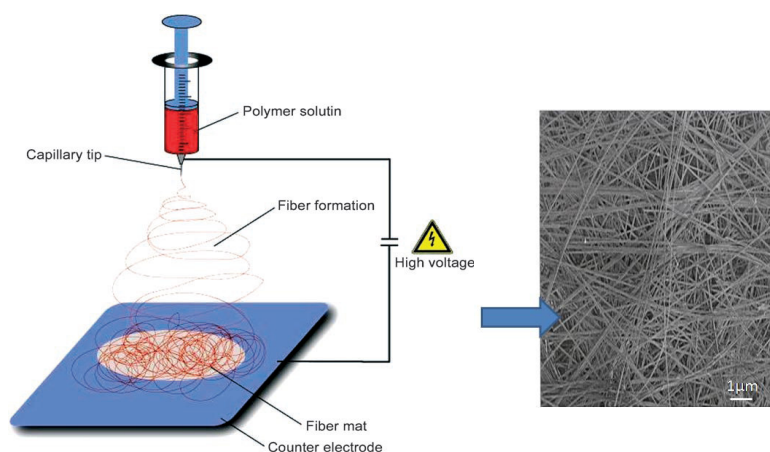


**Figure 1.14.** Schematic representation of the set-up for electrospinning nanofibers.

(Adapted from reference 55)

Another important physical method for nanofabrication is electrochemical approaches. These methods are very attractive since the material obtained is relatively defect free and more pure<sup>56</sup>. Liu et al. showed the creation of large arrays of uniform and oriented nanowires of PANI with diameters less than 100 nm on a variety of substrates by a three-step electrochemical deposition procedure in the absence of any templates<sup>56</sup>. This step wise growth produced exclusively very uniform and oriented nanowires on both flat substrates. Additionally, electrochemical polymerization in presence of templates like porous polymer films in acid media to synthesize nanostructured films of polyaniline are also known.

#### 1.4.2. Hard Template Synthesis

Hard template synthesis for architecting conducting polymers were developed by Martin et al. , which make use of the pores, channels of hard materials such as polymer membranes , zeolites, anodic aluminium oxide etc. as template for polymer growth<sup>57,58</sup>. Here the monomer was filled in pores of template and up on polymerising the polymer formed will take the shape of the channel. In a typical synthesis, the hard templates were firstly immersed in a pre-cooled acidic solution of aniline, and the oxidant solution at the same temperature was added then to start the polymerization. During the course of time, polyaniline was produced and deposited within the pores or channels of the templates (see figure 1.15). With the templates eliminated, partly or completely, one-dimensional nano-structured polyaniline was isolated. Using this method one-dimensional micro- or nano-structures of a variety of conducting polymers like polyaniline, polypyrrole, polythiophene etc with controllable diameter, length and orientation were synthesized. The main advantage of this approach is by selecting suitable template characteristics it is possible to precisely tune the morphological features like diameter, length etc. However, the main drawback of the method is that a rather tedious post-synthesis process is required in order to remove the templates and also the nano-structure may be destroyed or form undesirable aggregated structures after released from the templates. In addition to the above mentioned chemical oxidative polymerization, polyaniline nanofibers, nanotubules and nanoribbons were also prepared by electrochemical oxidative polymerization with hard templates such as polycarbonate membranes, anodic alumina and enclosed

nanochannels. Using hard template method polyaniline nanotubules encapsulated metal nanowires can be prepared. These metal nanowires were protected from corrosion and oxidation from air by the polyaniline nanotubules.

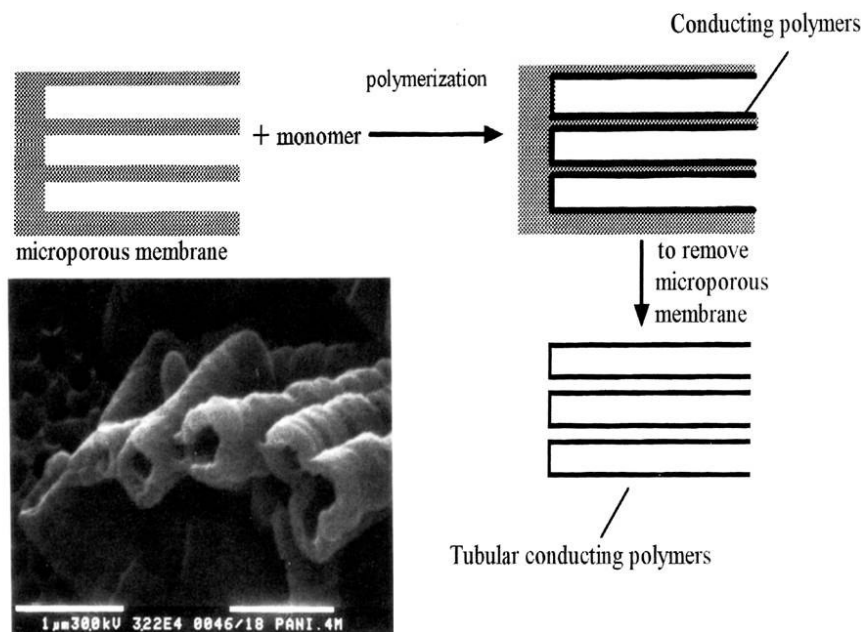


**Figure 1.15.** Hard template synthesis of polyaniline tubes. (Adapted from reference 58)

### 1.4.3. Soft Template Synthesis

The soft template or self-assembly method is an easy and widely used scalable method pioneered by Wan and co-workers<sup>59-64</sup>. This process involves the use of structure-directing molecules such as surfactants, functional dopants, amphiphilic polymers, liquid crystals, supramolecular assemblies as templates for production of the one-dimensional nanomaterials of polyaniline and polypyrrole. The widely used functional dopants are naphthalenesulfonic acid (NSA), camphorsulfonic acid (CSA), azobenzenesulfonic acid (ABSA), 2-acrylamido-2-methyl-1-propanesulfonic acid (AMPSA) and the polyelectrolytes include poly (acrylic acid), poly (styrene sulphonic acid) etc. This method is free of post synthesis processing since these molecules are good dopants for polyaniline. In a typical synthesis, aniline and functional dopant with different molar ratios were added to a certain amount of distilled water and stirred to result the formation of aniline-dopant complex. This soft template was oxidised by oxidants like ammonium per sulphate to get nanomaterials (see figure

1.16). The formation of the one-dimensional nano-structured polyaniline depended on the reaction conditions, such as the concentration of aniline, the molar ratio of aniline to oxidant, the soft template etc<sup>65,66</sup>.

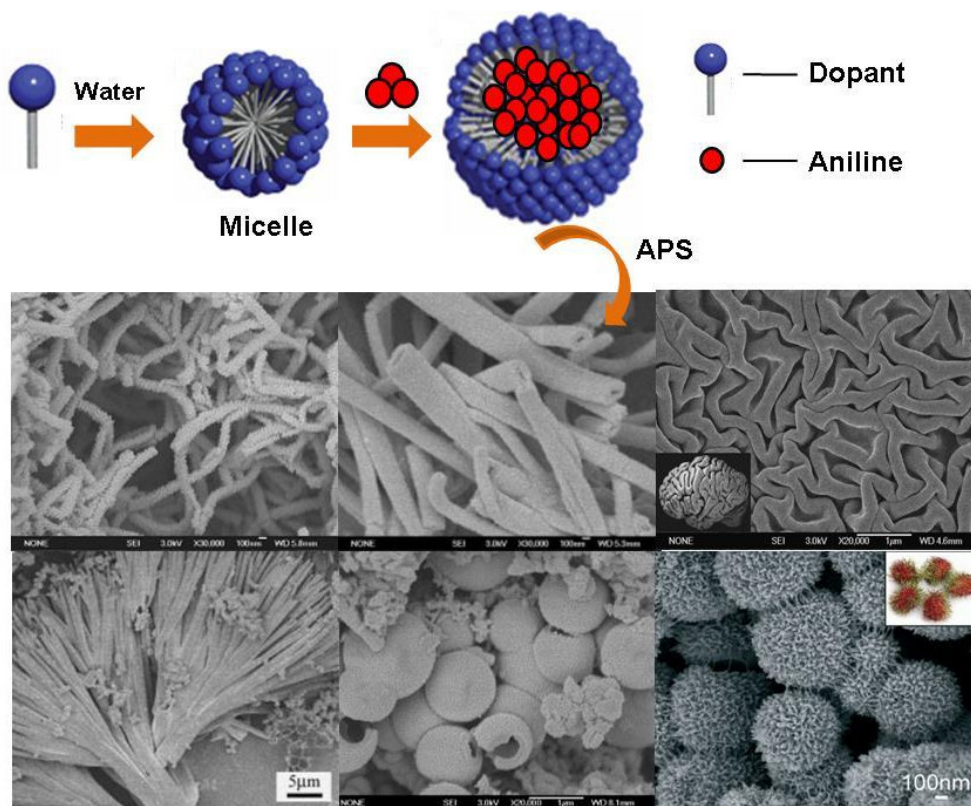


**Figure 1.16.** A schematic representation of soft template approach and various polyaniline morphologies synthesised this route. (Adapted from reference 51,53)

The same method was extended to inorganic dopants like HCl, H<sub>2</sub>SO<sub>4</sub>, HBF<sub>4</sub> and H<sub>3</sub>PO<sub>4</sub> also by introducing surfactants as structural directing agents<sup>67</sup>. By adopting soft template approach a variety of nanostructures including nanofibers, nanotubes, nanorods, nanospheres and nanoleaves etc were synthesised (see figure 1.16). It was found that the diameters and lengths of the one-dimensional nano-structured polyaniline were depended on the factors such as the soft templates, molar ratio of surfactant to aniline, reacting temperature, time and other synthetic conditions. So by selectively tuning the self assembly properties of the dopant template it is possible to create a variety of nanostructures. Another important advantage of this process is that after synthesis of nanostructures it is possible to

employ any dopant by a dedoping–redoping procedure without significantly changing the morphologies and diameters of the nanostructures. Shinkai et al. were very successfully translated the morphological features like helicity, lamellar packing etc. of self-assembled molecular template to the final polyaniline nanostructures<sup>68,69</sup>. The same group also used self assembled gels as template to architect various superstructures of polyaniline. This soft template self-assembly approach is very versatile and even extended to related conducting polymers like polypyrrole and poly(3,4-ethylenedioxythiophene) also<sup>70,71</sup>.

Regarding the mechanistic aspects of the nanostructure formation, it was proposed that the functional dopants or surfactants self assembled with or without their aniline salts into nano- or micro structured aggregates due to the amphiphilic nature, which played a template role in the formation of the one-dimensional nanostructured polyaniline<sup>51,53</sup>. Wan et al. were able to isolate these intermediates and showed the presence of the proposed templates by freeze fracture TEM. One-dimensional nano-structured polyaniline was also reported during electrochemical polymerization of aniline with soft templates like liquid crystalline assemblies. The nanofibers produced this way are very smooth, better aligned and very long<sup>72</sup>. Grady et al. used the adsorbed surfactant aggregates on a flat surface as soft templates for synthesizing nanostructured polyaniline and polypyrrole, with controlled morphology<sup>73</sup>. In this method, aniline and sodium dodecyl sulphate (SDS) were allowed to aggregate on highly oriented pyrolytic graphite surfaces and then the oxidant was added to start the polymerization which resulted in well aligned polyaniline nanowires parallel to the surface, as well as other morphologies on the substrates.

#### 1.4.4. Interfacial Polymerization

This facile non-template method for quality nanofibers was developed by Kaner's group and they found that when the polymerization is carried out at an aqueous/organic interface the polyaniline formed has fibrillar morphology<sup>74-78</sup>. In a typical synthesis, aniline was dissolved in the organic phase. Meanwhile, APS was dissolved in an aqueous acid solution taken in a separate vessel. And then, the two solutions were gently transferred to a reaction vessel, generating an interface between



the two layers. Green polyaniline was formed initially at the interface as the reaction proceeds and migrated gradually into the aqueous phase until the whole aqueous phase is filled homogeneously with dark-green polyaniline (see figure 1.17). The isolated polyaniline is in the form of nanofibers of diameter < 100 nm.

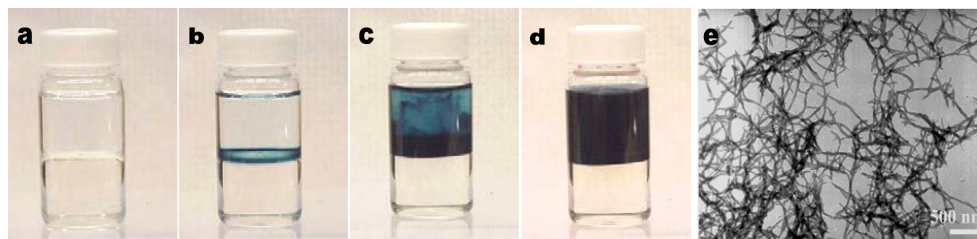


**Figure 1.17.** Snap shot showing the progress of interfacial polymerization and the SEM of nanofibers synthesized by this route. (*Adapter from reference 75*)

It was believed that polyaniline has an intrinsic nanofibrillar nature, but in single pot reactions the initially formed nanofibrillar morphology was lost due to secondary growth leading to agglomerated morphology, whereas in interfacial route the secondary growth was effectively suppressed due to the unavailability of excess monomer at the interface leading thus to the exclusive formation of nanofibers<sup>75</sup>. The nanofibers formed at the interface moved away rapidly from the interface and diffused into the water phase due to their hydrophilicity and allowing formation of new nanofibers at the interface. They have shown that diameters of the nanofibers prepared by interfacial polymerization can be controlled by using surface active dopants like AMPSA or CSA, and surfactants in the aqueous phase. Interfacial polymerization was also employed to graft a two-dimensional mesh of polyaniline nanofibers with diameters of 40–50 nm onto the Au surface through the covalent bonding between polyaniline and the amine created by the 4-aminothiophenol monolayer<sup>78</sup>. While using sulfonated polystyrene as both the host and the dopant in interfacial polymerization yielded transparent conductive nanocomposites with well-defined two-dimensional polyaniline nanofibers, rendering this procedure a unique and facile one in preparing robust conductive nanofibers based composites.

It was found that when the solution of APS mixed rapidly with that of aniline, rather than the conventional slow addition of the solution of APS to that of aniline, polyaniline nanofibers with comparable shapes and sizes to those of interfacial polymerization method were obtained<sup>79</sup>. It is believed that owing to the even distribution of aniline and APS molecules in the solution, all the initiator molecules

were consumed rapidly after the start of the polymerization and the secondary growth of polyaniline was suppressed, resulting exclusive nanofibers in the product. Another important approach to prevent secondary growth and preserve nanofibrillar morphology was carrying out polymerization at very dilute conditions so that new reactive aniline cation radicals and oligomeric intermediates generally do not diffuse quickly enough to newly formed nanofibers to affect secondary growth<sup>80,81</sup>. Epstein and co-workers showed using dilute polymerization approach it is possible to control the growth of polyaniline as well as the alignment of polyaniline nanofibers grown on a range of conducting and non-conducting substrates in a wide variety of sizes<sup>82</sup>. They found that these coatings display a range of properties including superhydrophilicity and superhydrophobicity etc. The addition of very small amount of nanomaterials to polymerization feed is found to be altering the growing polyaniline morphology<sup>83,84</sup>. The newly formed polymer chains will nucleate on these nano-surfaces and take up the shape of the seed. The nanomaterials used as seed are carbon nanotubes, nanofibers of hexapeptide etc<sup>83</sup>.

**Table.1.3.** Table summarizing the dopant used aniline amount, nano material type and corresponding reference.

Dopant	Aniline Amount	Nano type	References
HCl	0.3 mL	tube	Parthasarathy et al. <i>Chem. Mater.</i> <b>1994</b> , <i>6</i> , 1627-1632
NSA	1 mL	tube	Huang et al. <i>J. Polym. Sci: Part A: Polym. Chem</i> <b>1999</b> , <i>37</i> , 151.
Sulfonated - C-60	0.2 mL	tube	Qiu et al. <i>Macromolecules</i> <b>2001</b> , <i>34</i> , 675-677.
NSA	0.18 mL	tube	Wei et al. <i>Langmuir</i> , <b>2002</b> , <i>18</i> , 917-92.
Sulfonated CNT	18 $\mu$ L	tube	Wei et al. <i>Adv. Mater</i> , <b>2003</b> , <i>15</i> ,136-139.
HCl, PTSA, CSA	0.3 mL	fiber	Huang et al. <i>J. Am .Chem. Soc.</i> , <b>2004</b> , <i>126</i> , 851-855.
HCl	0.465 g	fiber	Wang et al. <i>Langmuir</i> <b>2005</b> , <i>21</i> , 833-836.
No dopant	0.06 g	plate	Zhou et al. <i>Macromolecules</i> , <b>2008</b> , <i>41</i> , 6473-6479.
HCl, SDS	0.045g	tube	Zhou et al. <i>Macromolecules</i> , <b>2009</b> , <i>42</i> ,1252–1257

To summarize various approaches for nano polyaniline a short literature survey spanning last one decade including some important research is given in table 1.3. It is clear that in most cases the synthesis of nanomaterials is in very small amount and there is a large discrepancy in the selection of dopant for specific polymerization routes. Further, polyaniline nanomaterial formation was found highly sensitive to experimental conditions such as stirring, rate of mixing, temperature, reactants compositions and concentrations, etc. Also most importantly there is fewer attempts that have been paid to understand the mechanistic aspects of polyaniline nanostructure formation. So the development of a multi-purpose amphiphilic dopant for simple, reproducible and scalable method for various types of polyaniline nanomaterials has been found to be a challenging task.

## **1.5. Applications of Polyaniline Nanomaterials**

Polyaniline nanostructures synthesised by chemical or electrochemical polymerization exhibit many similar physical properties as that of their conventional counterparts<sup>43,50</sup>. Besides these, nanostructured polyaniline exhibits certain unique properties related to miniaturization that make them advantageous over their bulk counterparts in certain type of applications<sup>85,86</sup>. The large surface area, improved processability, uniform morphology etc. of one-dimensional nanostructured polyaniline makes this important class of novel materials a promising candidate for applications ranging from sensors, microelectronics, energy storages and electron field emissions etc<sup>43</sup>. Polyaniline nanomaterials can also be used as a platform to grow inorganic nanoparticles and this composite material is an effective layer in molecular devices.

### **1.5.1. Chemical Sensors**

The highly sensitive electrical conductivity variations of the polyaniline upon exposure to acidic or basic vapours and liquids made them promising materials for sensor applications and much work was devoted in this area<sup>85,87-90</sup>. However, very poor sensitivity was observed for conventional polyaniline films due to poor diffusion of analyte molecules<sup>87,90</sup>. At the same time the nano-structured polyaniline showed an improved diffusion due to its greater exposure area and penetration depth for gas

molecules than the conventional polyaniline (see figure 1.18) and became an alternative material to improve the sensitivity of polyaniline based sensors<sup>91</sup>.

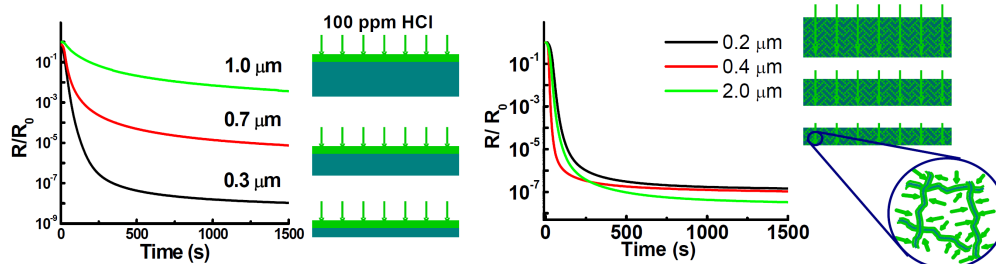


**Figure 1.18.** Difference in response of chemical vapors by conventional polyaniline film (left) and nanofiber film (right). (Adapted from reference 91)

### 1.5.2. Actuator Based on Flash Welded Polyaniline Nanofiber Film

The polyaniline fiber film can be welded by a camera flash in to a smooth and shiny film due to the high photo-thermal conversion and low thermal conductivity of polyaniline.<sup>92,93</sup> These flash welded asymmetric polyaniline film can be used as a monolithic actuator.<sup>92</sup> When the asymmetric film is exposed to acid, the nanofibrillar portion of the film expands as a result of charge repulsion of the anionic dopants. Since the welded side is much more dense and cross-linked, the entire film bends and coils towards the welded side (see figure 1.19). The reverse was happened when base vapour was introduced.

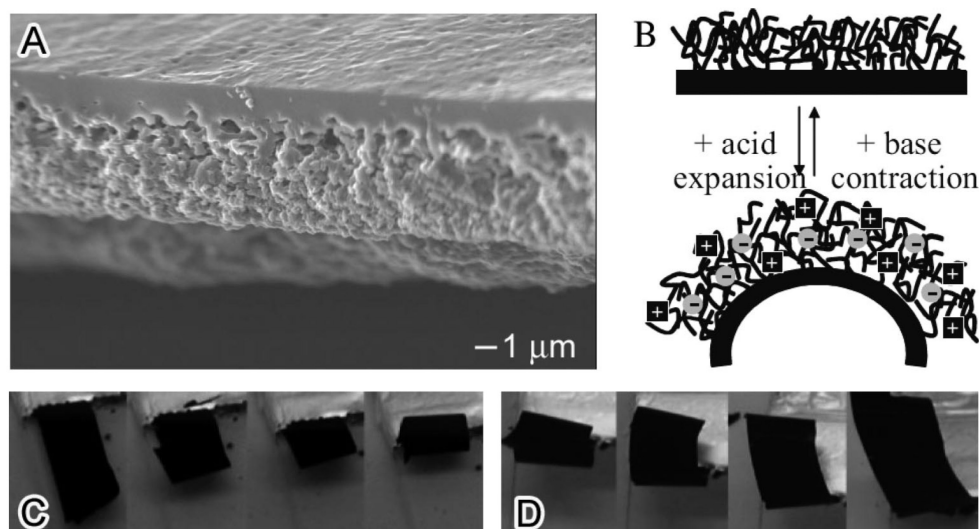


**Figure 1.19.** Flash welded polyaniline nanofiber film as an actuator. (Adapted from reference 93)

### 1.5.3. Digital Non-volatile Memory

Polyaniline nanofibers–gold nanoparticle composite material was found to be good candidate for memory devices. The device showed a bi-stable electrical behaviour and can be switched electrically between two states with a conductivity difference of about three orders of magnitude<sup>50,94</sup>. The switching mechanism was postulated to an electric field-induced charge transfer from the polyaniline nanofibers to the gold nanoparticles. The prolonged retention time and good write-read-erase cycle results suggested the device promising for digital non volatile memory applications<sup>91,94</sup>.

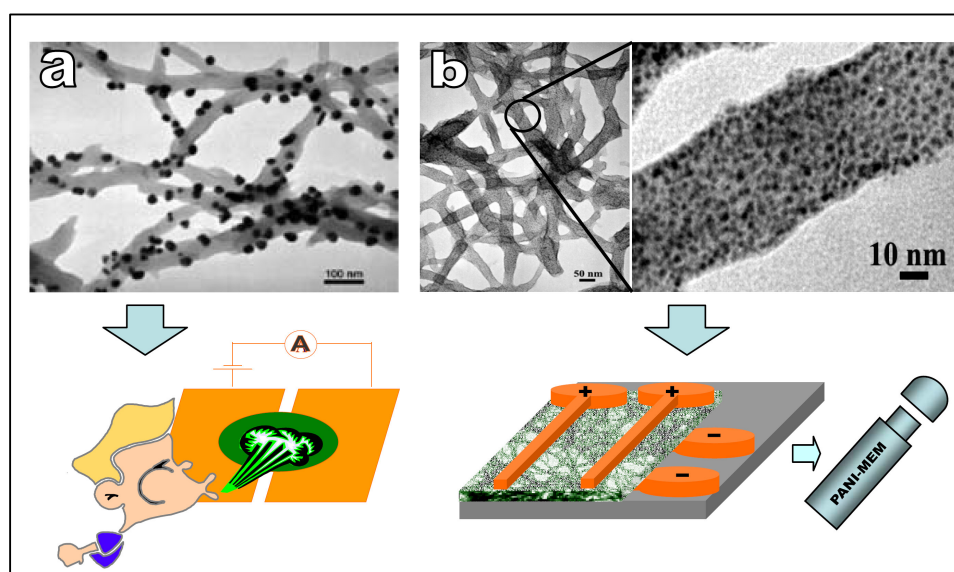


**Figure 1.20.** Schematic of polyaniline nanofiber/gold nanoparticle memory device and TEM images of nanofiber/gold composite. (Adapted from reference 91)

### 1.6. Aim of the Thesis

It is clear from the previous discussions that for the synthesis of one dimensional polyaniline nanostructures different kinds of synthesizing methods have been established, but synthesis of nano-structured polyaniline with controllable morphologies and sizes is still a major challenge. Similarly the exact formation mechanisms of the nanostructures need to be understood from a scientific point of view, which will be very useful in morphological control of polyaniline. We have come across with a new molecular design based on renewable resource starting material to address these issues. Additionally, the idea of interconnecting both

renewable resources and conducting nanomaterials is very new and have tremendous opportunities for fundamental and applied research. In this thesis, a renewable resource raw material cardanol, which is an industrial waste and pollutant from cashew nut industry, is utilized for the synthesis of novel amphiphilic dopants for conducting polyaniline nanomaterials. Additionally, efforts were also put to study the effect of functionalization from aniline monomer level on the self-assembly as well as surface properties of resulting polyaniline nanomaterials.

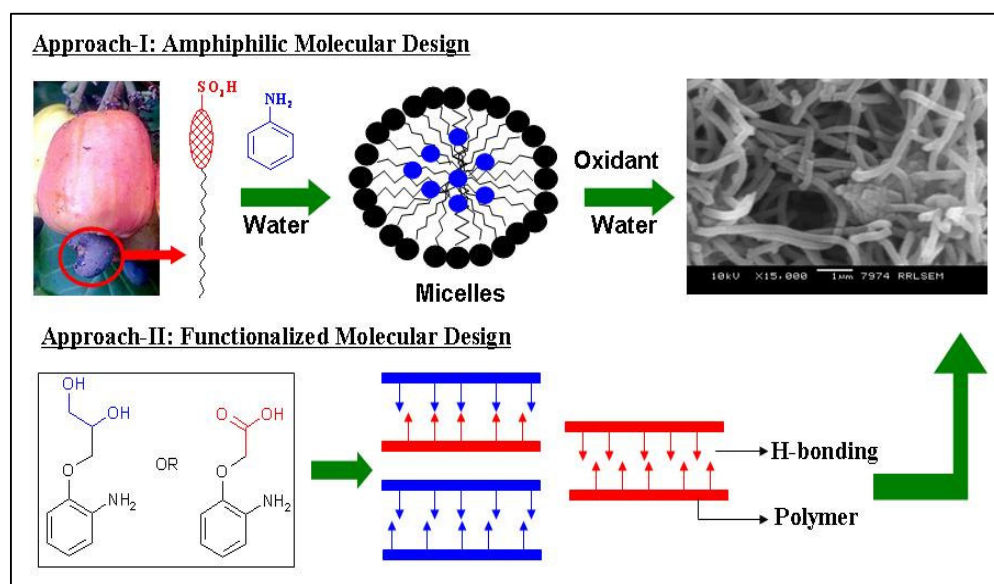


**Figure 1.21.** Schematic representation of the approach for the synthesis of polyaniline nanostructures.

The major aspects discussed in the thesis are

- (i) Design and development of novel amphiphilic azobenzene sulfonic acid molecule from renewable resource cardanol and employ it as structure-directing molecular template for polyaniline nanofibers.
- (ii) Selective micellar template approach for divergent polyaniline nanostructures.
- (iii) Cylindrical and vesicular templates for polyaniline nanofibers and nanotapes.
- (iv) Amphiphilic dopant organogel templates for polyaniline nanofibers.
- (v) Functionalized polyaniline nanospheres as a sensor material for vitamin C.

In this thesis, a unique amphiphilic azobenzene dopant molecule from a renewable resource cardanol was developed and utilized as structure-directing agent

for polyaniline nanomaterials. This surfactant dopant was employed to produce polyaniline nanomaterials by emulsion route by varying [aniline]/[dopant] ratio and its effect on the morphology and other physical properties were studied. Efforts have been paid to understand the mechanistic aspects of nanomaterials formation by DLS and TEM techniques. The feasibility of this approach to bulk-scale synthesis of nanofibers up to 100 gram was also tested. Since this dopant has a built-in amphiphilic structure its selective templating under emulsion, dilution and interfacial polymerizations were included in chapter 3. Dilution of thick emulsion produce uniform smaller micellar aggregates and similarly the dopant micelles form spherical aggregates with oxidizing agent ammonium persulfate (APS) in water; the templating effects of these novel templates were studied. The detailed studies using DLS, TEM were carried out to understand the mechanistic aspects of nanomaterials formation. The optical and solid-state properties of these nanostructures were understood by UV-Vis and WXR D techniques.

A soft template approach of a custom-designed novel surfactant-cum-dopant synthesised by ring opening of 1, 4 - butanesultone by cardanol is described in chapter 4. The micellar template formed by this amphiphilic dopant was utilized in emulsion and dispersion routes for polyaniline nanostructures. The fifth chapter comprises the supramolecular gel templating of polyaniline nanomaterials by the saturated counter part of the above dopant. The self assembled morphology of the gel was studied by SEM, TEM and AFM studies. The gel template formed between aniline and dopant is oxidised to produce polyaniline nanostructures. Gel-assisted polymerization was carried out at various temperatures to investigate the role of the physical state of the gel on the morphology of the final product. The effects of gel-template on solid-state and electrical conductance properties of nanomaterials were also tested.

The synthesis of novel polyaniline nanomaterials bearing mono and bis-hydroxyl functional groups to trace the molecular interactions at the nano-surfaces constitute chapter 6. Vitamin-C was employed as an analyte to trace the molecular interaction at the nano-surface and study the influence of functionalization on the sensing ability of biomolecules. Finally, overall conclusion of the thesis is summarized.

**1.7. References:**

1. Sergeev, G. B.; *Nanochemistry* (1<sup>st</sup> ed), Elsevier, Amsterdam, **2006**, pp 30-32
2. Bandyopadhyay, A.K. *Nanomaterials*, (1<sup>st</sup> ed) New Age, New Delhi, **2008**, pp 2-10.
3. Brechignac, C.; Houdy, P.; Lahmani, M. *Nanomaterials and Nanochemistry*, Springer-Verlag, Berlin, **2007**, pp10-15
4. Wang, Z. M. *One-Dimensional Nanostructures* (1<sup>st</sup> ed), Springer, New York, **2008**, pp 3-9.
5. Nabok, A. *Organic and Inorganic Nanostructures* (1<sup>st</sup> ed), Artec. Inc., Norwood, MA, **2005**, pp 2-9
6. Dai, H. *Nanotube Growth and Characterization. Carbon Nanotubes* (2<sup>nd</sup> ed), Springer, Berlin, **2001**, pp 29-53.
7. Niemeyer, C. M.; Mirkin, C. A. *Nanobiotechnology* (1<sup>st</sup> ed), Wiley-VCH, **2004**, pp 227-240
8. Rao C. N. R.; Muller, A.; Cheetham, A. K. *The Chemistry of Nanomaterials* (1<sup>st</sup> ed), Wiley-VCH, **2004**, Weinheim, pp 3-11
9. Thassu, D.; Deleers, M.; Pathak, Y. *Nanoparticulate Drug Delivery Systems* (1<sup>st</sup> ed), Informa, New York, **2007**, 1-5
10. Xia, Y.; Rogers, J. A.; Paul, K. E.; Whitesides, G. M. *Chem. Rev.* **1999**, *99*, 1823-1848
11. Loi, S.; Wiesler, U.-M.; Butt, H.J.; Mullen, K. *Chem. Commun.* **2000**, 1169.
12. Daniel, M.C.; Astruc, D. *Chem. Rev.* **2004**, *104*, 293-346
13. Barnard, A.S.; Young, N. P.; Kirkland, A. I.; van Huis, M. A.; Xu, H. *ACS Nano*, **2009**, *3*,1431–1436.
14. Faraday, M. *Philos. Trans.* **1857**, *147*, 145-181.
15. Rao, C.N. R.; Biswas, K.; Subrahmanyama, K. S.; Govindaraj, A. *J. Mater. Chem.* **2009**, *19*, 2457–2469
16. Dai, H. *Acc. Chem. Res.* **2002**, *35*, 1035-1044
17. Ramakrishnan, S. *Nanostructured Polymers; The Chemistry of Nanomaterials* (Eds: Rao, C. N.R. and Cheetham, A. K.) , Wiley-VCH, Weinheim, **2004**, pp 484-495



18. Alexandridis, P.; Lindman, B. *Amphiphilic Block Copolymers: Self-Assembly and Applications* (1st Ed) Elsevier, Amsterdam, **2000**.
19. Blanazs, A.; Armes, S. P.; Ryan, A. J. *Macromol. Rapid Commun.* **2009**, *30*, 267–277.
20. Ruokolainen, J.; Mäkinen, R.; Torkkeli, M.; Mäkelä, T.; Serimaa, R.; ten Brinke, G.; Ikkala, O. *Science*, **1998**, *280*, 557–560.
21. Muthukumar, M.; Ober, C. K.; Thomas, E. L. *Science*, **1997**, *277*, 1225.
22. Tiitu, M.; Volk, N.; Torkkeli, M.; Serimaa, R.; ten Brinke, G.; Ikkala, O. *Macromolecules* **2004**, *37*, 7364–7370
23. Ikkala, O.; ten Brinke, G. *Science*. **2002**, *295*, 2407–2409.
24. Valkama, S.; Kosunen, H.; Ruokolainen, J.; Haatainen, T.; Torkkeli, M.; Serimaa, R.; ten Brinke, G.; Ikkala, O. *Nat. Mater.* **2004**, *3*, 872–876.
25. MacDiarmid, A.G.; *Angew. Chem., Int. Ed.* **2001**, *40*, 2581–2590
26. Bredas, J. L. *Conjugated Oligomers, Polymers and Dendrimers: From Polyacetylene to DNA*, Proceedings of the Fourth Francqui Colloquium, Brussels, **1998**.
27. Skotheim, T. A.; Elsenbaumer, R. L.; Reynolds, J. R. *Handbook of Conducting Polymer* (2nd Ed). CRC Press, New York, **1998**.
28. Wise, D. L. *Electrical and Optical Polymer Systems: Fundamentals: Methods and Applications*, CRC Press, New York, **1998**.
29. Shirakawa, H. *Angew. Chem. Int. Ed.* **2001**, *40*, 2574.
30. Saxena, V., and B. D. Malhotra, *Current Appl. Phys.* **2003**, *3*, 293–305.
31. Stejskal, J.; Gilbert, G. *Pure Appl. Chem*, **2002**, *74*, 857–867.
32. Kang, E. T.; Neoh, K. G.; Tan, K. L. *Prog. Polym. Sci.* **1998**, *23*, 211–324
33. MacDiarmid, A.G.; Epstein, A. J.; *Faraday Discuss. Chem. Soc.* **1989**, *88*, 317
34. Palaniappan, S.; John, A. *Prog. Polym. Sci.* **2008**, *33*, 732–758
35. MacDiarmid, A.G.; Epstein, A. J.; *Science and Applications of Conducting Polymers* (Eds.: Salaneck, W. R.; Clark, D. T.; and Samuelsen, E. J.), Adam Hilger, Bristol, **1990**, p. 117.
36. MacDiarmid, A. G.; Epstein, A. J.; *Synth. Met.* **1995**, *69*, 85–92.
37. Chiang, J. C.; MacDiarmid, A. G. *Synth. Met.* **1986**, *13*, 193.

38. MacDiarmid, A.G.; Chiang, J.C.; Richter, A. F.; Epstein, A. J.; *Synth. Met.* **1987**, *18*, 285.
39. Norris, D.; Shaker, M. M.; Ko, F. K.; MacDiarmid, A. G. *Synth. Met.* **2000**, *114*, 109.
40. Glarum, S. H.; Marshall, J. H. *J. Electrochem. Soc.* **1987**, *134*,142.
41. Han, D.H.; Park, S. M. *J. Phys. Chem. B* **2004**, *108*, 13921-13927
42. Cao, Y.; Smith, P.; Heeger, A. J. *Synth Met* , **1992**, *48*, 91–97
43. Zhang, D. H; Wang, Y. Y. *Mater. Sci. Eng. B*, **2006**, *134*, 9-19
44. Armes, S. P.; Aldissi, M.; Hawley, M.; Berry, J. G.; Gottesfeld, S. *Langmuir* **1991**, *7*, 1447
45. Armes, S. P.; Aldissi, M.; Hawley, M.; Berry, J. G.; Gottesfeld, S. *Langmuir* **1991**, *7*, 1447.
46. Chattopadhyay, D.; Mandal, B. M. *Langmuir* **1996**, *12*, 1585-1588
47. Dufour, B.; Rannou, P.; Fedorko, P.; Djurado, D.; Travers, J.P.; Pron, A. *Chem. Mater.* **2001**, *13*, 4032-4040
48. Jana, T.; Nandi, A. K. *Langmuir* **2000**, *16*, 3141
49. Laska, J.; Djurado, D.; Lunzy, W. *Eur. Polym. J.* **2002**, *38*, 947-951.
50. Tran, H. D.; Li, D; Kaner, R. B. *Adv. Mater.* **2009**, *21*, 1–13
51. Wan, M. X. *Macromol. Rapid. Commun.* **2009**, *30*, 963–975
52. Li, D; Huang, J; Kaner, R. B. *Acc. Chem. Res.*, **2009**,*42*,135-145
53. Wan, M. X. *Adv. Mater.* **2008**, *20*, 2926–2932
54. MacDiarmid, A.G.; Jones, Jr., W. E.; Norris, I. D.; Gao, J.; Johnson, Jr., A. T.; Pinto, N. J.; Hone, J.; Han, B.; Ko, F. K.; Okuzaki, H.; Llagune, M. *Synth. Met.* **2001**, *119*, 27.
55. Greiner, A.; Wendorff, J. H. *Angew. Chem. Int. Ed.* **2007**, *46*, 5670 – 5703
56. Liu, J.; Lin, Y.; Liang, L.; Voigt, J. A.; Huber, D. L.; Tian, Z. R.; Coker, E.; Mckenzie, B.; Mcdermott, M. J. *Chem. Eur. J.* **2003**, *9*, 604.
57. Martin, C. R. *Acc. Chem. Res.*, **1995**, *28*, 61.
58. Parthasarathy, R. V; Martin, C. R; *Chem. Mater.*, **1994**, *6*, 1627-1632
59. Zhang, Z.; Sui, J.; Zhang, L.; Wan, M.X.; Wei, Y.; Yu, L. *Adv. Mater.* **2005**
60. Wei, Y.; Wan, M.X. *Adv. Mater.* **2002**, *14*, 1314-1317

61. Wei, Y.; Zhang, L.; Yu, M.; Yang, Y.; Wan, M.X, *Adv. Mater.* **2003**, *15*, 1382-1385
62. Zhang, L.; Wan, M.X. *Adv. Funct. Mater.* **2003**, *13*, 815-820
63. Qiu, H.; Zhai, J.; Li, S.; Jiang, L.; Wan, M.X. *Adv. Funct. Mater.* **2003**, *13*, 925-928
64. Zhang, L.; Long, Y.; Chen, Z.; Wan, M.X. *Adv. Funct. Mater.* **2004**, *14*, 693-698
65. Haung, K.; Wan, M.X. *Chem. Mater.* **2002**, *14*, 3486-3492
66. Yang, Y.S.; Liu, J.; Wan, M.X. *Nanotechnology*, **2002**, *13*, 771-773.
67. Zhang, Z.M.; Wei, Z.X.; Wan, M.X.; *Macromolecules*, **2002**, *35*, 5937-5942.
68. Hatano, T.; Takeuchi, M.; Ikeda, A.; Shinkai, S. *Chem. Lett.* **2003**, *32*, 314-315.
69. Li, C.; Hatano, T.; Takeuchi, M.; Shinkai, S. *Chem. Commun*, **2004**, 2350-2351
70. Jang, J.; Oh, J. H.; Stucky, G. D. *Angew. Chem., Int. Ed.* **2002**, *41*, 4016.
71. Tovar, J. D.; Rabatic, B. M.; Stupp, S. I. *Small*. **2007**, *3*, 2024 - 2028
72. L. Huang, Z. Wang, H. Wang, X. Cheng, A. Mitra, Y. Yan, *J Mater. Chem.* **2002**, *12*, 388-391
73. Carswell, A.D.W.; O'Rear, E.A.; Grady, B.P. *J. Am. Chem. Soc.*, 2003, *125*, 14793-14800.
74. Haung, J.; Virji, S.; Weiller, B. H.; Kaner, R. B. *J. Am. Chem. Soc.* **2003**, *125*, 314.
75. Huang, J.X.; Kaner, R.B. *J. Am. Chem. Soc.* **2004**, *126*, 851-855.
76. Haung, J.; Kaner, R. B. *Chem. Commun*, **2006**, 367-376
77. Zhang, X.Y.; Chan-Yu-King, R.; Jose, A.; Manohar, S.K.; *Synth. Met.* **2004**, 14523-14529.
78. Sawall, D.D.; Villahermosa, R.M.; Lipeles, R.A.; Hopkins, A.R. *Chem. Mater.* **2004**, *16*, 1606-1608.
79. Haung, J.; Kaner, R. B. *Angew. Chem.* **2004**, *116*, 5941-5945
80. Chiou, N.R.; Epstein, A.J. *Adv. Mater.*, **2005**, *73*, 1679-1683.

81. Chiou, N.R.; Epstein, A.J. *Synth. Met.* **2005**, *153*, 69–72.
82. Chiou, N.R.; Lu, C.; Guan, J.; Lee L. J , Epstein A. J. *Nat. Nanotech.* **2007**,*2*, 354 - 357
83. Zhang, X.; Goux,J.W. Manohar, S. K. *J. Am .Chem. Soc.* **2004**, *126*, 4502-4503.
84. Li, W.; Wang, H. L. *J. Am. Chem. Soc.* **2004**, *126*, 2278-2279
85. Hatchett, D. W.; Josowicz, M.; *Chem. Rev.* **2008**, *108*, 746-769
86. Janata, J.; Josowicz, M. *Nat. Mater.* **2002**, *2*, 19-24
87. Haung, J.; Virji, S.; Weiller, B. H.; Kaner, R. B. *Chem. Eur. J.* **2004**, *10*, 1314-1319
88. Virji, S.; Fowler, J.D.; Baker, C.O.; Haung, J.; Kaner, R.B.; Weiller, B.H. *Small.* **2005**, *1*, 624-627.
89. Sadek, A. Z.; Baker, C. O.; Powell, D. A.; Wlodarski, W.; Kaner, R. B.; Kalantar-zadeh, K.; *IEEE Sens. J.* **2007**, *7*, 213.
90. Virji, S.; Haung, J.; Kaner, R.B.; Weiller, B. H. *Nano.Lett*, **2004**, *4*, 491-496.
91. Huang, J. X. *Pure Appl. Chem.* **2006**, *78*, 15–27.
92. Baker, C. O; Shedd, B; Innis, P. C; Whitten, P. G; Spinks, G. M; Wallace, G. G; Kaner, R. B. *Adv. Mater.* **2008**, *20*, 155.
93. Huang, J.X.; Kaner, R.B. *Nat. Mater.* **2004**, *3*, 783–784.
94. Tseng, R. J.; Huang, J. X.; Ouyang, J.; Kaner, R. B.; Yang, Y. *Nano Lett.* **2005**, *5*, 1077–1080.

## ***Chapter-2***

---

### ***Development of Renewable Amphiphilic Molecular Template for Polyaniline Nanomaterials***

## 2.1. Introduction

In recent times polyaniline nanomaterials have gained significant interest due to their easy synthesis; simple non-redox doping/dedoping chemistry based on acid/base reactions, and environmental stability<sup>1-5</sup>. These unique properties associated with polyaniline nanomaterials made them very attractive for potential application in sensors, electronic and optical devices. Polymerization approaches such as ‘hard and soft’ templates, interfacial, rapid mixing, seeding, oligomer assisted and dilute polymerization techniques have been reported for one and three (1D and 3D) dimensional polyaniline nanomaterials<sup>4</sup>. Mineral acids like HCl, H<sub>2</sub>SO<sub>4</sub>, and HClO<sub>4</sub> etc. were employed as dopants for polyaniline nanomaterials and the materials were successfully tested for sensor applications<sup>4,5</sup>. However, low yield, poor environmental stability, need of large excess mineral acids for synthesis and amorphous nature of the nanomaterials are some of the limitations associated with mineral acid dopants<sup>6,7</sup>. Organic dopants such as aliphatic or aromatic sulfonic acids are very promising for polyaniline nanomaterials because of their high thermal and environmental stability compared to that of inorganic counterparts<sup>8-10</sup>. Most often the synthesis of polyaniline nanomaterials based on sulfonic acids were found highly susceptible to the [aniline]/[dopant] ratio in the feed and good morphology of the nanomaterials was produced only for selected compositions<sup>11</sup>. The reason for the in-homogeneity in the morphology was associated to the poor and unstable micelles formation of aniline-dopant complex in water. Efforts have also been taken by researchers to address these issues and the nanomaterial formation was found sensitive to various experimental conditions such as ultrasonic stirring, magnetic stirring, rate of mixing, reaction time and temperature, reactants compositions and their concentrations, etc<sup>12-15</sup>. Additionally, most of the research works in this area report the synthesis in very small amount, for example, varying from 30 milligram to < 1 gram scale. The important question is why the synthesis of polyaniline nano-materials restricted to such low gram scales even though all the starting materials such as monomer (aniline), oxidizing agent (ammonium persulphate, APS), dopant (like HCl or sulfonic acid) and the solvent (water) are commercially available and not expensive. The nanomaterial synthetic approaches at these very low quantity scales would be difficult to reproduce and the resultant materials may not be sufficient for practical applications which

required at least few grams of samples (~10 g). Therefore, design and development of novel surfactant cum dopant molecules for the reproducible synthesis of polyaniline nanomaterials under various composition and adaptable to wider experimental conditions are important issues to be addressed. These approaches should also be able to utilize for the large scale synthesis of polyaniline nanofibers for reproducible and sustainable polyaniline nanomaterials research.

In this thesis, a renewable resource strategy has developed for conducting nanomaterials research. The building blocks currently used in nanochemistry are synthesized mainly from petroleum-based starting materials<sup>16</sup>. However, plant resource based organic synthesis has distinct advantages for the generation of new building blocks since a) they are obtainable from renewable resources and b) they are cheap and widely available<sup>17</sup>. Additionally, the idea of interconnecting both renewable resources and conducting nanomaterials is very new and has tremendous opportunities for fundamental and applied research. This study is an effort to combine the principles of green chemistry and nanochemistry, making use of renewable plant-derived resources as the starting materials for the synthesis of advanced conducting polymer nanomaterials. Renewable resource raw material cardanol, which is an industrial waste and pollutant from cashew nut (*Anacardium occidentale*) processing industry<sup>18</sup>, is utilized for the synthesis of new amphiphilic sulfonic acid, which template for polyaniline nanomaterials.

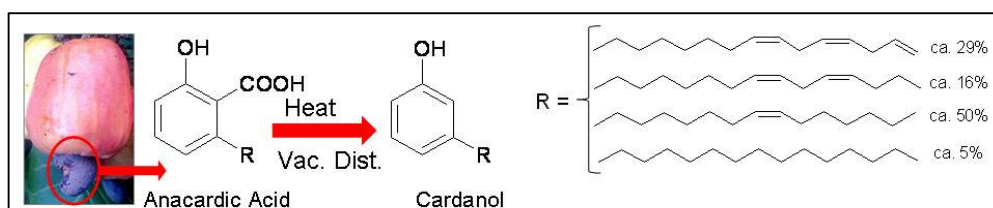


**Figure 2.1.** Cardanol from renewable resource based CNSL.

Cashew nut shell liquid (CNSL) is a unique natural source for unsaturated long-chain phenols. Cardanol is a phenol obtained from anacardic acid, the main component of technical CNSL, by thermal decarboxylation during vacuum distillation<sup>16,18</sup>. Cardanol consists of four *meta*-alkyl phenols with alkyl chains differing in their degree of un-saturation - saturated side chain, 8-ene, 8, 11- dienes and 8, 11, 14-trienes (see figure 2.1.). The amount and types of these components

vary depending up on the species of the plant. This renewable material has wide applications in the form of brake linings, surface coatings, paints, and varnishes.

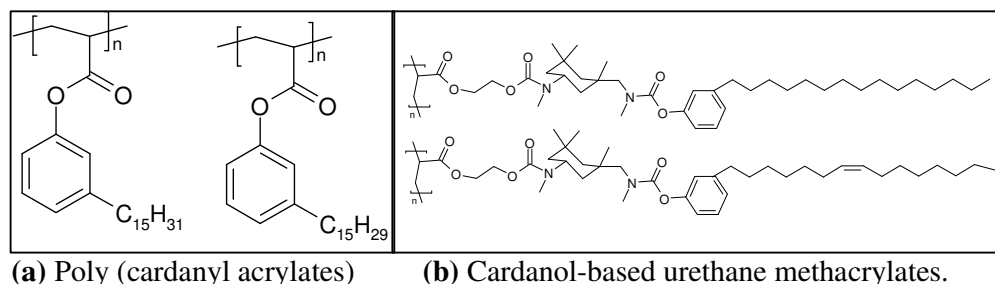


**Figure 2.2.** *Polymers based on cardanol.*

A variety of functional groups can be attached to the reactive free hydroxyl group of cardanol for derivatization. For example, cardanyl acrylate was synthesized by the reaction of cardanol with acryloyl chloride, which produced a linear polymer upon solution polymerization in toluene using radical initiator (see figure 2.2.a).<sup>19,20</sup> Upon removal of solvent and exposure to either air or UV light, the polymer underwent cross-linking to produce an insoluble transparent film. In a recent approach hydrogen bonding urethane group has been introduced as a spacer between hydrophobic cardanol unit and polymeric back bone to induce self-assembly properties (see figure 2.2.b).<sup>21</sup> These polymers were undergone self assembly into pores, spheres, vesicles, tubes etc.

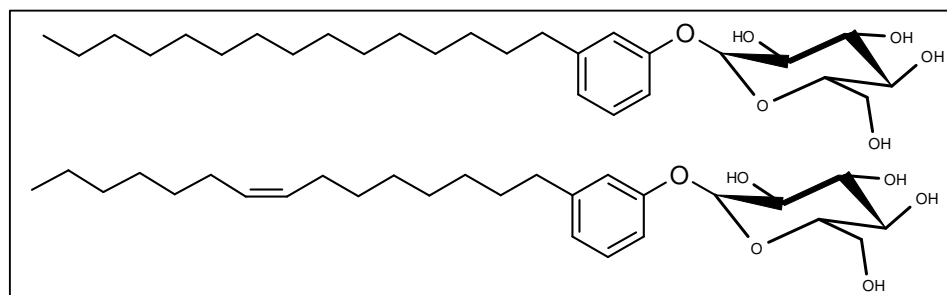


**Figure 2.3.** *Cardanol based glyco-lipids.*

Cardanol can be easily functionalized in to an amphiphile molecule by simple chemistry. The synthesis of cardanyl glycolipids by attaching glucopyranose to cardanol was reported (see figure 2.3).<sup>22,23</sup> These amphiphile were found to be self-assemble in aqueous/organic solution to generate nanostructures, such as helical and twisted fibers and nanotubes.



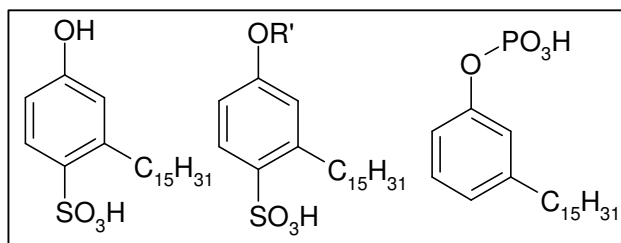


**Figure 2.4.** Cardanol based sulfonic and phosphoric acids.

The synthesis of novel amphiphilic sulfonic and phosphonic acids from cardanol based materials was established by Pillai and co-workers from our institute (see figure 2.4.)<sup>24,25</sup>. It was found that when cardanol was treated directly with  $\text{H}_2\text{SO}_4$  the resin formation takes place instead of ring sulfonation due to the presence of unsaturation in the pentadecyl side chain. Hence the hydrogenation of cardanol was carried out to saturate the side chain and the saturated cardanol (3-pentadecylphenol) was sulfonated to give the sulfonic acids<sup>24</sup>. These molecules were found to be good dopants for normal polyaniline. But these dopants are insoluble in water (due to hydrophobic saturated side chain) at room temperatures and not explored as soft templates for polyaniline nanomaterials. Therefore, the direct utilization of cardanol based dopants as soft templates for polyaniline nanomaterials is a challenging problem to be addressed. Similarly renewable resource lignosulfonic acid (LSA), a waste from the paper pulp industry, is used for the preparation of conducting polyaniline, polyaniline-ferromagnetic composites, preparation of self-assembled films of poly (o-ethoxyaniline) and exploration of polyaniline for biomedical applications<sup>26,27</sup>. The complex formation of ligno sulfonic acid sodium salt (LSA) with polyaniline has been studied and found that lignosulfonic acid was showing the doping behaviour like any other dopants and yields highly conducting polyaniline. These lignosulfonic acid polyaniline complexes provide a unique combination of properties such as electronic conductivity, processability and biodegradability.<sup>27</sup> However, so far no attempts for synthesizing and controlling the properties of polyaniline nanomaterials based on lignosulfonic acid, cardanol or any other renewable resource material was reported.

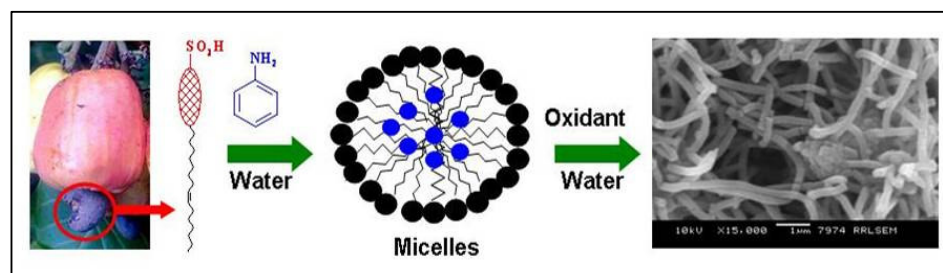


**Figure 2.5.** Scheme of the approach for polyaniline nanomaterials synthesis.

Here, a novel renewable resource amphiphilic dopant [4-[4-hydroxy-2((Z)-pentadec-8-enyl) phenylazo]-benzenesulfonic acid (dopant 1) has developed from cardanol. The new dopant possesses unique amphiphilic geometry with a hydrophilic polar head and hydrophobic alkyl chain and produce micelles or aggregates. These aggregates behaved as template for polyaniline nanomaterial synthesis in emulsion route. The micellar behaviour and critical micelle concentration (CMC) of the dopant was obtained from the dynamic light scattering (DLS), dye encapsulation, surface tension, and ionic conductance studies. The polyaniline nanomaterials morphology, three dimensional solid states ordering, and absorption properties were analyzed by using microscopic and spectroscopic electron techniques. To study the influence of experimental conditions on the nanomaterials morphology, control experiments were carried out under ultrasonic stirring, magnetic stirring and without any stirring or disturbance. This facile emulsion approach was also tested for large-scale synthesis of nanofibers up to 100g without losing morphology and other physical properties.

## 2.2. Experimental Section

**2.2.1. Materials:** Aniline, ammonium persulfate (APS) and sulfanilic acid were purchased from Aldrich Chemicals. Aniline was distilled and kept under nitrogen prior to use. Hydrochloric acid, HPLC water and sodium hydroxide were purchased from Merck India. Technical grade CNSL was obtained from Quilon export enterprises, Quilon, Kerala and purified by vacuum distillation.

**2.2.2. General Procedures:** NMR spectra of the molecules and polymers were recorded using 500-MHz (or 300-MHz) Bruker Avance ii NMR Spectrometer. Infrared spectra of the polymers were recorded using a Perkin Elmer, spectrum one FT-IR spectrophotometer in the range of 4000 to 400  $\text{cm}^{-1}$ . The purity of the

compounds was determined by JEOL JSM600 fast atom bombardment (FAB) mass spectrometry. For SEM measurements, polymer samples were subjected for thin gold coating using JEOL JFC-1200 fine coater and analysed by JEOL JSM- 5600 LV scanning electron microscope. Wide angle X-ray diffractions of the finely powdered polymer samples were recorded by Philips Analytical diffractometer using CuK-alpha emission. The spectra were recorded in the range of  $2\theta = 0- 50^\circ$  and analyzed using X'Pert software. UV-vis spectra of the polyaniline in water were recorded using Perkin Elmer Lambda-35 UV-VIS Spectrophotometer. Transmission electron microscope images were recorded using a Hitachi H-600 instrument at 75 KV. For TEM measurements, the water suspension of nanomaterials were prepared under ultrasonic and deposited on Formvar coated copper grid. For dynamic light scattering (DLS) measurements, a Nano ZS Malvern instrument employing a 4mW He-Ne laser ( $\lambda=632.8$  nm) equipped with a thermo stated sample chamber was used. For conductivity measurements, the polymer samples were pressed into a 10 mm diameter disc and analyzed using a Keithley four probe conductivity instrument.

### 2.2.3. Synthesis of Azobenzene Dopant

**Purification of Cardanol:** Technical CNSL (2.5 L) was taken in a 4 L round bottomed flask equipped with a distillation set up. The contents were heated at  $120^\circ\text{C}$  for 30 minutes to remove low volatile impurities and water. Then, the contents were allowed to boil for 2 h under sufficient vacuum. During this time most of the anacardic acid was decarboxylated to form cardanol. This conversion was indicated by the evolution of plenty of smoke due to the generation of carbon dioxide. Finally, the temperature of the mixture was elevated to  $230^\circ\text{C}$  and vacuum distilled (5 mm of Hg) to get a yellow liquid. The collected yellow liquid was again vacuum distilled ( $230^\circ\text{C}$  under 5 mm of Hg) to get 1 L of pale yellow pure cardanol.  $^1\text{H-NMR}$  (300 MHz,  $\text{CDCl}_3$ ),  $\delta$ : 7.15 (t, 1H, Ar-H), 6.70 (m, 3H, Ar-H), 5.45 (b, 2H, CH=CH), and 2.9 – 0.6 ppm (m, 27H, aliphatic-H). FT-IR (in  $\text{cm}^{-1}$ ): 3353, 3006, 2929, 1590, 1305, 1456, 1265, 984, 873, 811, 702 and 515. FAB-MS (MW: 302.0):  $m/z = 303.1$  (M+1).

**Synthesis of 4-[4-hydroxy-2((Z)-pentadec-8-enyl)phenylazo]-benzene- sulfonic acid (dopant 1):** Sulfanilic acid (47.25 g, 0.27 mol) and sodium carbonate (12 g, 0.11 mol) were added into 450 mL of water and heated to  $60-70^\circ\text{C}$  to dissolve the entire

solid. It was further cooled to 5 °C and a cold solution of sodium nitrite (16.65 g, 0.24 mol) in water (48 mL) was added. The resultant yellow solution was poured into ice (300 g) containing conc. HCl (31.5 mL) and stirred using mechanical stirrer for 30 min at 5 °C. It was added into a flask containing sodium hydroxide in 225 mL water (27 g, 0.68 mol) and distilled cardanol (67.5 mL, 0.23 mol) in methanol (115 mL). The coupling reaction was continued with stirring for 3 h in the ice-cold condition using a mechanical stirrer. The reaction mixture was neutralized by addition of conc. HCl (225 mL) in crushed ice (450 g). The red precipitate was filtered using Buckner funnel and washed with water. It was further purified by silicagel column chromatography using ethylacetate/methanol mixture (4:1 v/v). The dried product weighed 65 g (60 % yield). <sup>1</sup>H-NMR (300 MHz, d<sub>6</sub>-DMSO) δ: 7.75 ppm (b, 4H, Ar-H); 7.59 ppm (d, 1H, Ar-H); 6.77 ppm (s, 1H, Ar-H); 6.72 ppm (d, 1H, Ar-H); 5.3 ppm (b, 2H, CH=CH); 3.1 – 0.6 ppm (m, 27H, aliphatic-H). <sup>13</sup>C-NMR (75 MHz, d<sub>6</sub>-DMSO) δ: 161.25, 152.59, 149.14, 145.82, 142.98, 129.69, 126.75, 121.76, 116.88, 116.36, 114.23, 31.75, 31.24, 30.77, 29.14, 28.85, 28.59, 28.38, 26.70, 26.62 and 25.33. FT-IR (KBr, in cm<sup>-1</sup>): 3444, 2923, 2852, 1600, 1533, 1498, 1369, 1338, 1236, 1174, 1116, 1033, 1007, 820, 706 and 55. UV-Vis (in water): λ<sub>max</sub> = 360 nm. FAB-MS (MW: 486.0): m/z = 487.3 (M+1).

#### 2.2.4. Synthesis of Polyaniline Nanomaterials

**Synthesis of Polyaniline Nanomaterials:** Typical procedure for the synthesis of polyaniline nanofiber is described in detail for **E-150**. The dopant 1 (0.035 g, 0.07 mmol) was dissolved in doubly distilled water (20 mL) and stirred under ultrasonic for 1 h at 30 °C. Distilled aniline (1 mL, 1.02 g, 11 mmol, [aniline]/ [dopant] =150) was added to the dopant solution and stirred under ultrasonic for additional 1 h at 30 °C. To the emulsion ammonium persulfate (10 mL, 1.1 M solution) was added at 5 °C and stirred under ultrasonic for 1 h at 5 °C. The resultant green color content was allowed to stand at 5 °C for 15 h without disturbing in the refrigerator. The solid was filtered, washed with distilled water, methanol and diethyl ether for several times till the filtrate become colourless. The solid product was dried in a vacuum oven at 60 °C for 48 h (0.01 mm Hg). Yield = 0.8 g (76 %). <sup>1</sup>H-NMR (500 MHz, DMSO-d<sub>6</sub>) δ: 7.81

(b, 4H, Ar-H, dopant) 7.55 (b, 2H, Ar-H), 7.52 (b, 2H, Ar-H), 7.11, 7.18, 7.29 (1/1/1 triplet, 1H, -NH+), 6.91 (b, 1H, Ar-H, dopant), 6.81 (b, 1H, Ar-H, dopant), 5.3 ppm (b, 2H, CH=CH, dopant); 0.5-3.5 (27H, aliphatic-H, dopant). FT-IR (KBr, in  $\text{cm}^{-1}$ ): 3010, 1579, 1500, 1305, 1224, 1159, 1031, 825, 705 and 628.

The polyaniline samples **E-1** to **E-1500** were prepared by varying [aniline]/[dopant] ratio as 1, 1.5, 7.5, 15, 35, 70, 100, 150, 300, 450, 600, 900, 1200 and 1500 (in moles) by following the above procedure. The controlled synthesis have been carried out by varying experimental conditions like temperature ( $5^\circ$  and  $30^\circ\text{C}$ ), ultrasonic stirring and without stirring, etc. The experimental conditions for varying the temperature and stirring/no stirring are same as that of 1 g scale procedure and [aniline]/[dopant] ratio was kept a constant value of 100.

**Large-scale Synthesis of Polyaniline Nanofibers (100g Scale):** The dopant 1 (5.30 g, 11 mmol) was dissolved in doubly distilled water (2 L) and stirred under ultrasonic for 1h at  $30^\circ\text{C}$ . Distilled aniline (100 mL, 102 g, 1.09 mol; [aniline]/ [dopant] =100) was added to the dopant solution and stirred under ultrasonic for additional 1h at  $30^\circ\text{C}$ . The pale yellow emulsion was oxidized by ammonium persulfate (1 L, 1.1 M solution) and further stirred under ultrasonic for 1 h at  $30^\circ\text{C}$ . The rest of the procedures are same as described for 1 g scale. Yield = 75 g (74 %).  $^1\text{H-NMR}$  (500 MHz,  $\text{DMSO-d}_6$ )  $\delta$ : 7.81 (b, 4H, Ar-H, dopant) 7.55 (b, 2H, Ar-H), 7.52 (b, 2H, Ar-H), 7.11, 7.18, 7.29 (1/1/1 triplet, 1H, -NH+), 6.91 (b, 1H, Ar-H, dopant), 6.81 (b, 1H, Ar-H, dopant), 5.3 ppm (b, 2H, CH=CH, dopant), 0.5-3.5 (27H, aliphatic-H, dopant). FT-IR (KBr, in  $\text{cm}^{-1}$ ): 3011, 1577, 1502, 1306, 1225, 1158, 1032, 825, 706 and 627. The 10 and 50g scale synthesis also carried out in a similar manner by keeping [aniline]/ [dopant] ratio as 100 (in moles) and aniline concentration as 0.36 M.

## 2.3. Results and Discussion

### 2.3.1. Synthesis of New Azobenzene Amphiphilic Dopant

Cashew nut shell liquid (CNSL) is an agricultural renewable resource and the by-product of the cashew processing industry, which contains anacardic acid as major component<sup>16</sup>. Heat treatment and consecutive vacuum distillation (230 °C at 5 mm of Hg) of CNSL undergo decarboxylation to yield pure cardanol<sup>18</sup>. Cardanol is meta-pentadecadienyl phenol; the aliphatic side chain usually consists of mixture of one, two and three double bonds in a linear chain with a saturated side chain<sup>16</sup>. The cardanol used in this study is obtained from local resources in Quilon, Kerala. Cardanol was purified by double vacuum distillation at 5 mm of Hg and the fraction distilled at 230 - 235 °C was collected. The NMR and mass spectrum confirms this molecule has only one double bond at 8<sup>th</sup> carbon atom in the side chain. Four aromatic protons from the cardanol aromatic ring appear at 7.15 and 6.70 ppm. The unsaturated double bonds in the side chains appear at 5.43 ppm. The rest of the protons in the side chain appear from 3 to 0.76 ppm. The integration of the peaks is very well matched with the required number of protons and it confirms (Z)-(pentadec-8-enyl) phenol.

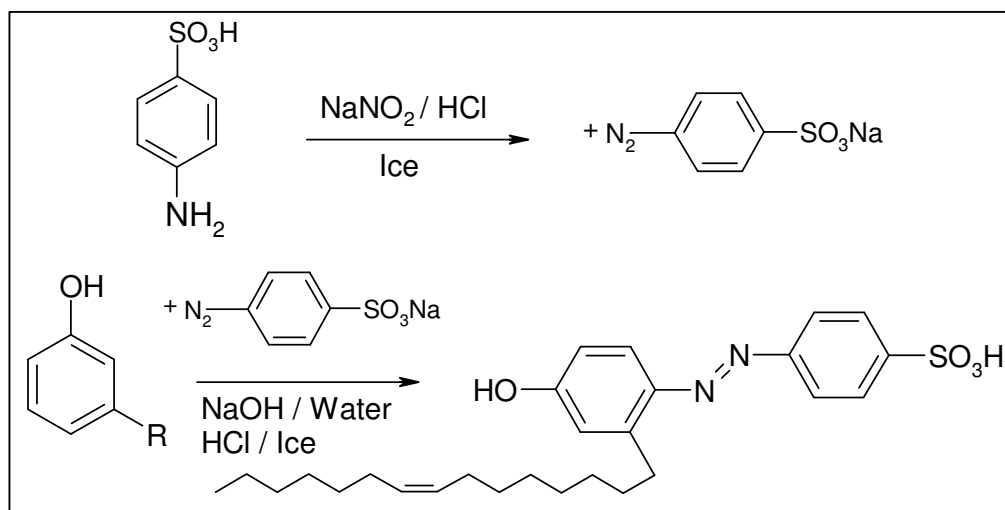


**Figure 2.6.** Synthesis of novel amphiphilic azobenzene dopant from cardanol.

The synthesis of sulfonic acid derivatives through a direct sulfonation at phenyl ring was not possible because of the presence of unsaturated double bonds in the pendent chains. Therefore, a diazotization coupling reaction in water using

diazonium salt of sulphanilic acid to prepare cardanol based novel dopant is adopted. Diazotized sulphanilic acid was coupled with cardanol under basic conditions to yield, 4-[4-hydroxy-2((Z)-pentadec-8-enyl)phenylazo]-benzenesulfonic acid (dopant 1). Under these basic reaction conditions, the side chain double bond is inactive and does not affect the diazotization reactions. The synthesis of dopant 1 is represented in figure 2.6.

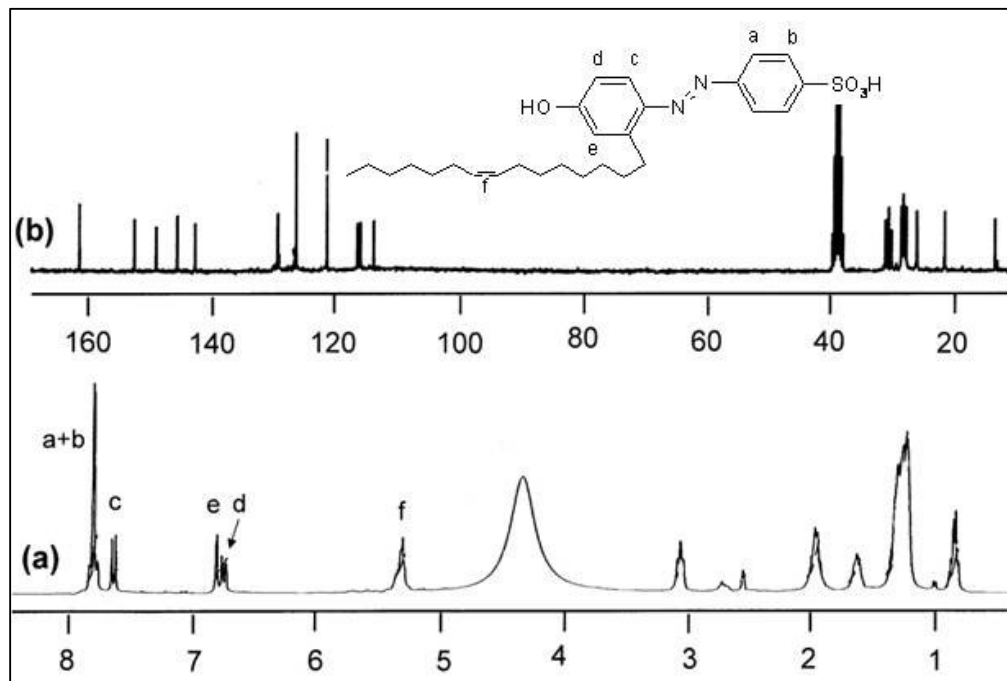


**Figure 2.7.** Characterization of dopant 1 by (a) <sup>1</sup>H-NMR and (b) <sup>13</sup>C-NMR.

The structure of the dopant 1 is confirmed by NMR, FT-IR and Mass techniques. The <sup>1</sup>H-NMR spectrum of dopant 1 is given in figure 2.7.a and all different types of the protons in the structure are assigned with alphabets. The four protons in the aromatic ring containing the sulfonic acid group appears together at 7.8 ppm whereas the aromatic protons from the other ring appears with characteristic splitting pattern at 7.6, 6.85 and 6.80 ppm. The double bond in the pendent group appears at 5.4 ppm and all other aliphatic protons appear below 3.2 ppm. The <sup>13</sup>C-NMR spectrum also has the required amount of peaks for dopant 1 (see figure 2.7.b). The peak intensities are in accordance to the expected structure, which confirm the formation of the expected amphiphilic dopant. FT-IR analysis showed a broad peak at 3444 cm<sup>-1</sup> corresponds to the -OH stretching of the sulfonic acid group. The C-H

stretching vibration bands appeared at 2923 and 2852  $\text{cm}^{-1}$ . The peak at 1600  $\text{cm}^{-1}$  is for the C=C vibrations (see figure 2.16). The peak at 1496  $\text{cm}^{-1}$  is arisen from the stretching vibrations of aromatic rings and the peak at 1033  $\text{cm}^{-1}$  is due to sulfonic acid vibrations. Thermal analysis using TGA showed that the dopant is very stable up to 250  $^{\circ}\text{C}$  (see figure 2.17.) and undergo slow decomposition above this temperature.

### 2.3.2. Dynamic Light Scattering (DLS) Studies of the Dopant 1

The molecule was subjected to dynamic light scattering (DLS) in water to study the aggregation behaviour<sup>28,29</sup>. The photograph of vials containing various concentration of the dopant 1 is shown in figure 2.8. It is clear that the visibility of the dopant solution changes in the range of  $2 \times 10^{-4}$  M, which is corresponding to surfactant-like behaviour. Also above this concentration owing to the amphiphilic surfactant nature, the dopant molecule in water forms soap like foamy solution (see figure 2.8). Dynamic light scattering (DLS) is an efficient tool to understand the size of aggregates like micelles in solution and so DLS analysis of the dopant at various concentration in water have been carried out.

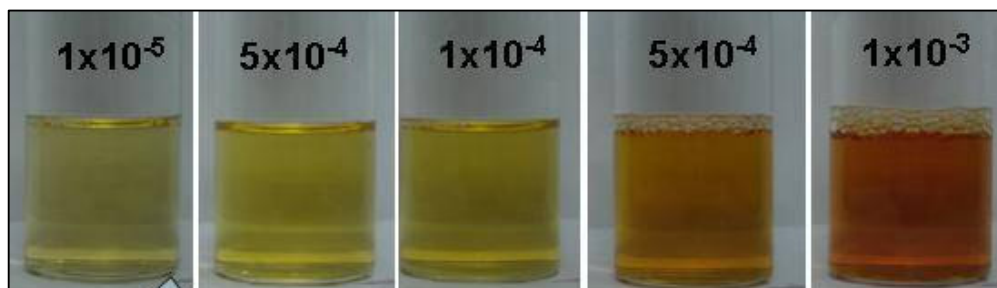


**Figure 2.8.** Photographs of the dopant 1 solution in water at various concentrations.

DLS data for the dopant for concentrations  $10^{-3}$  to  $10^{-5}$  M are given in the figure 2.9. DLS data indicate the azobenzenesulfonic acid molecule exists in the form of the micelles (at  $1 \times 10^{-3}$  M) in water and their average diameters were obtained as 4.29 nm. DLS profile of  $1 \times 10^{-4}$  M dopant solution shows a bimodal distribution with maxima centred at 25 nm and 600 nm. This indicates that as the concentration of dopant decreases in water, the strongly aggregated micelles are transformed into weakly aggregated species. Further decrease in the dopant concentration ( $1 \times 10^{-5}$  M) increases the aggregate size to 600 nm. DLS measurement clearly demonstrates that at very lower concentrations ( $1 \times 10^{-5}$  M to  $5 \times 10^{-4}$  M) the dopant molecules in water are



existing as open-aggregates (like layers) and completely transformed to micelles as the concentration dopant become  $1 \times 10^{-3}$  M.

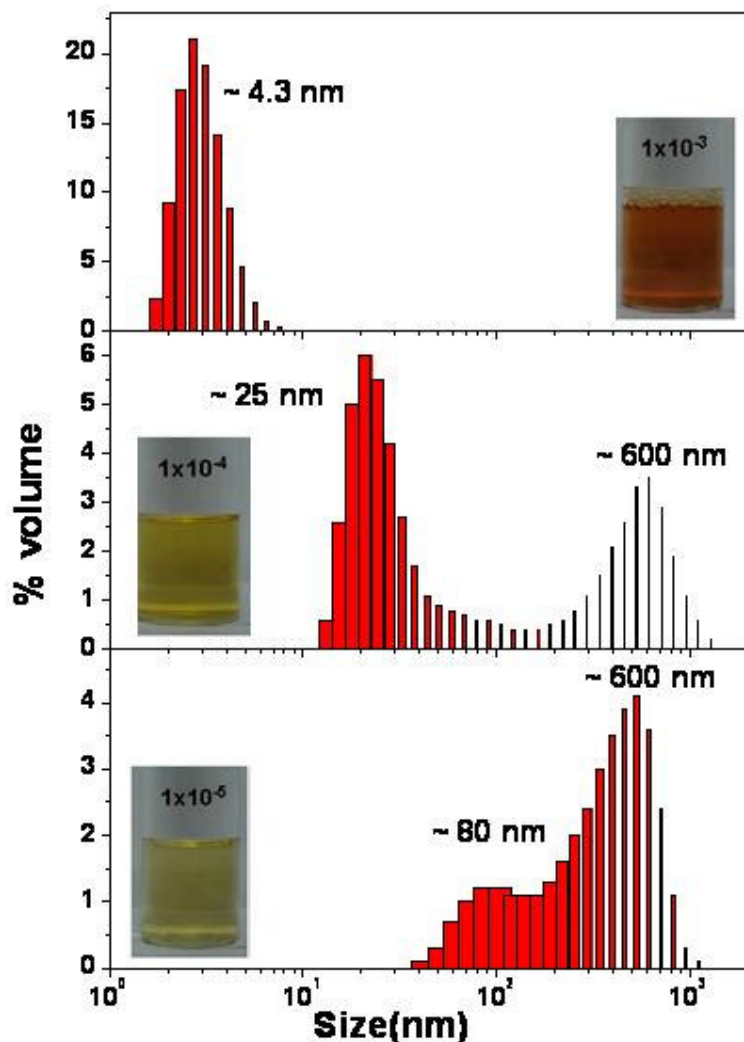


**Figure 2.9.** DLS histograms of dopant solution in water.

DLS data for the dopant 1 in water ( $1 \times 10^{-3}$  M) confirmed that it exists as 4.3 nm micelles. The micellisation process in solvent was controlled by two opposing forces: (i) Van der Waals attractive forces between hydrocarbon tails and (ii) electrostatic repulsion between polar hydrophilic head groups<sup>30</sup>. The formation of micelles by a particular surfactant can be predicted by the critical packing parameter,  $P_c = V/al$ , where 'V' is the volume occupied by hydrophobic part of the molecule, 'a' is the head group area, and 'l' is the length of the molecule<sup>31,32</sup>. The  $P_c$  directly correlates the expected geometry of the amphiphilic molecule self-assembly: for

spherical micelles ( $P_c = <0.33$ ), cylindrical micelles ( $P_c = 0.33-0.50$ ), bilayers ( $P_c=0.50-1.0$ ) and reverse or inverted micelles ( $P_c>1$ ).

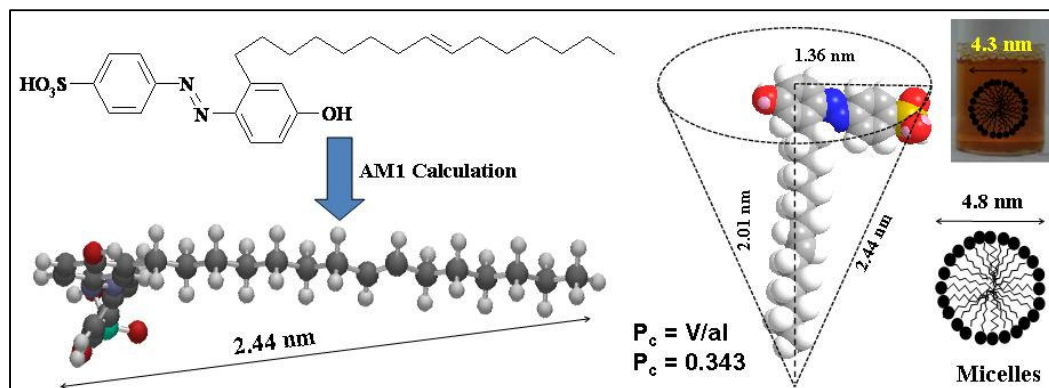


**Figure 2.10.** Molecular geometry and theoretical packing factor.

In order to get more insight in to the dopant packing factor, energy minimized AM1 structure calculations have been utilized (see figure 2.10)<sup>32</sup>. The molecule has a bend shape with a head group radius of 1.36 nm, tail length of 2.01 nm with overall molecular length of 2.44 nm. It appears as a cone shape with large head and a long hydrophobic tail. The  $P_c$  for the new amphiphilic dopant molecule was obtained as 0.34, which predicts the shape of the micelles as spherical one. Based on the energy minimized structure, the theoretical diameter of the spherical micelle (which is equivalent to the twice the end-to-end distance of the dopant) was calculated as 4.8 nm (see figure 2.10). The calculated diameter of the micelle (4.8 nm) is well matching with that of the DLS experimental value (4.3 nm) with in experimental error.

### 2.3.3. Determination of Critical Micelle Concentration (CMC) of the Dopant 1

The dopant 1 molecule was subjected to dye encapsulation, ionic conductance and surface tension studies to determine CMC<sup>33-35</sup>.  $\beta$ -Diketones [benzoylacetone or 1-phenyl-1, 3-butadione] was chosen as dye for encapsulation studies because it exhibits keto-enol tautomorphism in water<sup>33</sup>. The abundance of these two isomeric forms is highly dependent upon the hydrophobic or hydrophilic environment of the dye<sup>36</sup>. Typically inner part of the micelles provide hydrophobic environment, and therefore,  $\beta$ -diketone is expected to show large enhancement of the enol form above the CMC of the surfactant. Either the decrease in the abundance of keto-form or enhancement of

enol-form directly provides information about CMC of the surfactant.  $\beta$ -Diketone has two strong absorption peaks at 254 and 310 nm for the  $\pi$ - $\pi^*$  transition corresponding to keto and enol-form, respectively (see figure 2.11)<sup>33</sup>. Amphiphilic azobenzene dopant has two absorption peaks at 254 and 360 nm for the  $\pi$ - $\pi^*$  transition corresponding to cis and trans-form, respectively (see figure 2.11). Therefore, the absorption spectra of  $\beta$ -diketone and dopant were compared to identify the spectral overlap. The absorption spectra (figure 2.11) clearly indicate that the enol-form (at 310 nm) of the  $\beta$ -diketone in the presence of the azobenzene surfactant is not disturbed and can be directly utilized for determining the CMC (the keto-form overlap with the dopant absorption peak at 254 nm).

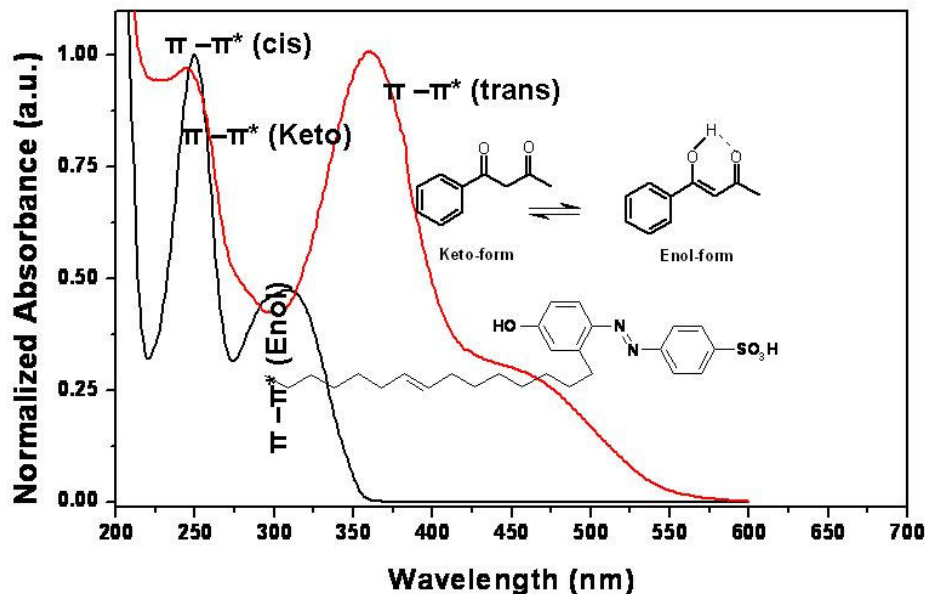


**Figure 2.11.** Absorption spectra of dopant 1 and bezoyl acetone in water.

Encapsulation experiments was carried out by keeping the amount of  $\beta$ -diketones constant ( $3.5 \times 10^{-5}$  M) and varying the concentration of the dopant from  $10^{-6}$  to  $10^{-3}$  M in water. The concentration variation spectra are shown in figure 2.12 and the intensity of the peak corresponding to enol-form (at 310 nm) was plotted against the variation of the concentration of the dopant (see inset of figure 2.12). At lower concentration of the dopant 1 ( $< 10^{-4}$  M) there is no considerable change in the absorption at 310 nm, but as the concentration become above this value there is a gradual increase and showed a drastic increase above  $4 \times 10^{-4}$  M. From this it is concluded that the CMC of the azobenzene surfactant dopant was  $4 \times 10^{-4}$  M in water.

Since aniline is also an aromatic molecule like  $\beta$ -Diketone, it can be assumed that it can also be trapped in the hydrophobic environment provided by the amphiphilic dopant.

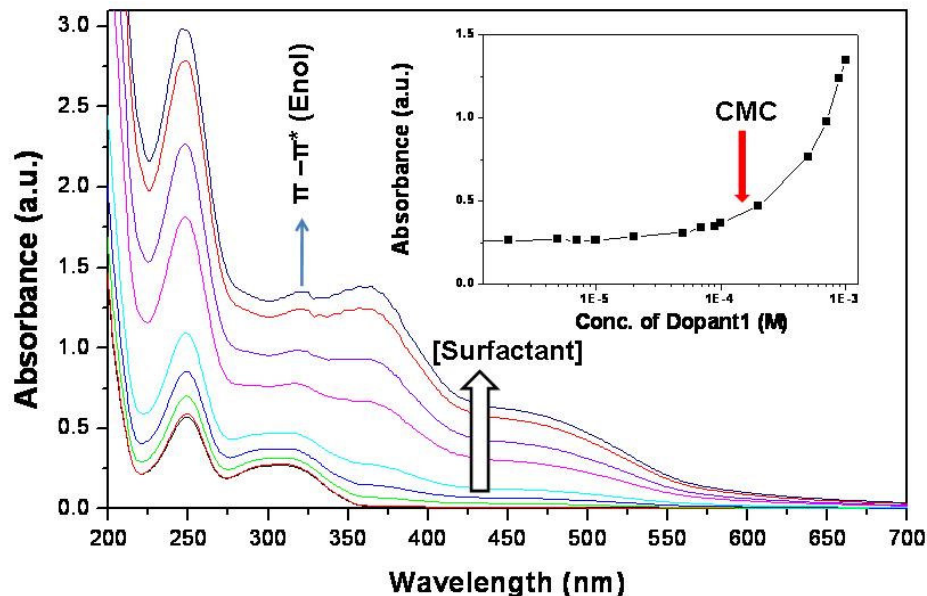


**Figure 2.12.** Concentration dependent UV-Vis of dopant 1 with benzoyl acetone ( $3.5 \times 10^{-5} \text{ M}$ ). Inset is the plot of conc. dependent variation of absorption at 310 nm.

To further confirm this CMC value, concentration dependent surface tension measurement of the dopant solution in water have been carried out<sup>35</sup>. The surface tension measurement (Wilhelmy Plate method) was carried out in double distilled water at 29 °C and the plot of surface tension against surfactant concentration is given in figure 2.13. Below the CMC, the surface tension decreased with increase in surfactant concentration and the surface tension did not change considerably above the CMC. The CMC is taken as the concentration where the surface tension changes its trend and is found to be  $4 \times 10^{-4} \text{ M}$  at 29 °C. Another important physical property which gives an idea about the CMC as well the structural changes in anionic surfactant molecules is its specific conductance measurements<sup>34</sup>. The plot of specific conductance versus concentration of the dopant is given in figure 2.13. At the dopant concentration  $1 \times 10^{-5} \text{ M}$  the specific conductance is very low, which may be due to the number of molecules to carry the charge is very less. As the concentration of the dopant increases above  $1 \times 10^{-4} \text{ M}$ , the specific conductance showed gradual increment marking the transformation of loose large aggregates to small highly mobile spherical micelles, which can conduct more current. The break point of specific conductance

plot directly gives the CMC as  $\sim 4 \times 10^{-4}$  M. These two independent experiments also confirmed that the surfactant dopant forms micelles above its CMC of  $4 \times 10^{-4}$  M.

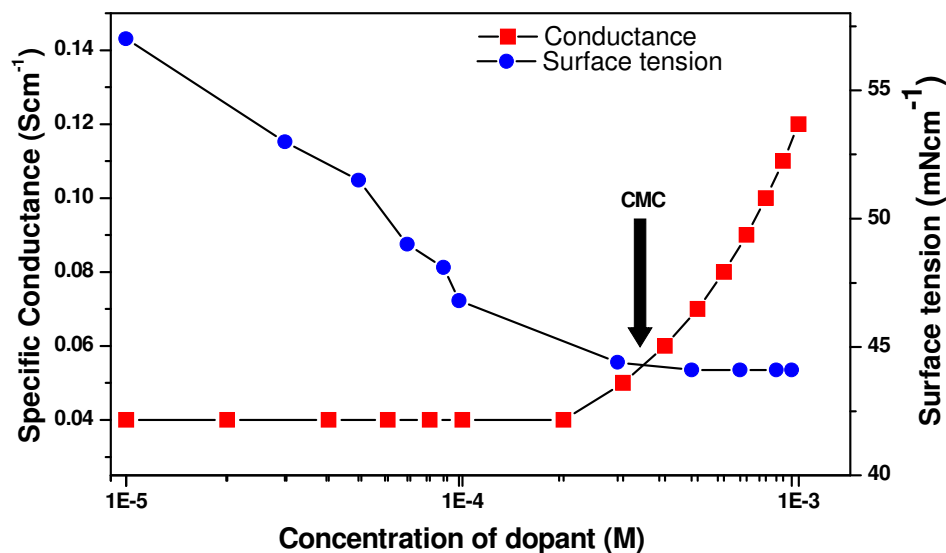


**Figure 2.13.** Concentration dependent changes in surface tension and ionic conductance.

### 2.3.4. Synthesis of Polyaniline Nanomaterials

The dopant 1 is soluble in water and its complex with aniline form stable emulsion in water that will acts as self-assisted template for polyaniline nanomaterials.

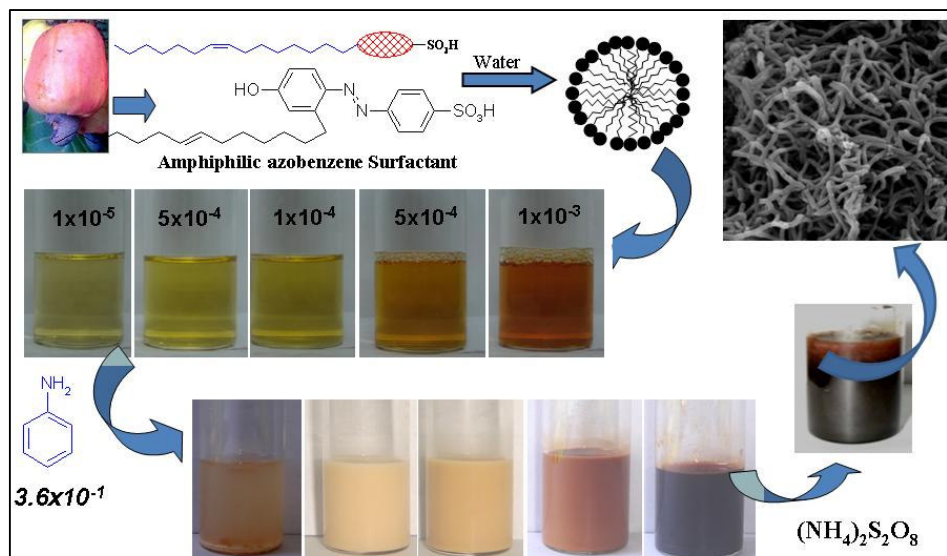


**Figure 2.14.** Synthesis of polyaniline nanomaterials by emulsion route.

The polyaniline nanomaterials were synthesized by varying the [aniline]/[dopant] composition over a wide range from 1 to 1500 in moles (up to 1/1500 moles

less amount of dopant with respect to aniline). The concentration of the aniline was fixed as  $3.6 \times 10^{-1}$  M for all the compositions in water and the concentration of dopant was varied by dissolving various amounts in water ( $3.6 \times 10^{-1}$  to  $2.3 \times 10^{-4}$  M). Typically the polymerization was carried out by dissolving aniline and dopant in water and subsequently stirring under ultrasonic at ambient conditions for 30 minutes. The resultant milky emulsion was oxidized by adding ammonium persulphate (1.1 M solution) in water and stirred at 0-5 °C under ultrasonic for 1 h. The green solution was kept at 5 °C without disturbing in the refrigerator for 15 h. The green nanomaterials was filtered and purified by washing with water and methanol until the filtrate become colourless. It was dried under vacuum for 24 h (0.05 mm of Hg) at 60 °C in vacuum over prior to further analysis.

**Table 1.1.** Table summarising concentration of dopant, [aniline]/[dopant], yield and S/N ratio.

Sample	Conc. of Dopant <sup>a</sup> (M)	[Aniline]/[Dopant] (moles)	Yield <sup>b</sup> (%)	S/N <sup>c</sup> (%)
<b>E-1</b>	$3.6 \times 10^{-1}$	1	2	39.4
<b>E-1.5</b>	$2.4 \times 10^{-1}$	1.5	16	34.8
<b>E-7.5</b>	$4.6 \times 10^{-2}$	7.5	26	30.1
<b>E-15</b>	$2.4 \times 10^{-2}$	15	78	29.4
<b>E-35</b>	$9.6 \times 10^{-3}$	35	68	28.3
<b>E-70</b>	$5.1 \times 10^{-3}$	70	90	30.1
<b>E-100</b>	$3.2 \times 10^{-3}$	100	71	30.1
<b>E-150</b>	$2.4 \times 10^{-3}$	150	76	29.8
<b>E-300</b>	$1.2 \times 10^{-3}$	300	75	29.9
<b>E-450</b>	$8.2 \times 10^{-4}$	450	81	29.7
<b>E-600</b>	$5.9 \times 10^{-4}$	600	60	28.8
<b>E-900</b>	$4.1 \times 10^{-4}$	900	60	27.9
<b>E-1200</b>	$3.1 \times 10^{-4}$	1200	65	27.4
<b>E-1500</b>	$2.3 \times 10^{-4}$	1500	55	27.6

a) The concentration of aniline was maintained as  $3.6 \times 10^{-1} \text{M}^{-1}$  for all the compositions.

b) Calculated for isolated product.

c) From elemental analysis.

The yield and composition of the polyaniline nanomaterials **E-1** to **E-1500** are summarized in table 1.1. The polymers are denoted as **E-X**, where ‘E’ represents emulsion and ‘X’ is corresponding to the [aniline]/[dopant] in the feed (for example

**E-1500** indicate the polyaniline synthesized using 1500 moles less amount of dopant with respect to aniline

### 2.3.5. Characterization of Polyaniline Nanomaterials

The amphiphilic molecule makes these conducting structures easily dispersible in organic solvents like DMSO for complete structural characterization by NMR and the  $^1\text{H}$ -NMR spectra for **E-150** is given in figure 2.15. It is clearly evident from the NMR spectra of the nanomaterials that the peaks corresponding to the dopant molecule was present in addition to the peaks for the polymer structures. The two broad peaks at 7.65 and 7.52 ppm were assigned to the two aromatic peaks in the polyaniline aromatic ring<sup>37,38</sup>. The three equally intense peaks (triplet) at 7.1, 7.2 and 7.3 ppm are attributed to the free radical NH proton resonance due to the  $^{14}\text{N}$  with unit spin which makes the proton attached to it split into three lines<sup>37</sup>. It confirms the strong binding of anionic sulfonic acid dopant to the polymer structure and also the doped stage of the conducting polyaniline. The amount of dopant incorporated in the polyaniline was determined by comparing the integral intensities of the aromatic peak intensities of the dopant (at 7.81 ppm/ three protons) versus polyaniline (7.65 and 7.52 ppm together/four protons) and found to be 34%.

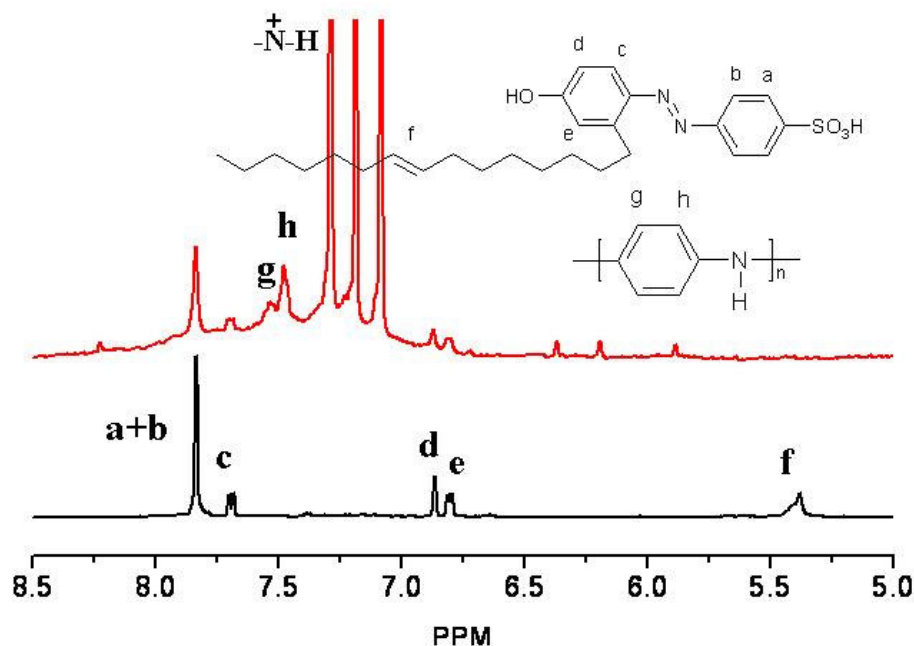


**Figure 2.15.**  $^1\text{H}$ -NMR spectra of dopant 1 and polyaniline (Aromatic region expanded) in  $d_6$ -DMSO at 30 °C.

The FT-IR analysis of the samples (see figure 2.16) showed all the characteristic bands of polyaniline, i.e., the C=C stretching of quinoid ring ( $1574\text{ cm}^{-1}$ ), the C=C stretching of benzenoid ring ( $1492\text{ cm}^{-1}$ ), the C-N stretching of secondary aromatic amine ( $1300\text{ cm}^{-1}$  and the out of plane deformation of C-H in the 1,4-disubstituted benzene rings ( $820\text{ cm}^{-1}$ )<sup>39</sup>. The doping of the polyaniline by the sulfonic acid have been confirmed by the presence of peaks at  $1145, 1025, 703$  and  $618\text{ cm}^{-1}$  corresponds to the O=S=O, S=O, S-O and C-S stretching vibrations, respectively<sup>40</sup>.

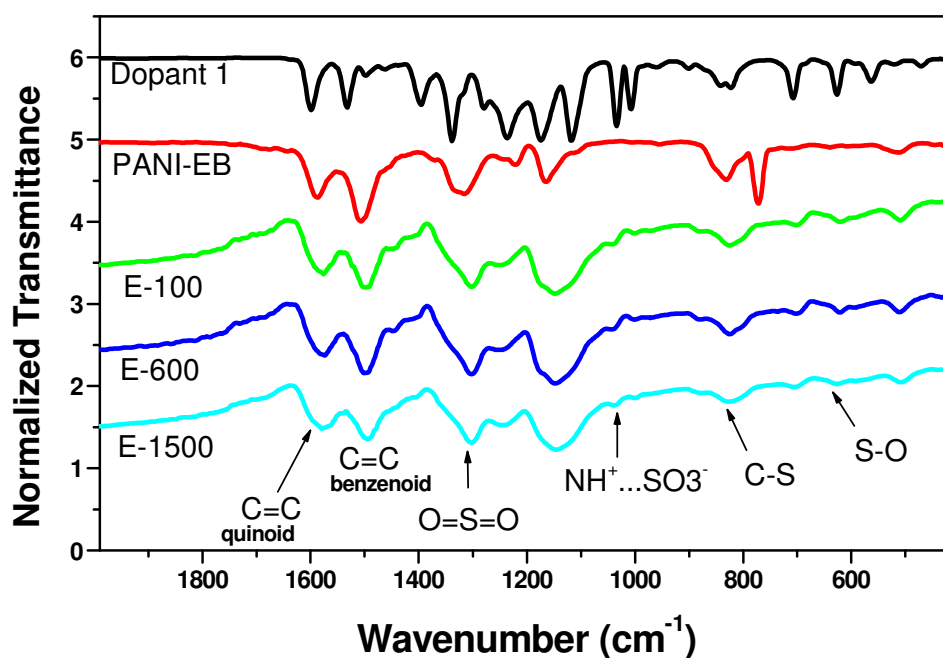


**Figure 2. 16.** FT-IR spectra of dopant and polyaniline nanomaterials.

In order to check the molecular weights of the synthesized polyaniline nanofibers, the inherent viscosity ( $\eta_{inh}$ ) of the samples (PANI-EB form) were determined in N-methylpyrrolidinone (NMP) using an Ubbelohde viscometer. The polymer sample was dissolved in NMP, filtered and 0.5 wt % solutions was subjected to measurements at  $30\text{ }^{\circ}\text{C}$ . The inherent viscosities of the polymers were obtained in the range of  $\eta_{inh}$  0.24-0.29 dL/g. The viscosities of the samples indicate the formation of moderate molecular weight samples and the values are in accordance with the earlier reports for polyaniline materials<sup>41,42</sup>.



The thermal properties of polyaniline nanomaterials were measured by means of thermogravimetric analysis (TGA). Typical TGA curves for nanomaterials are given in figure 2.17. All typical TGA curves have a typical three step weight loss behavior: the loss of water or solvent, dedoping and decomposition of dopant and decomposition of polyaniline chain. Thermal analysis showed that all the polyaniline nanomaterials are stable up to 300°C and so good for high temperature applications.

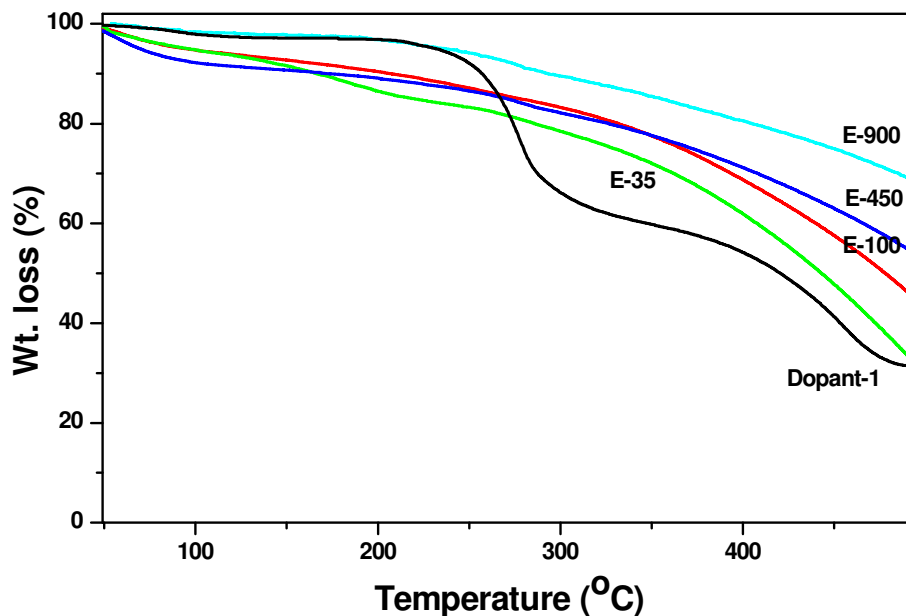
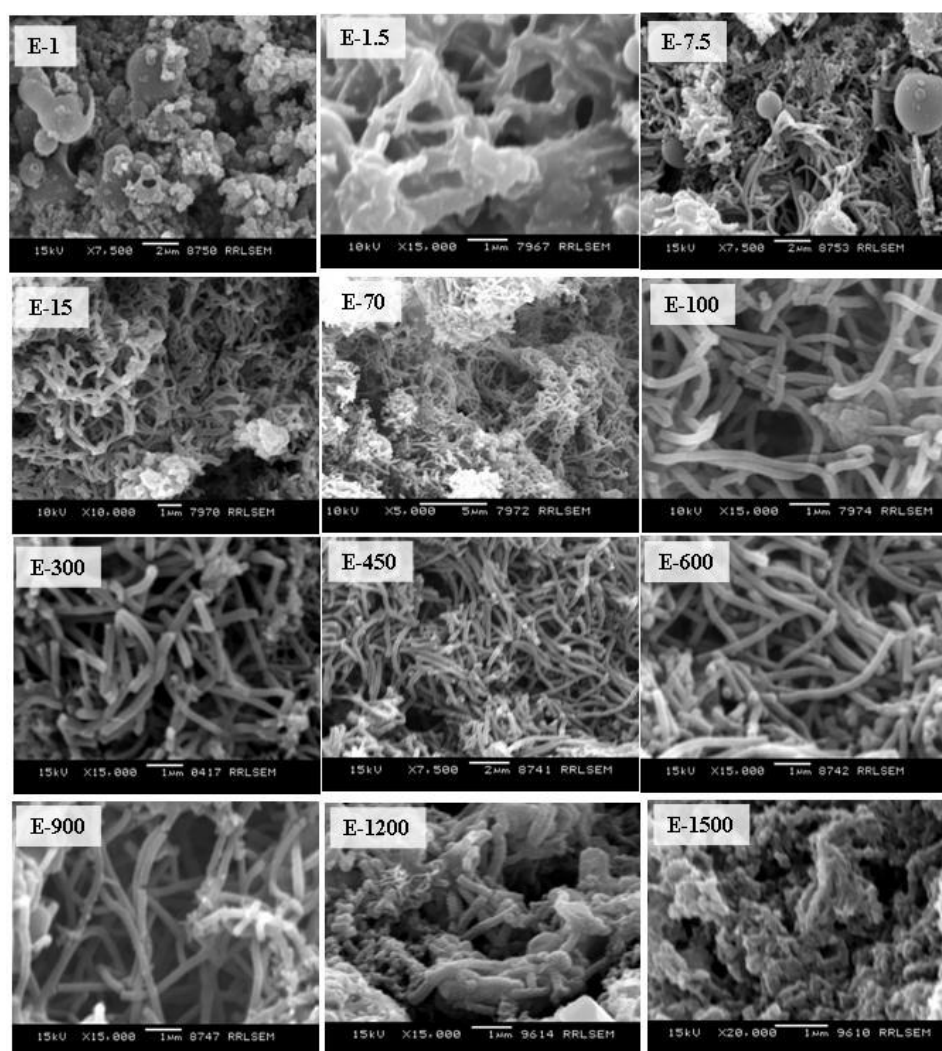


Figure 2.17. TGA plots for dopant and polyaniline nanomaterials.

### 2.3.6. Morphology of the Nanomaterials

The sulfonic acid doped polyaniline nanomaterials prepared through emulsion polymerization were highly sensitive to the micelle formation in water and different morphologies were produced depending up on nature and stability of these micelles<sup>43,44</sup>. At higher dopant concentration ( $3.6 \times 10^{-1} \text{M}$ ) in the feed (**E-1**), the anilinium salt formed was found to be partially soluble in water and the entire polymerization mixture appeared as a mixture of emulsion plus precipitate (see vial in figure 2.14). In this highly concentrated solution the micelles are not stable and the high anilinium salt concentration enhances the formation of micron sized hollow spheres rather than nanofibers. The formation of hollow spheres has also been noticed by others for higher dopant concentration and it is correlated to the existence of aniline-dopant complex in the form of salt. As the dopant amount further decreases in

the feed ( $5.4 \times 10^{-1}$  to  $3.6 \times 10^{-2}$ , from **E-1** to **E-15**), the concentration of anilinium salt also decreases, which in turn induce dendritic nanofiber along with micro spheres. Upon further dilution of dopant in the polymerization medium ( $9.6 \times 10^{-3}$  to  $4.1 \times 10^{-4}$  M), the resultant polyaniline samples **E-35** to **E-900** were obtained linear nanofibers and the length of the fibres were found to be as long as 8-10  $\mu$ M. It is very surprising to notice that nanofibers are produced even at very low concentration of the dopant, which is almost 1/1200 to 1/1500 moles lower than that of aniline in the feed (see figure 2.18, **E-1200** and **E-1500**).



**Figure 2.18.** SEM images of the polyaniline nanomaterials.

It is very clearly evident from the SEM images that the new renewable resource molecule is very effective structure directing agent and the [aniline]/[dopant]

ratio plays a major role in the formation of various types of polyaniline nanomaterials such as micro-hollow spheres, branched nanofibers to linear nanofibers. The average length and the diameter of the polyaniline nanofibers are measured from the SEM images and summarized in table 2.2. The diameter of the nanofibers are almost in the same range (140-180 nm) whereas the average length of the fibres initially increases from 1 to 8  $\mu\text{m}$  (up to **E-450**) and further decreased with the dilution of the dopant in the feed (see table 2.2). It suggests that the variation in the [aniline]/ [dopant] ratio in the emulsion polymerization strongly influence on the length of the nanofibers rather than their widths (or diameters). The SEM technique has limitation and it is very difficult to differentiate between nanotubes and nanofibers, and therefore, the samples have been subjected for transmission electron microscopic (TEM) analysis<sup>45</sup>.

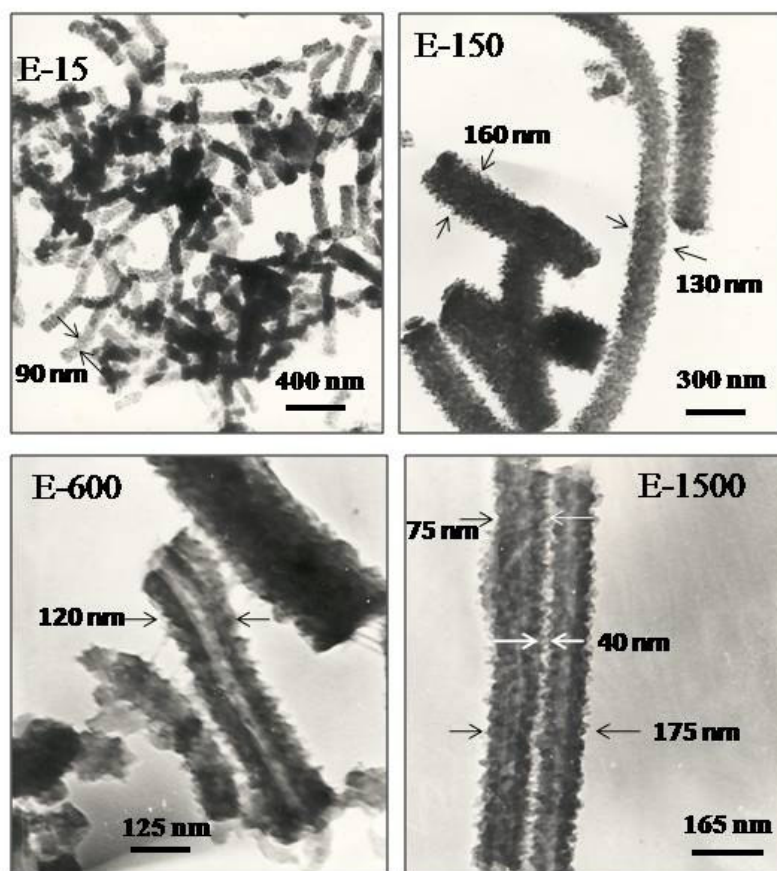


**Figure 2.19.** TEM images of the polyaniline nanomaterials.

The TEM images of **E-15**, **E-150**, **E-600** and **E-1500** are shown in figure 2.19. For TEM analysis, the samples were dispersed in water under ultrasonic and a drop of

the solution was evaporated on the Cu grid for TEM analysis. TEM-images of **E-15** and **E-150** clearly indicate that the entire nanomaterials have uniform fibrous morphology and their diameters and lengths are in the range of 120 – 200 nm and 800 nm -1.2  $\mu\text{M}$ , respectively. The comparison of the TEM and SEM images of these samples reveals that the nanofiber diameters are almost matching, but their length was somewhat shorter in TEM images. It is assumed that the nanofiber length was disturbed by the mode of the sample preparation for TEM analysis. Interestingly at very low concentration, the amphiphilic dopant produces mixtures of both polyaniline nanotubes and nanofibers. In **E-600** and **E-1500**, polyaniline nanotubes with 20-40 nm pore and 60-80 nm wall thickness can be clearly visible (see figure 2.19).

**Table 2.2.** Table summarising nanomaterials dimension, conductivity and WXR D details.

Sample	Nano dimension <sup>a</sup>		Conductivity <sup>c</sup> (S/cm)	WXR D Data <sup>b</sup>	
	Diameter (nm)	Length ( $\mu\text{m}$ )		[ $A_{(2\theta=6.4)}/$ $A_{\text{total}}$ ]	[ $I_{(2\theta=6.4)}/$ $I_{(2\theta=25.9)}$ ]
<b>E-1</b>	Sphere	-	-	-	-
<b>E-1.5</b>	Sphere	-	$6 \times 10^{-5}$	-	-
<b>E-7.5</b>	125-160	1.0-3.0	$5 \times 10^{-4}$	0.0108	0.15
<b>E-15</b>	130-165	0.9-1.8	$9 \times 10^{-3}$	0.0091	0.15
<b>E-35</b>	140-175	0.9 -2.2	$3 \times 10^{-3}$	0.0104	0.14
<b>E-70</b>	160-205	0.8-2.6	$1 \times 10^{-2}$	0.0147	0.25
<b>E-100</b>	150-200	1.0-3.1	$7.5 \times 10^{-3}$	0.0165	0.31
<b>E-150</b>	185-260	1.0- 8.1	$1.1 \times 10^{-2}$	0.0188	0.29
<b>E-300</b>	180-250	1.2-6.0	$9.5 \times 10^{-3}$	0.0172	0.37
<b>E-450</b>	175-165	1.3-6.4	$3 \times 10^{-3}$	0.0167	0.49
<b>E-600</b>	175-240	1.0-3.8	$7 \times 10^{-3}$	0.0086	0.19
<b>E-900</b>	190-270	2.0-5.6	$2.4 \times 10^{-2}$	0.0104	0.18
<b>E-1200</b>	180-260	0.5-2.0	$6.6 \times 10^{-2}$	0.0084	0.16
<b>E-1500</b>	175-265	0.4-2.1	$4.4 \times 10^{-2}$	0.0055	0.11

- a) The values are determined from the SEM images.  
 b) From wide angle X-ray diffraction measurements at 30° C.  
 c) Values are obtained using four probe conductivity unit at ambient conditions.

The combination of SEM and TEM analysis suggests that the specially designed renewable resource amphiphilic dopant is very efficient structural director for polyaniline nanomaterials, and found that the size, type and nature of the

nanomaterials can be fine-tuned for a wide composition range of [aniline]/[dopant] in the feed.

### 2.3.7. Mechanism of Nanomaterial Formation

Morphological studies using SEM and TEM of nanomaterials showed that at higher dopant concentration, hollow micro-spheres or dendritic short nanofibers are formed whereas at medium-to-low concentration of the dopant produces a long nanofibers or combination of nanofibers and nanotubes. It suggests that the dopant-aniline complex in the present system may exist in more than one form of supramolecular aggregates like layers and micelles and subsequent oxidation of these various aggregates produces hollow-spheres, dendritic fibers, linear fibers and nanotubes. Therefore, it is very important to study the behaviour of the amphiphilic dopant 1 and dopant1+aniline complex in water to understand the formation of various types of nanomaterials<sup>29,46</sup>. Upon adding aniline in to the dopant micelles in water and stirring under sonication for few minutes, the solution became pale yellow thick milky emulsion. DLS histograms of the aniline + dopant complexes for nanomaterials **E-100**, **E-450** and **E-600** are shown in figure 2.20. In all the three cases upon adding aniline into the dopant micelles in water (4.3 nm) resulted the formation of thick pale yellow emulsion (see vials in figure 2.20), which is stable for more than a week. DLS studies of these emulsions showed a bimodal distribution with majority of the aggregates in the range of 3- 5  $\mu\text{m}$  (see figure 2.20). It confirms that the aniline can form a stable micrometer sized aggregated templates with amphiphilic dopant for a wider [aniline] / [dopant] compositions. All attempts to get good DLS data for the polymerization mixture at [aniline]/[dopant]  $\geq 900$  (corresponding to the polyaniline nanotubes) was not successful because of higher aniline concentration compared to that of dopant (see vial figure 2.14), which made emulsion less stable and easily phase separated.

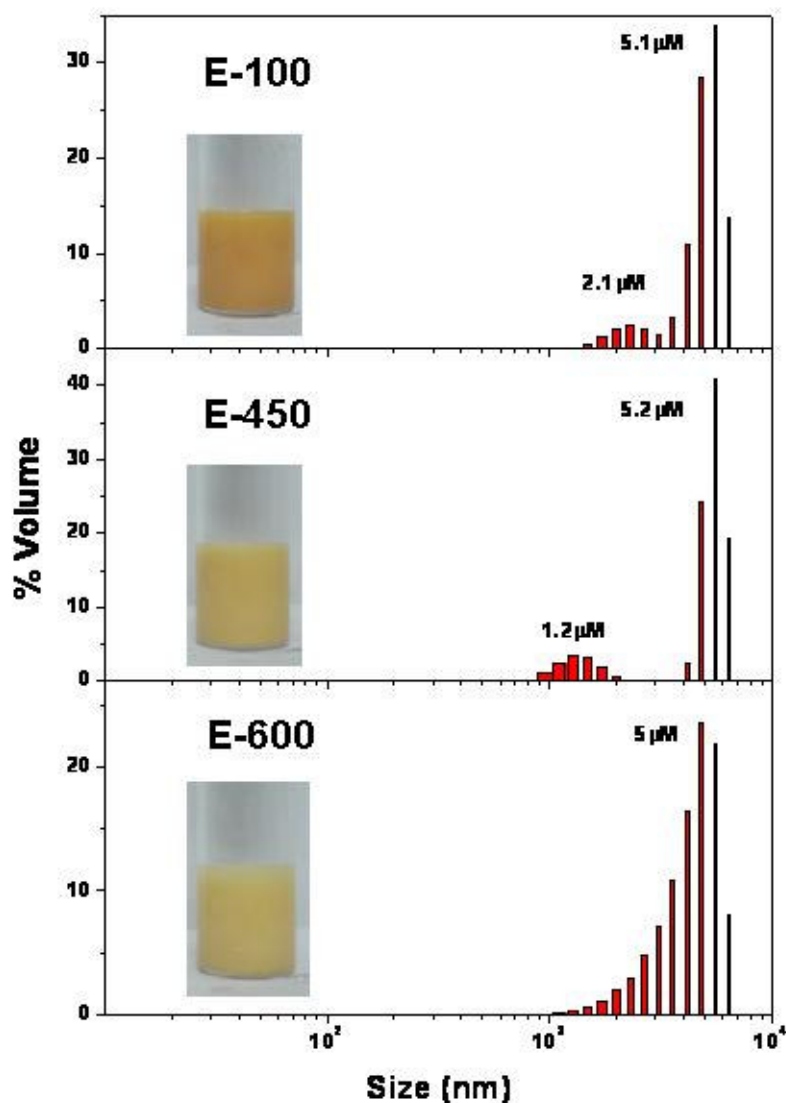


**Figure 2.20.** DLS histograms of emulsion template.

The good stability of the template (aniline+dopant) enabled us to characterize the morphology by SEM and HR-TEM<sup>28,46</sup>. For the microscopic analysis the dopant+aniline emulsion (in water) was drop casted on SEM-stud (for TEM on farmar Cu grid) and the samples was dried under desiccator containing anhydrous calcium chloride for one week. SEM and TEM images of the templates are shown in figure 2.21. SEM image indicates the existence of net-work morphology of cylindrical micelles, which is a typical texture observed for micellar templates<sup>46</sup>. High resolution TEM images evident the presence of two types of long cylindrical micelles, one type with diameter around 80 nm with a length of 6  $\mu\text{m}$  and other short one with 180 nm

average diameter. It is reasonable to believe that the complexation of aniline induces the transformation of dopant micelles into long cylindrical aggregates of 80-180 nm, which template for nanomaterials. Further oxidation of these aggregates by APS produces polyaniline nanofibers.

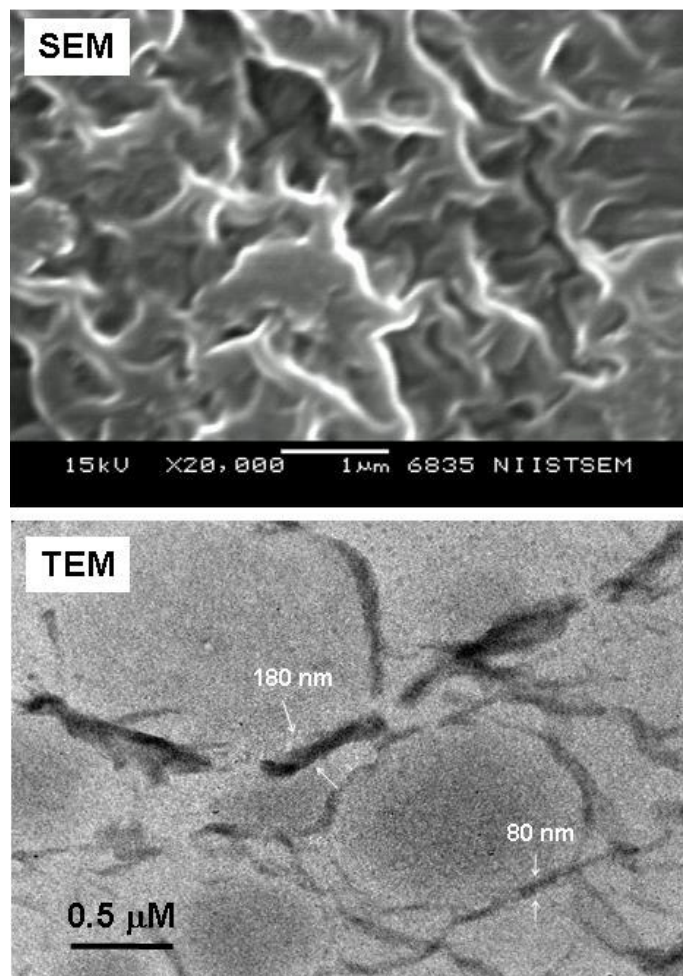


**Figure 2. 21.** SEM and TEM images of the emulsion template.

In order to understand the interactions of aromatic moieties like aniline with anionic surfactant in water, the pH of the polymerization mixtures were also measured. The pH of the dopant (alone) and surfactant+aniline in water were obtained as 2.86 and 7.29, respectively. As expected the aromatic sulfonic surfactant is highly acidic in nature in water with lower pH of 2.86. Aniline is a strong base and effectively reacted with the surfactant to form the neutral anilinium-salt which drastic increase the pH of the solution from 2.86 to 7.29 (towards neutral). This results supports that the aniline molecules not only occupy the hydrophobic core of the

micelle and it also reacts with the hydrophilic portion at the surface of the micelles to bring the micelles together to produce large size aggregates (as seen in TEM images and supported by DLS).

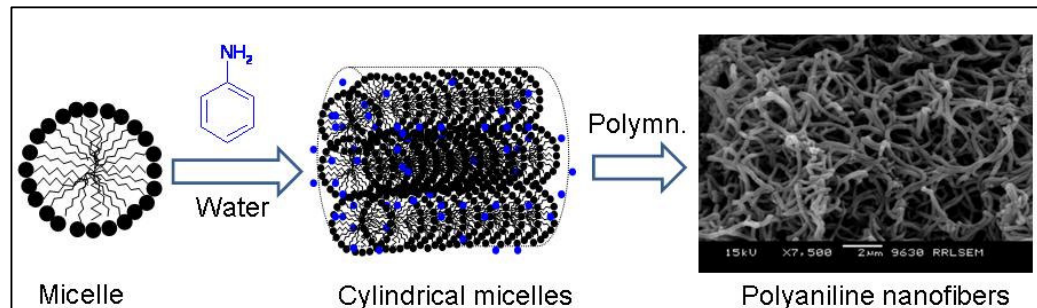


**Figure 2. 22.** A plausible mechanism for nanofiber formation.

A plausible mechanism of nanofiber formation was shown in figure 2.22. It can be summarized that the cylindrical micelle template plays a major role for the formation nanofibers. At lower dopant concentration ( $[\text{aniline}]/[\text{dopant}] > 600$ ), the aniline molecule trapped in the layer assemblies of dopant, which template for the polyaniline nanotubes. Due to the phase separation of aniline + dopant complex, the template for the nanotubes was not able to characterize by DLS and TEM. Since azobenzene surfactants are well-known to form layer-assemblies below CMC in water (evident DLS measurements), even in the absence of in-ability to view the layers assemblies, the proposed template model is anticipated to template for polyaniline nanotubes<sup>47</sup>. At very high dopant concentration (**E-1** to **E-15**), the dopant-anilinium salts form inhomogeneous emulsion and the subsequent oxidation leads to hollow micro-spheres or spheres plus short dendritic fibers. In this study the  $[\text{aniline}]/[\text{dopant}]$  ratio in the feed was varied from 1 to 1500, and the DLS and microscopic studies of the dopant template was utilized to trace the mechanism of the polyaniline nanomaterials formation.

### 2.3.8. Properties of Nanomaterials

The polyaniline nanomaterials prepared by dopant 1 is freely dispersible in water by stirring under ultrasonic at room temperature and produce a stable green solution which is stable for more 2-3 days at ambient conditions. Few representative absorption spectra of **E-1** to **E-1500** are shown in figure 2.23. It is very clear from the spectra that the peak corresponding to quinoid ring (at 650 nm) is essentially absent



which confirmed the doping of polyaniline nanofibers. Two distinct peaks at 420-450 nm and at near-IR region above 850 nm are corresponding to the formation of polaron species in the nanofibers<sup>48,49</sup>. However **E-1** did not show any absorption for polaron indicating the incomplete doping.

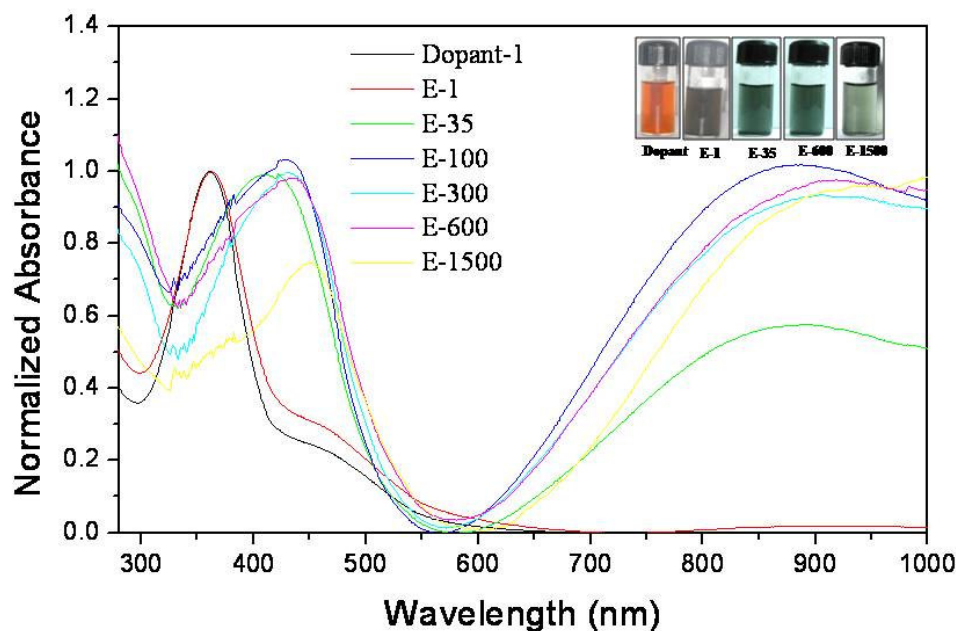


**Figure 2.23.** Absorption spectra of the dopant 1 and polyaniline nanomaterial solution in water at 30 °C. The inset is corresponding solution.

The degree of doping is calculated from the elemental analysis of the doped materials and the sulphur/nitrogen ratios were obtained as 39.4, 30.1, 28.8 and 27.6 % for **E-1**, **E-100**, **E-600** and **E-1500**, respectively. The values are in the range reported for the sulfonic acid doped polyaniline and as expected the degree of doping decreases with the decrease in the amount of dopant in the feed<sup>11,50</sup>.



**Figure 2.24.** Photograph of Keithley Four Probe set up.

For electrical conductivity measurements, the nanomaterials are pressed to make pellets in a press. Thickness ( $d$ ) of the pellets is measured at four different positions and the results were averaged. The conductivity is measured at room temperature (28 °C) by the standard spring-loaded pressure-contact four-probe method (see figure 2.24). A constant current ( $I$ ) from a current source is allowed to pass through two adjacent leads of the four probes, and the voltage ( $V$ ) across the other two leads is measured using a nano-voltmeter. The conductivity ( $\sigma$ ) is calculated from the relation <sup>51</sup>.

$$\sigma = (ln2/\pi d) I/V$$

The conductivity values of the polyaniline nanomaterials were given in table 2.2. The polyaniline samples with higher dopant amount (**E-1** to **E-7.5**) showed very low conductivity in the range of  $6 \times 10^{-5}$  to  $5 \times 10^{-4}$  S/cm, whereas the conductivity of **E-15** to **E-1500** was obtained in the range of  $\sim 10^{-3}$ - $10^{-2}$  S/cm. The conductivity of **E-1** and **E-1.5** are very low despite the high dopant concentration indicate that the extent of doping is not directly increasing the conductivity of the polyaniline nanofibers, whereas the morphology was found to be the determining factor for the conductivity<sup>52</sup>. It is evident from the SEM images that the **E-1** and **E-1.5** has poor morphology compared to that of **E-7.5** to **E-900**, and therefore, the morphology plays a major role in the conductivity of the polyaniline nanofibers rather than the extent of doping.

The solid-state properties of polyaniline nanomaterials were also studied for finely powdered samples using wide angle X-ray diffraction analysis (WXRd). Polyaniline backbone is highly rigid due to their linear structure and less flexible to chain folding to induce crystalline domain. Therefore, un-doped polyaniline (emeraldine base) chains as well as mineral acid doped polyaniline normally observed as highly amorphous polymer <sup>41,53</sup>. In the presence of organic dopants, the dopant-polymer undergoes various interactions, which tend to organize the polymer chains in three-dimensional highly ordered fashions (see figure 2.25). The WXRd patterns of polyaniline nanofibers are shown in figure 2.25.

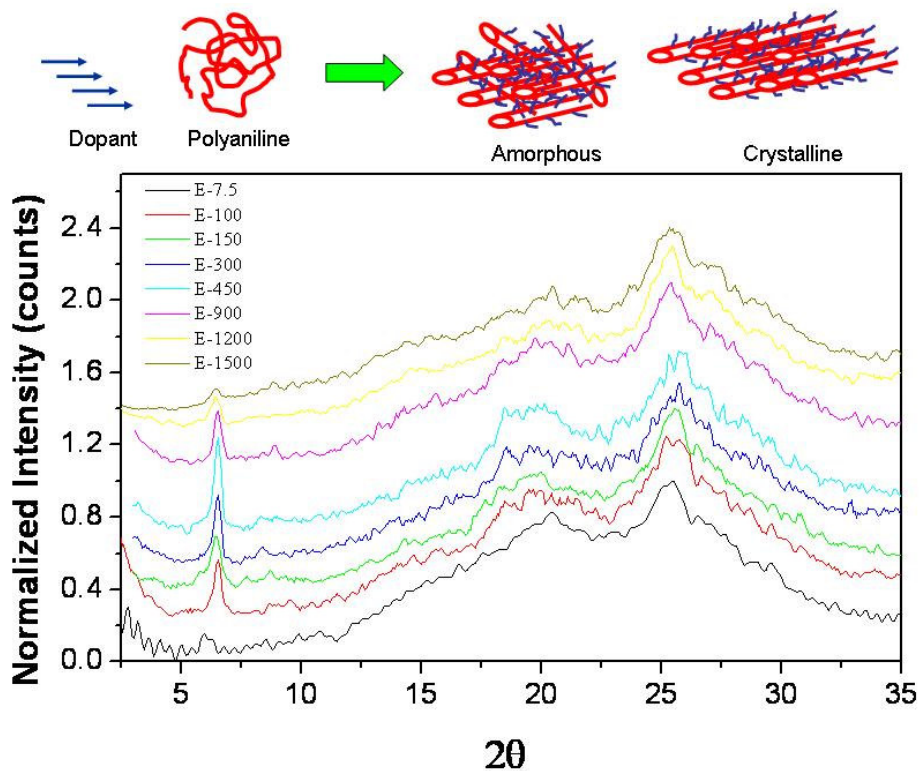


**Figure 2.25.** WXR D plots of polyaniline nanomaterials.

The WXR D patterns of nanomaterials showed three distinct peaks at  $2\theta = 6.4, 20.1$  and  $25.5$  ( $d$ -spacing =  $13.6, 4.4$  and  $3.5 \text{ \AA}$ ). The two peaks at  $20.1$  and  $25.5$  are generally observed in doped polyaniline, but the new peak at  $2\theta = 6.4$  is only observed for highly ordered samples in which the polyaniline chain to chain distance increased by the effective inter -digitations of dopant molecules<sup>54</sup>. The peak at  $2\theta = 6.4$  ( $d = 13.6 \text{ \AA}$ ) is present in all other polyaniline samples. Interestingly, this peak intensity increases and reaches a maximum value at sample **E-450** (up to CMC) and then decreases gradually. The ratio of the intensities of the peaks at  $2\theta = 6.4$  and  $25.9$  (also peak area ratio) were plotted and shown in figure 2.26. The percent (%) crystallinity of this peak was determined by dividing its peak area by the total area<sup>53</sup>. It is very clear from the plots that both the intensity and percent crystallinity of the peak at  $2\theta = 6.4$  increase with the dopant concentration up to CMC ( $4 \times 10^{-4} \text{ M}$ , up to **E-450**) and further decreases below CMC. It suggest that the above CMC, the dopant in micelles not only increase the length and linearity of the polyaniline fibers (see SEM figure 2.18), it also effectively penetrate into the polymer interlayer and

produces highly three dimensionally ordered solid state nano-fibers. Below the CMC, the dopant molecule is isolated and loses the collective penetration ability to form highly ordered fibers. It is clear that the [aniline]/[dopant] ratio in the feed plays a major role in formation of highly ordered, lengthy and linear polyaniline nanofibers. The micellar type of the dopant-aniline complex determines the length, shape and solid state ordering of the polyaniline nanomaterials.

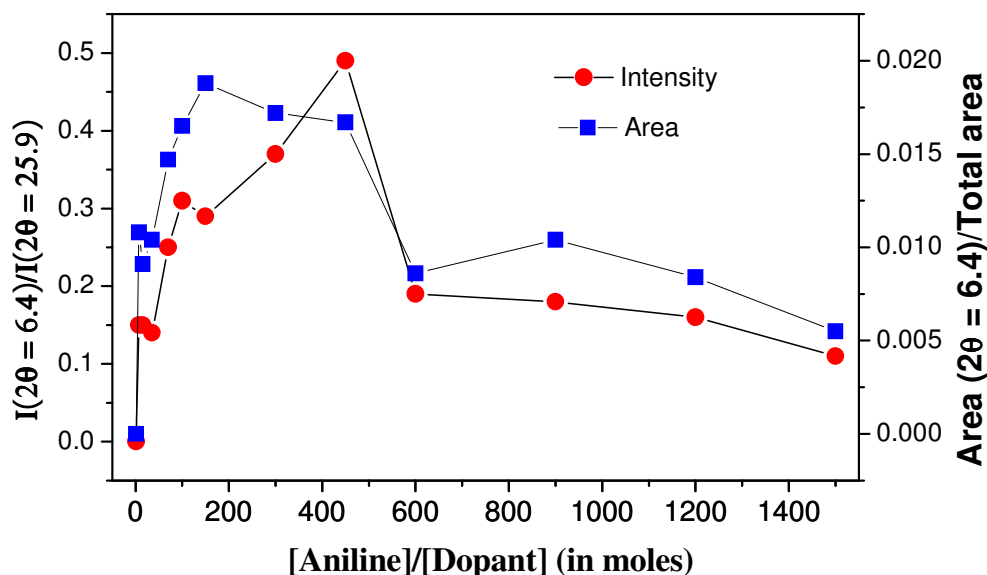


**Figure 2.26.** Plot of intensity and area of WXR peak versus [Aniline]/[Dopant].

### 2.3.9. Effect of Experimental Conditions on Morphology

To study the influence of experimental conditions on the nanomaterials morphology, control experiments (at 1 g scale by keeping [aniline]/[dopant] = 100) by varying temperature (5 and 30°C), under ultrasonic stirring, magnetic stirring and without any stirring or disturbance were carried out<sup>12,13</sup>. SEM images of the resultant samples under these various conditions are given in figure 2.27. All the cases showed nanofibrillar morphology confirming that the dopant 1 soft-templte approach is not sensitive to any variation in the experimental conditions. Therefore, the present approach is very unique in the sense polyaniline nanofibers can be prepared in reproducible manner with less or no influence of experimental variation.

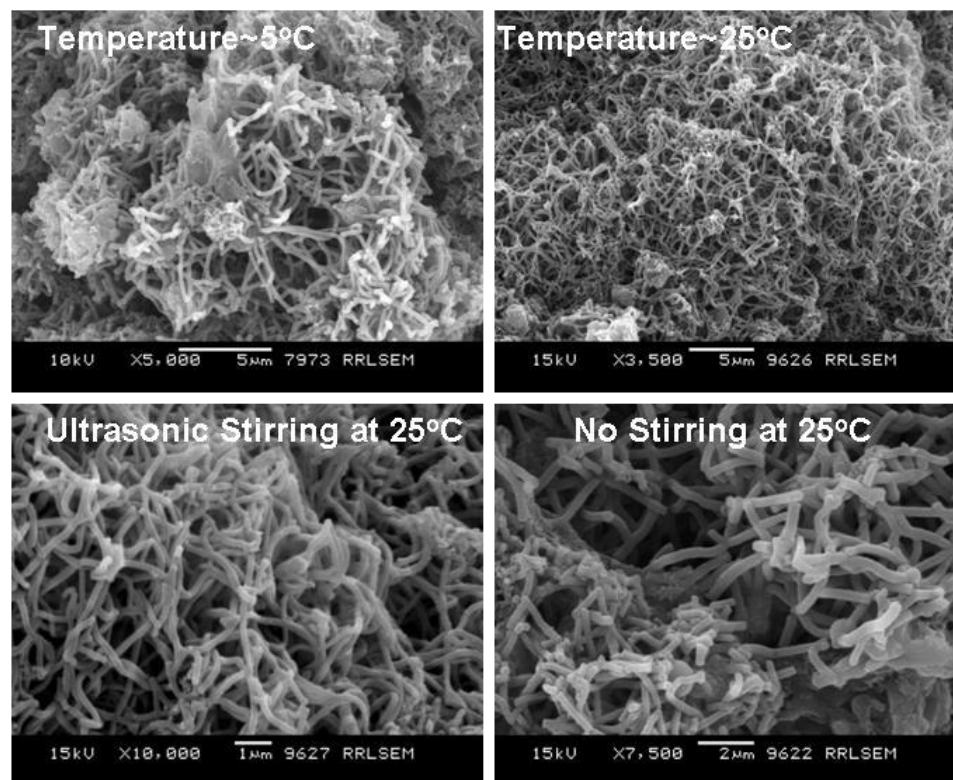


**Figure 2.27.** SEM images nanofibers synthesised under various conditions.

In the entire polyaniline nanomaterials research large-scale synthesis is un-addressed issue. To check the viability of approach for large-scale synthesis in 10, 50 and 100 g scale ([aniline]/[dopant] is kept 100) were carried out and the sample are denoted by **E-10g**, **E-50g** and **E-100g**. The SEM images of the nanomaterials **E-10g** to **E-100g** is given in figure 2.28 and evident the formation of nanofibers of 160 nm diameters and long up to 4  $\mu\text{m}$ . TEM-images (**E-100g**) of the nanomaterials have further confirmed the fibrous morphology and their diameters were almost same as noticed in the SEM. SEM and TEM-images confirmed that the nanofiber morphology was un-altered from 1 to 100 g scale synthesis. Therefore, the present approach is very unique and polyaniline nanofibers can be prepared in reproducible manner from 1 to 100 g scale without altering its morphology.

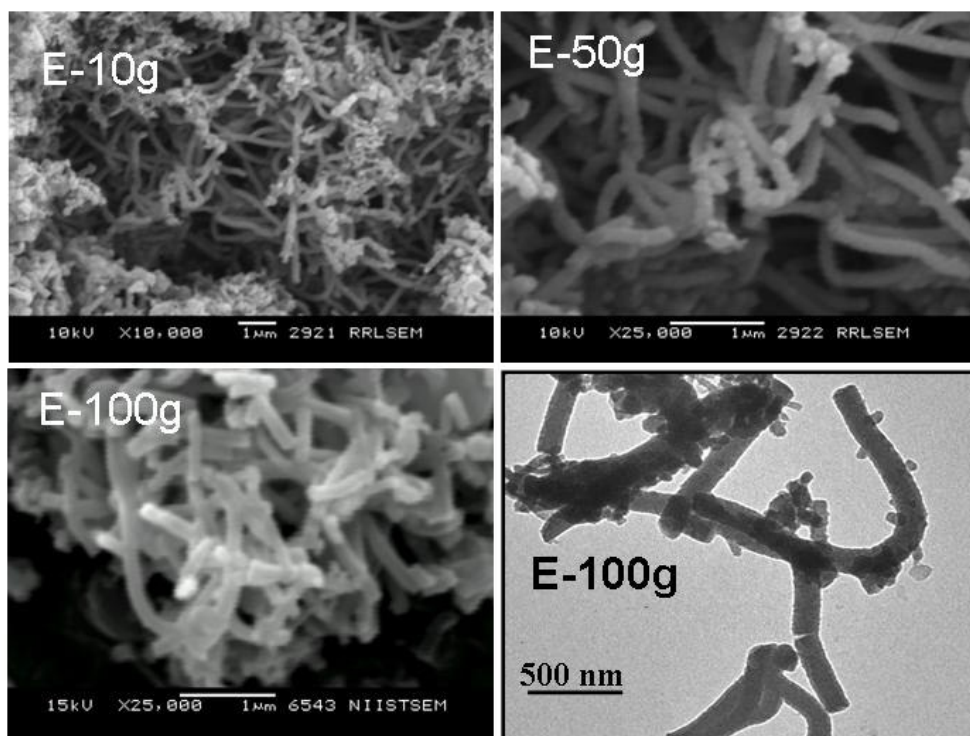


**Figure 2.28.** SEM images of large-scale synthesised polyaniline nanofibers.

In order to check any effect on the properties of nanofibers on scale up, the absorption and WXR D of large-scale synthesised products were carried out. The absorption spectra of polyaniline nanofibers **E-10g** to **E-100g** are given in figure 2.29a. All the nanofibers showed three distinct absorption at 380 nm, 430 nm and at above 850 nm corresponding to the transitions of  $\pi$ -band to  $\pi^*$ -band, polaron band to  $\pi^*$ -band and  $\pi$ -band to polaron band as observed in doped conventional polyaniline samples. It is interesting to note that unlike the 1 g scale nanofibers, the samples **E-10g**, **E-50g** and **E-100g** showed a tail-like behaviour above 890 nm and indicating a more expanded chain conformation<sup>48,49</sup>. It suggests that the more expanded conformation of polyaniline chains in large-scale products increases the delocalization of charge carriers (evident by UV-Vis spectra, see figure 2.29a). The difference in the conformation of the polymer chains may be associated with the temperature of the polymerization of the 1 to 100 g scale. Oxidation of aniline in to PANI is an exothermic reaction, and therefore, the temperature of the polymerization medium was monitored at regular intervals. Before the addition of APS (before polymerization starts), the temperature of emulsion was noticed as 29 °C in all the cases (1g and

large-scale). After the addition of APS, within 30 minutes, the temperature of the reaction medium increased to a constant high temperature of 39, 54, 63 and 67 °C for the 1 g, 10 g 50 g and 100g scale, respectively. The temperature of the polymerization medium gradually decreased to 29 °C after 6 h of reaction.

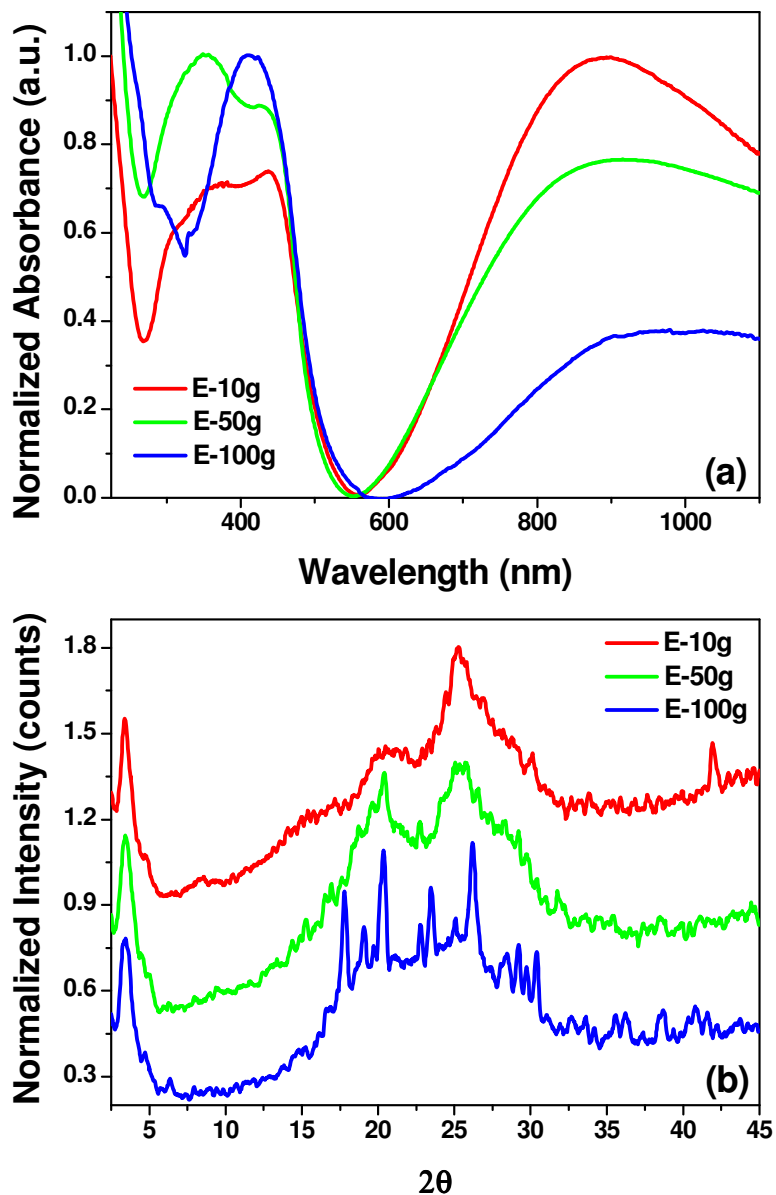


**Figure 2.29.** Absorption and WXR D plots of large-scale synthesized nanofibers.

In the small scale (1g) reaction the volume of reaction is relatively small and also the reacting sites are more exposed to atmosphere which will dissipate the heat evolved during polymerization. But in the large-scale synthesis (10g, 50g and 100g),

most of the reaction sites are occupied well beneath in the bulk and so the heat generated is trapped inside the reaction medium. This higher temperature favored the effective uncoiling of polyaniline chains into a more expanded conformation due to the increased thermal motions of polyaniline chain and subsequent doping by amphiphilic dopant molecules allows crystallization of side chains of dopant to produce highly ordered polymer chains in nanofibers<sup>55,56</sup>.

To further confirm the conformational changes in the polyaniline chains (nanofibers) and also to study the solid state behaviour of the polyaniline nanofibers, the finely powdered samples were subjected for Wide angle X-ray diffraction analysis at 30 °C. The WXR D plots of the polyaniline nanofibers are shown in figure 2.29b. The WXR D patterns of the nanofiber samples showed three distinct peaks at  $2\theta = 3.4$ , 20.1 and 25.5° (d-spacing = 25.5, 4.4 and 3.5 Å). The two peaks at 20.1 and 25.5° are generally observed in doped polyaniline and in this case these peaks are more or less super imposed with amorphous scattering<sup>53</sup>. The new peak at  $2\theta = 3.4^\circ$  (d-spacing of 25.5 Å), which is not observed in 1g scale nanofibers (see figure 2.25), observed in bulk scale sample is strongly indicating for the existence of a lamellar structure<sup>54,57</sup>. This lamella is formed due to the inter-digitations and crystallization of side chains of the comb-shaped doped polyaniline. In order to get more idea regarding d-spacing values, the theoretical geometry of the dopant molecule calculated by AM1 calculations (see figure 2.10) was correlated to the d-spacing of the WXR D patterns. The polar head of the dopant molecules penetrated in to the tunnel between the polymer chains and give d-spacing value (d =25.5 Å,) equivalent to molecular length (end to end distance= 24.4 Å). Among the bulk scale products **E-100g** is appeared to be more crystalline and showed sharp peaks at even higher angles ( $2\theta = 15$  to 35°). This may be due to the more expanded nature of the polymer chains (evident from absorption spectra, figure 2.29a) in this sample which can pack in a more ordered fashion to increase the solid state ordering of the nanofibers. It is reasonable to believe that this observed difference in solid state packing is also a consequence of heat generated during polymerization. In bulk scale polymerization (**E-10g**, **E-50g** and **E-100g**), the excess generated heat will improve the diffusion of dopant molecules into the polymer matrix and hence results in peaks with increased d-spacing in WXR D<sup>58,59</sup>. So the observed differences in absorption and solid-state



properties are due to the conformational variation among polymer chains originated from the difference in the temperature of reaction medium. It is very important to add here that despite the variation in the temperature of the polymerization, the morphology of the nanofiber synthesis is highly reproducible.

### 2.3.10. Property Reversibility of Polyaniline Nanofibers

The polyaniline nanofiber is a promising material for many applications since acidic and basic chemicals change polyanilines conductivity. The major difficulty in this aspect is the availability of pure, uniform diameter polyaniline nanofibers in desirable quantities. Due to the ease of the synthetic method developed by us, sufficient nanofiber material is now readily available. For the facile use of these large scale synthesized materials, the morphology should be stable and the physical properties such as conductivity, ordering and absorption characteristics should also be retained in consecutive reversible cycles of doping/de-doping processes<sup>60</sup>.

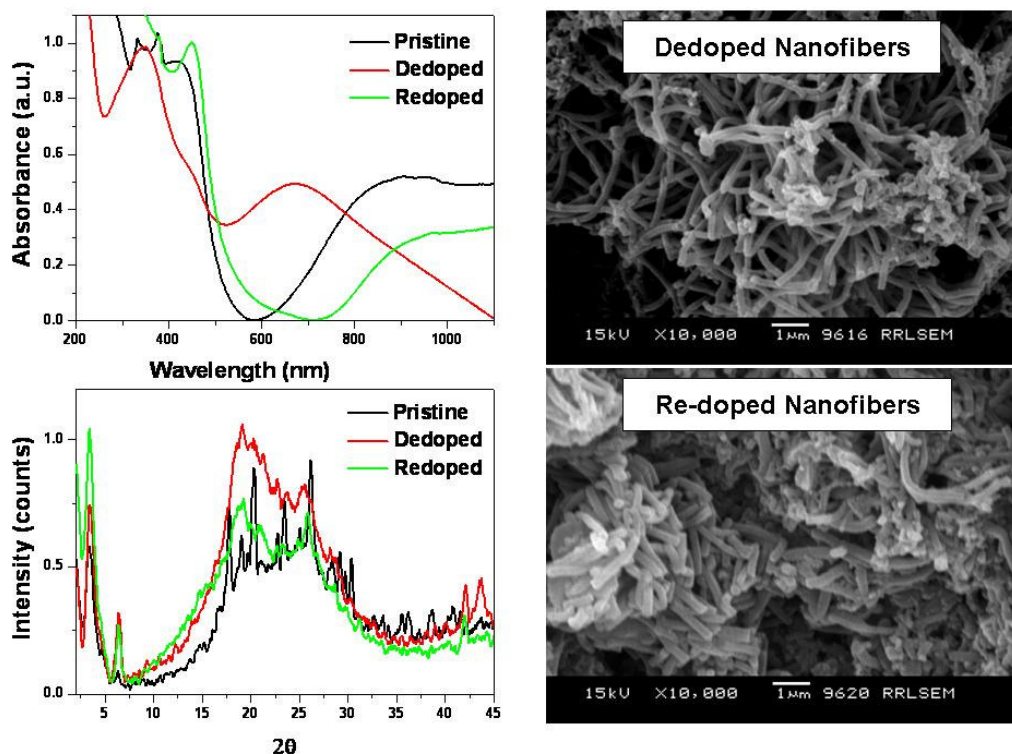


**Figure 2.30.** Reversibility in properties of polyaniline nanofibers on acid-base doping / dedoping process.

In order to check the reversibility of the nanomaterials, the sample **E-100g** was subjected to doping/de-doping experiments. The sample was de-doped by stirring

with 25 mL of 10 % solution of aq.NH<sub>3</sub> for 4 h to get PANI-EB form. The sample was purified by washing with water till the filtrate become colourless and dried in vacuum oven for 24 h. The morphology and other properties of dedoped sample were given along with the parent sample in figure 2.30.

**Table 2.3.** Conductivity data for de-doping and re-doping experiments

Sample	$\sigma^a$ (pristine) (S/cm)	$\sigma$ (de-doped) (S/cm)	$\sigma$ (re-doped) (S/cm)
<b>E-70</b>	$0.85 \times 10^{-2}$	$1.8 \times 10^{-6}$	$2.5 \times 10^{-2}$
<b>E-100</b>	$0.93 \times 10^{-2}$	$1.2 \times 10^{-6}$	$0.6 \times 10^{-2}$
<b>E-150</b>	$0.76 \times 10^{-2}$	$3.0 \times 10^{-6}$	$1.0 \times 10^{-2}$
<b>E-100g</b>	$5.8 \times 10^{-2}$	$2.1 \times 10^{-7}$	$1.8 \times 10^{-1}$

Absorption spectra of the de-doped sample showed a peak at 650 nm characteristic of quinoid ring in the emeraldine base which confirmed the complete de-doped stage. The SEM image of de-doped sample indicated that the fibrous morphology was not altered by the de-doping process. The WXRd plot of the de-doped sample showed the presence of lower angle peak confirming the retaining of ordered polymer chains even after the removal of the dopant. The conductivity of the de-doped sample was obtained in the range of  $10^{-6} - 10^{-7}$  S/cm which is 4 order less than that of the original sample (in the range of  $10^{-2}$  S/cm) (see table 2.3). The de-doped sample was re-doped by treating with camphor sulfonic acid in ethanol (or HCl in water) at 60 °C to result green coloured emeraldine salt form. The UV-Vis spectrum showed the formation of polaron peak at 850 nm due to the doping and vanishing of peak at 650 nm indicating efficient doping. It is very clear from SEM image that the fiber morphology is still preserved and WXRd confirmed the complete reversal of solid state properties of polyaniline. The conductivity values of green colour re-doped pellets showed  $10^4$  times (in the range of  $10^{-2}$ - $10^{-1}$  S/cm) increase compared to the de-doped pellets. The combinations of SEM, WXRd, UV-Vis and conductivity measurements reveal that the morphological, solid-state, electronic and optical properties of the polyaniline nanofibers are reversible.

## 2.4. Conclusion

In summary, a renewable resource dopant based self-assembly strategy for high quality polyaniline nanomaterials were developed. The renewable amphiphilic azobenzene sulfonic acid dopant designed and developed based on cardanol is an efficient structure directing agent for the polyaniline nanomaterials. The approach demonstrated here many unique features and advantages: (i) the dopant is very cheap and can be easily synthesized from naturally available resource cardanol, the main component of cashew nut shell liquid (CNSL) (ii) the dopant has unique built-in amphiphilic nature to form micelles in water and micellation behaviour was confirmed by dynamic light scattering (DLS), dye encapsulation, surface tension, emission and ionic conductance studies (iii) these micellar aggregates can form stable emulsion with aniline for a wide concentration ranging from  $10^{-1}$  to  $10^{-4}$  M in water, which is very rarely reported for any types of dopant in polyaniline synthesis (iv) the dopant-aniline templates were characterized by DLS, SEM and TEM studies (v) the dopant-aniline complex selectively exist in various forms such as salt, aggregated cylindrical micelles and layers in water depending upon the [aniline]/[dopant] ratio in the feed, which subsequently results in spheres, fibres and nanotubes (vi) the polyaniline nanomaterials are soluble in high polar solvents like DMSO and water that enabled the complete structural characterization by NMR and UV-Vis. (vii) the dopant molecule can penetrate into the polyaniline chain via inter-digitations and highly ordered solid state properties can be preciously controlled by the [aniline]/[dopant] ratio in the feed and (viii) the self-organized cylindrical micellar template was extended to reproducible large synthesis of polyaniline nanofibers up to 100 gram and (ix) the nanofibers showed high reversibility in morphology, optical and solid state properties in the repetitive doping/de-doping analysis for practical applications.

**2.5. References**

1. Li, D.; Huang, J.; Kaner, R. B. *Acc. Chem. Res.*, **2009**, *42*, 135-145
2. Wan, M. X. *Adv. Mater.* **2008**, *20*, 2926–2932
3. Wan, M. X. *Macromol. Rapid. Commun.* **2009**, *30*, 963–975
4. Zhang, D. H.; Wang, Y. Y. *Mater. Sci. Eng. B*, **2006**, *134*, 9-19
5. Tran, H. D.; Li, D.; Kaner, R. B. *Adv. Mater.* **2009**, *21*, 1–13
6. Haung, J.; Virji, S.; Weiller, B. H.; Kaner, R. B. *J. Am. Chem. Soc.* **2003**, *125*, 314.
7. Chiou, N. R.; Epstein, A. J. *Adv. Mater.* **2005**, *17*, 1679-1683
8. Zhang, X.; Manohar, S. K. *Chem. Commun.* **2004**, 2360-2361
9. Zhang, L.; Wan, M. X. *Adv. Funct. Mater.* **2003**, *13*, 815-820
10. Wei, Y.; Zhang, L.; Yu, M.; Yang, Y.; Wan, M. X. *Adv. Mater.* **2003**, *15*, 1382-1385
11. Haung, K.; Wan, M. X. *Chem. Mater.* **2002**, *14*, 3486-3492
12. Jing, X.; Wang, Y.; Wu, D.; She, L.; Guo, Y. *J. Polym. Sci. Part A: Polym. Chem.* **2006**, *44*, 1014-1019
13. Li, D.; Kaner, R. B. *J. Am. Chem. Soc.* **2006**, *128*, 968-975
14. Wang, Y.; Jing, X. *J. Phys. Chem. B*, **2008**, *112*, 1157–1162
15. Haung, J.; Kaner, R. B. *Angew. Chem.* **2004**, *116*, 5941-5945
16. Vemula, P. K.; John G. *Acc. Chem. Res.*, **2008**, *41*, 769-782
17. John, G.; Masuda, M.; Okada, Y.; Yase, K.; Shimizu, T. *Adv. Mater.* **2001**, *13*, 715–718.
18. Santos, M. L.; Magabhaes, G. C. *J. Braz. Chem. Soc.* **1999**, *10*, 13-20.
19. John, G.; Pillai, C. K. S. *Polym. Bull.* **1989**, *22*, 89–94.
20. John, G.; Pillai, C. K. S. *J. Polym. Sci., Part A: Polym. Chem.* **1993**, *31*, 1069–1073.
21. Rekha, N.; Asha, S. K. *J. Polym. Sci. Polym. Chem.* **2009**, *47*, 2996–3009.
22. Yui, H.; Guo, Y.; Koyama, K.; Sawada, T.; John, G.; Yang, B.; Masuda, M.; Shimizu, T. *Langmuir* **2005**, *21*, 721–727.

23. John, G.; Jung, J. H.; Minamikawa, H.; Yoshida, K.; Shimizu, T. *Chem. Eur. J.* **2002**, *8*, 5494–5500.
24. Paul, R.K.; Vijayanathan, V.; Pillai, C.K.S. *Synth Met.* **1999**, *104*, 189–195
25. Antony, R.; Pillai, C. K. S.; Scariah, K. J. *J. Appl. Polym. Sci.* **1990**, *41*, 1765–1775.
26. Jayakannan, M.; Amrutha, S. R.; Sindhu, K. V. *J. Appl. Polym. Sci.* **2006**, *101*, 2650-2655.
27. Roy, S.; Fortier, J. M.; Nagarajan, R.; Tripathy, S.; Kumar, J.; Samuelson, L. A.; Bruno, F. F. *Biomacromolecules.* **2002**, *3*, 937-941
28. Bucholz, T.; Sunb, Y.; Loo, Y.L. *J. Mater. Chem.*, **2008**, *18*, 5835–5842
29. Zhang, X.; Kolla, H.S.; Wang X.; Raja, K.; Manohar S.K. *Adv. Funct. Mater.*, **2006**, *16*, 1145-1152.
30. Tanford, C. *Proc. Nat. Acad. Sci. USA.* **1974**, *71*, 1811-1815.
31. Israelachvili, J. N.; Mitchell, D. J.; Ninham, B. W. *J. Chem. Soc. Faraday Trans.* **1976**, *72*, 1525.
32. Hamley, I.W. *Introduction to Soft Matter*, (2 nd Edn), Wiley, **2007**, pp-200-04
33. Dominguez, A.; Fernandez, A.; Gonzalez, N.; Iglesias, E.; Montenegro, L. *J. Che. Edu.* , **1997**, *74* , 1227-1231
34. Atkins, P.; de Paula, J. *Atkin's Physical Chemistry*, (7th Edn), Oxford University Press, **2002**, Chapter 21, pp-755.
35. Franke, D.; Egger, C.C.; Smarsly, B.; Faul, C. F. J.; Tiddy, G. J. T. *Langmuir*, **2005**, *21*, 2704-271
36. Iglesias, E. *J. Phys. Chem.* **1996**, *100*, 12592-12599
37. Mu, S.; Yang, Y. *J. Phys. Chem. B*, **2008**, *112* , 11558.
38. Zhou, C.; Han, J.; Song, G.; Guo, R. *J. Polym. Sci., Polym. Chem.* **2008**, *46*, 3563
39. Zheng, W.; Angelopoulos, M.; Epstein, A. J.; MacDiarmid, A. G. *Macromolecules* **1997**, *30*, 7634-763.
40. Kang, E. T.; Neoh, K. G.; Tan, K. L. *Prog. Polym. Sci.*, **1998**, *23*, 211-324
41. Jayakannan, M.; Annu, S. ; Ramalekshmi, S. *J. Polym. Sci. Polym. Phys.* **2005**, *43*, 1321
42. Erdem , E.; Karakısla, M.; Sacak , M. *Eur Poly J*, **2004**, *40*, 785–791

43. Wei, Z.; Zhnag, Z.; Wan, M. *Langmuir*, **2002**, *18*, 917-921.
44. Zhang, Z.; Wei, Z.; Wan, M. *Macromolecules* **2002**, *35*, 5937-5942.
45. Yan , Y.; Yu , Z.; Huang, Y. W.; Yuan, W. X.; Wei, Z. X. *Adv. Mater.* **2007**, *19*, 3353
46. Zhang, L.; Wan, M. X. *Adv.Funct.Mater.* **2003**, *13*, 815-820
47. Shimomura, M.; Kunitake, T. *J. Am. Chem. Soc.* **1987**, *109*, 5175-5183.
48. Xis, Y.; Wiesinger, J. M.; MacDiarmid, A. G. *Chem. Mater.* **1995**, *7*, 443-445
49. MacDiarmid, A. G.; Epstein, A, J.; *Synth. Met.* **1995**, *69*, 85-92.
50. Wei,Y.; Wan, M. X.; Lin, T.; Dai, L. *Adv .Mater.* **2003**, *15*, 136-139
51. Jana, T.; Nandi, A. K. *Langmuir* **2000**, *16*, 3141
52. Parthasarathy, R. V.; Martin, C. R. *Chem. Mater.* 1994, *6*, 1627-1632.
53. Lunzy, W.; Banka, E.; *Macromolecules* **2000**, *33*, 425.
54. Dufour, B.; Rannou, P.; Fedorko, P.; Djurado, D.; Travers, J.P.; Pron, A. *Chem. Mater.* **2001**, *13*, 4032-4040
55. Dawn, A.; Nandi A.K. *Macromolecules* **2005**, *38*, 10067-10073.
56. Dawn, A.; Nandi A.K. *Langmuir* **2006**, *22*, 3273-3279.
57. Laska, J.; Djurado, D.; Lunzy, W. *Eur. Polym. J.* **2002**, *38*, 947-951.
58. Levon, K.; Ho, K.H.; Zheng, W.Y.; Laakso, J.; Karna, T.; Taka, T.; Osterholm, J.E. *Polymer* , **1995**, *36* , 2733-2738
59. Banka, E.; Luzny, W.; *Synth Met* **1999**, *101*, 715.
60. Sarno, D. M.; Manohar, S. K.; MacDiarmid, A. G. *Synth Met*, **2005**, *148* ,237–243

## ***Chapter-3***

---

### ***Selective Micellar Templating for Divergent Polyaniline Nanostructures***

### 3.1. Introduction

Tuning the morphology of the nanostructures is a challenging task in conducting polymer nanomaterials research<sup>1-4</sup>. In emulsion route for polyaniline nanomaterials the polymerization is carried out in aniline in water emulsion stabilized by surfactants or functionalized dopants<sup>5-7</sup>. The underlying principle in emulsion route is that the micellar soft template formed by the surfactant (or dopant) directs the morphology of the resulting polymer. In interfacial route for polyaniline nanofibers, the polymerization is performed in an immiscible aqueous/organic two phase system<sup>8,9</sup>. The polymerization occurs at the interface and the resultant polyaniline in its hydrophilic emeraldine salt form diffuses away from the reactive interface which makes more reaction sites available at the interface. The interfacial route is mostly restricted to < 1 g scale (also low yield) due to the difficulty in controlling the diffusion process at the interfaces for large scale synthesis of polyaniline nanomaterials. Interestingly, the nanofibers produced through interfacial route were thin (< 100 nm), free from agglomerates and easily dispersible in water compared to other synthetic routes<sup>10</sup>.

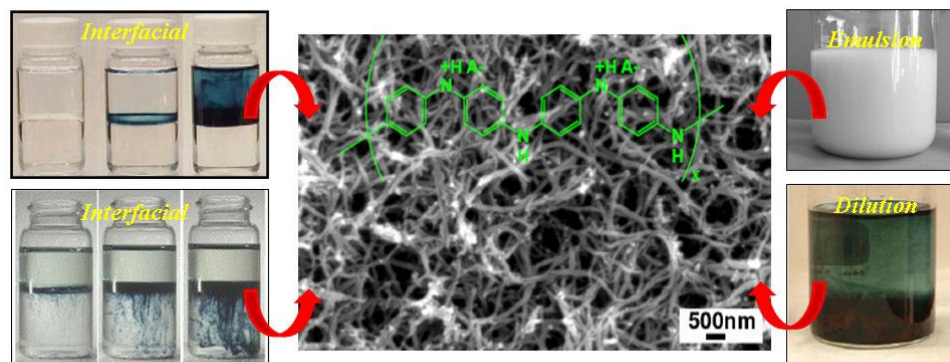


**Figure 3.1.** Polyaniline nanostructures by interfacial, emulsion and dilution routes (Adapted from references 9,11).

A dilute polymerisation route for polyaniline nanofibers developed by Epstein group has been carried out at very low concentration of monomer and thus prevents excessive aggregation tendencies of polymer chains leading to agglomerates<sup>11,12</sup>. In dilute polymerization the kinetics of polymerization is relatively very low so it is very advantageous to tune the morphology of the forming polymer by adjusting experimental conditions. For example, Guo and co-workers fabricated polyaniline rectangular sub-micron tubes by carrying out the polymerization of aniline in dilute



anionic surfactant solutions<sup>13</sup>. Both interfacial and dilute polymerizations are important non-template routes to synthesize high quality polyaniline nanofibers. The advantage of these polymerization approaches is that the aniline monomer concentration is very low and hence the secondary growths of nanofibers leading to particulate aggregates are well prevented<sup>9</sup>. However, low yield, inability to large scale synthesis and structural restriction to a few acid dopants are unsolved problems associated with these superior processes. So far there is no detailed study has been done to analyze the influence of the structural changes of templates in emulsion, dilute or interfacial route on polyaniline nanomaterials morphology. Further, a wider discrepancy was also noticed in the polyaniline nanomaterials synthesis over the selection of dopant molecules and polymerization routes: for instance, an emulsion friendly dopant failed as a good candidate for interfacial or dilution routes and vice-versa. It restricts the deep understanding of the mechanistic aspects of polymerization processes and their dependency on the formation of nanomaterials. Therefore, the development of a single amphiphilic surfactant (or dopant) based templates for the synthesis of various polyaniline nanostructures under emulsion, interfacial and dilution conditions is very much demanding.

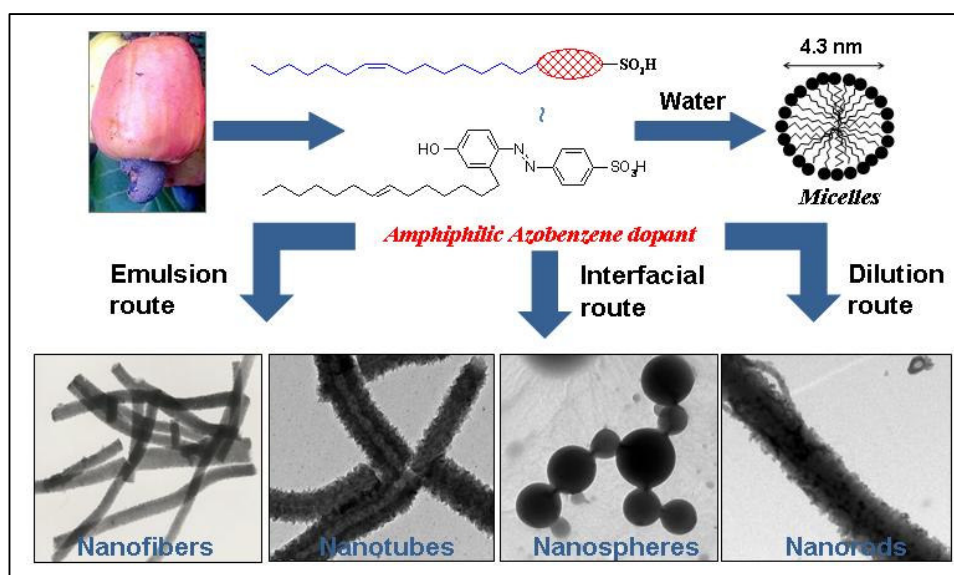


**Figure 3.2.** Amphiphilic azobenzene soft-template mediated synthesis of polyaniline nanostructures-fibers, tubes, spheres and rods.

This chapter is focused on the use of the unique micellar soft template approach based on an in-built amphiphilic molecule, 4-[4-hydroxy-2((Z)-pentadec-8-

enyl)phenylazo]-benzenesulfonic acid (developed in chapter-2), for tuning various types of polyaniline nano materials such as fibers, rods, spheres and tubes through selective templating process in water. This approach is very unique in the sense that all the starting materials are same (amphiphilic dopant, aniline, ammonium persulfate (APS) and water), but various nanomaterials were produced in a controlled way depending on how these constituents are self-organized and polymerized in water under normal conditions. During the chemical oxidative polymerization of aniline via self-assembly process, amphiphilic dopant molecules form thermodynamically stable aggregates of inherent nanoscale dimensions in solution, which act as template for the overall morphology of the resulting polyaniline. Templates formed by the dopant aniline complex in emulsion, dilute and interfacial polymerization is characterized by DLS (in solution) and TEM (in solid state). In emulsion route the dopants form either cylindrical micelles or bilayers with aniline monomer and their oxidation yields nanofibers and nanotubes respectively. Up on diluting the emulsion, it transformed into micelle aggregates of 175 nm size, which seeds for nanorods. In the interfacial route the spherical aggregates formed by the dopant-APS complex acts as template for nanospheres. The nanomaterials were characterized by SEM, TEM, absorption spectroscopy and X-ray diffraction to understand the morphology, electronic and solid state ordering. In summary, a unique amphiphilic sulfonic acid was developed to form variety of templates with aniline and APS to produce wide range of nanomaterials of fibers, rods, tubes and spheres. The idea of utilizing a single molecular dopant system in both emulsion (dilution) and interfacial routes to trace the factors which control the morphology of the nanomaterials is crucial and important for fundamental understanding of polyaniline nanomaterials.

## 3.2. Experimental Procedures

**3.2.1. Materials:** Aniline, ammonium persulfate (APS) and sulfanilic acid were purchased from Aldrich. Aniline was distilled and kept under nitrogen prior to use. The renewable dopant molecule 4-[4-hydroxy-2((Z)-pentadec-8-enyl)phenylazo]-benzenesulfonic acid was synthesised by following the procedure given in chapter 2.

The polyaniline nanomaterials **E-1** to **E-900** synthesised by emulsion route (see chapter-2) is used for current studies also.

**3.2.2. General Procedures:** For SEM measurements, polymer samples were subjected to thin gold coating using JEOL JFC-1200 fine coater. The probing side was inserted into JEOL JSM- 5600 LV scanning electron microscope for taking photographs. Transmission electron microscope images were recorded using a FEI Tecnai 30G<sup>2</sup> S Twin HRTEM instrument at 100kV. For TEM measurements, the water suspension of nanomaterials were prepared under ultrasonic stirring and deposited on Formvar coated copper grid. Wide angle X-ray diffractions of the finely powdered polymer samples were recorded by Philips Analytical diffractometer using CuK-alpha emission. Dynamic light scattering (DLS) measurements were carried out using a Nano ZS Malvern instrument employing a 4mW He-Ne laser ( $\lambda=632.8$  nm) and equipped with a thermo stated sample chamber. For all the DLS measurements HPLC quality (Merck, India) double distilled water is used. All the dopant solutions are centrifuged (2000 rpm, 5 min) prior to DLS measurements in order to remove any suspended particles, whereas the emulsions and dopant + APS complexes are not centrifuged since centrifugation may destabilize the emulsion. Infrared spectra of the polymers were recorded using a Perkin Elmer, spectrum one FTIR spectrophotometer in the range of 4000 to 400  $\text{cm}^{-1}$ . For conductivity measurements, the polymer samples were pressed into a 10 mm diameter disc and analyzed using a Keithley four probe conductivity instrument by applying a constant current. The resistivity of the samples was measured at five different positions and at least two pellets were measured for each sample: the average of 10 readings was used for conductivity calculations. The thermal stability of the polymers was determined using TGA-50 Shimadzu Thermo gravimetric Analyzer at a heating rate of 10 °C/min in nitrogen. UV-Vis spectra of the PANI in water were recorded using Perkin Elmer Lambda-35 UV-VIS Spectro Photometer. The emission studies were performed by a SPEX Fluorolog F112X spectrofluorimeter. The fluorescence quantum yields of the dopant and nanomaterials were determined in water using quinine sulfate in water ( $\phi=0.546$ ) as standard by exciting at 360 nm. The concentration of polymer solution (also dopant) and standard were adjusted in such a way to obtain the absorbance equal to

0.1 at 360 nm. The quantum yields of the samples are calculated by the following equation:

$$\phi_s = \phi_r [F_s A_r / F_r A_s] (n_r/n_s)^2$$

Where,  $\phi_s$  is the fluorescence quantum yield of the sample, F is the area for the emission peak, n is the refractive index of solution, and A is the absorbance of the solution at the exciting wavelength. The subscripts r and s denote reference and sample respectively. The resonance Raman peak for water appeared at 420 nm, which was deconvoluted computationally from the sample spectra for the calculating the area of the emission peaks.

**3.2.3. Dilute Polymerization Route to Polyaniline Nanomaterials:** Typical procedure for the synthesis of polyaniline nanomaterials is described in detail for **D-100a** and other samples were prepared following the same procedure. The dopant (0.053 g, 0.11 mmol) was dissolved in doubly distilled water (20 mL) and stirred under ultrasonic for 1h at 30 °C. Distilled aniline (1mL, 1.02 g, 11 mmol, [aniline]/[dopant] = 100) was added to the dopant solution and stirred under ultrasonic for additional 1h at 30 °C. The resulting emulsion was diluted by adding 15 mL of water. To this ammonium persulfate (10 mL, 1.1 M solution) was added at 30 °C. The resultant green color content was allowed to stand at 30 °C for 15 h. The solid was filtered, washed with distilled water, methanol and diethyl ether for several times till the filtrate become colorless. The solid product was dried in a vacuum oven at 60 °C for 48 h (0.01 mm Hg). <sup>1</sup>H-NMR (500 MHz, DMSO-d<sub>6</sub>)  $\delta$ : 7.81 (b, 4H, Ar-H, dopant) 7.55 (b, 2H, Ar-H), 7.52 (b, 2H, Ar-H), 7.11, 7.18, 7.29 (1/1/1 triplet, 1H, -NH+), 6.91 (b, 1H, Ar-H, dopant), 6.81 (b, 1H, Ar-H, dopant), 5.3 ppm (b, 2H, CH=CH, dopant), 0.5-3.5 (27H, aliphatic-H, dopant); FTIR (KBr, in cm<sup>-1</sup>): 3013, 1561, 1486, 1304, 1251, 1153, 1103, 1029, 812, 705 and 616. In a similar way the total volume of the reaction feed is varied by adding 30 mL, 60 mL, 90 mL and 120 mL water by keeping the [aniline]/[dopant] as 100 to synthesize samples **D-100b**, **D-100c**, **D-100d**, and **D-100e**, respectively.

**3.2.4. Interfacial Polymerization Route for Polyaniline Nanomaterials:** The dopant (0.053 g, 0.11 mmol) and ammonium persulfate (2.5 g, 11mmol) were

dissolved in doubly distilled water (30 mL) in a 50 mL glass vial. In a separate glass vial distilled aniline (1 mL, 1.02 g, 11 mmol, [aniline]/[dopant] = 100) was dissolved in dichloromethane. To the dichloromethane solution, dopant plus oxidant in water was carefully added without disturbing the interface. The interfacial polymerization was allowed to stand at 30 °C for 15 h without disturbing. Then the polyaniline solid mass was formed in the aqueous phase which was centrifuged, washed with distilled water and methanol for several times till the filtrate become colourless. The solid product was dried in a vacuum oven at 60 °C for 48 h (0.01 mm Hg). Yield = 0.36 g (35 %). <sup>1</sup>H-NMR (500 MHz, DMSO-d<sub>6</sub>) δ: 7.81 (b, 4H, Ar-H, dopant) 7.55 (b, 2H, Ar-H), 7.52 (b, 2H, Ar-H), 7.11, 7.18, 7.29 (1/1/1 triplet, 1H, -NH+), 6.91 (b, 1H, Ar-H, dopant), 6.81 (b, 1H, Ar-H, dopant), 5.3 ppm (b, 2H, CH=CH, dopant); 0.5-3.5 (27H, aliphatic-H, dopant); FTIR (in cm<sup>-1</sup>): 3015, 1563, 1484, 1301, 1248, 1151, 1106, 1027, 812, 707 and 618. Similarly **I-300** and **I-450** were prepared by varying [aniline]/ [dopant] ratio as 300 and 450 (in moles) respectively.

### 3.3. Results and Discussion

#### 3.3.1. Dilute Route Synthesis of Polyaniline Nanomaterials:

The amphiphilic azobenzene dopant molecule, 4-[4-hydroxy-2-((Z)-pentadec-8-enyl) phenylazo]-benzenesulfonic acid (see figure 3.2) was employed as structural directing dopant for polyaniline nanomaterials. From previous studies (chapter 2), it is found that renewable resource based amphiphilic azobenzenesulfonic acid is a good water soluble surfactant and exists in the form of ~ 4.3 nm spherical micelles above CMC value. These dopant micelles are efficient structure directing soft templates for polyaniline nanofibers in emulsion route for a wide range of [aniline]/[dopant] ratios. Here, in order to tune the morphology of nanomaterials as well as to thoroughly understand the mechanism of formation of nanomaterials, three synthetic approaches were employed. (i) Emulsions with varied ratio of [aniline]/[dopant] in the feed [from [aniline]/[dopant] = 1 to 900] as discussed in chapter 2 (ii) Dilution polymerization by the addition of water in to pre-templated emulsion ([aniline]/[dopant] = 100) results in the decrease in both aniline and dopant concentration (see figure 3.3) and (iii) interfacial polymerization which is carried out in an aqueous/organic bi-phasic interfacial

system by varying the [aniline]/[dopant] ratio in the feed as 100, 300 and 450 (in moles) (see figure 3.4).

**Table 3.1.** [Dopant], [aniline], yield, S/N ratio, dimensions, conductivity, and WXR D-data of polyaniline nanomaterials.

Sample	[Dopant] (M)	[Aniline] (M)	Yield <sup>a</sup> (%)	S/N (%)	Diameter <sup>c</sup> (nm)	$\sigma^d$ (Scm <sup>-1</sup> )	$[I(2\theta)6.4]/I(2\theta)25.9]^e$
D-100a	$2.4 \times 10^{-3}$	0.24	76	29.5	125-210	$7.8 \times 10^{-3}$	0.44
D-100b	$1.8 \times 10^{-3}$	0.18	59	28.6	140-220	$1.5 \times 10^{-2}$	0.68
D-100c	$1.2 \times 10^{-3}$	0.12	68	29.1	130-225	$4.6 \times 10^{-3}$	0.69
D-100d	$9 \times 10^{-4}$	0.09	58	27.5	0.7-1.3 $\mu\text{m}$	$7.3 \times 10^{-3}$	0.82
D-100e	$7.2 \times 10^{-4}$	0.07	63	27.1	0.6-1.4 $\mu\text{m}$	$2.4 \times 10^{-3}$	0.82

- Calculated for isolated product.
- Calculated from elemental analysis data.
- The values are determined from the SEM images.
- Values are obtained using four probe conductivity units at 30° C.
- From wide angle X-ray diffraction measurements at 30° C.

The amphiphilic azobenzene dopant is freely soluble in water and its complex with aniline form stable emulsion, which acts as self-assisted template for polyaniline nanomaterials. The emulsion formed is very stable for a wide range of [aniline]/[dopant] ratios and are very stable for more than one month under normal ambient conditions. This gives the opportunity to trace both the effect of composition and concentration of the reactant constituents on the formation of nanomaterials. Emulsion polymerization details were described in chapter 2.

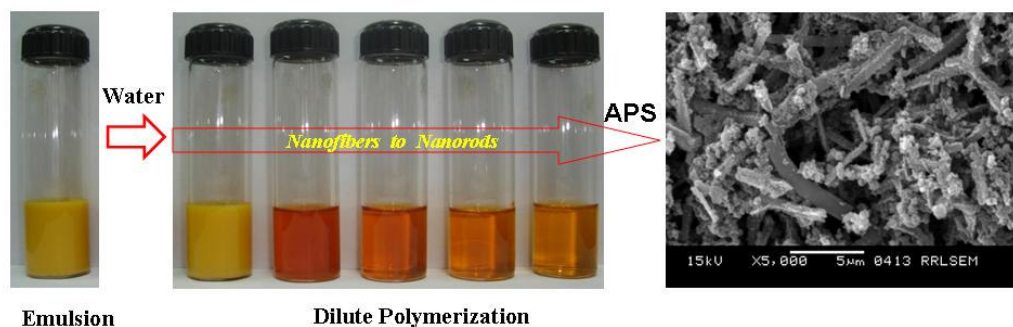


**Figure 3.3.** Dilute polymerization route for polyaniline nanorods.

In dilution route by gradually adding water into the pre-formed thick emulsion transformed into a clear solution without phase separation (see figure 3.3). Unlike the

emulsion route, in the dilution route the concentration of the aniline also decreases along with dopant, which account for the homogenous solution. It suggests that the amphiphilic dopant is very versatile in nature and wide range of composition of the reactants as well as their concentration can be fine-tuned for nanomaterials synthesis. The dilution polymerization mixtures were oxidised by APS solution to obtain green polyaniline nanomaterials. Typically the polymerization was carried out by dissolving aniline and dopant in water and subsequently stirring under ultrasonic at ambient conditions for 30 minutes. The resultant milky emulsion was diluted by adding required amount of water and oxidized by adding ammonium persulfate (1.1 M solution) in water under ultrasonic for 1 h. The green solution was kept at 30 °C without any disturbance. The green polymer was filtered and purified by washing with water and methanol until the filtrate become colourless. The samples prepared by dilution method were denoted as **D-100x**, where **x= a, b, c, d** and **e** (see table 3.1). The concentration of the aniline and dopant are given in table 3.1. The polymer samples were dried under vacuum for 24 h (0.05 mm of Hg) at 60 °C prior to further analysis. Polyaniline nanomaterials were produced in 60-80 % yield. The yield, composition and elemental analysis data (S/N ratio) of the polyaniline nanomaterials are summarized in table 3.1.

### 3.3.2. Interfacial Route Synthesis of Polyaniline Nanomaterials:

Interfacial polymerization is performed in an aqueous/organic two phase system with aniline dissolved in dichloromethane as solvent and ammonium peroxydisulfate +dopant were dissolved in an aqueous solution<sup>9</sup>.

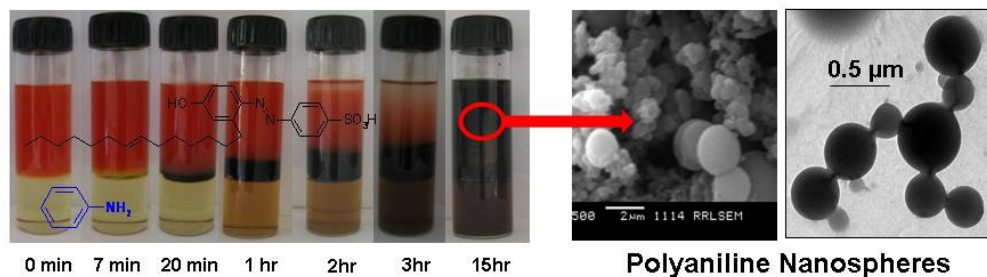


**Figure 3.4.** Snap shot showing the progress of interfacial polymerization.

The polyaniline samples were prepared by varying the [aniline]/ [dopant] ratio in the feed as 100, 300 and 450 (in moles), respectively. The polymer were denoted as

**I-X (I-100, I-300 and I-450)**, where **I** and **X** refer the interfacial route and ratio of [aniline]/ [dopant] in the feed, respectively. Ammonium persulfate and dopant-1 were dissolved in water and immediately transferred to a vial containing aniline in dichloromethane. It is observed (within two minutes) that upon adding APS solution, the aqueous dopant layer slowly transform to yellow turbid (see vials in figure 3.4). After an induction period of 10 minutes, the polymerization started and green layer of polyaniline emeraldine appears at the interface (see vials in figure 3.4). As the reaction proceeds, the green layer became thick and after 15 h the entire aqueous layer turned to a dark solid. The aqueous layer was separated carefully, centrifuged and washed well with water and methanol to remove all oligomers, excess dopant and inorganic impurities. The samples were dried under vacuum for 24 h (0.05 mm of Hg) at 60 °C prior to further analysis. Polyaniline nanomaterials were produced in 40 % yield, which is relatively much higher than that reported for other sulfonic acid dopants<sup>8</sup> (for example camphoresulfonic acid, 8 % yield). The polyaniline structure and doping of emeraldine salt by the sulfonic acid was confirmed by FTIR analysis and the degree of doping (S/N ratio) was determined from elemental analysis (see table 3.2).

**Table3.2.** [Dopant]/[aniline], S/N, yield, conductivity, dimensions and WXRd-data of polyaniline nanomaterials.

Sample	[Aniline]/[Dopant] (moles)	Yield <sup>a</sup> (%)	S/N <sup>b</sup> (%)	$\sigma^c$ (S/cm)	Diameter <sup>d</sup> (nm)	WXRd d-spacing (Å)
<b>I-100</b>	100	34	33.3	$2 \times 10^{-2}$	0.4-2.1 $\mu\text{m}$	14.4, 13.6, 4.8
<b>I-300</b>	300	36	41.3	$5 \times 10^{-2}$	300-400nm	14.5, 13.6, 4.8
<b>I-450</b>	450	41	32.4	$1 \times 10^{-2}$	50- 120nm	13.6, 4.4, 3.4

a) Calculated for isolated product.

b) Calculated from elemental analysis data.

c) Values are obtained using four probe conductivity units at 30° C.

d) The values are determined from the SEM images.



### 3.3.3. Morphology of Nanomaterials:

The SEM and TEM images of dilute polymerization route samples are given in figure 3.5. The samples **D-100a** and **D-100c** consists of nanofibers of ~100 nm thickness, which are thin compared to that of emulsion route fibres. Largely diluted sample, **D-100d** mainly comprises of nanorods plus spheres instead of nanofibers. As the polymerization medium become very dilute, (as in the case of **D-100e**), the sample comprises of only nanorods of diameter ranging from 175 nm – 800 nm.

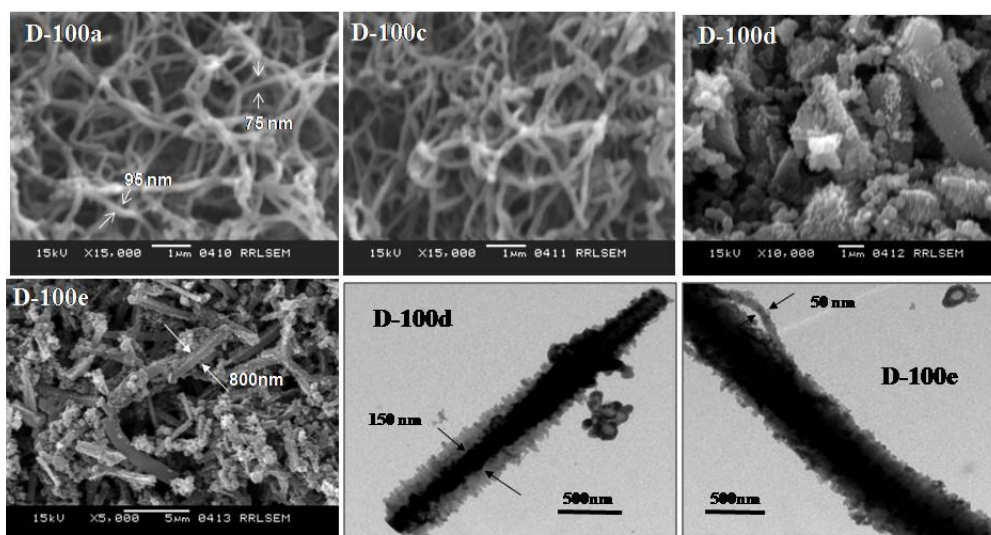


**Figure 3.5.** SEM and TEM images of polyaniline nanomaterials synthesized by dilute emulsion route.

The TEM images of **D-100d** (see figure 3.5) revealed that the nanorods are formed by the aggregation of nanospheres. The contrast difference of the interior part and exterior part clearly suggests the non-cylindrical shape of the nanorods and the whiskers like growth seen in rod surface indicates the adsorption of nanospheres. It is also interesting to see from the TEM images of **D-100e** that the rod composed of nanofibers of diameter ~75 nm. Based on the TEM (also SEM) images, it is reasonable to believe that during the initial stages of polyaniline formation in very dilute polymerization both nanospheres and nanofibers are formed. During the course of reaction the spheres are adsorbed on nanofiber surface that leads to nanorod formation. The above assumption is supported by the fact that the SEM and TEM image of rod clearly indicates the non-cylindrical in shape mostly due to the surface adsorption of nanospheres over the initially formed nanofiber fragments.

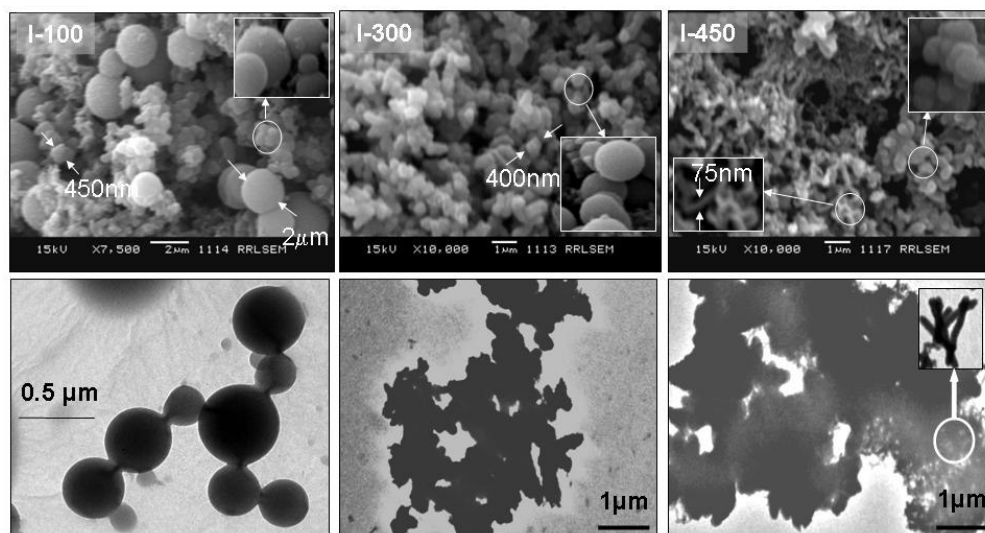


**Figure 3.6.** SEM and TEM images of polyaniline nanomaterials synthesised by interfacial polymerization.

The SEM and TEM images of the interfacial polymerized polyaniline nanomaterials are given in figure 3.6. The SEM images of interfacial samples showed an interesting observation that the morphology of the materials changing from microspheres to nanospheres plus fibres with the decreasing the amount of dopant in the feed (from [aniline]/[dopant] = 100 to 450 in moles). **I-100** consists of both micron and nanospheres whereas **I-300** predominately has only nanospheres of ~ 400 nm diameter. The sample **I-450** has nanospheres (~400 nm) and also thin nanofibers of < 150 nm diameter. SEM technique is inadequate to distinguish whether the nanomaterials are hollow or rigid and also poor resolution for <150 nm size (see figure 3.6) Therefore, the polyaniline nanomaterials samples were subjected to TEM analysis and the TEM images of **I-100**, **I-300** and **I-450** are given in figure 3.6. TEM image of **I-100** appeared as well separated nanospheres with diameter 300-400 nm, whereas **I-300** is seen as a cluster of highly aggregated nanospheres of 300 nm. In **I-450** the presence mixtures of thin nanofibers with nanospheres were clearly visible. The charged conducting nanomaterials have very strong affinity to each other and cluster together during the sample preparation (for TEM analysis) via solvent evaporation method. This leads to the TEM images of the materials (**I-300** and **I-450**) looks like meso-structures<sup>14</sup>. It is clear from the morphological analysis by SEM and TEM that the polyaniline nanomaterials prepared by interfacial method are predominantly nanospheres. In general, polyaniline nanofibers are commonly reported

for interfacial route (for HCl and CSA), but here the formation of nanospheres was observed. This suggests that the mechanism of formation of nanomaterials in interfacial route for the amphiphilic azobenzene dopant is different compared to other dopants known. Additionally, the formations of different morphologies in the emulsion dilute, and interfacial routes (fibres, rods and spheres) also indicate that same dopant molecule follows different mechanistic pathways in these three routes.

The morphological analysis of nanomaterials clearly indicates that (i) the decrease in the dopant amount in emulsion route (decrease in the aniline / dopant ratio), the nanomaterials are transformed from nanofibers to nanotubes, (ii) the decrease in the concentration of both aniline and dopant (for fixed [aniline]/[dopant] ratio = 100), results in the transformation of thin-fibres to nanorods and (iii) the interfacial route produced exclusively nanospheres rather than nanofibers. It strongly suggests that the amphiphilic dopant follows an entirely different pathway in the interfacial route to produce nanospheres compared to that of emulsion and dilution routes. It is very important to note that in all the cases the starting materials are same (aniline, dopant, APS and water) and different nanomaterials are produced depending upon their composition, concentration, combination of the constituents and types of the polymerization processes were employed.

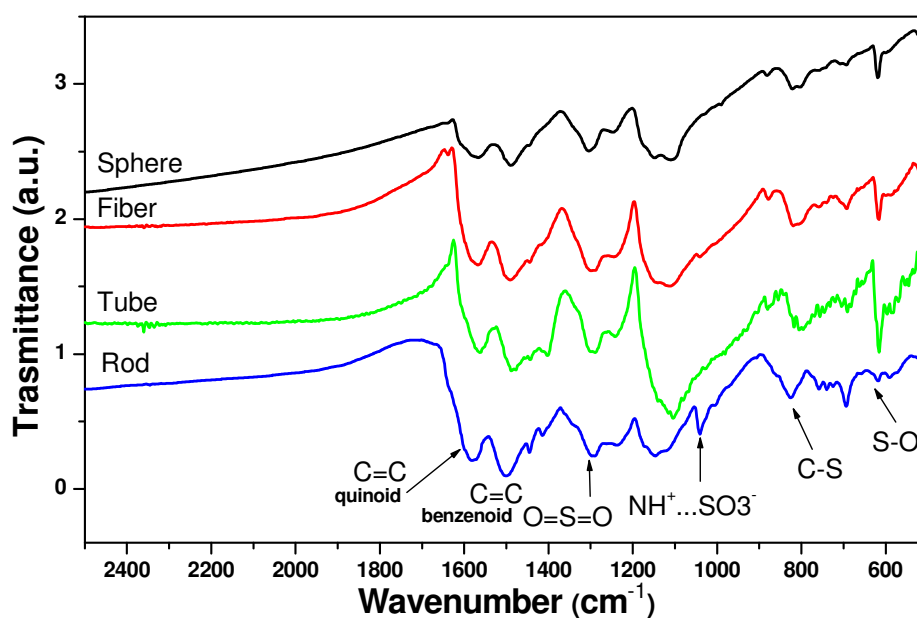
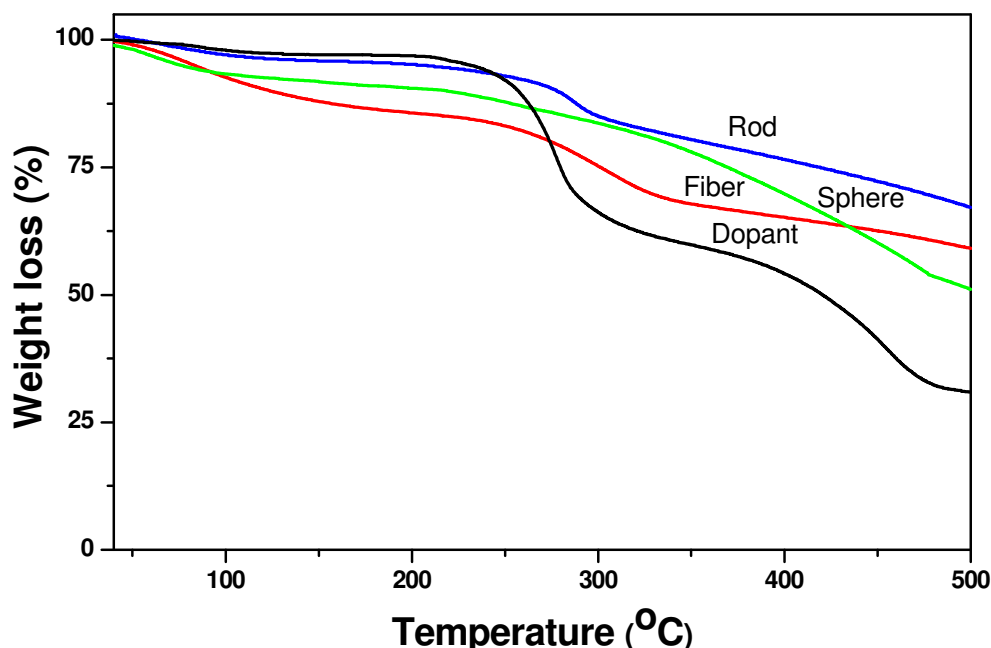


Figure 3.7. FTIR spectra of polyaniline nanomaterials.

The FTIR spectra of polyaniline nanomaterials (fibres, tubes, spheres and rods) are given in figure 3.7 and found that almost similar to conventional polyaniline. The two peaks at 1583 and 1481 are corresponding to the quinoid and benzenoid ring C=C stretching ring deformations, respectively<sup>15,16</sup>. The peak at 1315 and 832 are corresponding to C-N stretching and C-H out-of-plane vibrations of 1, 4-disubstituted benzene ring, respectively. The appearance of new peaks in the dopant doped samples at 1304 and  $\sim 632\text{ cm}^{-1}$  are attributed to symmetric and un-symmetric stretching vibrations of O=S=O and S-O groups. The peak at 1021  $\text{cm}^{-1}$  is corresponding to  $\text{NH}^+\dots\text{SO}_3^-$  interactions between the polymers chain and the dopant<sup>17</sup>. This analysis confirmed the doping in polyaniline nanomaterials.



**Figure 3.8.** TGA plots of dopant 1, polyaniline nano-fibres, spheres and rods.

The thermal properties of the polyaniline nanomaterials were measured by means of thermo gravimetric analysis (TGA). TGA curves for dopant 1 and polyaniline nanomaterials are given in figure 3.8. It is clear from the TGA of dopant that it very stable up to 250 °C and started decomposing above this temperature. The TGA curves for polyaniline nanomaterials have a typical three step weight loss behavior: the loss of water or solvent around 100 °C, dedoping and decomposition of dopant at 250 °C and decomposition of the polymer chain above 300 °C. Thermal

analysis showed that all the polyaniline nanomaterials are stable up to 300°C and so suitable for higher temperature applications.

#### 3.3.4. Mechanism of Nanomaterials Formation:

It is very clear from morphological analysis of nanomaterials that the formations of different morphologies in the interfacial, dilution and emulsion routes (spheres, rods, tubes and fibres). At the same time it is important note that in all routes the reactants used were same (aniline, dopant 1, water and ammonium per sulphate), which indicates that the same dopant molecule follows different mechanistic pathways in different routes<sup>18,19</sup>. In order to get more light on the templating behaviour of the amphiphilic azobenzene dopant DLS measurements were carried out for (i) aniline +dopant and (ii) APS+ dopant to trace factors which influence on the morphology of the nanomaterials in the emulsion, dilution and interfacial routes and shown in figure 3.9. Upon adding aniline into the dopant micelles in water, a thick emulsion was formed and it showed a bimodal distributions with majority of the aggregates in the range of 3- 5  $\mu\text{m}$  (see figure 3.9). It confirms that the aniline can form a stable aggregated emulsion with amphiphilic dopant. As the emulsion is diluted by adding water the milky appearance vanishes and the resultant aniline-dopant complex showed a pale turbidity (see vials in figure 3.9). DLS data showed a shift in the distribution of the aggregates size and shape from micro-meter to less than 600 nm (see figure 3.9 for **D-100b**). At higher dilution, the aniline+dopant complex (**D-100e**) almost become transparent and showed narrow uniform distribution with aggregates of 175 nm (see figure 3.9). It suggests that the dilution of pre-aggregated micro-emulsion leads to small nano-aggregates (**D-100e**) without any phase separation. During the interfacial polymerization, it was noticed that the addition of ammonium persulfate solution into dopant in water resulted in the formation of red turbidity. The DLS profile of the turbid APS+ dopant complex indicates that the amphiphilic dopant has also tendency to form a large 3- 5  $\mu\text{m}$  micrometer size aggregates with the APS. However, the nature of the distribution plot was different from that of the aniline+dopant complex. It confirms that upon adding APS to dopant in water larger aggregates of 3-5  $\mu\text{M}$  in size were produced which are stable and dispersed in the aqueous phase.

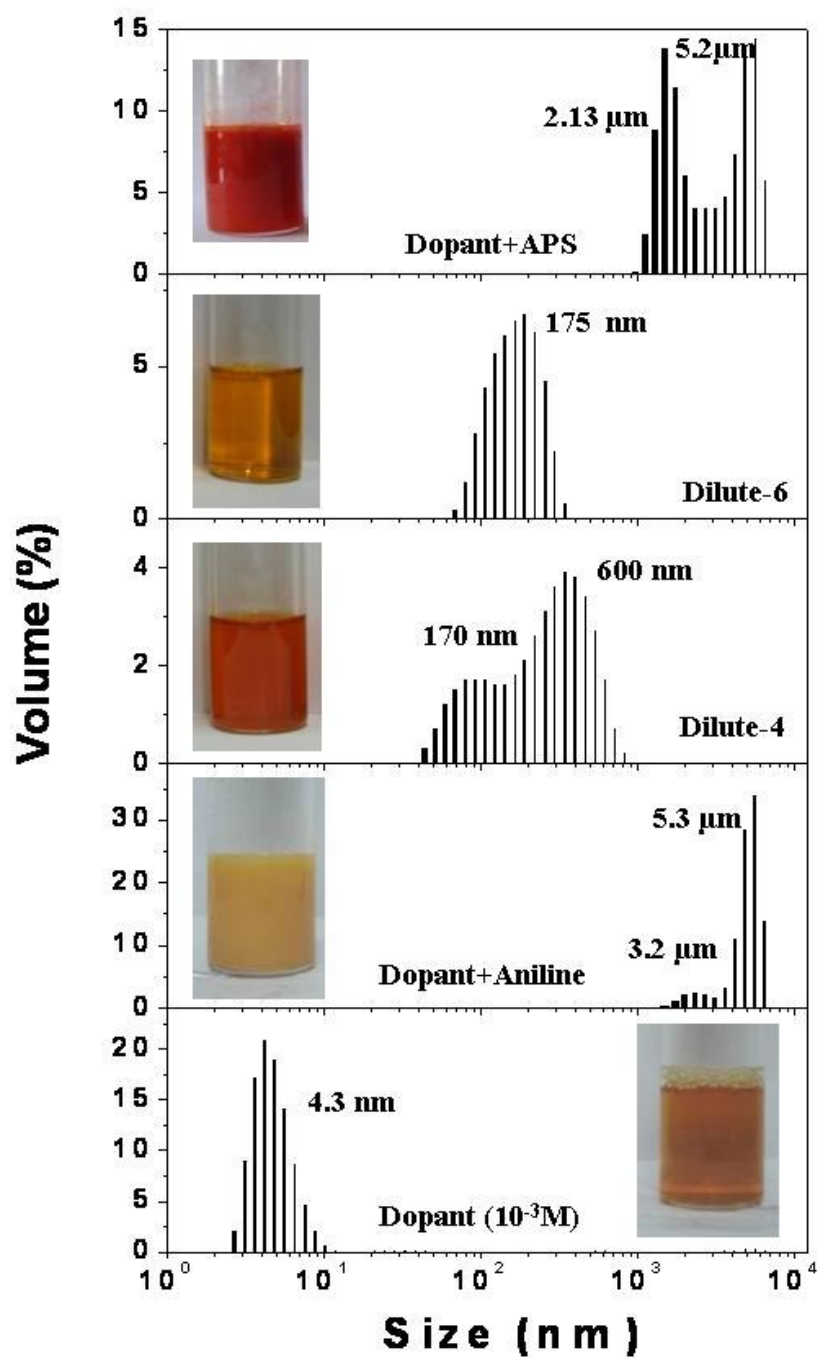


**Figure 3.9.** DLS histograms of dopant and various polymerization templates in water.

The dopant+aniline and dopant+APS complexes were stable for more than 24 h in water, which gives us opportunity to characterize them by TEM<sup>20,21</sup>. High resolution TEM images of the templates were recorded and shown in figure 3.10. The TEM images of dilute templates (**D-100e**) shows that it contains both spherical

aggregates of 200 nm size plus small number of rod type aggregates (up to micrometer size). It suggests that upon dilution, the long cylindrical aggregates (see chapter 2) are truncated into smaller spherical or rod like aggregates. These spheres + rods has template for polyaniline nanorods formation in the dilute route. Interestingly, the TEM image of dopant +APS complex (interfacial template) showed completely different trend and the templates appeared as exclusively spheres of 0.5 micrometers to 200 nm. It clearly proves that dopant +APS complex has unusual spherical templating behaviour in the interfacial route, which produces exclusively nanospheres.

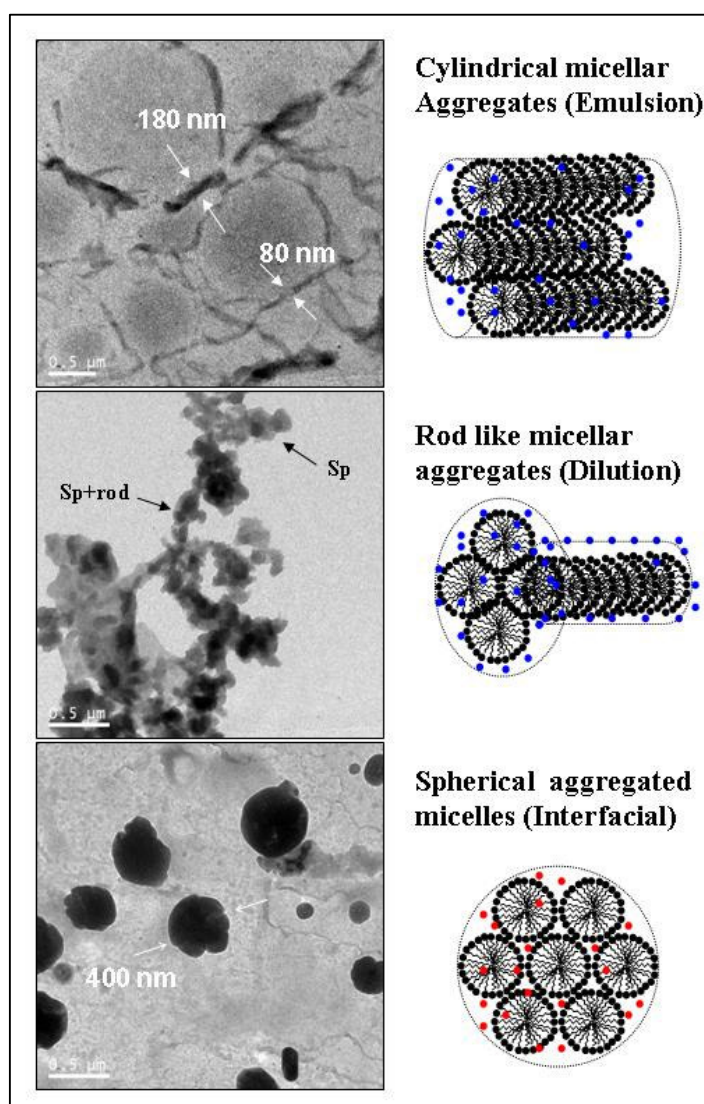


**Figure 3.10.** Template morphology by high resolution TEM.

Based on the SEM and TEM morphology of the synthesized samples and template characterization by TEM and DLS, the formation of various types of nanomaterials from amphiphilic dopant is proposed in figure 3.11. The studies from chapter 2 showed that the dopant molecules exist in the form of 4.3 nm micelles or layer-like assemblies depending upon its concentration in water. The addition of aniline produces long micrometer range cylindrical aggregates for  $[\text{aniline}]/[\text{dopant}] < 600$ , which template for polyaniline nanofibers. At lower dopant concentration ( $[\text{aniline}]/[\text{dopant}] > 600$ ), the aniline molecule trapped in the layer assemblies of dopant, which template for the polyaniline nanotubes. The dilution of emulsion template (for fixed  $[\text{aniline}]/[\text{dopant}] = 100$ ) produces micron range spheres plus rods, which aggregated together to template for polyaniline nanorods. It suggests that the effect of composition ( $[\text{aniline}]/[\text{dopant}]$  ratio) in the dopant + aniline varies the morphology from fibres to tubes whereas the concentration gradient transforms from fibres to nanorods. In the interfacial route, the dopant forms spherical aggregates with APS. During the course of polymerization aniline monomers will diffuse from organic layer and adsorbed over the spherical template surface. The subsequent oxidation of these aggregates will lead to formation of nanospheres. The SEM pictures of interfacial samples indicate that the morphology of the materials in this route was more sensitive to the  $[\text{aniline}]/[\text{dopant}]$  ratio in feed. The samples **I-100** and **I-300** were predominantly spheres, however, the decreasing the amount of dopant changes the morphology from spheres to fibres in **I-450**. In **I-100** and **I-300** relatively higher dopant amount in aqueous layer results in homogeneous aggregates, this produces more uniform nanospheres. Further dilution of dopant in the APS+ dopant mixture in the aqueous layer; disturb the aggregates formation and results in the formation of fiber plus spheres in **I-450**. Here, conducting polyaniline nanomaterials with variety of nanostructures are produced from same reaction constituents through selective polymerization in water at ambient conditions. The renewable amphiphilic dopant is very unique and it can form stable and aggregated micelles of cylindrical and layered shape for wider range of concentrations and compositions in reaction medium to tune polyaniline nanomaterials in a single system.



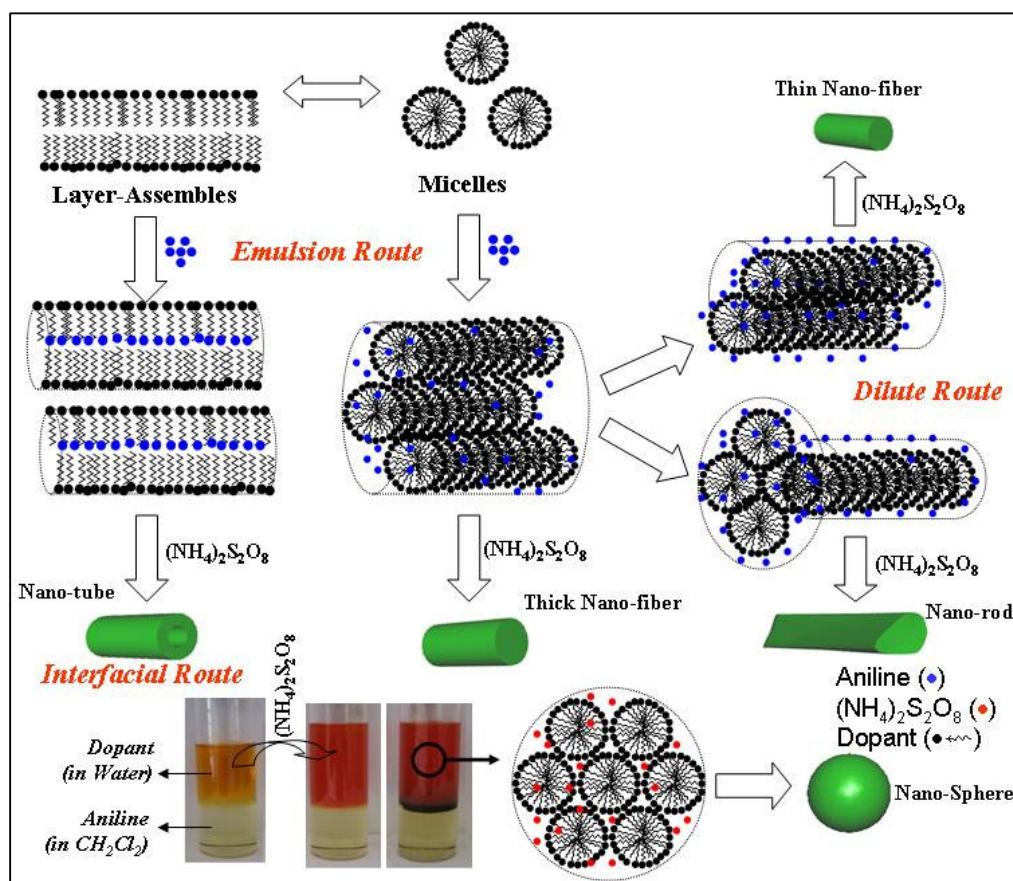


**Figure 3.11.** A plausible mechanism for the formation polyaniline nano-fibers, tubes, spheres and rods by emulsion, interfacial and dilution polymerization route respectively.

### 3.3.5. Optical and Solid-state Properties of Nanospheres and Nanorods:

The polyaniline nanomaterials were freely suspendable in water and other organic solvents by simple mixing under ultrasonic stirring at room temperature. UV-vis spectra of the nanospheres and nanorod samples are recorded in water are shown in figure 3.12. It is clear from the figure that the absorption spectra of polyaniline nanomaterials are free from quinoid ring (at 650 nm), which confirm the efficient doping of dopant. Generally, the absorption spectra of polyaniline show three characteristic absorption at 360, 450 and 800 nm, which are assigned as the transitions from  $\pi$ - $\pi^*$  band, polaron band to  $\pi^*$  band,  $\pi$  band to polaron band, respectively<sup>22,23</sup>. Whereas in nanospheres the peak at 360nm is absent and the near-IR region absorption was completely different (above 850nm).

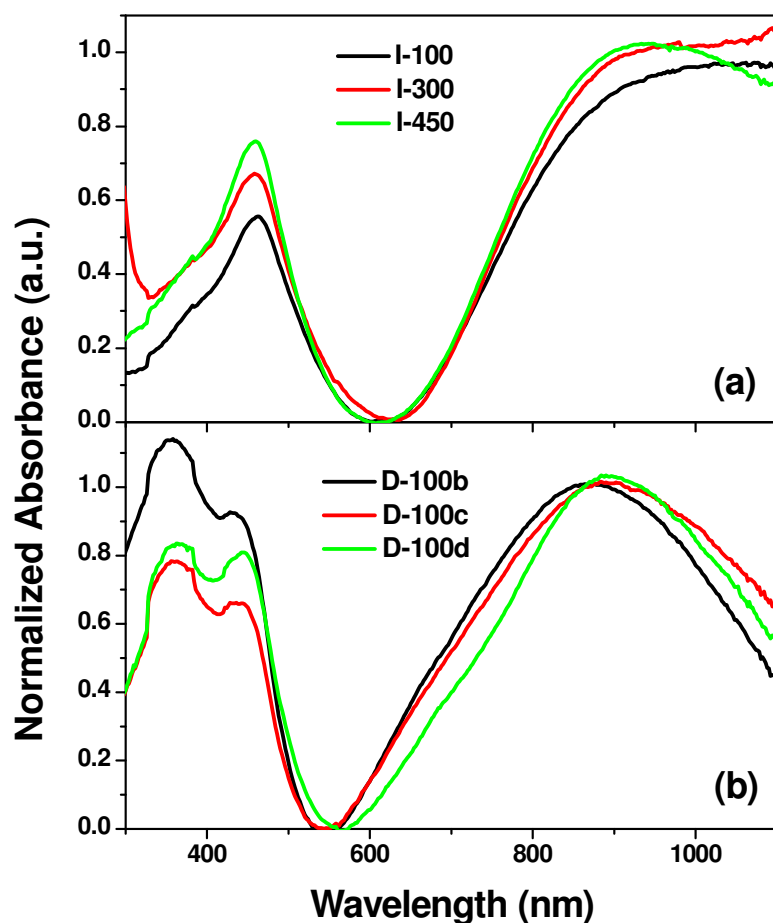


**Figure 3.12.** UV-Vis spectra of polyaniline nanomaterials.

MacDiarmid and co-workers studied the secondary doping of simple polyaniline-CSA doped materials (not nanomaterials) by *m*-cresol solvent<sup>23,24</sup>. They found that the more coil-like conformation in polyaniline chains produce peak characteristics at 800 nm whereas expanded chain conformation showed a free carrier tail commencing at 950-1000 nm in near IR-region<sup>22,25</sup>. The absorption spectra of the nanospheres showed the disappearance of peak at 360 nm and free carrier tail-characteristics in the near-IR region above 850 nm which confirms the delocalization of polaron band with respect to more expanded chain conformation in the polyaniline nanospheres (prepared via interfacial route). It is important to note that the presence of spheres plus fibres in **I-450** (see figure 3.12a) partially disturb the expanded conformation of the polymer chains, which is further reflected on the absorbance spectra. The samples **I-100** and **I-300** (see figure 3.12a) predominantly have only nanospheres and their absorbance spectra confirmed that they are in expanded

polymer chain conformation. In the same time the polyaniline nanorods (or fibers) produced via dilution route (or emulsion) showed a characteristic peak at 800 nm corresponding to more coil-like chain conformation (see figure 3.12b). The conformational changes in the polyaniline nanomaterials actually arise from their difference in the mode of chemical reactions in the polymerization processes. The interfacial polymerization is mainly driven by the selective solubility of the polymer chains specifically in one of the solvent medium at the interface for driving the equilibrium to form of higher molecular weight chains. In interfacial polymerization route, the resultant hydrophilic (also charged) polyaniline emeraldine salt has more affinity towards water rather than the organic phase. The higher water affinity of the charged chains drives the polymerization equilibrium towards the aqueous phase for the formation of higher molecular weight chains. Since the polymer chains have more tendencies to adopt expanded conformation in good solvents, the diffused charged chains in their expanded conformation in water behave as a nucleating site for subsequent growth of polymer chains. On the other hand, in the dilute route (or emulsion route) such a solvent-driven uni-directional growth is not possible, and therefore, the nanorods were obtained in entangled coil-like conformation compared to that of the interfacial route. The four probe conductivity of nanospheres were obtained in the range of  $\sim 10^{-2}$  S/cm, which is one order higher than that of nanofibers and nanorods ( $\sim 10^{-3}$  S/cm) (see table 3.1 and 3.2). The conductivity of the polyaniline nanomaterials matched with that of the reported values. It suggest that the expanded conformation of polyaniline chains in spheres increase the delocalization of charge carriers (evident by UV-Vis spectra, see figure 3.12a) and produced conductivity one order higher than that of nanofibers. Since the degree of doping (S/N ratio see table 3.1 and 3.2) in both fibres and spheres are comparable, so it is concluded that the more expanded conformation chains increase the electrical conductivity of the polyaniline nanomaterials.

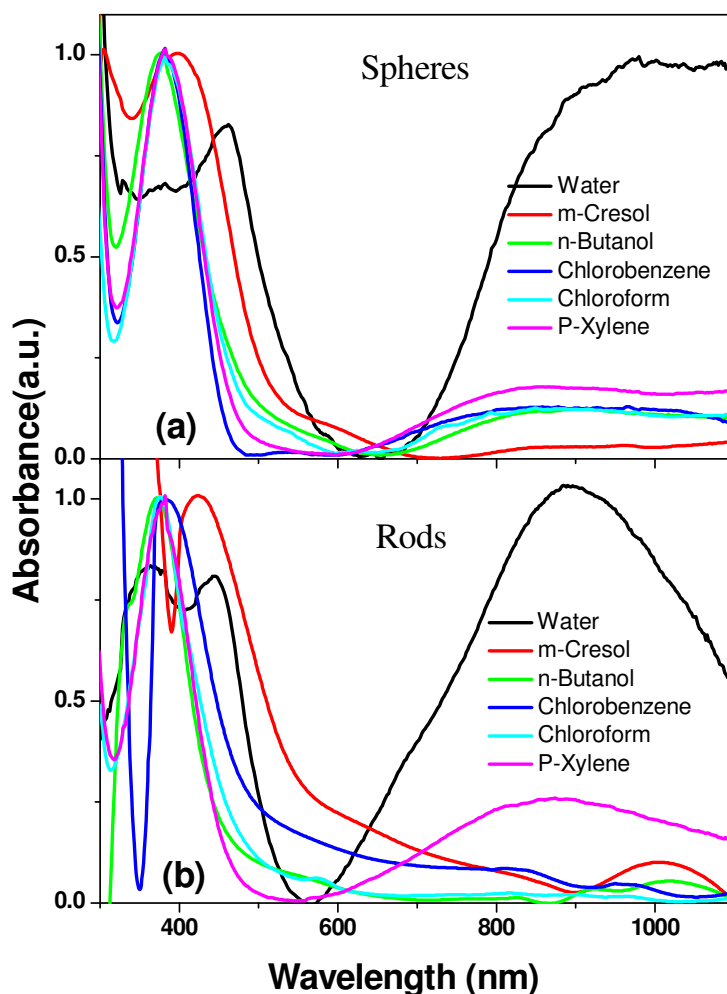


**Figure 3.13.** UV-Vis spectra of polyaniline nano-spheres and rods in various solvents.

In general, polyaniline nanomaterials are not soluble due to the highly aromatic nature of the polymer back bone. This is one of the major disadvantages of this versatile material that hampers its uses. In the present case, the amphiphilic surfactant molecule makes these conducting nanostructures easily dispersible in almost all organic solvents and results a transparent suspension which behaves like a solution. The presence of hydrophobic tail in the amphiphilic dopant increases the solubility of both polyaniline nanospheres and nanorods in common organic solvents. The materials can be easily suspended in chloroform, n-butanol, chlorobenzene, xylene and m-cresol, etc. To study the effect of solvents on the expanded chain to coil-like conformation, the UV-vis spectra of the **I-300** (spheres) and **D-100d** (rods)

were recorded in various solvents and shown in figure 3.13. In organic solvents also the nanomaterials showed all the characteristic absorptions of polyaniline. It is clear from the spectra that optical density of the polaron transition is affected by the organic solvents, however, the conformations of the polymer nanomaterials are retained and less influenced by the solvent in which they were suspended. The absorption of polaron peaks at the lower wavelength region ( $\sim 400$  nm) was blue shifted for samples recorded in organic solvents (except m-cresol) compared to that of water. The optical density of the absorption band corresponding to the polaron of polyaniline rods and spheres (above 950 nm) were more susceptible in organic solvents, however the chain conformations were not affected. It confirms that the conformations of the polymer chains in the nanomaterials are predominately controlled during the chemical polymerization techniques and not affected by the solvents in which they were dispersed. Since the conformation of polymer chains in polyaniline nanomaterials (both nanospheres and nanofibers) are almost unaltered by the various solvent, it can be assumed that once the polymer chains are confined to particular topology at nanometre level they are less influenced by the external stimuli such as solvent nature and its polarity.

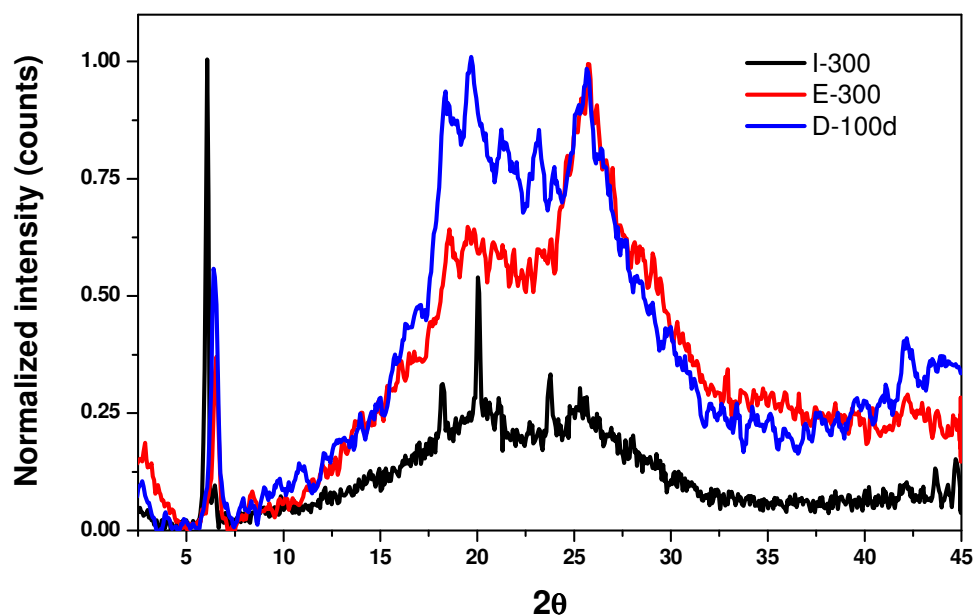


**Figure 3.14.** WAXRD plots of polyaniline nano-fibres, spheres and rods.

To further confirm the conformational changes in the polyaniline chains (nanofibers, nanorods and nanospheres) and also to study the solid state behaviour of the dopant molecule with polyaniline nanomaterials, the finely powdered samples were subjected for wide angle X-ray diffraction analysis at 30 °C. It is reasonable to expect that the expanded chain conformation of the polymer chains in nanospheres will show further increase in the solid state ordering (or crystalline) than nanofiber and nanorods, which possess a coil-like polymer chain conformation<sup>22</sup>. WXR D patterns of **I-100**, **E-100** and **D-100d** are given in figure 3.14. All the three samples are semi-crystalline with characteristic peaks. The WXR D patterns of nanofibers and nanorods (**E-100** and **D-100d**) showed three distinct peaks at  $2\theta = 6.4$ , 20.1 and 25.5 (d-spacing = 13.6, 4.4 and 3.5 Å, respectively). The two peaks at 20.1 and 25.5, which is mostly superimposed with amorphous background scattering, are generally observed in doped polyaniline, but the peak at  $2\theta = 6.4$  is only observed for highly ordered samples in which the polyaniline chain distance increased by effective interdigitations of dopant molecules<sup>26-28</sup>. In the case of nanospheres (**I-100**), a new intense peak at  $2\theta = 6.05$  (d-spacing 14.3 Å) is observed in addition to a peak at  $2\theta = 6.4$  (d-spacing 13.6 Å, as observed in fibres and rods). The presence of new peak at  $2\theta = 6.05$  indicates that the polymer chains in nanospheres possess more expanded chain conformation for increased solid state ordering compared to that of the nanofibers or nanorods. It was also noted that in nanospheres the amorphous region at higher angles ( $2\theta = 15$  to  $35^\circ$ ) very much suppressed and peaks become well resolved and sharp. This is due to the more expanded nature of the polymer chains in this sample which can pack in a more ordered fashion to increase the solid state ordering. The WXR D analysis of polyaniline nanomaterials demonstrated that nanospheres (interfacial route) have a high degree of ordering due to more expanded like polymer chain conformation compared to nanofibers and nanorods (emulsion or dilute route) possessing coil-like chain conformation. This suggests that the polymerization routes as well as corresponding soft-template have significant effect on the crystallinity of polyaniline nanomaterials.

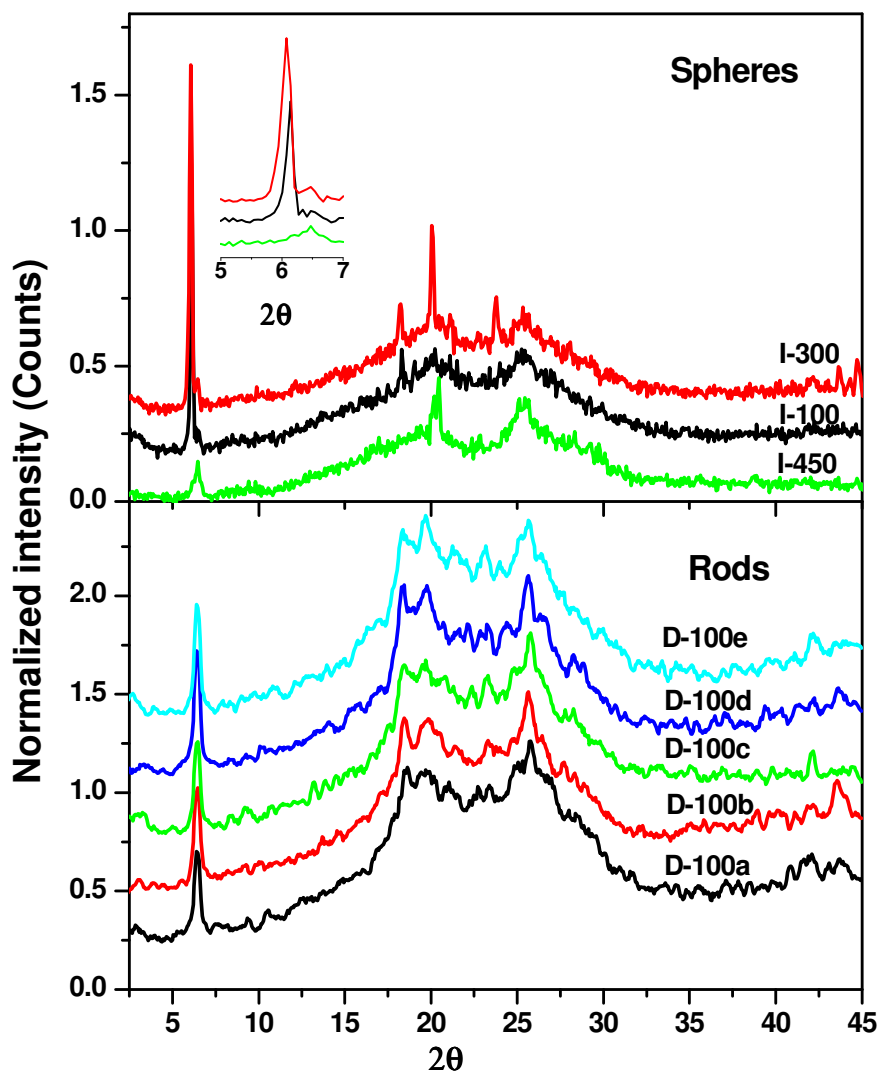


**Figure 3.15.** WXR D plots of polyaniline nanomaterials synthesised by interfacial and dilution routes.

Among interfacial samples there are some noticeable differences in solid state packing between samples. Samples **I-100** and **I-300** the peak at  $2\theta = 6.05$  (d-spacing  $14.3 \text{ \AA}$ ) is observed in addition to a peak at  $2\theta = 6.4$  (d-spacing  $13.6 \text{ \AA}$ ). The lower angle peak at  $2\theta = 6.05$  is more intense for uniformly distributed nanospheres **I-300** compared to broadly distributed sample **I-100** (see figure 3.15). **I-450** has mixture of nanospheres+ fibres, and therefore, the expanded conformation of polymer chains were disturbed, which account for the vanishing of the low angle peak at  $2\theta = 6.05$ .

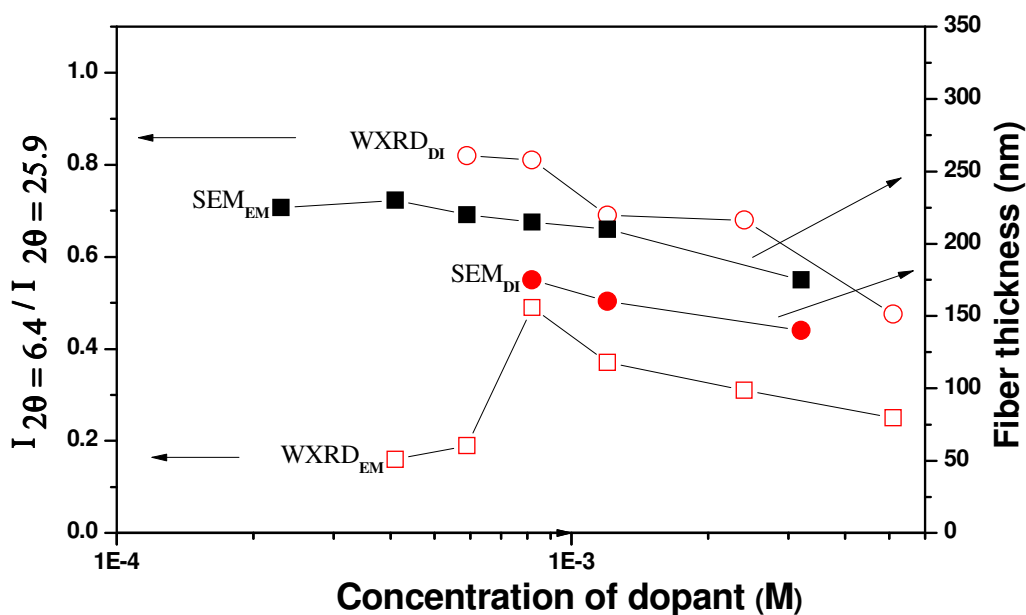


**Figure 3.16.** Plots of  $I_{2\theta=6.4}/I_{2\theta=25.9}$  and fiber thickness versus the amount of dopant in the feed). The symbol DI indicates dilute route and EM for emulsion route.

Lunzy et al. studied various kinds of polyaniline materials and shown that the ratio of the intensities of the peaks at  $2\theta = 6.4^\circ$  and  $26^\circ$  is directly related to crystallinity of polyaniline samples<sup>29</sup>. The ratio of the intensities of the peaks at  $2\theta = 6.4^\circ$  and  $25.9^\circ$  of both emulsion and dilute route polyaniline nanomaterials and fiber thickness (from SEM images) are plotted against the concentration of dopant present in the reaction feed and are shown in figure 3.16. In the case of emulsion route sample the peak intensity ratio initially increases up on decreasing dopant concentration and reaches a maximum value for sample **E-450** (see chapter-2) and then gradually decreases for low concentration of dopant. But in the case of dilution route, the peak intensity ratio increases as the volume of added water increases and finally attained the maxima at nanorods. Similarly the average fiber thickness of the emulsion route samples ranges 150-200 nm, whereas the thickness of the dilute route nanofibers is lower than 150 nm. This clearly indicates that upon dilution, the aggregated templates break in to smaller templates which lead to the formation of thinner fibers. From XRD studies it is clear that in the case of nanorods the polymer chains are more ordered compared with nanofibers. The reason for the enhanced ordering in the dilute route may be correlated to the effective penetration ability of the dopant in to the polymer



matrix because of the availability of isolated polymer chains. Therefore, besides the amount of dopant in the reaction mixture, the type of the polymerization routes also play a major role in controlling the solid state properties of nanomaterials. The WXR D investigations of various polyaniline nanomaterials clearly demonstrate that the polymerization routes have significant effect on the crystallinity of polyaniline nanomaterials.

### 3.3.6. Luminescence Properties of the Polyaniline Nanomaterials:

The dopant possesses an integral photo-responsive azobenzene chromophore, which gives an opportunity to study the photo-physical behaviour of dopant and nanomaterials in solution by spectroscopic methods. Azobenzene molecule has lone pair of electrons on the nitrogen atoms, and therefore, the absorption spectra shows  $n-\pi^*$  ( $S_0 \rightarrow S_1$ ) transition in addition to the  $\pi-\pi^*$  ( $S_0 \rightarrow S_2$ ) transition<sup>30,31</sup>. The absorbance spectrum of dopant 1 has three characteristic peaks at 245, 360 and 460 nm corresponding to  $\pi-\pi^*$  (cis),  $\pi-\pi^*$  (trans) and  $n-\pi^*$  (cis), respectively (see figure 3.17).

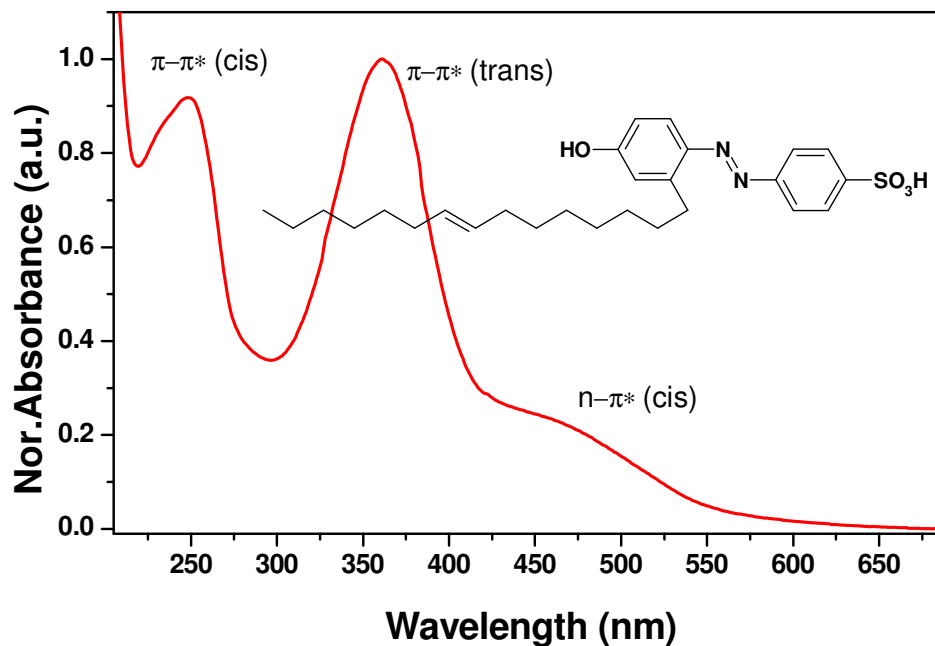
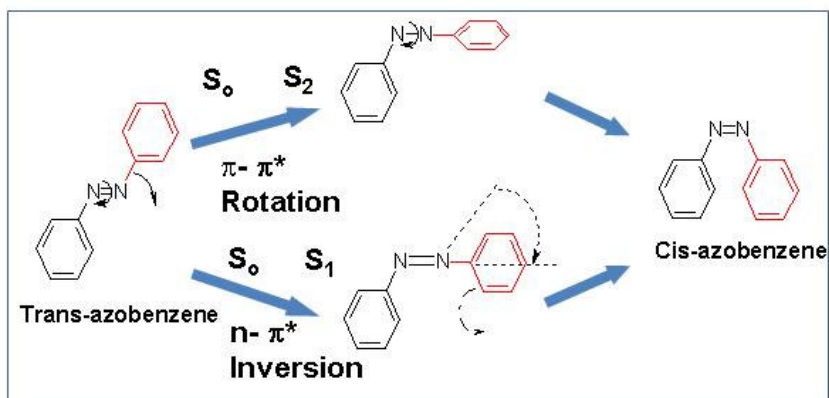


**Figure 3.17.** UV-Vis spectra of dopant 1 in water.

The photoisomerization of azobenzene molecules are highly dependent on the excitation wavelength: the  $n-\pi^*$  excitation induces the isomerization via inversion mechanism whereas the cis-trans isomerization proceeds via rotation mechanism for

the  $\pi$ - $\pi^*$  excitation (see figure 3.18a)<sup>30,32</sup>. The  $n$ - $\pi^*$  state ( $S_1$ ) of trans-azobenzene is generally non-fluorescent because of the forbidden transition and isomerization in the  $S_1$  manifold<sup>30</sup>. Researchers had found that the  $S_2 \rightarrow S_0$  of trans azo-benzene chromophores showed enhanced fluorescence for self-organized supramolecular aggregates such as bi-layers or micelles in water (see figure 3.18b)<sup>32,33</sup>. Similar observations were also known for fluorescence enhancement from self-assembled amphiphilic trans-azobenzene chromophores in organic solutions under UV-radiations<sup>34-36</sup>. Basically in these self-assembled structures the photoisomerization is more or less prevented and so the excitation energy is used for emission instead of isomerisation<sup>37</sup>. Interestingly the renewable resource amphiphilic dopant is found to be luminescent for excitation at 360 nm.

### (a) Photoisomerization



### (b) Prevention of Photoisomerization

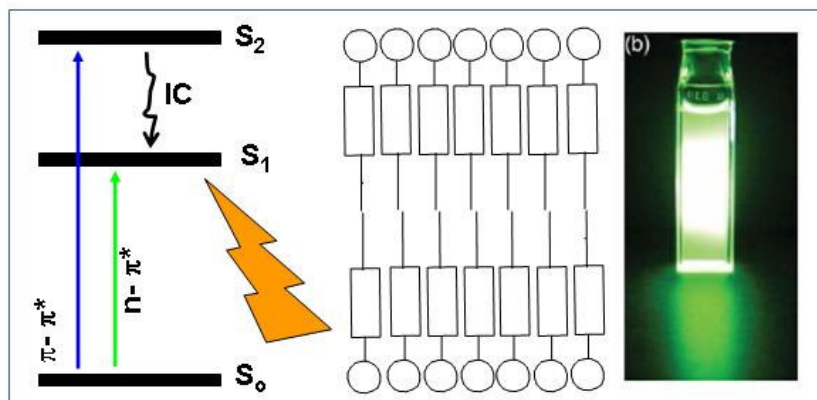


**Figure 3.18.** Emission from azobenzene chromophore-photoisomerization of azobenzene (a) restricted photoisomerization in bi-layer aggregates (b).

The fluorescence spectra of the dopant at different concentrations in water excited at 360 nm is given in figure 3.19. It is very clearly evident from the plots that the fluorescent intensity of the dopant is highly dependent on its concentration in water. The emission spectra of dopant has a shoulder at 420 nm corresponding to the resonance Raman of water and, as expected, it vanished completely for the increased dopant concentration in water. The emission maximum of azobenzene chromophore is centered at 450 nm and it is not disturbed by the resonance Raman of water for further analysis. It is understood in the literature that in restricted azo-benzene chromophores, the photoisomerization (via rotation mechanism) for  $S_2$  excitation is normally restricted due to steric hindrance<sup>38</sup>. It suggests that the luminescent behavior of dopant-1 could arise by the prevention of the cis-trans photo-isomerization at the excited state by steric hindrance induced by the long alkyl chain in dopant **1**, which facilitate the radiative decay from  $S_2 \rightarrow S_0$ . The formation of the supramolecular aggregates like layers and micelles in water by the amphiphilic dopant is also accountable for enhancement of emission (see chapter 2).

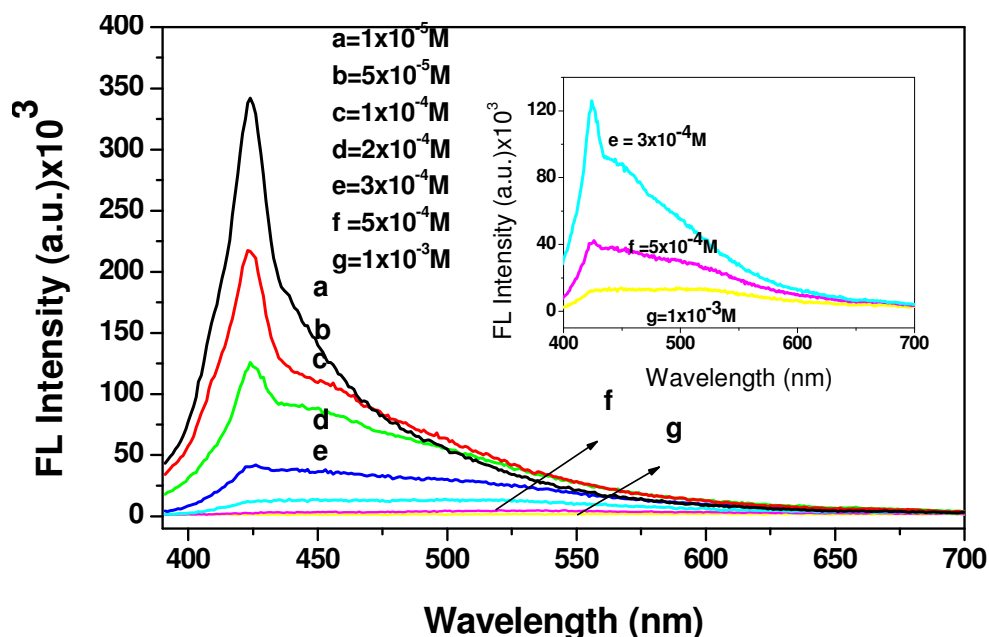


**Figure 3.19.** Fluorescent spectra of dopant **1** at various concentration in water.

In general, at low concentration, the amphiphilic azobenzene molecules (like dopant **1**) are known to form weak aggregates like layers through head-to-tail packing of chromophores in water and increase in concentration leads to higher order supramolecular aggregates (evident from DLS study, chapter 2)<sup>39</sup>. The fluorescence

intensity of the dopant in water was plotted for various concentrations and shown in figure 3.20. The emission intensity of the dopant increases with the increase in the dopant concentration ( $1 \times 10^{-6}$  to  $1 \times 10^{-5}$  M) and attained maxima at  $1 \times 10^{-5}$  to  $7 \times 10^{-5}$  M. Further increase in the dopant concentration ( $6 \times 10^{-5}$  to  $6 \times 10^{-4}$  M) decreases the emission intensity and the fluorescence nature is completely lost above  $1 \times 10^{-3}$  M. This non-linear trend suggests that the dopant 1 exist in more than one form in water depending up on its concentration. At low concentration, the dopant 1 may exist as isolated molecules and with increase in concentration they tend to aggregate to form a layer structure. At still higher concentration, the layer structure of the dopant is disturbed by the formation of micelles, which known to quench the luminescent intensity. At concentrations higher than  $10^{-3}$  M, both the higher concentration of dopant and also the existence of micelles are accountable for quenching the luminescent intensity. This is also further supported by the shift in the emission maxima of the dopant 1 (see figure 3.19, in set).

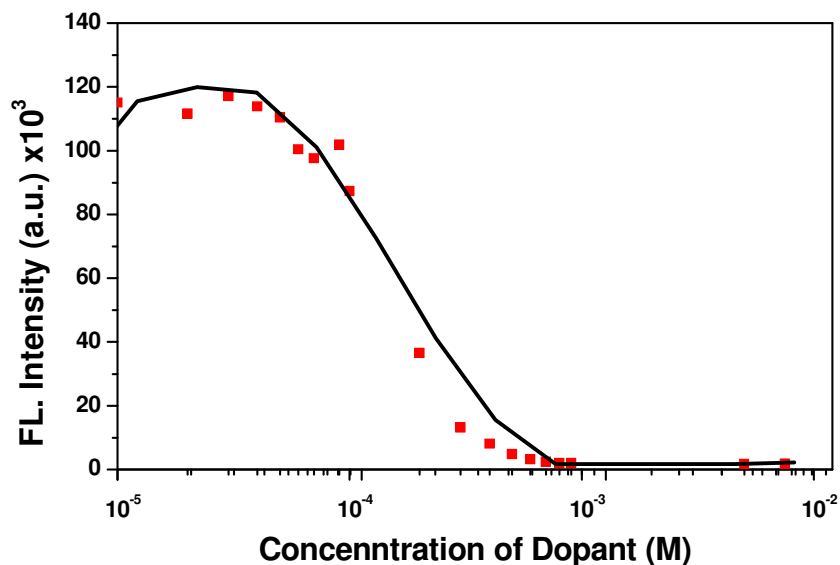


**Figure 3.20.** Plot of fluorescent intensity versus of dopant 1 concentration in water.

The emission maximum was not affected at very low concentration; however at very high concentration (expanded emission spectra were provided as in-set) there is a red shift of more than 100 nm. This large red shift reveals that luminescent azobenzene chromophore transformed from layer structures to aggregated micelles, which rapidly quenches the luminescent intensity. This transformation from layer-like to spherical micelle is also supported by DLS studies (see chapter 2).

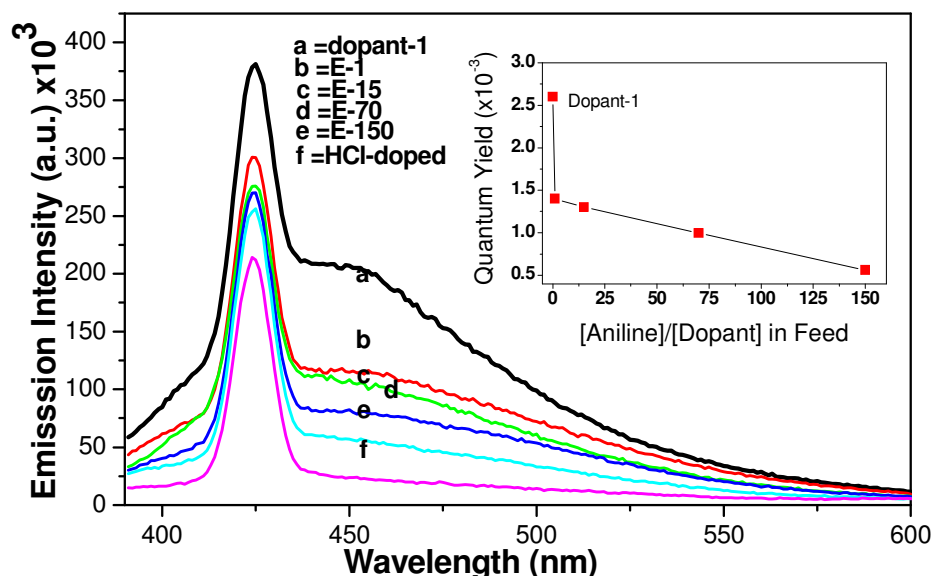


**Figure 3.21.** Fluorescent spectra of dopant and polyaniline fibers in water.

Polyaniline nanofibers doped by luminescent azobenzene dopant were expected to exhibit emission properties. The emission properties nanomaterials were studied in water and the spectra were recorded followed by exciting at 360 nm corresponding to the  $\pi$ - $\pi^*$  (trans) of the azobenzene part in the renewable resource dopant. The emission spectra for dopant 1, and few representative nanofibers **E-1**, **E-15**, **E-70** and **E-150** are shown in figure 3.21. The optical densities of all the solutions were maintained as 0.1. The resonance Raman peak for water at 420 nm is very intense because of the low concentration of the molecules in water (similarly observed in figures 3.21), however, the nanomaterials showed a broad peak at 450 nm corresponding to the luminescence of azo- groups. The HCl-doped polyaniline nanomaterials did not show any peak at 450 nm, which confirm that the luminescent behavior of **E-1.5** to **E-150** is mainly arising from the dopant 1 and not arise from the polyaniline backbone. The luminescence intensity of the nanomaterials drastically decreases with the decrease in dopant concentration in the feed. The quantum yield of the nanofibers were obtained using quinine sulfate as reference in water and shown in figure 3.21 (see in-set). The quantum yield of dopant is  $2.6 \times 10^{-3}$ , which is in the same range for azobenzene amphiphilic chromophores<sup>40</sup>.

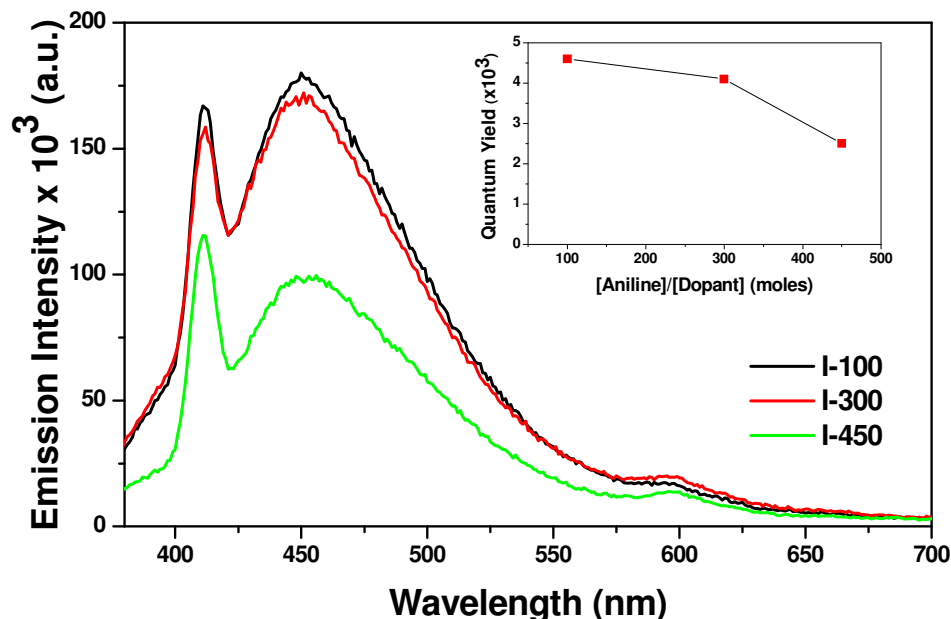


**Figure 3.22.** Fluorescent spectra of the nanospheres in water.

The emission spectra for interfacially synthesised nanomaterials **I-100**, **I-300** and **I-450** were shown in figure 3.22. All the nanomaterials showed a broad peak at 450 nm corresponding to the luminescence of azo-group. The luminescence intensity of the nanospheres (azo-groups) is relatively higher than that of polyaniline nanofibers produced by emulsion route. The quantum yield of the nanospheres in water is shown in figure 3.22 (see in-set). This relatively higher quantum yield for nanospheres than nanofibers is correlated to the more expanded chain conformation, which will help the effective packing of azo chromophore in nanospheres. The nanorods obtained by dilute route are found to be very weakly luminescent since the dilute reaction conditions will make the dopant well dispersed in polymer matrix and prevent chromophore-chromophore interactions in resulting sample. In the present case, a single molecular dopant approach was utilized to tune the morphology and other properties of polyaniline nanomaterials via selective self-organization in the interfacial, dilution and emulsion routes. Therefore, it may be assumed that the pre-templating behaviour of the dopant complex and also the types of the polymerization determine the luminescent property of polyaniline nanomaterials.

### 3.4. Conclusion

The self-organization properties of the renewable resource based amphiphilic azobenzene sulfonic acid dopant have been utilized to template various polyaniline nanomaterials like nanofibers, nanotubes, nanospheres and nanorods. The amphiphilic molecule is efficient structure directing dopant for polyaniline nanomaterials and has template selectivity depending upon the [dopant]/ [aniline] ratio as well as concentration of dopant and aniline. DLS and TEM techniques have been successfully utilized to trace the nature and shape of polymerization templates to understand the mechanism the nanomaterials formation. The present investigation brought the following outcomes: (i) the dopant micelles have shape selective self-organization with aniline and APS, (ii) at concentration higher than CMC of the dopant, well defined micrometer sized cylindrical micelles filled with aniline acts as templates for the growth of long nanofibers, (iii) as the concentration of the dopant below CMC, the layers filled with aniline are acting as templates for the growth of nanotubes, (iv) in the dilute polymerization, the size of the aggregates become 175 nm and consists of spherical plus short cylindrical micelle aggregates, which upon chemical oxidation yields nanorods, (v) in interfacial route, the dopant micelles form spherical aggregates with APS in the aqueous layer and the diffusion of aniline (through interfacial layer) into these spherical aggregates and get oxidized to form polyaniline spheres of 200-400 nm, (vi) the structure of the cylindrical and spherical micelle templates were characterized by DLS and TEM, (vii) absorption spectra of the nanomaterials revealed that the nanospheres possesses expanded confirmation and the fibres, rods and tubes were found to have coil-like confirmation and (viii) wide angle X-ray diffraction showed that the nanomaterials exhibit good solid state ordering because of the high penetrating power of amphiphilic dopant in to polymer matrix (ix) the polyaniline nanomaterials exclusively doped with fluorescing azobenzene sulfonic acid dopant showed enhanced emission in water and the amount of the dopant in the nanomaterial and chain conformation plays a crucial role in luminescent intensity and quantum yields. In summary, it is shown that divergent polyaniline nanomaterials such as fibres, rods, tubes and spheres can be synthesized from identical reactant ingredients by carefully choosing the amphiphilic dopant templates under emulsion, dilution and interfacial polymerizations.

**3.5. References:**

1. Wan, M. X. *Adv. Mater.* **2008**, *20*, 2926–2932
2. Wan, M. X. *Macromol. Rapid. Commun.* **2009**, *30*, 963–975
3. Zhang, D. H.; Wang, Y. Y. *Mater. Sci. Eng. B*, **2006**, *134*, 9-19
4. Li, D.; Huang, J.; Kaner, R. B. *Acc. Chem. Res.*, **2009**, *42*, 135-145
5. Zhang, X.; Manohar, S. K. *Chem. Commun.* **2004**, 2360-2361
6. Wei, Z.; Zhnag, Z.; Wan, M. *Langmuir*, **2002**, *18*, 917-921.
7. Zhang, Z.; Wei, Z.; Wan, M. *Macromolecules* **2002**, *35*, 5937-5942.
8. Haung, J.; Virji, S.; Weiller, B. H.; Kaner, R. B. *J. Am. Chem. Soc.* **2003**, *125*, 314.
9. Haung, J.; Kaner, R. B. *J. Am. Chem. Soc.* **2004**, *126*, 851-855
10. Haung, J.; Virji, S.; Weiller, B.H.; Kaner, R.B. *Chem.Eur.J.* **2004**, *10*, 1314-1319
11. Chiou, N. R.; Epstein, A. J. *Adv. Mater.* **2005**, *17*, 1679-1683
12. Chiou, N. R.; Epstein, A. J. *Synth. Met*, **2005**, *153*, 69-72
13. Zhou, C.; Han, J.; Guo, R. *J. Phys. Chem. B.*; **2008**; *112*; 5014-5019
14. Li, X. G.; Lu, Q. F.; Huang, M. R. *Chem. Eur. J.* **2006**, *12*, 1349-1359.
15. Zheng, W.; Angelopoulos, M.; Epstein, A. J.; MacDiarmid, A. G. *Macromolecules* **1997**, *30*, 7634-763.
16. Kang, E. T.; Neoh, K. G.; Tan, K. L. *Prog. Polym. Sci*, **1998**, *23*, 211-324
17. Jayakannan, M.; Annu, S.; Ramalekshmi, S. *J. Polym. Sci. Polym. Phys.* **2005**, *43*, 1321
18. Zhang, X.; Kolla, H.S.; Wang X.; Raja, K.; Manohar S.K. *Adv. Funct. Mater*, **2006**, *16*, 1145-1152.
19. Hassan, P. A; Sawant, S. N; Bagkar, N. C; Yakhmi, J. V. *Langmuir*, **2004**, *20*, 4874-4880
20. Zhang, L.; Wan, M. X. *Adv.Funct.Mater.* **2003**, *13*, 815-820
21. Bucholz, T.; Sunb, Y.; Loo, Y.L. *J. Mater. Chem.*, **2008**, *18*, 5835–5842
22. Xis, Y.; Wiesinger, J. M.; MacDiarmid, A. G. *Chem. Mater.* **1995**, *7*, 443-445
23. MacDiarmid, A. G.; Epstein, A, J.; *Synth. Met.* **1995**, *69*, 85-92.



24. Min, Y.; Xia, Y.; MacDiarmid, A. G.; Epstein, A. J. *Synth Met*, **1995**, *69*, 159-160
25. Li, W.; Zhu, M.; Zhang, Q.; Chen, D. *Appl. Phys. Lett*, **2006**, *89*, 103110
26. Jana, T.; Nandi, A. K. *Langmuir*, **2000**, *16*, 3141.
27. Laska, J.; Djurado, D.; Lunzy, W. *Eur. Polym. J.* **2002**, *38*, 947-951.
28. Levon, K.; Ho, K.H.; Zheng, W.Y.; Laakso, J.; Karna, T.; Taka, T.; Osterholm, J.E. *Polymer*, **1995**, *36*, 2733-2738
29. Lunzy, W.; Banka, E.; *Macromolecules* **2000**, *33*, 425.
30. Tamai, N.; Miyasaka, H. *Chem. Rev.* **2000**, *100*, 1875-1890.
31. Ghedini, M.; Pucci, D.; Calogero, G.; Barigelletti, F. *Chem. Phys. Lett.* **1997**, *267*, 341.
32. Shimomura, M.; Kunitake, T. *J. Am. Chem. Soc.* **1987**, *109*, 5175-5183.
33. Moss, R. A.; Jiang, W. *Langmuir*. **1997**, *13*, 4498-4501
34. Han, M. R.; Hirayama, Y.; Hara, M. *Chem. Mater*, **2006**, *18*, 2784-2786.
35. Han, M.; Hara, M. *J. Am. Chem. Soc.*, **2005**, *127*, 10951-10955.
36. Rau, H.; Luddecke, E. *J. Am. Chem. Soc.* **1982**, *104*, 1616.
37. Yoshino, J.; Kano, N.; Kawashima, T. *Chem. Comm.* **2007**, *6*, 559.
38. Tsuda, K.; Dol, G. C.; Gensch, T.; Hofkens, J.; Latterini, L. Weener, J. W.; Meijer, E. W.; De Schryver, F. C. *J. Am. Chem. Soc.* **2000**, *122*, 3445
39. Marquez, F.; Marti, V.; Palomares, E.; Garcia, H.; Adem, W. Adam, J. *Am. Chem. Soc.* **2002**, *124*, 7264-7265
40. Constantino, C. J. L.; Aroca, R. F.; Mendonca, C. R.; Mello, S. V.; Balogh, D. T.; Oliveira, O. N. *Spectrochim. Acta. Part A* **2001**, *57*, 281.

***Chapter-4***

---

***Cylindrical and Vesicular Templates for Polyaniline  
Nanofibers and Nanotapes***

### 4.1. Introduction

Polyanilines uniqueness with its rich chemistry made one of the most studied research topic in conducting polymer<sup>1-5</sup>. But its reduced solubility in common solvents is one of the main factors that hamper its wide applications. So it is believed that if the growth of the polymer is confined in micro/nano dimension most of the processibility related issues can be solved<sup>6</sup>. The initial attempt in this direction is the introduction of dispersion polymerization in which a stabilizer is used to prevent the macroscopic precipitation of the polymer<sup>7,8</sup>. The first developed and employed stabilizers were polymeric type like poly (2-vinylpyridine-cop-aminostyrene), which produce stable colloidal dispersion of polyaniline<sup>9</sup>. These types of stabilizers were very effective in controlling the morphology of polyaniline in to micro/sub-micron particles like rice-grains and needles. After these initial findings a series of steric stabilizers like ploy (vinyl alcohol-co-acetate), poly (vinyl methyl ether), poly (vinylpyridine-co-p-aminostyrene), poly styrene latexes and even silica particles were used<sup>10-13</sup>.

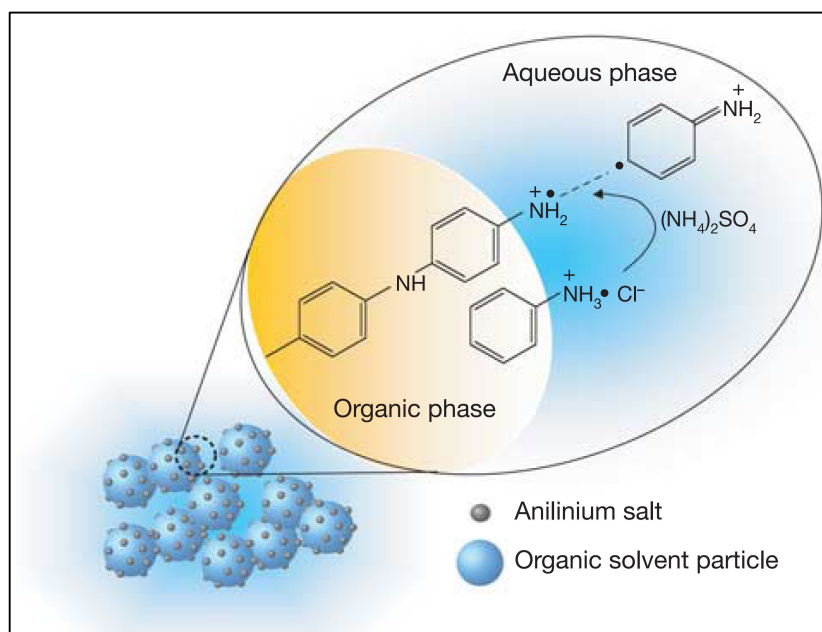


**Figure 4.1.** Schematic representation of dispersion polymerization of aniline (adapted from reference 15).

The dispersion approach was very successful in controlling morphology and improving the processibility of the material, but the product obtained is always a composite of polyaniline and stabilizer material. So in order to get pure polyaniline a

tedious post-synthetic treatment is required which mostly disrupts the morphological features of polyaniline. Self-stabilized dispersion method was also reported for dispersion polymerization routes in which the anilinium ions acts as interfacial stabilizer for the water-oil dispersion, however, poor control over the polyaniline morphology was observed<sup>14,15</sup>. Another approach known as counter-ion induced processibility of polyaniline was developed in which bulky sulfonic acids were employed as dopants for polyaniline<sup>16</sup>. It was found that when the emulsion polymerization is carried out in non-polar or weakly polar solvents in the presence of functionalized protonic acids fibrillar morphology can be produced, which have an exceptional degree of crystalline order and orientation<sup>17</sup>. It was also reported that polyaniline nanoparticles can be synthesized by using simple surfactants like sodium dodecyl sulfate (SDS)<sup>18</sup>. The polyaniline particles produced by surfactant micelles are very uniform and high quality than that of steric stabilizers, which underlines the importance of typical amphiphilic surfactants over sterical polymeric counterparts.

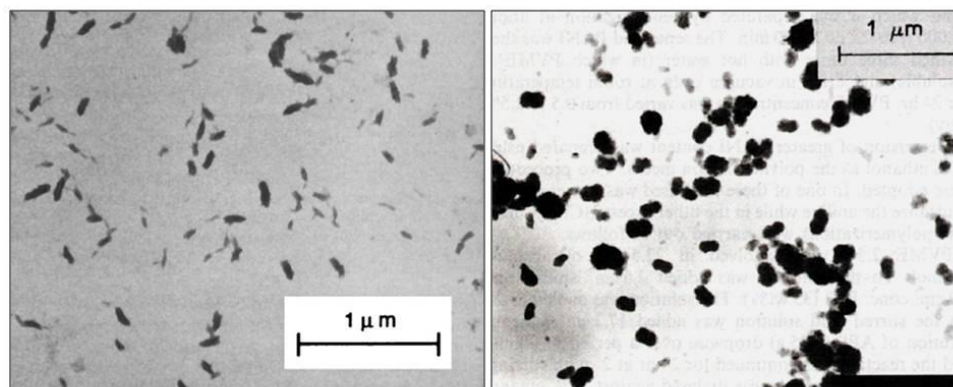


**Figure 4.2.** Polyaniline – rice-grains and sub-micron particles (Adapted from reference 11,12).

Among various approaches for polyaniline nanomaterials the emulsion and dispersion routes have paid more importance due to the formation of high quality materials and adaptable to simple synthetic conditions. The most commonly used dopants for polyaniline nanomaterials synthesis are commercial available mineral acids or custom designed sulfonic acids such as camphor sulfonic acid (CSA), naphthalene sulfonic acid (NSA), p-toluene sulfonic acid (PTSA) and azobenzene sulfonic acid (ABSA)<sup>19</sup>. Due to poor amphiphilic nature of the above mentioned dopants the morphology of polyaniline nanomaterials were found highly susceptible to the dopant/aniline ratio and other synthetic conditions<sup>20</sup>. Additionally, there is a

large discrepancy in the selection of dopant for specific polymerization routes: for example, an emulsion friendly dopant is not a suitable good candidate for dispersion routes and vice-versa. CSA is very good candidate for dispersion route and not suitable for emulsion polymerization. Similarly, DBSA forms stable micellar template for emulsion route, but not suitable for dispersion routes etc. The amphiphilic dopant 4-[4-hydroxy-2 ((Z)-pentadec-8-enyl) phenyl]-azobenzene sulfonic acid (see chapter 2) which is a good template for emulsion, interfacial and dilution route was found not suitable for dispersion polymerization due to poor solubility in organic solvents. Therefore, the development of a novel single dopant based templates for both emulsion and dispersion routes are still unsolved problem in polyaniline nanostructures. So it is an important issue to be addressed because of the following reasons: (i) single dopant based approach for emulsion and dispersion routes is attractive since tuning of nanostructures can be obtained without altering the chemical constituents, (ii) understanding the mechanistic aspects of emulsion and dispersion routes is essential for fundamental nanomaterials research, (iii) study the effect of polymerization routes on the size and shape of the polyaniline nanomaterials, (iv) and finally among all the synthetic approaches known for nanomaterials, only emulsion and dispersion routes have the possibility for large scale production, which further driven us to develop new approaches based on single dopant.



**Figure 4.3.** Schematic representation of the approach for synthesis of polyaniline nanofibers and nanotapes by emulsion and dispersion routes respectively.

This chapter is focused on the development of a novel amphiphilic surfactant-cum-dopant Z-4-(3-pentadec-8-enylphenoxy)-butane-1-sulfonic acid (see figure 4.4) by ring opening of 1,4-butanedisulfone with cardanol (3-pentadec-8-enyl-phenol) under basic conditions. The newly designed dopant almost looks like commercial dodecyl

benzene sulfonic acid (DBSA), but bears aliphatic sulfonic acid groups. Unlike DBSA, the new molecule is a crystalline solid, thermally stable and easy to handle under atmospheric conditions. Again this dopant was renewable resource based and so very attractive greener approach to polyaniline nanomaterials research due to their wide availability and lower cost. The newly synthesized amphiphilic sulfonic acid dopant was employed as a structural directing agent for the creation of novel nanostructures by emulsion and dispersion polymerization routes. The dopant has built-in head to tail molecular design for amphiphilic nature and forms stable emulsion with aniline in water in wider compositions. The amphiphilic molecule was found to produce 5.3 nm micelles in water. The micelle behaviour of the dopant and its critical micelle concentration (CMC) was studied by surface tension, dye-encapsulation and dynamic light scattering measurements. The dopant micelle was found to produce cylindrical self-organized templates with aniline in emulsion route and produced well defined polyaniline nanofibers. In water/toluene solvent mixtures (in dispersion route), the dopant+aniline complex transformed into vesicles which exclusively yielded polyaniline nanotapes. The amphiphilic molecule solubilises the resultant nanomaterials in water and other organic solvents which facilitate the complete structural characterization by  $^1\text{H-NMR}$ , FT-IR and viscosity techniques. The mechanism of the nanomaterials formation was further studied in detail by DLS and HR-TEM. The nanomaterials were characterized by SEM, TEM, absorption spectroscopy and wide angle X-ray diffraction to understand the morphology, electronic and solid state ordering properties. X-ray analysis revealed that the resultant nanomaterials were highly crystalline and possessed lamellar-type self organization in the solid state which contribute their high electrical conductivity in the range of 1-10 S/cm.

## 4.2. Experimental Procedures

**4.2.1. Materials:** Aniline, ammonium persulfate (APS), 1, 4-butanediol, and potassium tertiary butoxide were purchased from Aldrich. Aniline was distilled and kept under nitrogen prior to use. Cardanol was purified by double vacuum distillation at 3-5 mm of Hg and the fraction distilled at 220 - 235 °C was collected (see chapter 2).

**4.2.2. General Procedures:** The NMR analysis of the samples was carried out in 500-MHz Bruker Avance ii NMR Spectrometer at 30 °C. The purity of the compounds was determined by JEOL JSM600 fast atom bombardment (FAB) mass spectrometry. For SEM measurements, polymer samples were subjected for thin gold coating using JEOL JFC-1200 fine coater. The probing side was inserted into JEOL JSM- 5600 LV scanning electron microscope for taking photographs. Transmission electron microscope images were recorded using a FEI Tecnai 30G<sup>2</sup> S Twin HRTEM instrument at 100 kV. For TEM measurements, the water suspension of nanomaterials were prepared under ultrasonic stirring and deposited on Formvar coated copper grid. Wide angle X-ray diffractions of the finely powdered polymer samples were recorded by Philips Analytical diffractometer using CuK-alpha emission. Dynamic light scattering (DLS) measurements were carried out using a Nano ZS Malvern instrument employing a 4 mW He-Ne laser ( $\lambda=632.8$  nm) and equipped with a thermo stated sample chamber. For all the DLS measurements HPLC quality (Merck, India) double distilled water is used. Infrared spectra of the polymers were recorded using a Perkin Elmer, spectrum one FTIR spectrophotometer in the range of 4000 to 400 cm<sup>-1</sup>. For conductivity measurements, the polymer samples were pressed into a 10 mm diameter disc and analyzed using a Keithley four probe conductivity instrument. The resistivity of the samples was measured at five different positions and at least two pellets were measured for each sample: the average of 10 readings was used for conductivity calculations. Thermal analyses of the samples were performed with a PerkinElmer Pyris-6 differential scanning calorimetry (DSC) instrument under nitrogen at a heating rate of 5 °C/min, and the instrument was calibrated with indium, tin, and lead standards. The thermal stability of the polymers was determined using TGA-50 Shimadzu Thermo gravimetric Analyzer (TGA) at a heating rate of 10

°C/min in nitrogen. Uv-Vis spectra of the PANI in water were recorded using Perkin Elmer Lambda-35 UV-VIS Spectro Photometer.

### 4.2.3. Synthesis of Amphiphilic Dopant

**Synthesis of (Z)-4-(3-pentadec-8-enyl) phenoxy butane-1-sulfonic acid (dopant 2):** Distilled cardanol (10 g, 33 mmol) was added into a round bottom flask containing potassium tertiary butoxide (7.52 g, 66 mmol) in dry ethanol (100 mL). The solution was warmed for 30 minutes under nitrogen atmosphere. It was cooled and 1, 4-butanediol (9 g, 66 mmol) was added dropwise and the reaction mixture was refluxed for 40 h under nitrogen atmosphere. It was cooled and the precipitate was isolated by filtration. The solid mass was dissolved in water (30 mL) and acidified by HCl solution (30 mL of 50% v/v HCl). The white mass obtained was purified by passing through silica gel column using 20/80 v/v methanol/chloroform as eluent. Yield = 6.5 g (45 %). m. p. = 56-62 °C. <sup>1</sup>H-NMR (DMSO-d<sub>6</sub>, 500 MHz) δ: 7.26 (t, 1H, Ar-H), 6.83 (b, 3H, Ar-H), 5.44 (b, 2H, -CH=CH-), 4.02 (t, 2H, Ar-OCH<sub>2</sub>), 3.42 (t, 2H, HO<sub>3</sub>SCH<sub>2</sub>), 3-0.8 (27H, Aliphatic); <sup>13</sup>C-NMR (DMSO-d<sub>6</sub>, 75 MHz) δ: 158.1, 143.8, 130.1, 129.6, 129.1, 120.3, 114.3, 111.4, 67.1, 51.1, 35.2, 30.8, 28.9, 28.6, 28.5, 26.5, and 13.9. FT-IR (KBr, cm<sup>-1</sup>): 3450, 2926, 2852, 1646, 1583, 1452, 1384.2, 1264, 1174, 1054, 970, 876, 786, 734, 692, 613 and 529. FAB-MS (MW: 438.0): m/z = 461.1 (M +Na).

### 4.2.3. Synthesis of Polyaniline Nanomaterials

**Dispersion Route for Polyaniline Nanomaterials:** The synthesis of polyaniline is described in detail for **DP-100** and other samples were prepared following the same procedure. The dopant (0.048 g, 0.11 mmol) was dissolved in doubly distilled water (20 mL) in a 50 mL glass vial. In a separate glass vial distilled aniline (1 mL, 1.02g, 11 mmol, [aniline]/[dopant]=100) was dissolved in toluene. To the dopant solution, aniline in toluene was added and the mixture was sonicated for 1 h to obtain a milky white dispersion. Ammonium persulfate solution (1.35 M) was added to the dispersion and stirred under ultrasonic for 5 minute at 30 °C. The polymerization was allowed to continue at 30 °C for 15 h without further disturbance. The dark green polyaniline solid mass was filtered, washed with distilled water and methanol for



several times till the filtrate become colourless. The solid product was dried in a vacuum oven at 60 °C for 48 h (0.01 mm Hg). Yield = 0.67 g (65 %). <sup>1</sup>HNMR (DMSO-d<sub>6</sub>, 500 MHz) δ: 7.55 (t, 2H, Ar-H, PANI), 7.48 (d, 2H, Ar-H, PANI), 7.25 (b, 1H, Ar-H, dopant), 7.11, 7.21, 7.31 (1/1/1 triplet, 1H, -NH<sup>+</sup>, PANI), 6.83 (b, 3H, Ar-H, dopant), 5.91(1H, -N-H, PANI), 5.43 (b, 2H, CH=CH, dopant), 0.5-4.5 (35H, aliphatic-H, dopant). FT-IR (KBr, in cm<sup>-1</sup>): 3011, 1577, 1502, 1306, 1225, 1158, 1032, 825, 706 and 627.

**Emulsion Route for Polyaniline Nanomaterials:** Typical procedure for the synthesis of polyaniline nanofiber is described in detail for **EM-100** and other samples were prepared following the same procedure. The dopant (0.048 g, 0.11 mmol) was dissolved in doubly distilled water (20 mL) in a 50mL glass vial. Distilled aniline (1mL, 1.02g, 11 mmol, [aniline]/[dopant]=100) was added to the dopant solution in water and stirred under ultrasonic for additional 1 h at 30 °C. At the end of the stirring, the formation of milky white emulsion was noticed. Ammonium per sulfate (1.35 M solution) was added at 30°C and stirred under ultrasonic for 1 more hour. The resultant green content was allowed polymerize at 30 °C for 15 h without disturbance. The solid mass was filtered, washed with distilled water and methanol for several times till the filtrate become colourless. The solid product was dried in a vacuum oven at 60 °C for 48 h (0.01 mm Hg). Yield = 0.78 g (76 %). <sup>1</sup>HNMR (DMSO-d<sub>6</sub>, 500 MHz) δ: 7.55 (t, 2H Ar-H, PANI), 7.48 (d, 2H,Ar-H, PANI), 7.25 (b, 1H, Ar-H, dopant), 7.11, 7.21, 7.31 (1/1/1 triplet,1H -NH<sup>+</sup>, PANI), 6.83 (b, 3H Ar-H, dopant), 5.91(1H, -N-H, PANI), 5.43 (b, 2H, CH=CH, dopant), 0.5-4.5 (35H, aliphatic-H, dopant),. FT-IR (in cm<sup>-1</sup>): 3010, 1579, 1500, 1305, 1224, 1159, 1031, 825, 705 and 628.

The polyaniline nanomaterials **DP-10**, **DP-50**, **DP-75**, **EM-10**, **EM-50** and **EM-75** were prepared by varying [aniline]/[dopant] ratio as 10, 50, and 75 (in moles) by following the above dispersion and emulsion procedures. The compositions, concentration of dopant were summarized in table 4.1.

### 4.3. Results and Discussion

#### 4.3.1. Synthesis and Characterization Dopant 2.

A new renewable resource amphiphilic butane sulfonic acid was synthesized by reacting cardanol with 1, 4-bultonesultone using KtOBu as a base. The synthetic scheme of the dopant is given in figure 4.4.

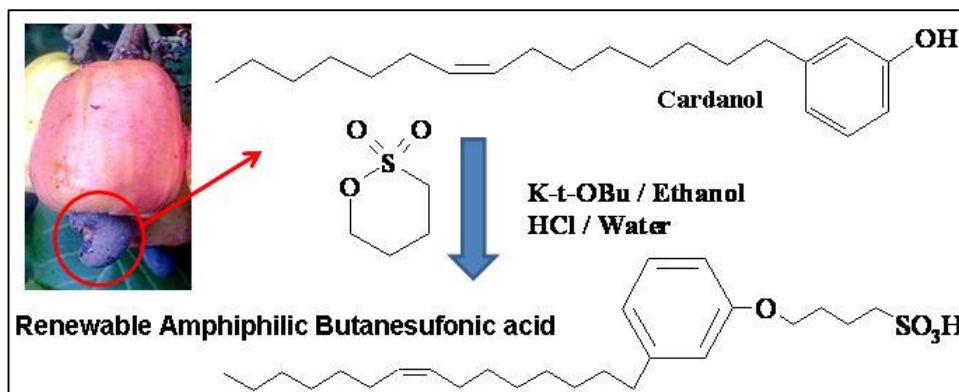


**Figure 4.4.** Synthesis of novel renewable amphiphilic dopant.

The structure of the dopant was confirmed by  $^1\text{H-NMR}$ ,  $^{13}\text{C-NMR}$ , FT-IR and Mass techniques. NMR spectrum of the dopant is shown in figure 4.5 and the different types of the protons were assigned by alphabets. The four protons in the aromatic ring appear with characteristic splitting pattern at 7.26, and 6.83 ppm. The double bond in the pendent alkyl chain appears at 5.44 ppm and the protons with respect to  $\text{Ar-OCH}_2$  and  $\text{CH}_2\text{-SO}_3\text{H}$  were appeared at 4.02 and 3.42, respectively. All other aliphatic protons appear below 3 ppm. The  $^{13}\text{C-NMR}$  spectrum also showed 8 peaks above 100 ppm corresponding to 6 aromatic and 2 vinylene carbon atoms. The peak intensities are in accordance to the expected structure, which confirm the formation of the new renewable resource amphiphilic dopant.

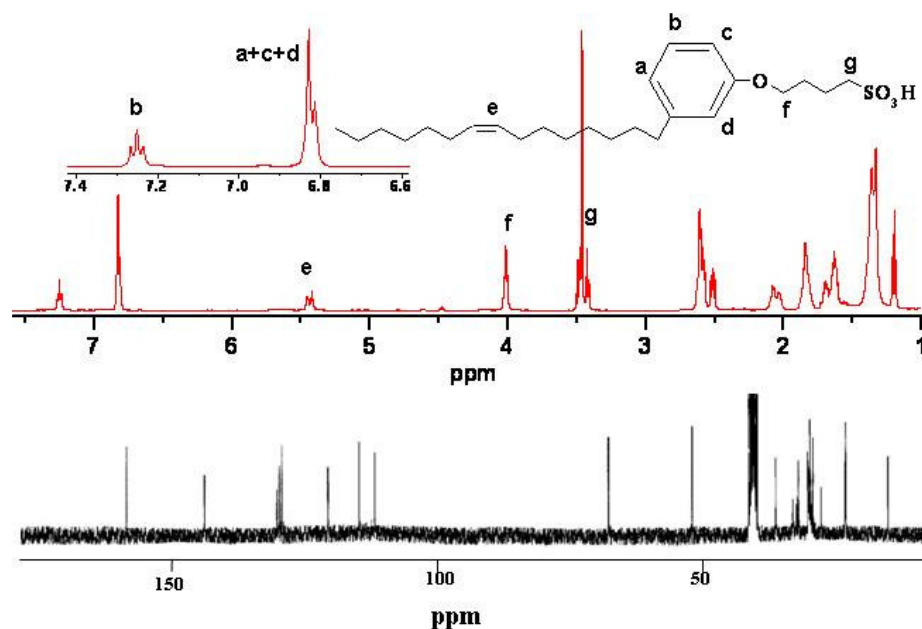


**Figure 4.5.** The  $^1\text{H}$  and  $^{13}\text{C}$ -NMR spectra of dopant 2.

FT-IR analysis (see figure 4.14) showed a broad peak at  $3454\text{ cm}^{-1}$  corresponds to the -OH stretching of the sulfonic acid group. The C-H stretching vibration bands appeared at  $2929$  and  $2859\text{ cm}^{-1}$ . The peak at  $1610\text{ cm}^{-1}$  is for the C=C vibrations. The peak at  $1456\text{ cm}^{-1}$  is arisen from the stretching vibrations of aromatic rings and the peak at  $1051\text{ cm}^{-1}$  is due to sulfonic acid vibrations. The sulfonic acid dopant is a white waxy solid and the thermo gravimetric analysis (TGA) showed that it is thermally very stable up to  $300\text{ }^\circ\text{C}$  (see figure 4.15). The heating cycle of DSC analysis showed a broad peak around  $59\text{ }^\circ\text{C}$  corresponding to the melting of the dopant and up on cooling the crystallization peak was appeared around  $44^\circ\text{C}$  (see figure 4.6). It suggested that newly designed dopant is more thermally stable and crystalline compared to earlier renewable resource dopant and may be suitable for various applications.

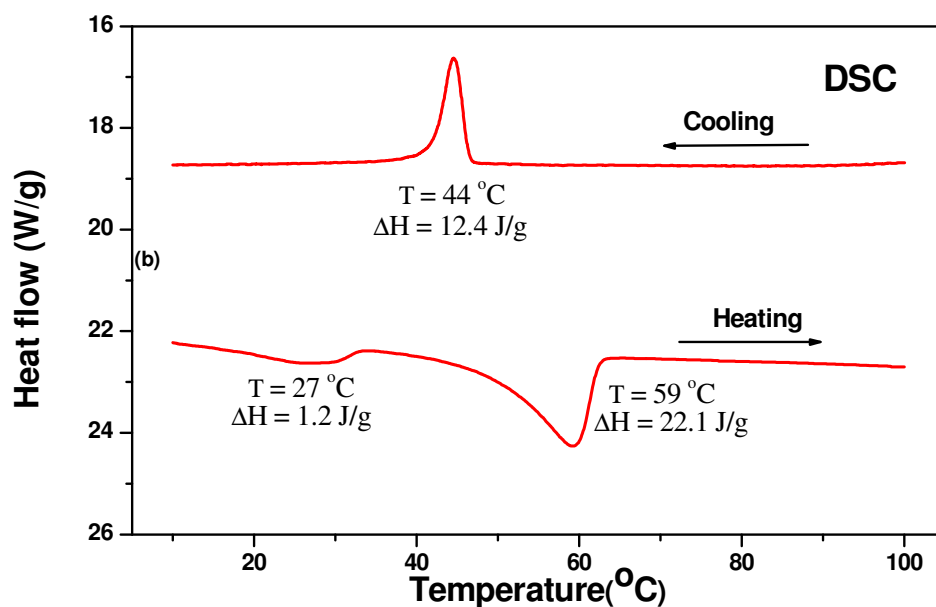


Figure 4.6. DSC plot of dopant 2.

#### 4.3.2. Study of Micellar Behaviour of Dopant 2:

The new dopant has typical amphiphilic structure with long flexible alkyl tail and highly polar hydrophilic head bearing sulfonic acid functional groups. The dopant was highly soluble in water and formed foamy solution (see figure 4.7).

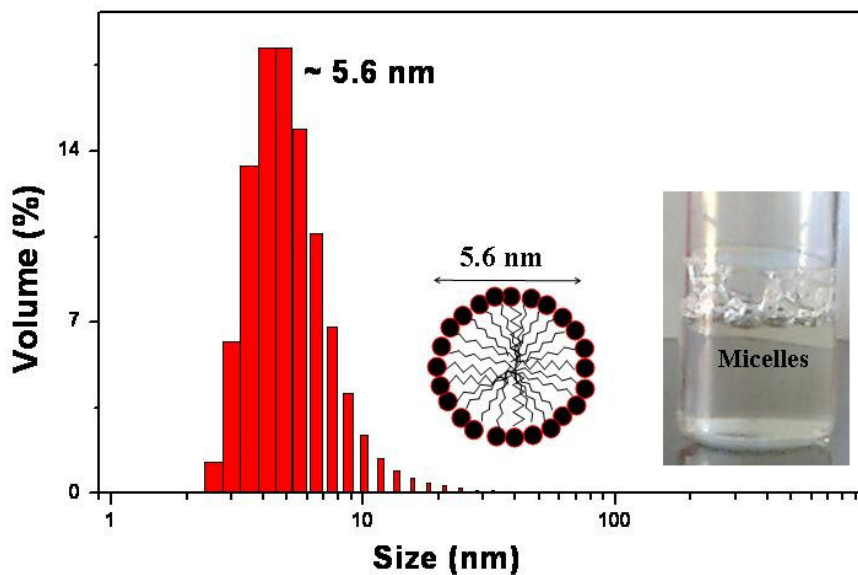
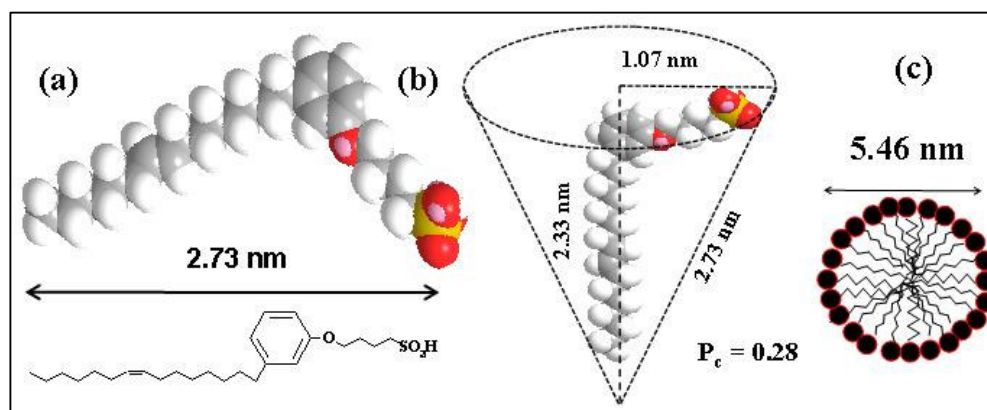


Figure 4.7. DLS histogram of dopant 2 in water ( $1.1 \times 10^{-2}\text{ M}$ ).

Dynamic light scattering (DLS) technique is an efficient tool to measure the size of the surfactant micelles<sup>21,22</sup>. DLS data for the dopant in water for the concentration of  $1.1 \times 10^{-2}$  M was shown in figure 4.7. The distribution plot showed that the amphiphilic butane sulfonic acid exists as 5.6 nm micelle in water (see figure 4.7). In order to get more insight in to the dopant packing factor, energy minimized MM2 structure for calculations were utilized (see figure 4.8). The molecule has a bend shape with a head group radius of 1.07 nm, tail length of 2.33 nm with overall molecular length of 2.73 nm. It appears as a cone shape with large head and a long hydrophobic tail. The packing parameter,  $P_c$  for the new amphiphilic dopant molecule was obtained as 0.28, which predicts the shape of the micelles as spherical one<sup>23,24</sup>. Based on the energy minimized structure, the end-to-end distance of the polar head to hydrophobic tail was obtained as 2.73 nm. The diameter of the tightly packed spherical micelle is expected to be equal to the double length of the end-to-end distance of the molecule. It was calculated as  $2 \times 2.73 \text{ nm} = 5.46 \text{ nm}$ , which is almost matching with the value of 5.6 nm obtained by dynamic light scattering measurements (see figure 4.7).



**Figure 4.8.** MM2 structure and packing parameter of dopant 2.

In order to understand the micellar behaviour of the new amphiphilic dopant, dye encapsulation studies were carried out using absorbance spectroscopy in water<sup>25,26</sup>. The dye encapsulation technique is useful to determine the critical micelle concentration (CMC) of the amphiphilic dopant and also to establish the evidence for the encapsulation of organic molecules like aniline and toluene (which are similar to dye molecules) in the hydrophobic core of the dopant micelles in water.

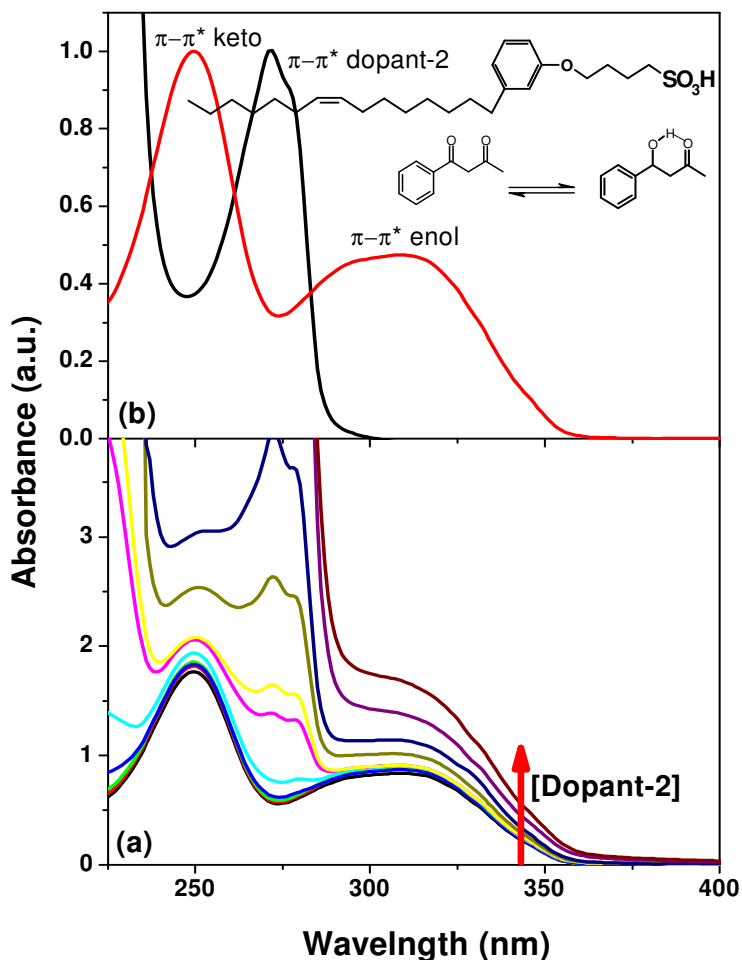


**Figure 4.9.** Dye encapsulation studies of dopant 2.

As discussed in chapter 2 for azobenzene dopant, this study also did using 1-Phenyl-1, 3-butanedione ( $\beta$ -diketone) dye. The amphiphilic dopant has an absorption peak at 270 nm for the  $\pi-\pi^*$  transition corresponding to phenyl ring (see figure 4.9b). The comparison of the absorption spectra of  $\beta$ -diketone and dopant indicate that the enol-form (at 310 nm) of the  $\beta$ -diketone is not disturbed by the absorbance characteristics of dopant. Therefore, the changes occurred in the enol-form of the  $\beta$ -diketone during the dye-encapsulation studies can be directly utilized for determining the CMC of the amphiphilic dopant (surfactant) in water<sup>25</sup>. Encapsulation experiments was carried out by keeping the amount of  $\beta$ -diketones constant ( $3.5 \times 10^{-5} \text{M}$ ) and varying the concentration of the dopant from  $7 \times 10^{-5}$  to  $10^{-2} \text{M}$  in water. The concentration variation spectra are shown in figure 4.9a. The intensity of the peak

corresponding to enol-form (at 310 nm) was plotted against the variation of the concentration of the dopant (figure 4.10). From the plot, the CMC of the amphiphilic surfactant dopant was determined as  $2 \times 10^{-3}$  M. To further validate this CMC value, the concentration dependent surface tension measurements of the dopant solution were carried out<sup>27</sup>. The surface tension measurement (Wilhelmy plate method) was carried out in double distilled water at 29 °C and the plot of surface tension against surfactant concentration is depicted in figure 4.10. Below the CMC, the surface tension decreased with increase in surfactant concentration and the surface tension did not change considerably above the CMC. The CMC is taken as the concentration where the surface tension changes its trend and is found to be  $2 \times 10^{-3}$  M at 29 °C. These two independent experiments confirmed that the surfactant dopant forms micelles above its CMC value of  $2 \times 10^{-3}$  M.

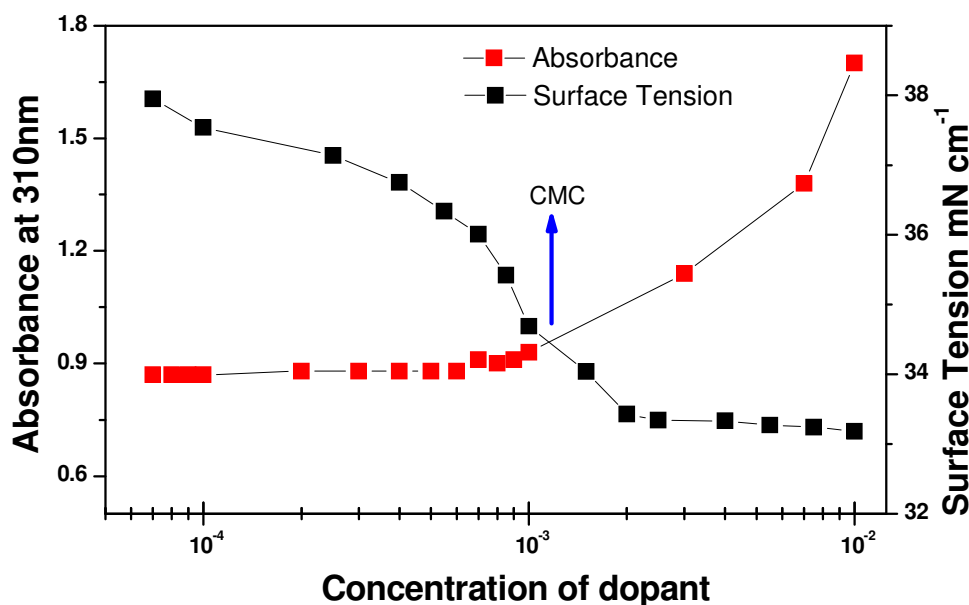


**Figure 4.10.** CMC of the dopant 2 by dye encapsulation and surface tension methods.

All the independent experiments (dye encapsulation, surface tension, dynamic light scattering and theoretical packing factor calculation) directly evident that the newly synthesized renewable resource butane sulfonic acid amphiphilic dopant exists in the form of 5.6 nm spherical micelles in water above its critical micellar concentration value.

### 4.3.3. Synthesis of Polyaniline Nanomaterials:

Two polymerization approaches (emulsion and dispersion routes) were adopted for tuning the size and shape of the polyaniline nanostructures (see figure 4.11). In emulsion route aniline monomer (0.55 M) is added to the micellar solution of dopant in water and stirred under ultrasonic stirring to produce a milky white emulsion (see vial in figure 4.11). In the dispersion approach, aniline is dissolved in an organic solvent toluene and was added into dopant micelles in water and stirred under ultrasonic to result a milky white dispersion (see vial in figure 4.11). In both the routes, the dopant concentration is above the CMC value ( $>2 \times 10^{-3}$  M, see table 4.1). The composition of [aniline]/[dopant] was also varied in the feed as 10, 50, 75 and 100 (in moles) to investigate the influence of the composition as well as for reproducible nanomaterials synthesis. The resultant emulsion or dispersion were further oxidised by ammonium persulfate to yield the polyaniline nanomaterials.

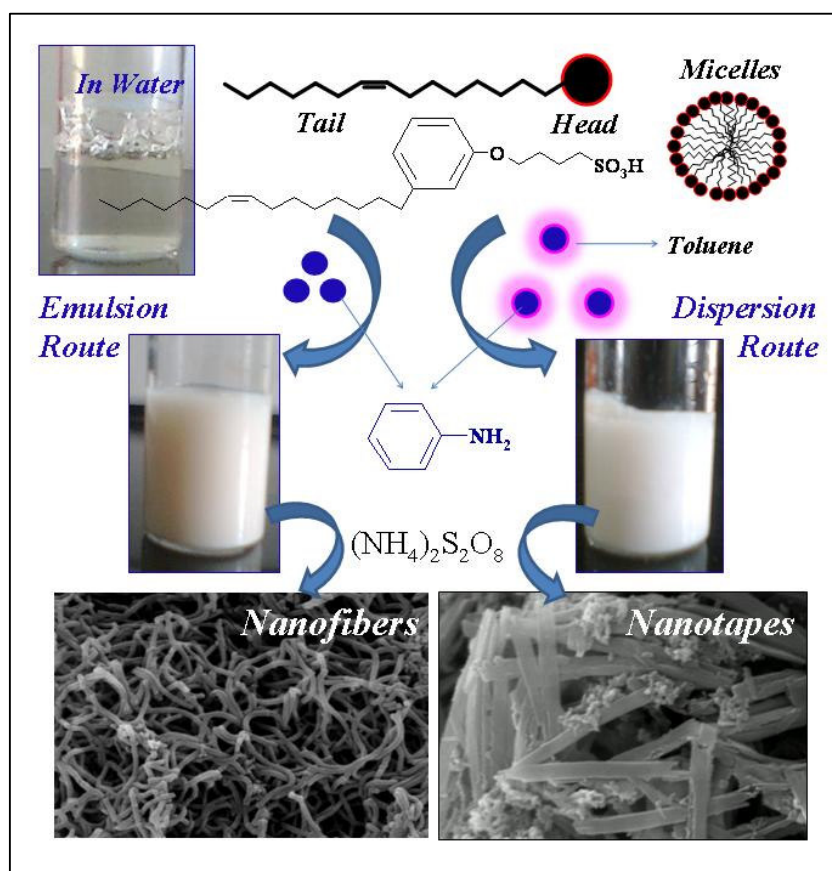


**Figure 4.11.** Schematic representation for the synthesis of polyaniline nanomaterials.



In both the cases the polymerization was allowed to continue 15 h at room temperature without any agitation and during this period the entire reaction mixture is transformed into a dark green solid mass. It was filtered in a Buchner funnel and washed many times with distilled water followed by methanol until the filtrate became colourless. The dark green coloured product was dried in a vacuum oven kept at 55 °C for 48 h and obtained in 60-80% in yield. The samples prepared by emulsion and dispersion routes were denoted as **EM-X** and **DP-X**, respectively (**EM**= emulsion, **DP**= dispersion and **X**= [aniline]/[dopant] ratio in the feed, see table 4.1). (In chapter-2 and 3 emulsion and dilution route samples were denoted by **E** and **D**, so to avoid confusion new notation was used for emulsion and dispersion in this chapter)

**Table 4.1.** Concentration and amount of dopant, conductivity, dimensions and WXRd-data of polyaniline nanomaterials.

Sample <sup>a</sup>	[Dopant] (M)	Amt. of dopant <sup>b</sup> (mole%)	Conductivity <sup>c</sup> (S/cm)	Nanomaterial Dimensions <sup>d</sup>	WXRd d-spacing <sup>e</sup> (Å)
<b>EM-10</b>	5.5x10 <sup>-2</sup>	0.42	0.9 x 10 <sup>-1</sup> (4.2)	F, 100±20nm	25.6,13.8,4.8,3.5,2.1
<b>EM-50</b>	1.1x10 <sup>-2</sup>	0.39	1.3 x 10 <sup>-1</sup> (1.3)	F, 100±50nm	26.5,3.6,2.1, 2.1
<b>EM-75</b>	7.3x10 <sup>-3</sup>	0.21	4.4 x 10 <sup>-1</sup> (2.2)	F, 100±35nm	26.7,13.7,4.6,3.5, 1.8
<b>EM-100</b>	5.5x10 <sup>-3</sup>	0.21	0.8 x 10 <sup>-1</sup> (6.9)	F, 100±25nm	26.4,4.6,3.5, 2.1
<b>DP-10</b>	5.5x10 <sup>-2</sup>	0.28	0.3 x 10 <sup>-1</sup> (0.2)	T, 1±0.5µm	24.7,13.7,4.7,3.5,2.1
<b>DP-50</b>	1.1x10 <sup>-2</sup>	0.13	0.5 x 10 <sup>-1</sup> (0.7)	T, 175±50nm	25.4,13.8,4.7,3.5,2.1
<b>DP-75</b>	7.3x10 <sup>-3</sup>	0.14	1.1 x 10 <sup>-1</sup> (8.8)	T, 150±50nm	25.3,13.8,4.4,3.5,2.1
<b>DP-100</b>	5.5x10 <sup>-3</sup>	0.05	3.2 x 10 <sup>-1</sup> (7.1)	T, 200±50nm	26.2,13.7,4.84,3,2.1

- Concentration of aniline was fixed as 0.55 M and in the name of the samples **EM-X** and **DP-X**, where **X**= [aniline]/[dopant].
- Determined by <sup>1</sup>H-NMR spectroscopy.
- Determined by four probe conductivity unit at 30° C. The values given in the parentheses are that of m-cresol cast film.
- F-nanofibers and T-nanotapes. The average sizes were calculated from SEM images.
- Wide angle X-ray diffraction measurements were done for powdered sample at 30° C.

<sup>1</sup>H-NMR spectra of the polyaniline nanomaterials (**EM-10** and **DP-10**) were recorded in d<sub>6</sub>-DMSO and their corresponding spectra are shown in figure 4.12. The NMR spectra of the polymers showed peaks corresponding to their structures as well as dopant molecule (peaks are shown by alphabets). This confirms that the strong

binding of sulfonic acid dopant to the polymer structure and also the doped nature of the polyaniline chains. The two peaks with characteristic splitting at 7.55 and 7.49 were assigned to protons of polyaniline chains (see expanded region, figure 4.12)<sup>28,29</sup>. The three equally intense peaks (1/1/1 triplet) at 7.10, 7.20 and 7.30 ppm are attributed to the protonated -NH resonance due to the  $^{14}\text{N}$  with unit spin which makes the proton attached to it split into three lines<sup>28</sup>. The peak at 5.90 ppm was assigned to un-protonated -NH present in the polymer backbone. The spectra of **EM-10** and **DP-10** were almost identical indicating similarity of the polyaniline chemical structure produced via emulsion and dispersion routes.

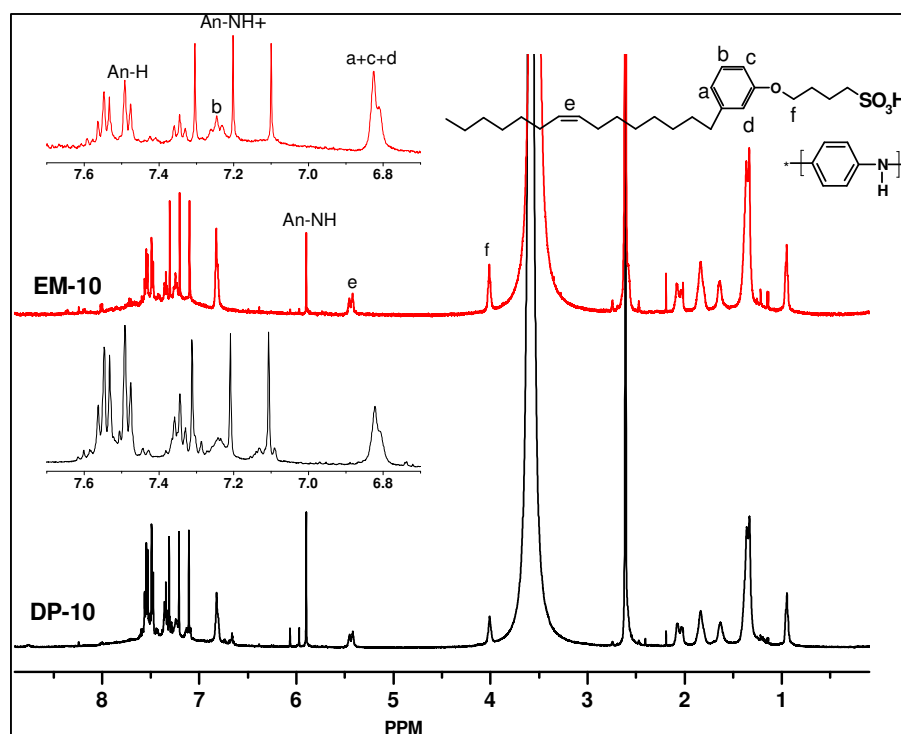


**Figure 4.12.**  $^1\text{H}$  NMR spectra of the polyaniline nanomaterials in  $d_6$ -DMSO solvent.

Polymers **EM-50** to **EM-100** and **DP-50** to **EM-100** were found soluble in DMSO and their NMR spectra are also similar to above samples. Anionic surfactant dopant behaved both as surfactant for polymerization as well as counter anion dopant for the positively charged conducting polymer chains. The anionic surfactants permanently bind to the polymer chains and become integral part of the resultant nanomaterials. The amount of sulfonic acid dopant incorporated in the polyaniline chain was determined by comparing the integral intensities of the aromatic peak

intensities of the dopant (at 7.28 ppm/ three protons) versus polyaniline (7.55 and 7.49 ppm together/four protons). The percentage incorporation (mole %) of dopant in the synthesized samples were plotted in figure 4.13 and revealed that upon decreasing the [aniline]/[dopant], the actual incorporation of dopant also decreased linearly. However, the decrease was found much more drastic for the dispersion route samples compare to that of synthesized by the emulsion routes. The custom-designed new renewable resource dopant is an efficient solubilising agent for the polyaniline chain in common organic solvents like DMSO and facilitate the complete structural characterization by NMR.

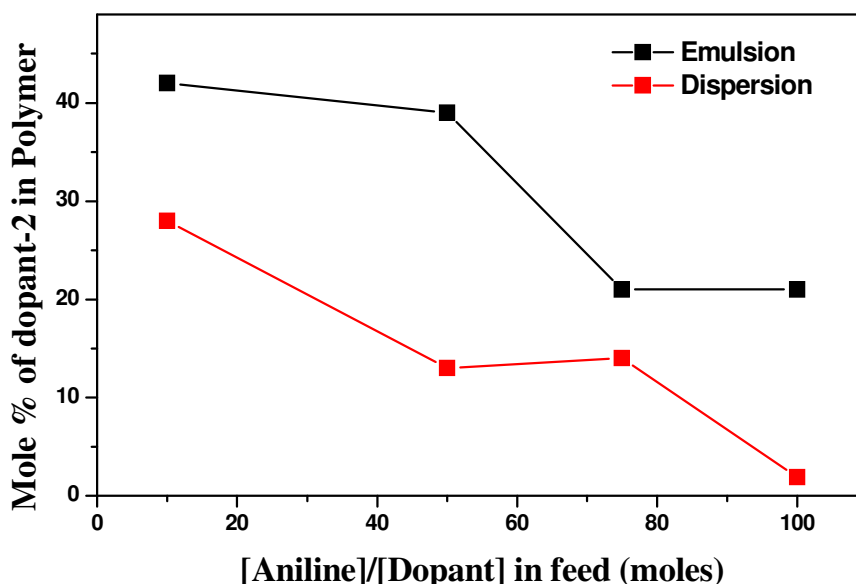


**Figure 4.13.** Mole fraction of dopant versus aniline/dopant ratio (from NMR).

The polyaniline samples were subjected to FT-IR analysis using KBr pellets (see figure 4.14). The two peaks were appeared at 1582 and 1501 are corresponding to the quinoid and benzenoid ring C=C stretching ring deformations, respectively<sup>30</sup>. The peak at 1315 and 832 are corresponding to C-N stretching and C-H out-of-plane vibrations of 1, 4-disubstituted benzene ring, respectively and the peak at 2932cm<sup>-1</sup> corresponds to -C-H vibrations<sup>31</sup>. Four peaks present in the nanostructure samples at 1307, 1026, 830 and 630 cm<sup>-1</sup> for O=S=O (sym), NH+....SO<sub>3</sub><sup>-</sup> interactions between the polymers chain and the dopant 1, S-O (un-sym) and C-S stretching vibrations, respectively<sup>32</sup>.

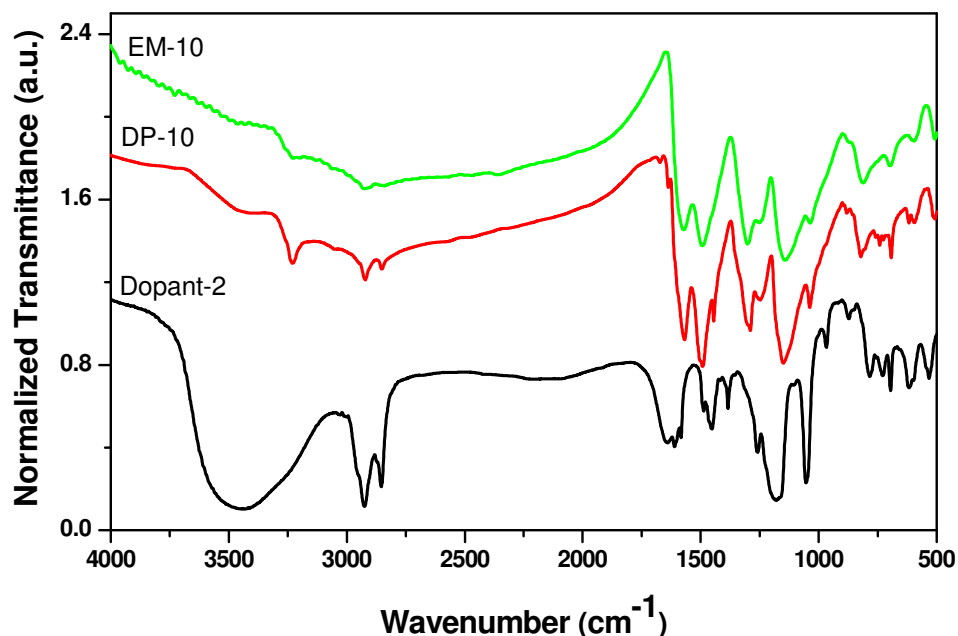


**Figure 4.14.** FTIR spectra of dopant and polyaniline nanomaterials.

The inherent viscosity of the polymer samples **EM-10** to **E-100** and **DP-10** to **DP-100** (in PANI-EB form) was determined for 0.5 wt % solutions in NMP at 30°C. The inherent viscosities of the polymers were obtained in the range of  $\eta_{inh} = 0.23$ - $0.28$  dL/g. The viscosities of the samples indicate the formation of good molecular weight samples and the values are similar to the earlier reports for polyaniline materials<sup>33,34</sup>.

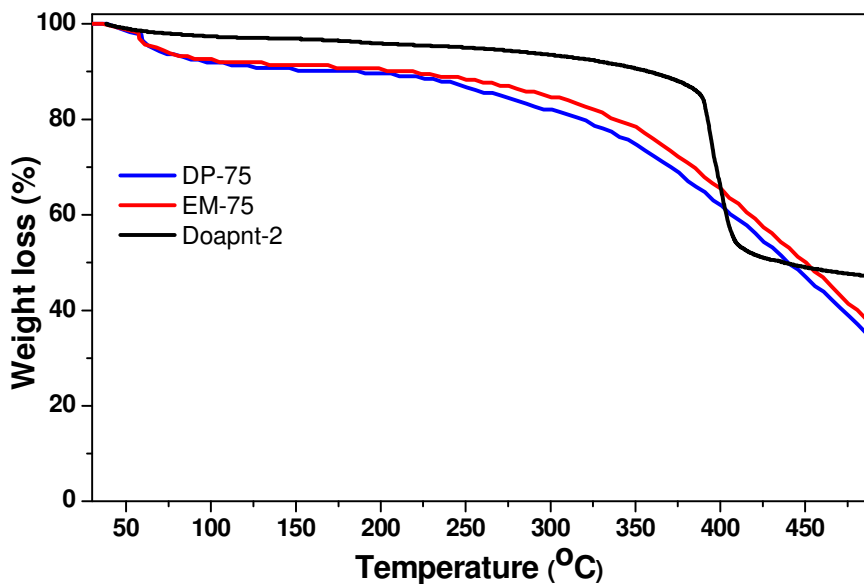


**Figure 4.15.** TGA plots of dopant and polyaniline nanomaterials.

The thermal properties of dopant and polyaniline nanomaterials were measured by means of thermogravimetric analysis (TGA) and given in figure 4.15. It is clear that both nanofibers and nanotapes are stable up to 300°C and so good for high temperature applications.

#### 4.3.4. Morphology of Polyaniline Nanomaterials:

The SEM images of the emulsion route nanomaterials **EM-10** to **EM-100** are given in figure 4.16. The sample **EM-10** has both dendritic nanofibers and micron size spheres. **EM-75** is seen as a very uniform mat of nanofibers of diameter ~80 nm with an average length up to 2 μm and there is no trace amount of microspheres. **EM-100** contains bundles of linear nanofibers with average 100 nm diameter and length of 3-5 μm. TEM image of **EM-75** (see figure 4.16) confirmed the morphology as nanofibers of diameter 100 nm and a length of 2.5 μm (similar to its SEM image) with trace amounts of smaller diameter nanofibers of <50 nm.

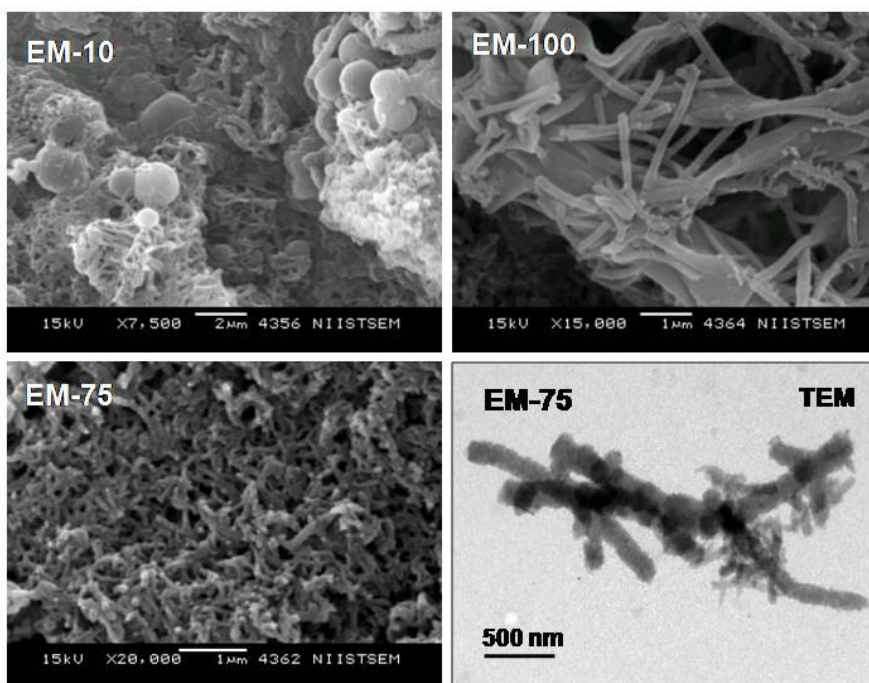


**Figure 4.16.** SEM and TEM images of emulsion route nanomaterials.

The SEM-images of dispersion route samples **DP-10** to **DP-100** was given in figure 4.17. It is very interesting to note that the samples synthesized through dispersion route were completely different from the emulsion route and contained exclusively planar nanotapes. **DP-10** contains very long tape but the morphology is

not very uniform. In **DP-50** and **DP-75**, the morphology of the nanotapes was very uniform and the width and thickness were obtained as 200 and 30 nm, respectively (see expanded SEM-image). The average lengths of the nanotapes were obtained as  $1.8 \pm 0.25 \mu\text{m}$ . The expanded image of nanotapes (**DP-50**) shows a saw tooth kind of edge with rough surface which is an indicative of template mediated growth of nanotapes. Sample **DP-100** contains stacked nanotapes with small amount of particulate aggregates. The TEM image (**DP-75**, figure 4.17) clearly demonstrated the flat and tape like nature of the nanostructures.

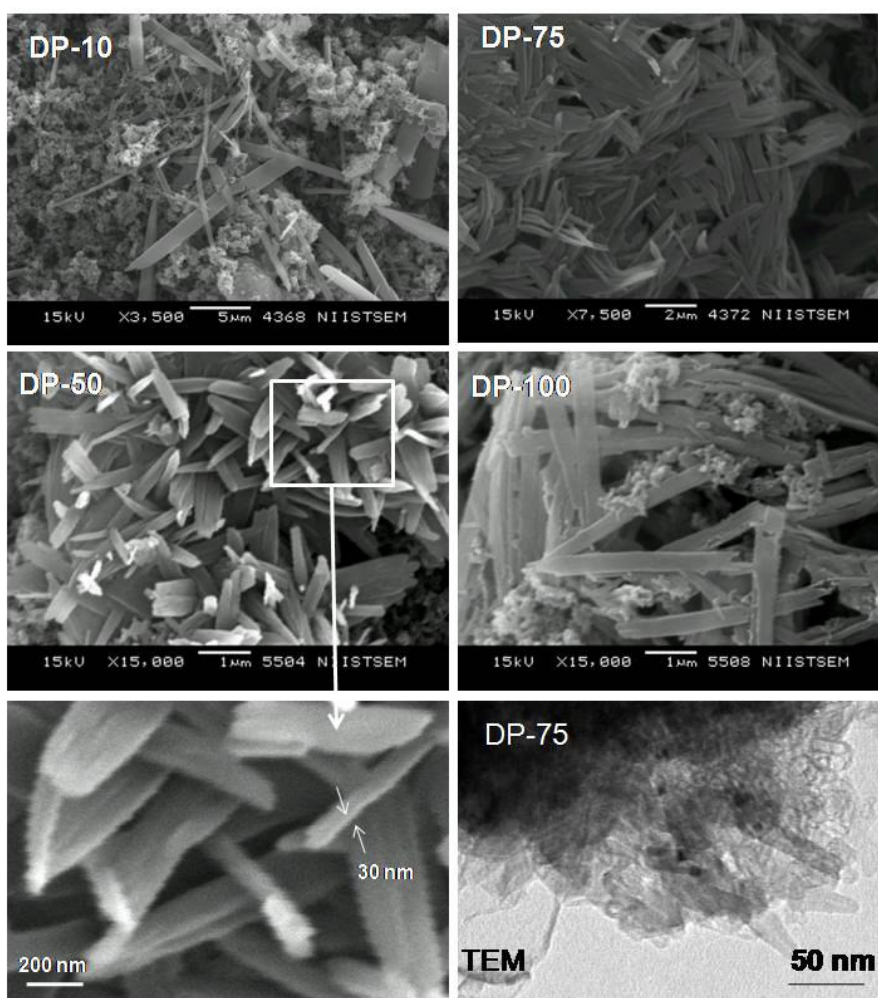


**Figure 4.17.** SEM and TEM images of dispersion route nanomaterials.

From the microscopic analysis of the nanomaterials, it is very clear that the type of polymerization plays a major role in the determination of the morphologies. The emulsion and dispersion routes exclusively produce nanofibers and nanotapes,

respectively and nanomaterials morphology were not altered for wider composition range {[aniline]/[dopant] = 50 to 100} which further confirmed that morphology evolution was driven by the polymerization processes.

#### 4.3.5. Mechanism of Nanomaterial Formation:

DLS measurements were carried out for both emulsion (dopant+aniline) and dispersion (dopant+aniline+toluene) templates in water and shown in figure 4.18<sup>35,36</sup>. The addition of aniline to dopant micelles in water produces milky white thick emulsion and DLS data of the resultant emulsion showed the presence of aggregates of 1.1  $\mu\text{m}$ . Similarly the addition of aniline in toluene into dopant micelles in water and subsequent ultra-sonication resulted in the formation of a white stable dispersion. The DLS of this dispersion showed the presence of aggregates of sizes around 2.8  $\mu\text{m}$ . DLS experiments evident that amphiphilic dopant molecule has behaved as a typical surfactant-cum-dopant and formed stable micellar aggregates with aniline or aniline in toluene under the polymerization conditions.

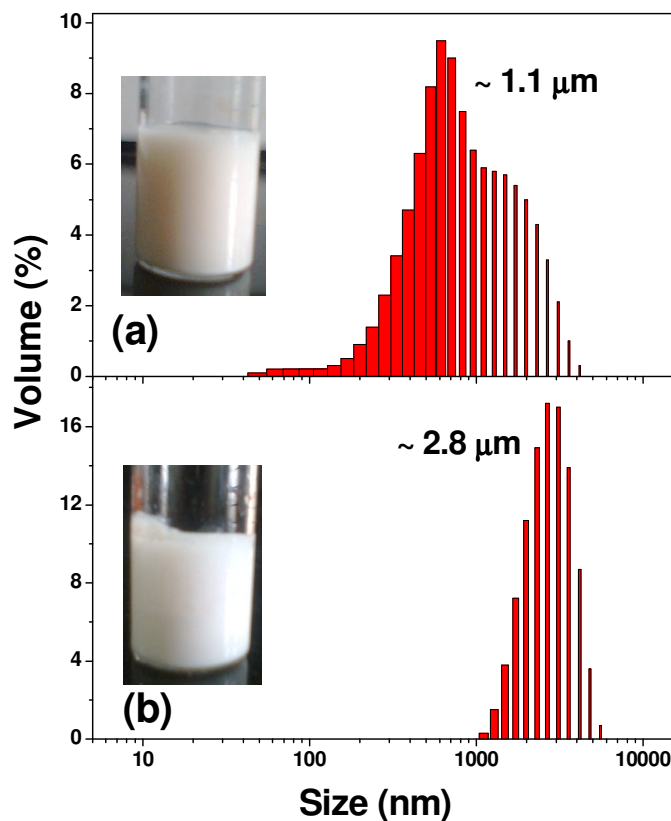


**Figure 4.18.** DLS histograms of emulsion (a) and dispersion (b) templates.

Though the DLS data provide the existence of the micrometer sized aggregates in emulsion and dispersion routes, but it cannot predict the shape and type of the aggregates. The polymerization mixtures were very stable and drop cast on TEM grid for visualizing these aggregates microscopically to map out the shape of the templates. TEM images of the polymerization templates are shown in figure 4.19

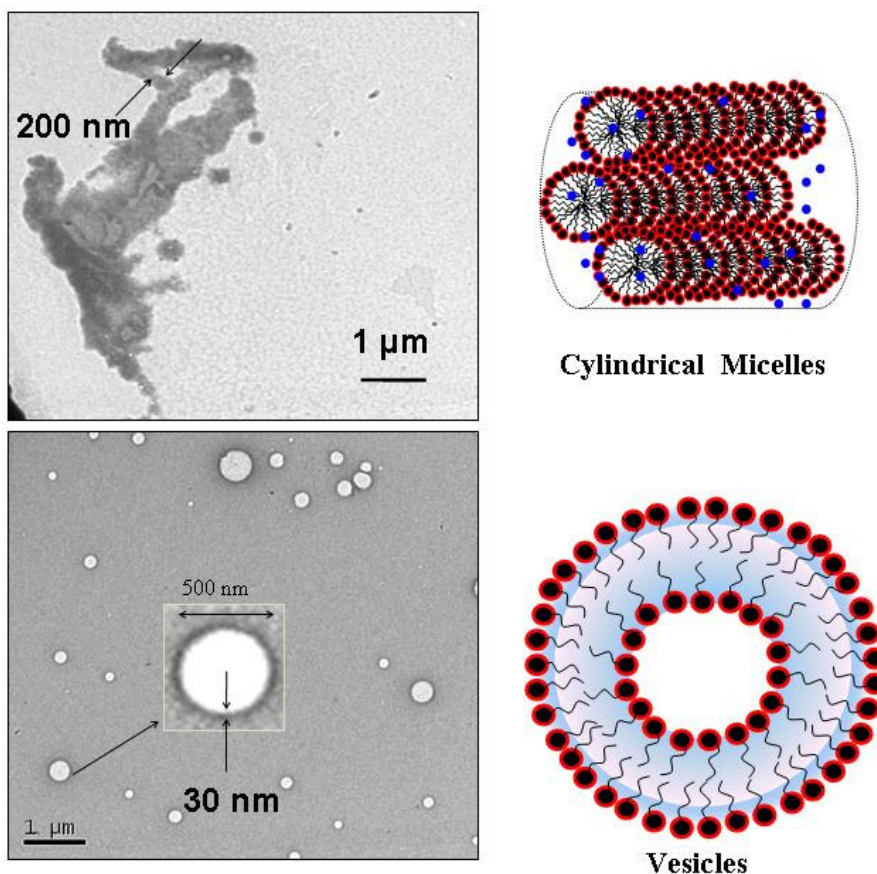


**Figure 4.19.** TEM images of emulsion and dispersion route templates.

The emulsion template (**EM-50**) showed cylindrical micellar aggregates of ~150 nm diameter with length upto 1-3 μm. It suggests that the addition of aniline induce self organization in the amphiphilic dopant micelles and the resultant cylindrical micelles template for the formation of polyaniline nanofibers. The transition from spherical to cylindrical micelles up on adding aniline was observed in earlier study also (chapter-2). The formation of cylindrical aggregated micelles can be explained by the acid-base interaction between the sulfonic acid head part of the amphiphilic dopant with basic aniline. The size of the miceller aggregates and the



synthesized nanofibers dimensions (SEM and TEM images) are matching well within experimental variation. This directly gives evidence for the cylindrical micellar aggregates template mediated process in the emulsion polymerization route. TEM image of dispersion route polymerization mixture (**DP-50**) showed completely different types of template morphology compare to emulsion route. The dispersion template contains exclusively spherical vesicles and the sizes of the vesicles were appeared as  $\sim 450 \pm 200$  nm in diameter and with wall thickness of  $20 \pm 10$  nm. The size of aggregates obtained by DLS showed a discrepancy with TEM observation; it may be due to the fact that in solution there are high degrees of aggregation among the vesicles which over estimate the values in DLS analysis. Since the TEM sample preparation was carried out much lower concentration, the isolate vesicles could be observed. It has been well known that typical amphiphilic molecules can exist in the dynamic equilibrium between vesicle and cylindrical micellar aggregates depending upon the concentration or external induction by organic molecules<sup>37</sup>. There are two types of competition interactions are possible when aniline+toluene was added into the dopant micelles in water: (i) first the basic aniline molecule can interact with sulfonic acid part of the micelles in water to produce cylindrical aggregates via acid-base interaction (as similar to emulsion route) and (ii) secondly the toluene molecules tend to stack in the aromatic part of the micelles which induced the transformation of the templates into vesicular aggregates<sup>38</sup>. Recently, Raghavan and co-workers had found a similar transformation of worm-like cylindrical micelles into unilamellar vesicles upon adding aromatic molecules like salicylic acid via selective aromatic ring interactions<sup>39</sup>. Hence, the addition of excess organic phase (toluene) is expected to increase the packing parameter ( $P_c$ ), and the spherical dopant micelles transformed into a shape with very low-curvature aggregate like vesicles<sup>23</sup>. These resultant vesicular aggregates behave as templates for nanotapes in dispersion route.

A plausible mechanism of self-organized renewable amphiphilic butane sultone sulfonicacid dopant mediated formation polyaniline nanostructures by emulsion and dispersion route is proposed as given in figure 4.20.

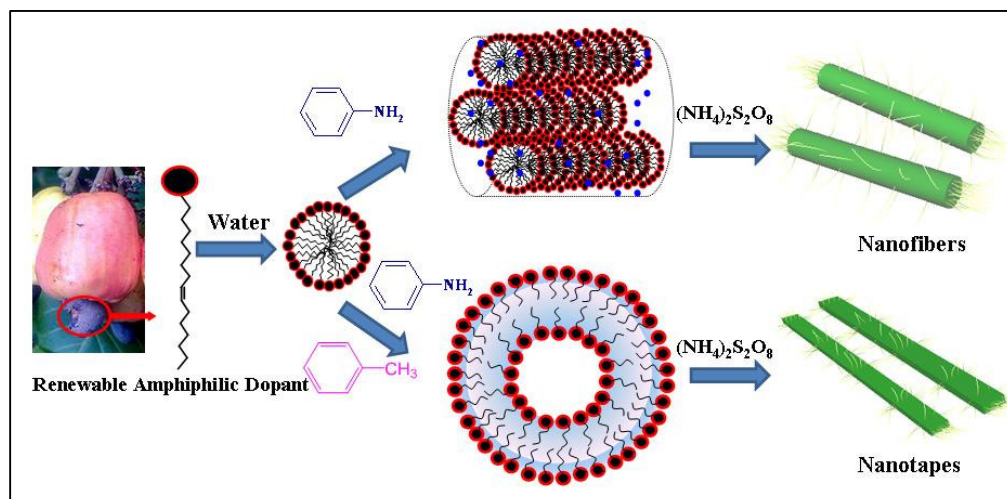


**Figure 4.20.** Plausible formation mechanism of polyaniline nanostructures by the soft templating of amphiphilic butane sulfonic acid.

The amphiphilic sulfonic acid dopant exists in the form of 5.6 nm micelles in water. The complexation of spherical micelles with aniline produce large micro-meter size (1.1  $\mu\text{m}$  range) cylindrical micellar aggregates which behave as templates in emulsion route for the formation of nanofibers. In the dispersion route, up on adding aniline dissolved in toluene into dopant micelles in water produced vesicular aggregates which template for nanotapes. One would immediate ask the question that how do nanotapes evolve from vesicular hollow structures? Recent reports based on the self-organization of sugar derivatives of cardanol (not conducting materials) documented the formation of vesicles and subsequent transformation of vesicles into long twisted tapes<sup>40,41</sup>. Though the mechanism of the opening of the vesicles to nanotapes is still under debate, the transformation was confirmed by many examples<sup>42</sup>. Therefore, in this case also the vesicular temple may open during subsequent oxidative polymerization process to form polyaniline nanotapes. The ripping of vesicles can be further confirmed from the saw tooth type edges in the surface of the nanotapes (see figure 4.17). In order to provide evidence for the ripping of vesicular templates, the dimensions of the vesicles and the resultant nanomaterials were compared. The average diameter ( $2r$ , where  $r$ -radius) of a vesicle is 0.6  $\mu\text{m}$  which give the circumference of the vesicle ( $2\pi r$ ) as 1.9  $\mu\text{m}$ . The average lengths of the nanotapes synthesized from the vesicular templates was obtained as  $1.7 \pm 0.4 \mu\text{m}$  (from SEM images). The circumference of vesicular template is very well matching with that of the average length of the nanotapes. Secondly, the thickness of the

nanotapes and vesicular templates were found almost identical (~ 30 nm). It is directly evident that during the chemical oxidation of the vesicular templates by APS, the vesicles are ripped in the surface to form the nanotapes. The above results suggest that the newly designed renewable resource amphiphilic dopant is an efficient structure directing agent for polyaniline nanofiber or nanotapes via selective self-assembled template processes. The newly designed amphiphilic surfactant bears an aliphatic sulfonic acid polar group with a long tail consisting of aromatic benzene ring and aliphatic pentadecylene chain. Therefore, the nature and behaviour of the new amphiphilic is expected to be different from the typical sulfonic acid surfactants like aromatic sulfonic acids (like DBSA) or aliphatic sodium dodecyl sulfonic acid (SDS). Amphiphilic azobenzene sulfonic acid studied in chapter-2 was found not soluble in organic medium which restrict its usage for dispersion route. Therefore, the appropriate sizes of the polar head and hydrophobic tail are crucial factors in the successful templating behaviour of amphiphilic dopants. The unique structural features associated with new dopant design enhances its solubility in variety of organic solvents as well as in water which facilitate its different types of template formation in emulsion and dispersion routes.

#### 4.3.6. Properties of Nanomaterials:

The nanostructures are highly water suspendable and the green coloured colloidal solutions are stable for 2-3 days at ambient conditions. In order to study the conformational as well as oxidation state of the polymer chains present in nanomaterials UV-vis spectra of the of nanostructures in water were recorded and shown in figure 4.21. It is clear from the plots of nanofiber samples that it contains all the characteristics peaks of doped polyaniline, the peaks at 360, 450 and 800 nm, which were assigned as the transitions from  $\pi$ - $\pi^*$  band, polaron band to  $\pi^*$  band,  $\pi$  band to polaron band, respectively<sup>43</sup>. It is also seen that in all four cases there is a tailing nature in the NIR region of the spectra indicating more expanded nature of polyaniline chain<sup>44</sup>. The spectra of **DP-75** and **DP-100** were very similar to that of nanofiber samples and exhibited the characteristic peaks of highly doped expanded emeraldine salt form of polyaniline, however, the intensity of polaron peak for **DP-10** and **DP-50** were relatively low. The spectra of dedoped form of all the nanofiber

samples (**EM-10** to **EM-100**, see figure 4.22a) showed peaks at 360 nm and 650 nm as similar to conventional emeraldine base (EB) form. The spectra of dedoped nanotapes **DP-75** and **DP-100** also showed similar characteristics of emeraldine base with absorption maxima at 650 nm. In the case of **DP-10** and **DP-50** (see figure 4.22b) the absorption maxima was blue shifted by 50 nm which indicate the presence of pernigraniline form along with EB form in nanotapes.<sup>31</sup> The reason for the pernigraniline structure in dispersion route may be correlated to over oxidation of polyaniline emeraldine chains at the organic/aqueous interface at the initial stages of polymerization.<sup>22,31</sup>

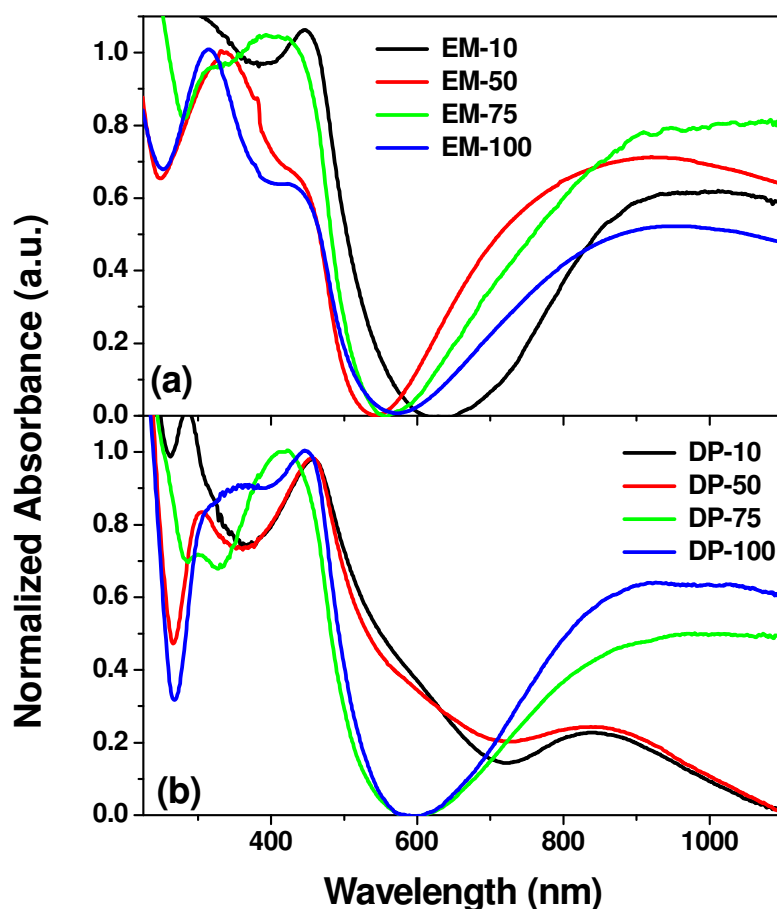


**Figure 4.21.** UV-vis absorption of polyaniline nanomaterials (doped) in water.

The bulk conductivity of the polyaniline nanostructures was determined by four probe conductivity measurement for compressed pellets at room temperature and the values are reported in table 4.1. The conductivities of the samples were found in the range of 0.03 - 0.44  $\text{Scm}^{-1}$  which is in accordance with sulfonic acid doped

polyaniline samples<sup>20</sup>. Additionally the four probe conductivity of m-cresol cast films of nanomaterials also measured and it showed a one order higher value in the range of 0.2-8.8 Scm<sup>-1</sup> than corresponding pellets (see table 4.1). It is well known in polyaniline literature that m-cresol has a secondary doping effect and also order the polyaniline chains for improved electrical properties of polyaniline<sup>44</sup>.

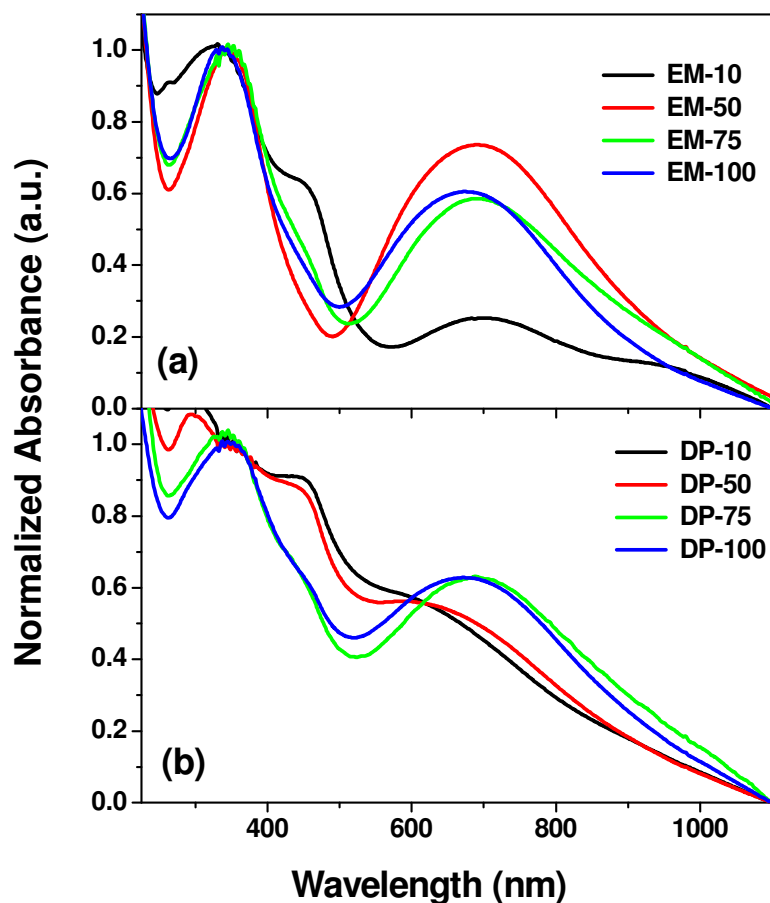


**Figure 4.22.** UV-vis absorption of polyaniline nanomaterials (dedoped) in water.

The new dopant has an amphiphilic structure so it is expected to penetrate in to polyaniline chains and may result in the formation of layered structures<sup>45</sup>. These types of layered dopant-polymer supramolecular structures are expected to reflect on the low angle region of the Wide angle X-ray diffraction (WXR) patterns (low  $2\theta$  values, higher d-spacing)<sup>46</sup>. In order to investigate the solid state properties of polyaniline nanostructures, the nanomaterials were finely powdered and subjected for WXR. The WXR patterns of polyaniline nanostructures synthesised by emulsion and dispersion method are shown in figure 4.23.

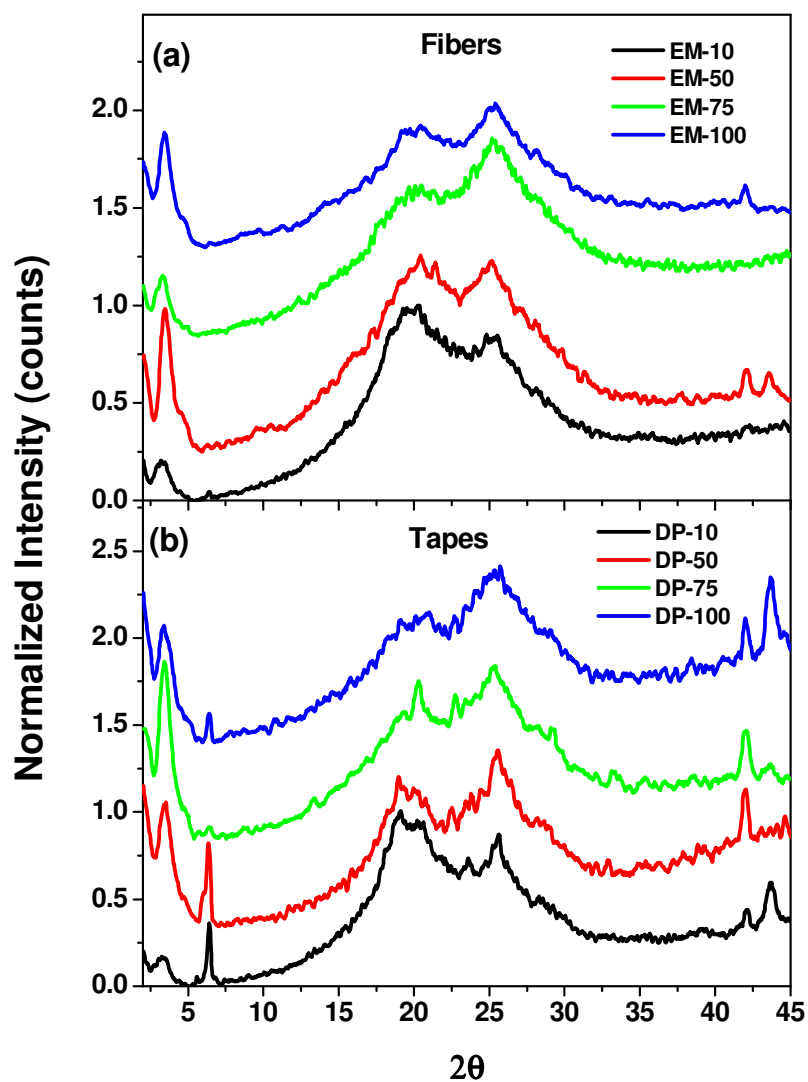


**Figure 4.23.** WXR D pattern of polyaniline nanomaterials at 30°C.

Both nanofibers and nanotapes showed a broad peak at  $2\theta = \sim 25^\circ$  with respect to aromatic chain interactions. Emulsion route synthesised nanofibers showed a sharp lower angle peak at  $2\theta = 3.3^\circ$  (d-spacing of 26 Å) corresponding to highly solid state ordered structure. Dispersion route nanotapes samples showed two peaks at the low angle region at  $2\theta = 3.3^\circ$  peak and  $2\theta = 6.4^\circ$  ( $d=13.7$  Å). The peak at  $2\theta = 6.4^\circ$  was observed for polyaniline structures in which sulfonic acids were employed as dopants. Therefore, the peak at  $d=13.7$  Å is the resultant of sulfonic acid interactions with polyaniline chains which induced short range solid state ordering. However, in this case both peaks at  $2\theta = 3.3^\circ$  (corresponding to long range ordering) and  $6.4^\circ$  (short range ordering) were observed in the same polyaniline nanomaterials doped by

amphiphilic dopants. In both nanofibers and nanotapes the  $3.3^\circ$  peak has d-spacing value of 26 Å, which is comparable to the molecular length 27 Å of the amphiphilic dopant molecule. This indicates that the peaks at 26 Å and 13.7 Å represent the first and second order reflection in the lamellae of the nanostructures<sup>47</sup>. It revealed that the polyaniline nanostructures may exist as lamellar type polyaniline-sulfonate supramolecular complex with stacks of polymer chains are separated by dopant anions<sup>48</sup>. These layered lamellae may be formed due to the inter-digitations and crystallization of side chains of the doped polyanilines.

#### 4.4. Conclusion

A novel amphiphilic sulfonic acid dopant from cardanol which is successfully utilized as structure directing agent for polyaniline nanomaterials- nanofibers and nanotapes by emulsion and dispersion routes, respectively. This dopant based approach has the following merits: (i) the dopant was developed from renewable resource waste product cardanol by ring opening of sultone under basic conditions, which open up new possibilities for designing novel amphiphilic molecules, (ii) the dopant forms micelle in water and its CMC value was determined by multiple techniques such as dye encapsulation, surface tension and DLS methods, (iii) the micelles formed by the dopant is utilized to grow polyaniline nanostructures under emulsion and dispersion routes, (iv) in emulsion route the cylindrical micellar soft template formed between dopant and aniline leads to the formation of nanofibers whereas in dispersion route the vesicular template of aniline+toluene produced nanotapes, (v) the polyaniline nanostructures are soluble in high polar solvents like DMSO that enabled us the complete structural characterization and composition determination by NMR, (vi) DLS and TEM techniques were successfully utilized to understand the mechanistic aspects of nanostructure formation, (vii) the absorption spectra of nanomaterials showed that all are in highly doped expanded chain nature and (viii) the WXRd studies confirmed the layered lamellar type packing of polymer chains in nanomaterials. In a nut shell, it is shown that a novel renewable resource amphiphilic dopant is a good candidate for the synthesis of high quality nanofibers and nanotapes by carefully choosing the amphiphilic dopant templates under emulsion and dispersion polymerizations in a single system. The polyaniline nanomaterials are highly soluble and therefore, they may suitable for various applications in bio and chemical sensors and optical devices.



**4.5. References:**

1. Li, D.; Huang, J.; Kaner, R. B. *Acc. Chem. Res.* **2009**, *42*, 135-145
2. Wan, M. X. *Adv. Mater.* **2008**, *20*, 2926–2932
3. Zhang, D. H.; Wang, Y. Y. *Mater. Sci. Eng. B*, **2006**, *134*, 9.-19
4. Tran, H. D.; Li, D; Kaner, R. B. *Adv. Mater.* **2009**, *21*, 1–13
5. MacDiarmid, A.G. *Angew. Chem., Int. Ed.* **2001**, *40*, 2581-25
6. Armes, S. P.; Aldissi, M. *J. Chem. Soc., Chem. Commun.* **1989**, 88-89.
7. Vincent, B.; Waterson, J. J. *Chem. Soc., Chem. Commun.* **1990**, 683-684
8. Gospodinova, N.; Mokreva P.; Terlemezyan L. *J. Chem. Soc., Chem. Commun.*, **1992**, *13*, 923-924
9. Chattopadhyay, D.; Mandal, B. M. *Langmuir* **1996**, *12*, 1585-1588
10. Armes, S. P.; Aldissi, M.; Hawley, M.; Berry, J. G.; Gottesfeld, S. *Langmuir* **1991**, *7*, 1447.
11. DeArmitt, C.; Armes, S. P. *J. Colloid Interface Sci.* **1992**, *150*, 134.
12. Armes S. P.; Aldissi M.; Agnew S.; Gottesfeld S. *Langmuir* **1990**, *6*, 1745.
13. Stejskal, J.; Kratochvil, P.; Gospodinova, N.; Terlemezyan, L.; Mokreva, P. *Polym. Commun.* **1992**, *33*, 4857.
14. Lee, S.H.; Lee, D.H.; Lee, K.; Lee, C.W. *Adv. Funct. Mater.* **2005**, *15*, 1495–1500.
15. Lee, K.; Cho, S.; Park, S. H.; Heeger, A. J.; Lee C.W.; Lee, S.H. *Nature*, **2006**, *441*, 65-68.
16. Cao, Y.; Smith, P.; Heeger, A. J. *Synth Met* , **1992**, *48*, 91–97
17. Palaniappan, S.; John, A. *Prog. Polym. Sci.* **2008**, *33*, 732–758
18. Kim, B.J.; Oh, S.G.; Han, M.G.; Im, S.S. *Synth Met* , **2001**, *122*, 297–304
19. Yan , Y.; Yu , Z.; Huang, Y. W.; Yuan, W. X.; Wei, Z. X. *Adv. Mater.* **2007**, *19*, 3353
20. Haung, K.; Wan, M. X. *Chem. Mater*, **2002**, *14*, 3486-3492
21. Vethamuthu, M. S.; Feitosa, E.; Brown, W. *Langmuir* **1998**, *14*, 1590-1596
22. Zhang, X.; Kolla, H.S.; Wang X.; Raja, K.; Manohar S.K. *Adv. Funct. Mater*, **2006**, *16*, 1145-1152.

23. Hamley, I.W. Introduction to Soft Matter ,( 2nd Edn), Wiley, **2007**, pp-200-204
24. Israelachvili, J. N.; Mitchell, D. J.; Ninham, B. W. *J. Chem. Soc. Faraday Trans.* **1976**, *72*, 1525.
25. Dominguez, A.; Fernandez, A.; Gonzalez, N.; Iglesias, E.; Montenegro, L. *J. Che. Edu.* , **1997**,*74* , 1227-1231
26. Iglesias, E. *J. Phys. Chem.* **1996**, *100*, 12592-12599
27. Franke, D.; Egger, C.C.; Smarsly, B.; Faul, C. F. J.; Tiddy, G. J. T. *Langmuir*, **2005**, *21*, 2704-271
28. Mu, S.; Yang, Y. *J. Phys. Chem. B*, **2008**, *112* , 11558
29. Zhou, C.; Han, J.; Song, G.; Guo, R. *J. Polym. Sci., Polym. Chem.* **2008**, *46*, 3563
30. Trchova, M.; Sedenkova, I.; Konyushenko, E. N.; Stejskal, J.; Holler, P.; Marjanovic, G. C. *J. Phys. Chem. B*, **2006**, *110* , 9461–9468
31. Kang, E. T.; Neoh, K. G.; Tan, K. L. *Prog. Polym. Sci.* **1998**, *23*, 211-324
32. Jayakannan, M.; Amrutha, S. R.; Sindhu, K. V. *J. Appl. Polym. Sci.* **2006**, *101*, 2650-2655.
33. Erdem , E.; Karakısla, M.; Sacak , M. *Eur Poly J*, **2004**, *40*, 785–791
34. Jayakannan, M.; Annu, S. ; Ramalekshmi, S. *J. Polym. Sci. Polym. Phys.* **2005**, *43*, 1321
35. Hassan, P. A; Sawant, S. N; Bagkar, N. C; Yakhmi, J. V; *Langmuir*, **2004**, *20*, 4874-4880
36. Bucholz, T.; Sunb, Y.; Loo, Y.L. *J. Mater. Chem.*, **2008**, *18*, 5835–5842
37. Hassan, P. A.; Valaulikar,B. S.; Manohar, C.; Kern, F.; Bourdieu, L.; Candau, S. J. *Langmuir* **1996**, *12*, 4350-4357
38. Yin, H.; Lei, S.; Zhu, S.; Huang, J.; Ye. J. *Chem. Eur. J.* **2006**, *12*, 2825 – 2835
39. Davies, T. S.; Ketner, A. M.; Raghavan, S.R. *J. Am. Chem. Soc.* **2006**, *128*, 6669-6675 9 6669
40. John, G.; Jung, J.H.; Masuda, M.; Shimizu, T. *Langmuir*, **2004**, *20*, 2060-2065

41. John, G.; Jung, J. H.; Minamikawa, H.; Yoshida K.; Shimizu, T. *Chem. Eur. J.* **2002**, 8, 5494
42. Nakashima, N.; Asakuma, S.; Kunitake, T. *J. Am. Chem. Soc.* **1985**, 107, 509-510
43. Xis, Y.; Wiesinger, J. M.; MacDiarmid, A. G. *Chem. Mater.* **1995**, 7, 443-445
44. MacDiarmid, A. G.; Epstein, A. J.; *Synth. Met.* **1995**, 69, 85-92.
45. Lunzy, W.; Banka, E.; *Macromolecules* **2000**, 33, 425.
46. Dufour, B.; Rannou, P.; Fedorko, P.; Djurado, D.; Travers, J.P.; Pron, A. *Chem. Mater.* **2001**, 13, 4032-4040
47. Laska, J.; Djurado, D.; Lunzy, W. *Eur. Polym. J.* **2002**, 38, 947-951.
48. Jana, T.; Nandi, A. K. *Langmuir* **2000**, 16, 3141

## ***Chapter-5***

---

### ***Amphiphilic Dopant Organogel Template for Polyaniline Nanofibers***

### 5.1. Introduction

The facile synthetic chemistry of conducting polyaniline prompted the development of different methods to fabricate and manipulate polyaniline nanostructures using hard or soft templates, emulsion, interfacial, seeding and dilute polymerization methods etc<sup>1-5</sup>. Among all the methods, the soft template method based on organic molecules was found most promising due to easy synthetic procedures and potential for large scale applications<sup>6-8</sup>. Amphiphilic surfactant micelles, block copolymer polymeric micelles, functional liquid crystals and peptide based supramolecular systems were found as good molecular templates for producing polyaniline nanostructures<sup>9-12</sup>. This approach in the development of novel polyaniline nanostructures continues to offer new and exciting alternatives to conventional synthetic strategies. Self-organized molecular gels are other classes of molecular templates and they have been utilized to tune the shape and size of the nanomaterials such as silica, titania, gold and silver<sup>13-16</sup>.

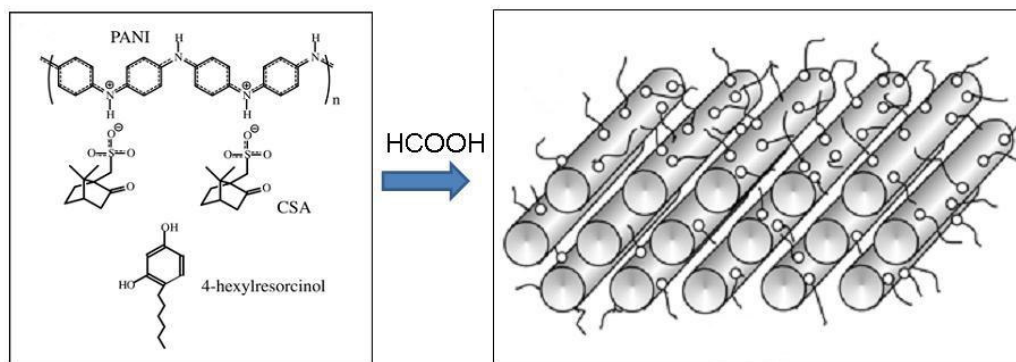


**Figure 5.1.** Schematic representation of post polymerization gel formation between polyaniline, camphor sulfonic acid and hexylresorcinol in formic acid. (Adapted from reference 19)

In polyaniline nanomaterials attempts were reported for gelation in the post polymerization step as well as hydro-gelators based on cholic acid+polyethylene glycol and hexadecyltrimethylammonium chloride etc<sup>17-21</sup>. Post-synthetically gels have usually been prepared by mixing the polyemeraldine base (PANI-EB) and suitable surfactant dopant such as camphorsulfonic acid (CSA), dinonylnaphthalenedisulfonic acid (DNNSA), and dodecylbenzenesulfonic acid (DBSA) in dry or wet conditions<sup>17-19</sup>. These gels were showed more mechanical

flexibility, crystallinity etc compared with parent polymer which is useful for their processing.

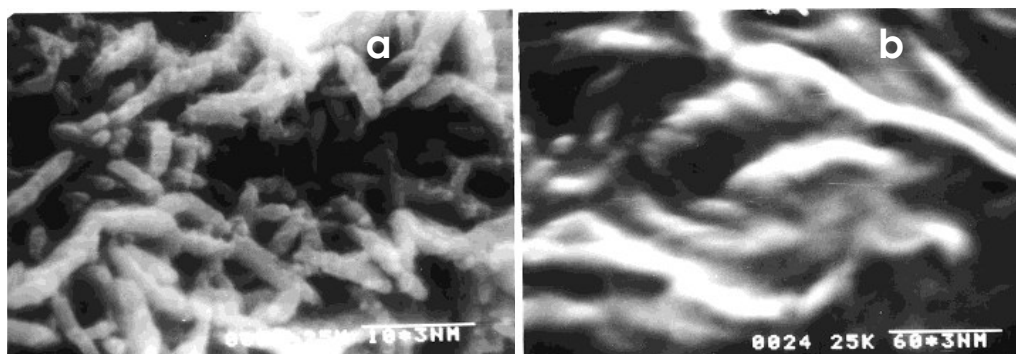


**Figure 5.2.** SEM images of polyaniline gel formed in presence of (a) CSA and DNNSA in formic acid medium. . (Adapted from reference 17,18)

Hydro and organol gels were emerging as important classes of templates for nanomaterials such as silica, titania, gold and silver. These molecular gels are good templates for the polymer nanostructures since the ability to store the sparingly soluble aromatic aniline within their hydrophobic channel regions<sup>22</sup>. During polymerization the growing polyaniline will take up the shape of gel network and then formed nanostructures are isolated by the selective degradation of the gel part of the self-assembly. Few commercially available organogelators were reported as templates for conducting polyaniline nanomaterials. Most often, the removal of the organic gelator molecules during the isolation of nanomaterials found induce instability in the polyaniline morphology<sup>22</sup>. Additionally, the presence of these gelator molecules behaves as insulating matrix and hampers the conductivity and other electronic properties of the conducting nanomaterials. But the advantage of gel based approach over other templates like micelles or liquid crystals is that it is possible to precisely control the morphological parameters of resulting polyaniline nanostructures by carefully tuning the gel template characteristics. The idea of developing new sulfonic acid based dopant-cum gelator molecule is very attractive since the same molecular system can act as both self-organize gel-template for polyaniline nanomaterials as well as anionic counterpart for the stabilizing the positively charged conducting chains. This approach is very much important because: (i) provide new synthetic approach for conducting nanomaterials based on self-templating molecular system, (ii) to understand the mechanism of the gel-templated nanomaterials synthesis and

(iii) provide opportunity for studying the superiority of the nanomaterials synthesized by gel-template approach. So far, there is no report known in the literature based on self gel-template dopant for polyaniline or other conducting nanomaterials.

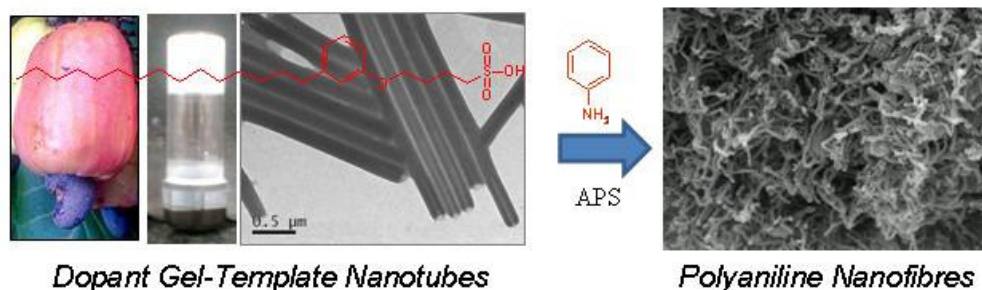


**Figure 5.3.** Dopant nanotube gel template for polyaniline nanofibers.

This chapter is emphasized to design and develop new dopant-cum-molecular gelator as novel soft templates for polyaniline nanostructures. The cardanol based 4-(3-dodecyl-8-enylphenoxy) butane sulfonic acid (dopant 2, see chapter-4)) were found showing gel forming tendencies in organic solvents, but the gel formed was not very stable. It is known that the presence of un-saturation in the aliphatic alkyl side chains of amphiphilic gelators reduces the gelling property<sup>23</sup>. Based on this knowledge a novel saturated counterpart gelator-cum-dopant, 4-(3-pentadecylphenoxy)butane-1-sulfonic acid from a renewable resource derivative, 3-pentadecylphenol was cleverly designed. It produces stable organo-gel nanotube in various organic solvents such as ethanol, methanol, chloroform and dimethylsulfoxide at room temperature. The addition of aniline monomer into the dopant nanotube results in the formation of filled nanotubular self-organization which template for the polyaniline nanofibers. Effects of gelation temperature, concentration and composition of the reactants on the gel mechanism of the gel-template assisted nanomaterials growth were investigated. The nanomaterials were found highly soluble in polar solvents like DMSO which further facilitate the structural characterization by <sup>1</sup>H-NMR, FT-IR and UV-Vis studies. The morphology of the synthesised polyaniline was analyzed by SEM and TEM, and the optical and electronic properties of nanomaterials were determined by UV-vis and four probe conductivity measurements. DSC and WXR D studies were utilized to study the thermo-reversible and solid state ordering of the resultant nanomaterials. Variable temperature electrical conductance measurements were carried out to study influence of molecular gel-template on the

electronic behaviour of polyaniline nanomaterials. The detailed investigation revealed that the nanomaterials synthesized by the gel-template assisted process possessed superior conductivity, crystallinity and solid state ordering.

## 5.2. Experimental Procedures

**5.2.1. Materials:** 3-Pentadecyl phenol, ammonium persulfate (APS), 1, 4-butane sultone, and potassium tertiary butoxide were purchased from Aldrich and used as such. Aniline (Aldrich) was double distilled and kept under nitrogen gas prior to use.

**5.2.2. General Procedures:** NMR analysis of the samples was carried out in 500-MHz Bruker Avance ii NMR Spectrometer at 30 °C. The purity of the compounds was determined by JEOL JSM600 fast atom bombardment (FAB) mass spectrometry. For scanning electron microscopy (SEM) measurements, samples were subjected for thin gold coating using JEOL JFC-1200 fine coater and analysed using a JEOL JSM-5600 LV scanning electron microscope. Atomic Force Microscopy (AFM) images of a thin gel films were recorded under ambient conditions using a NT-DMT Integra machine operating in the tapping mode regime. Samples for the AFM imaging were prepared by drop casting the ethanol solutions onto freshly cleaved mica. Transmission electron microscopy (TEM) images were recorded using a FEI Tecnai 30G<sup>2</sup> S Twin HRTEM instrument operating at 100kV. Wide angle X-ray diffractions of the finely powdered polymer samples were recorded by Philips Analytical diffractometer using CuK-alpha emission. Uv-Vis spectra of the polyaniline in water were recorded using Perkin Elmer Lambda-35 UV-VIS Spectrophotometer. Infrared spectra of the compounds were recorded using a Perkin Elmer, spectrum one FTIR spectrophotometer in the range of 4000 to 400 cm<sup>-1</sup>. For conductivity measurements, the polymer samples were pressed into a 10 mm diameter disc and analyzed using a Keithley 6881 programmable current source and 2128A nanovoltmeter instrument. Thermal analyses of the samples were performed with a DSC Q20 model (TA instruments) differential scanning calorimetry (DSC) instrument under dry nitrogen, and the instrument was calibrated with indium standards.



### 5.2.3. Synthesis of Dopant 3

**Synthesis of 4-(3-pentadecylphenoxy)butane-1-sulfonic acid:** 3-Pentadecylphenol (10 g, 33 mmol) was added into a flask containing potassium tertiary butoxide (7.52 g, 66 mmol) in dry ethanol (100 mL). This solution was heated (60 °C) for 30 minutes under nitrogen atmosphere. The contents were cooled and 1, 4-butane sultone (9 g, 66 mmol) was added drop wise. The reaction was continued by refluxing the content for 40 h under nitrogen atmosphere. It was cooled and the precipitated white solid mass was isolated by suction filtration. The white potassium salt of the product was suspended in water (40 mL) and acidified by 5M HCl (25 mL) to get white precipitate as sulfonic acid. The crude solid was purified by passing through silicagel column using 20/80 v/v methanol/chloroform as eluent. Yield=10.5 g (70 %) ; Melting point = 78 – 84 °C; <sup>1</sup>H-NMR (CDCl<sub>3</sub>, 500 MHz) δ: 6.96 (b, 1H, Ar-H), 6.59 (m, 3H, Ar-H), 3.71 (d, 2H, Ar-OCH<sub>2</sub>), 2.89 (d, 2H, -CH<sub>2</sub>-SO<sub>3</sub>H), 2.45 (b, 2H, Ar-CH<sub>2</sub>) and 2-0.8 (33H, Aliphatic). <sup>13</sup>C-NMR (DMSO-d<sub>6</sub>, 125 MHz) δ: 158.8, 143.9, 129.1, 120.3, 114.7, 111.7, 59.6, 65.1, 51.3, 39.8, 35.1, 31.4, 30.7, 28.6, 28.2, 22.9 and 14.9. FT-IR (KBr, cm<sup>-1</sup>): 3544, 3479, 2916, 2853, 1618, 1579, 1471, 1445, 1298, 1246, 1183, 1061, 970, 869, 774, 749, 723, 690, 684, 621, 588 and 524. FAB-MS (MW: 440.0): m/z = 463.2 (M<sup>+</sup>Na).

### 5.2.4. Synthesis of Polyaniline Nanomaterials

The synthesis of polyaniline is described in detail for **P-30** and other samples were prepared following the similar procedure. The dopant (0.5 g, 1.1 mmol) was dissolved in dry ethanol (50 mL) in a 100 mL beaker by heating in a water bath and cooled to 30 °C to obtain thick gel. To this gel added distilled aniline (1 mL, 1.02 g, 11 mmol; [aniline]/[dopant] = 10) and heated to 75 °C in a water bath for 5 minutes. The solution was allowed to cool in room temperature for 1 h which produced an opaque gel. Ammonium per sulfate solution (3.73 M, 5 mL) was slowly added on the top of the gel at 30 °C and the polymerization was allowed to continue at 30 °C for 24 h without any disturbance. Green coloured polyaniline solid was filtered, washed with distilled water and methanol for several times till the filtrate become colourless. The solid product was dried in a vacuum oven at 60 °C for 48 h (0.01 m Hg). Yield = 0.65 g (43 %). <sup>1</sup>H-NMR (DMSO-d<sub>6</sub>, 500M Hz) δ: 7.46 (2H, Ar-H, PANI), 7.41 (2H, Ar-H,

PANI), 7.14 (1H, Ar-H, dopant), 6.99, 7.11, 7.21 (1H, 1/1/1 triplet, -NH<sup>+</sup>, PANI), 6.73 (3H, Ar-H, dopant), 5.86 (1H, -N-H, PANI) and 4.5 - 0.5 (39H, aliphatic-H, dopant). FT-IR (KBr, in cm<sup>-1</sup>): 3449, 3228, 2920, 2850, 1570, 1494, 1298, 1254, 1153, 1038, 806, 693, 623 and 503.

The samples **P-45** and **P-65** were synthesised following similar procedure at 45 °C and 65 °C, respectively. The yield, elemental analysis data (S/N ratio) are provided in table 5.1.

### 5.3. Results and Discussion

#### 5.3.1. Synthesis of Gelator Dopant and Gelation Studies

The amphiphilic surfactant gelator molecule 4-(3-pentadecylphenoxy) butane-1-sulfonic acid was synthesised by ring opening of 1, 4- butanesultone by 3-pentadecyl phenol in basic conditions (see figure 5.4). The molecule was obtained as a white crystalline powder and the structure of the molecule was confirmed by NMR, FT-IR and Mass spectroscopic techniques.

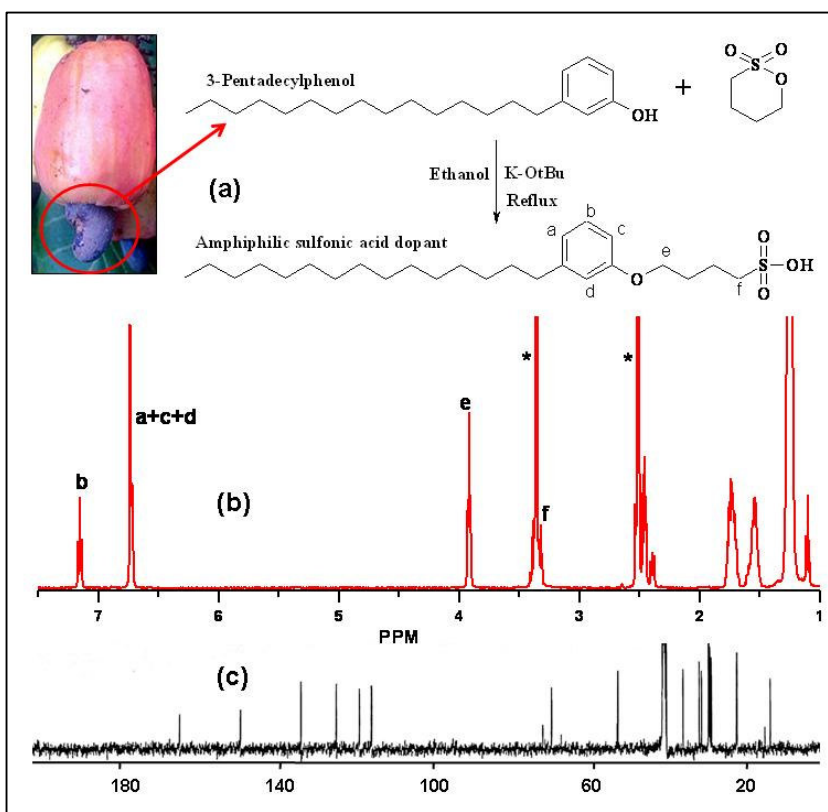


**Figure 5.4.** Synthesis scheme and NMR characterization (*d*<sub>6</sub>-DMSO) of gel forming dopant.

The four protons in the aromatic ring appear with characteristic splitting pattern at 7.16, and 6.74 ppm (see figure 5.4). The protons Ar-OCH<sub>2</sub> and CH<sub>2</sub>-SO<sub>3</sub>H were appeared at 3.92 and 3.32 ppm, respectively. All other aliphatic protons appear below 3 ppm and the intensities of the peaks matched with the expected structure. The new molecule possessed typical amphiphilic structure with a long flexible tail consisting of pentadecyl chain and rigid a polar hydrophilic head (-SO<sub>3</sub>H). The amphiphilic dopant molecule was found to produce opaque white gel in various organic solvents like ethanol, methanol, chloroform, DMSO, etc. Among all the solvents, ethanol produce stable gel for wider concentration range and the molecular gel were stable for more than a month. The photograph of the gel is shown in figure 5.5. Differential scanning calorimetric analysis of the gel in ethanol showed a broad melting peak at 65 °C with respect to gel-to-sol transitions and the sol-to-gel phase change occurred at 53 °C up on cooling (see figure 5.5). The gel was found to show reversible gel-sol transition in the repetitive heating/cooling process.

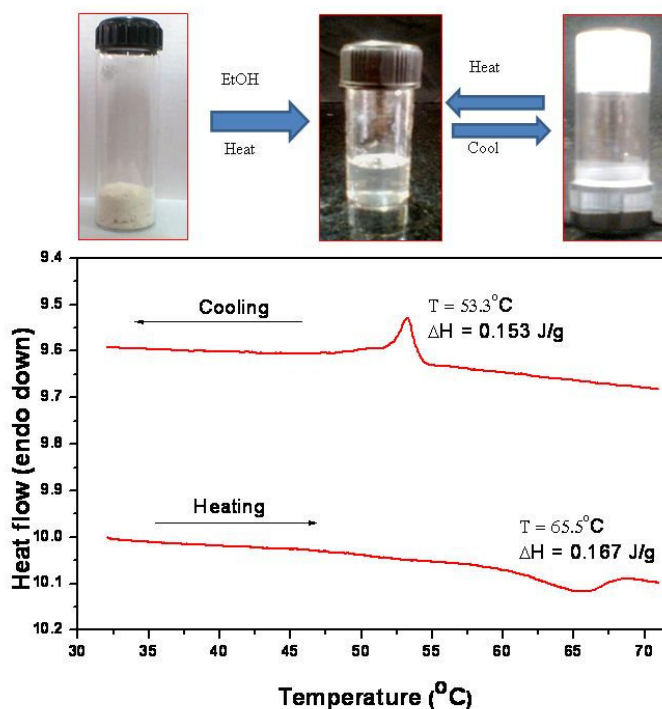


**Figure 5.5.** Photographs of thermo-reversible gel and DSC plot of dopant gel (in sealed hermetic pan).

Xerogels was subjected to various microscopic techniques such as SEM, AFM and TEM and the images were shown in figure 5.6. SEM image confirms the presence

of self-assembled long fibrillar tape like morphology which represents the typical organo-gels texture<sup>24,25</sup>. The average diameters of the long tapes were found 150–350 nm with length upto 8-10 micrometer. AFM image also supports the existence of gel network structure and the tapes were entangled to produce 3D network structure<sup>26</sup>. The average diameters of the fibrils were found as 200-300 nm and long up to 3  $\mu\text{m}$ . In order to get internal features of the nano-assemblies, the gel was subjected to high resolution TEM analysis. TEM images revealed that the inner part of the fibrils is hollowed and they are nothing but nanotubes of  $\sim 5$  micrometer length. The average inner and outer diameter of the nanotubes was found as 60 and 175 nm, respectively and the wall thickness is in the range of 70 nm. The end-to-end distance of the amphiphilic molecule (via MM2 calculation) was found 2.7 nm and so it is reasonable to believe that the nanotube is formed by a multilayer packing of dopant molecules.<sup>27</sup>

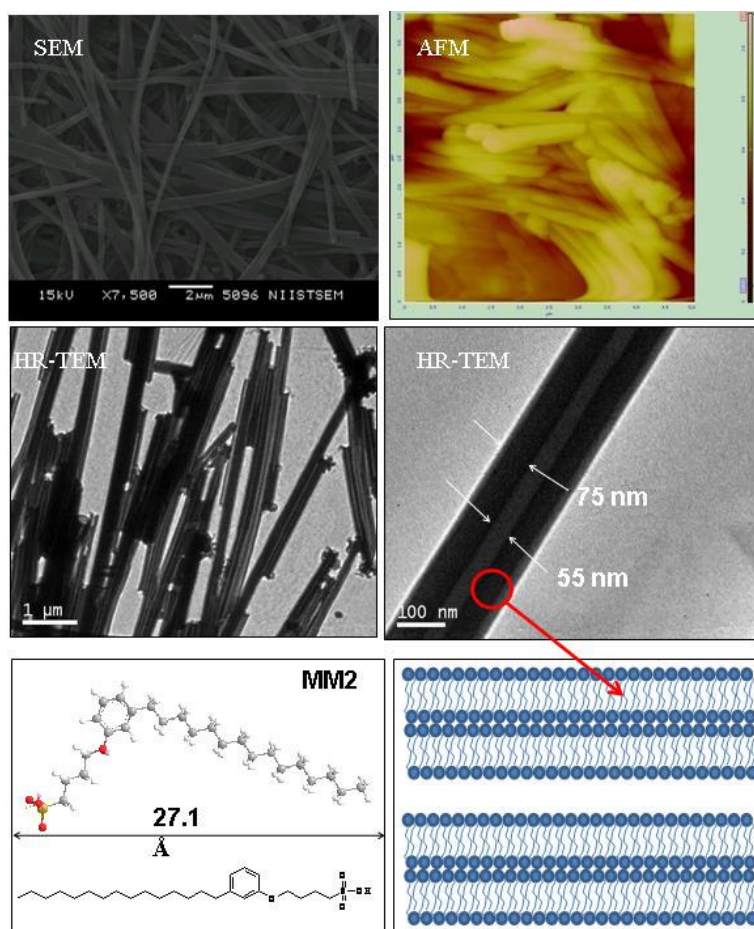


**Figure 5.6.** SEM, TEM and TEM images of dopant gel (xero gel), MM2 structure of the dopant and schematic representation of multilayer nanotube.

To transcribe the superstructures formed in the organogels into the conducting polyaniline structure, the dopant nanotubes were filled with aniline monomers and polymerized by standard chemical oxidative polymerization route (see figure 5.9). The amphiphilic dopant molecule was heated to dissolve completely in ethanol and cooled to get gel-template. Aniline was added to this gel and heated to dissolve completely. Upon cooling to 25 °C, the amphiphilic dopant+ aniline complex formed stable self assembled white gel (see figure 5.7).

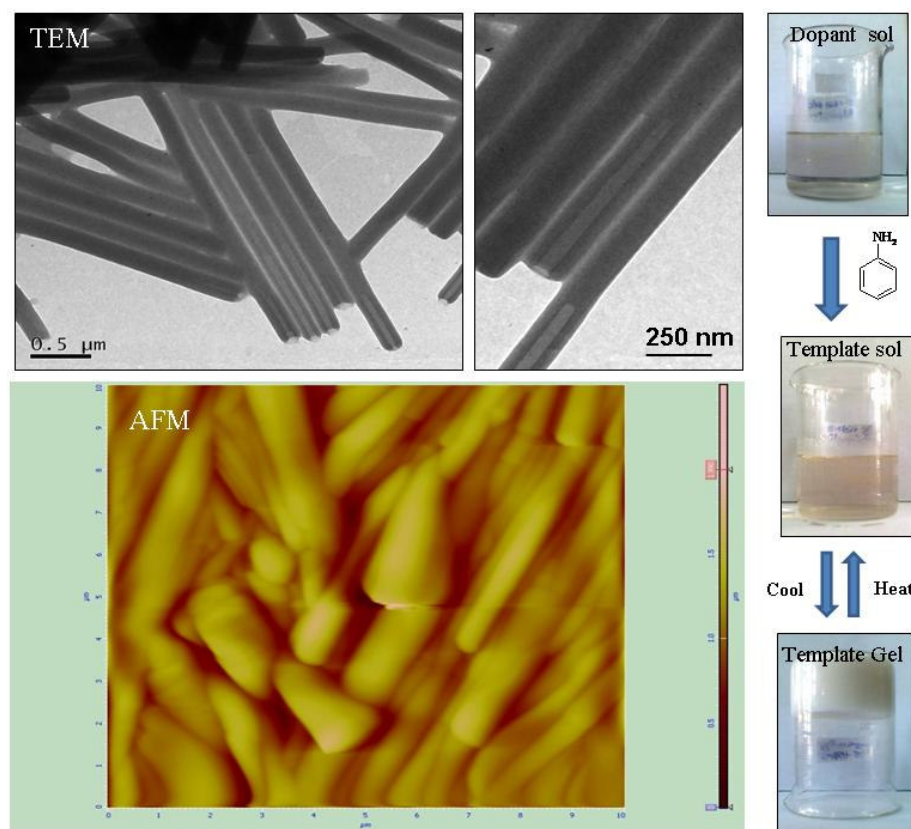


**Figure 5.7.** TEM, AFM images and photographs of gel-aniline template.

The stability of the gel-template was checked by varying the composition of [aniline]/[dopant] from 5 to 20 (in moles) and it was found that homogeneous and stable gel was formed for [aniline]/[dopant] ratio of 10 to 15. Therefore, in the present investigation, the composition of the [aniline]/[dopant] ratio as fixed at 10. AFM analysis of the aniline+dopant gel-template (see figure 5.7) confirmed the existence of uniform array of self-assembled bundles as similar to the morphology of the dopant gel (see figure 5.6). TEM images of the dopant+aniline template evident the presence

of self assembled nanotubes as similar to that of dopant gel (see figure 5.6). These average diameters of the dopant+aniline nanotubes were found 200 nm with length up to 4-5  $\mu\text{m}$ . A closer observation of the nanotubes revealed these nanostructures was not hollow rather that they were half-filled. It is reasonable to believe that during the gel formation the aniline monomers will preferentially occupied inside the cavity of the nanotubes formed by dopant molecules. The inner diameter of the dopant and dopant+aniline nanotubes were almost comparable, which further support the filling of aniline monomers inside the nanotubes.

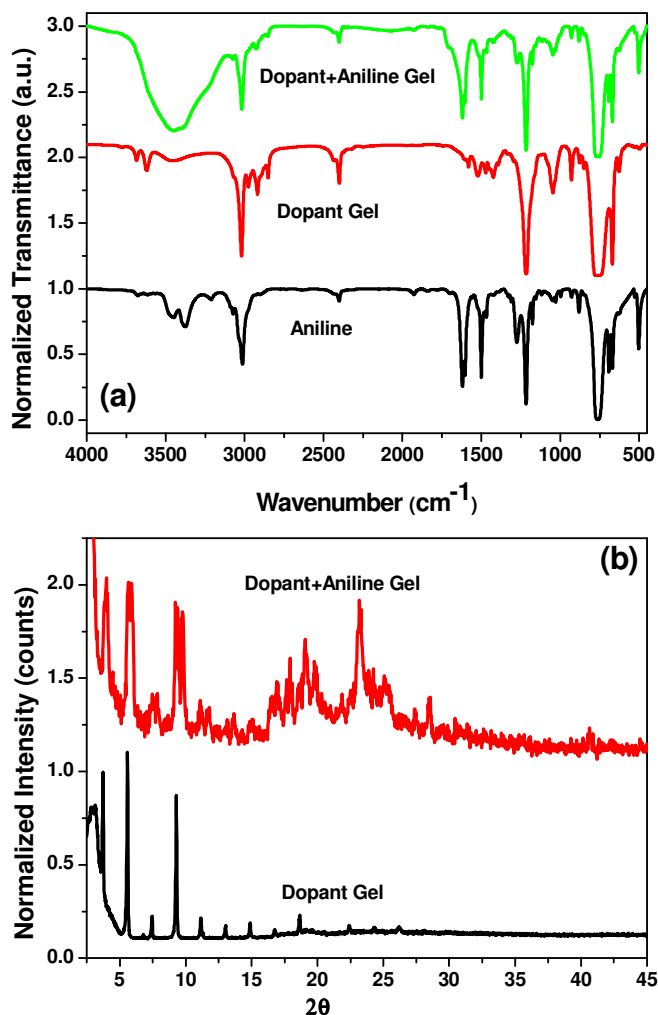


**Figure 5.8.** FTIR and WXR D plots of gel and gel template.

FT-IR is an efficient tool to trace the hydrogen bonding interactions between dopant and aniline molecules present in gel<sup>28</sup>. FT-IR spectra of dopant and dopant+aniline gels were recorded in chloroform solution ( $1 \times 10^{-3} \text{M}$ ) (see figure 5.8,

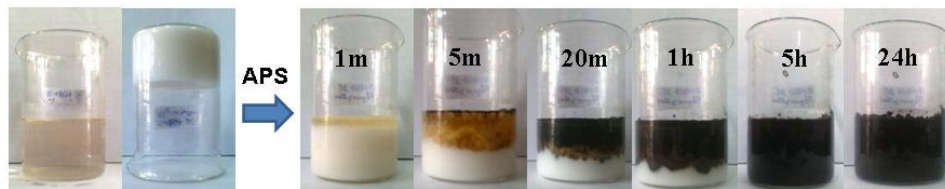
the gels are stable in chloroform also). FT-IR spectrum of the dopant-gel showed two peaks at higher wave numbers (3685 and 3619  $\text{cm}^{-1}$ ) with respect to anti-symmetric and symmetric stretching vibrations of the O-H group in the sulfonic acid, respectively<sup>29</sup>. A broad peak was also seen at lower wavenumber (3460  $\text{cm}^{-1}$ ) corresponding to the hydrogen-bonded O-H stretching vibration. FT-IR spectrum of aniline-dopant gel showed a broad peak at 3200-3600 regions indicating the presence of strong hydrogen bonding interaction between -NH and -OH groups of aniline and dopant molecules. To further confirm the aniline encapsulation and its effect on molecular packing, the gels were subjected to wide angle X-ray diffraction (WXR) studies (see figure 5.8). The self-assembled dopant showed a series of sharp reflections with the lower angle peak being the longest d-spacing of 31 Å (corresponds to  $2\theta = 2.8^\circ$ )<sup>23,27</sup>. The aniline-dopant gel showed all the peaks observed in the parent dopant gel. Additionally, broad peaks were also noticed at higher angle region in the dopant+aniline gel with d-spacing 4–3 Å ( $2\theta=16-26^\circ$ ) confirming the aromatic  $\pi$ - $\pi$  interaction among the dopant+ aniline molecules<sup>23</sup>. The theoretical geometry of the dopant molecule is calculated by MM2 calculations 27.1 Å was matching well with the d-spacing of the dopant gel. It suggests that the dopant molecule exist in the form of layer-like self-assembly in the organo-gel nanotubes. Based on the FT-IR and WXR studies, it is concluded that the dopant molecule self-assembled to form nanotubular gels in which the aniline molecules are stabilized via hydrogen bonding or aromatic  $\pi$ - $\pi$  interaction.

### 5.3.2. Synthesis and Morphology of Polyaniline Nanomaterials

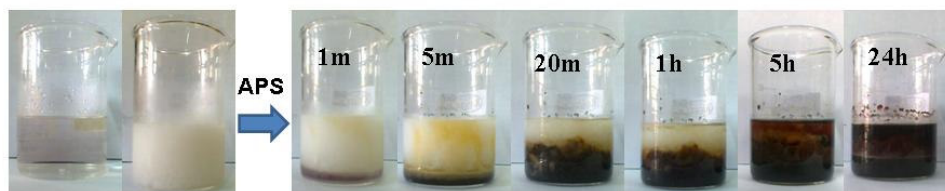
The dopant+aniline gel template was oxidized using concentrated aqueous ammonium perdisulfate (APS) solution to produce conducting polyaniline nanomaterials. To investigate the influence of the physical state of gel template on the morphology of the resulting conducting polymer, the polymerization was carried out at three different temperatures. Two polymerization temperatures were chosen in the gel state (below the gel-to-sol temperature at 30 °C and 45 °C) and one in the dissolved state of the molecules (65 °C, above gel-to-sol temperature). The snap shots of the polymerization reaction were given in the figure 5.9. After the addition of APS

solutions at respective temperatures, the polymerization was proceeded for 24 h at 28 °C during which the entire reaction mixture transformed in to a dark solid mass.

### 1) Polymerization at 30 °C



### 2) Polymerization at 45 °C



### 3) Polymerization at 65 °C

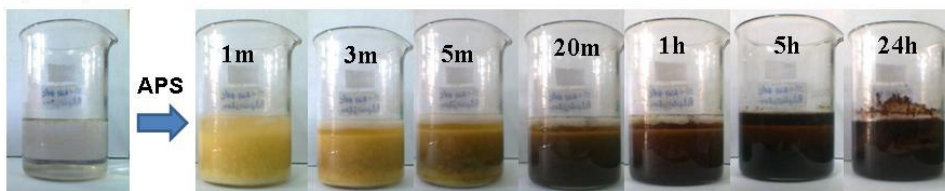


**Figure 5.9.** Snap shot showing the progress of gel-template polymerization.

At 30 °C, the dopant+aniline is very stable and the added APS solutions moved very slowly inside the self assembled gel phase and oxidize the aniline monomer. The gel was found semi-rigid when the polymerization temperature was 45 °C and the polymerization reaction (appearance of green colour) had occurred as soon as the oxidant solution was introduced. Polymerization at 65 °C (sol state) proceeded very fast as normally observed for polyaniline synthesis in aqueous or in organic solvents. The dark green powdered nanomaterial was filtered in a Buchner funnel and washed many times with distilled water followed by methanol until the filtrate become colourless. It was dried in a vacuum oven at 55 °C for 24 h prior to further analysis. The samples were denoted as **P-X**, where **X** denotes for the polymerization temperature (see table 5.1). The yield, S/N ration, viscosity details of the polyaniline nanomaterials are summarised in table 5.1.

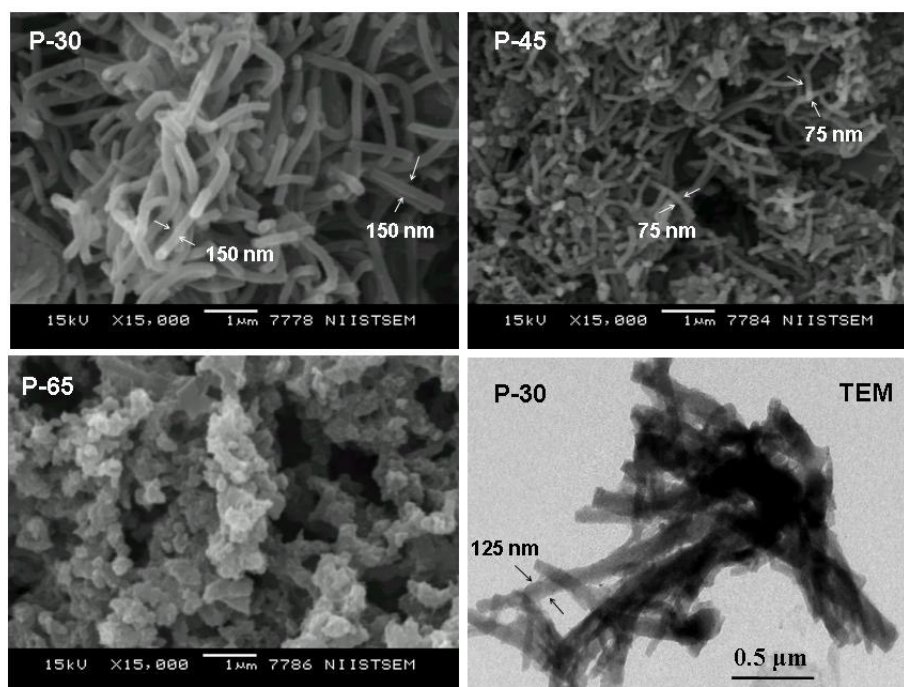


**Table 5.1.** Yield, S/N ratio, morphology, viscosity, and WXRd data of polyaniline nanomaterials.

Sample	Yield <sup>a</sup>	S/N <sup>b</sup> ratio	Morphology <sup>c</sup>	$\eta_{inh}$ (dL/g) <sup>d</sup>	WXRd peaks <sup>e</sup> d-spacing
P-30	43	45.6	Fiber, ~150nm	0.31	24.1, 13.5, 5.2, 4.7, 4.3
P-45	42	45.5	Fiber, ~75nm	0.29	25.6, 13.7, 4.7, 3.4, 3.1
P-65	39	35.3	Agglomerates	0.24	26.1, 13.7, 4.7, 4.3, 3.5

- For isolated product.
- From elemental analysis.
- From SEM images.
- Measured using Ubbelohde viscometer in NMP at 30 °C.
- From powder X-ray diffraction.

The morphologies of the polyaniline nanostructures are given in figure 5.10. The SEM images of **P-30** showed a mat of nanofibers with an average fiber diameter of ~135 nm and length up to 5  $\mu$ m long. The sample **P-45** was also should full of thin-nanofibers with average diameter of 75 nm with a length of 3  $\mu$ m. On the other hand, the sample synthesized at higher temperatures in non-gel state (sample **P-65**) did not produce good morphology and the image appeared as agglomerated particles.

**Figure 5.10.** SEM and TEM images of polyaniline nanomaterials.

To further identify whether the nanofibers were hollow or rigid, they were subjected to TEM analysis. TEM image of **P-30** showed the presence of bundle of solid nanofibers of ~100 nm diameter with a length of 3  $\mu\text{m}$  and there were no nanotubes present. SEM and TEM analysis of the gel templated polyaniline samples clearly indicated that the physical state of the supramolecular gel-assembly play a major role in determining the morphology of resulting polymer nanostructure. In **P-30** and **P-45**, the self-assembled gel template produce uniform nanofibers where as at 65  $^{\circ}\text{C}$  there was no self assembled template which yielded agglomerated polyaniline.

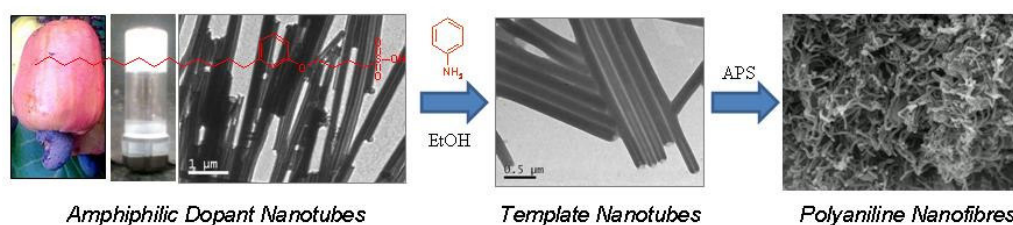


**Figure 5.11.** Proposed mechanism of polyaniline nanofiber formation.

Based on the microscopic studies of the polyaniline nanofiber formed and gel template characterization by SEM, AFM, TEM, WXR, and FT-IR a mechanism for polyaniline nanofiber synthesis via dopant molecular self-assembly in a gel state was proposed (see figure 5.11). The sulfonic acid dopant synthesised has a typical amphiphile structure and undergo self assembly in ethanol leading to the formation of open nanotubes with cavities of diameter ~75 nm. Upon gelation in presence of aniline monomer, the amphiphiles will form nanotubes and the aromatic aniline molecules will preferentially trap inside the hydrophobic regions of self-assembly and also tubular cavity due to the increased capillary action of nano-dimensional cavities<sup>16</sup>. These nano-confined aniline monomers on oxidation in to polyaniline take the shape of the host cavity to produce nanofibers. Subsequent to the polymerization reactions the amphiphilic sulfonic acid form strong complex with imine nitrogens of polyaniline and thereby acts as a dopant similar to any other sulfonic acid dopant. This in turn helps to arrest the nanofiber morphology in the network of gel. This mechanism also underlines the fact that in the case of **P-65** sample the self assembly of the template is not complete during oxidant addition since it is in the temperature range of gel melting (65 $^{\circ}\text{C}$ ) and so the polymerization proceeds just like conventional

polymerization in presence of amphiphilic dopants resulting the formation of polyaniline with agglomerated morphology.

### 5.3.3. Structural Characterization of Polyaniline Nanomaterials:

The long alkyl part of the amphiphilic molecule makes these conducting nanostructures soluble in highly polar solvents like DMSO for complete structural characterization by spectroscopic techniques.  $^1\text{H-NMR}$  spectra of the dopant and polyaniline nanomaterials were recorded in  $d_6\text{-DMSO}$  and their spectra are shown in figure 5.12.

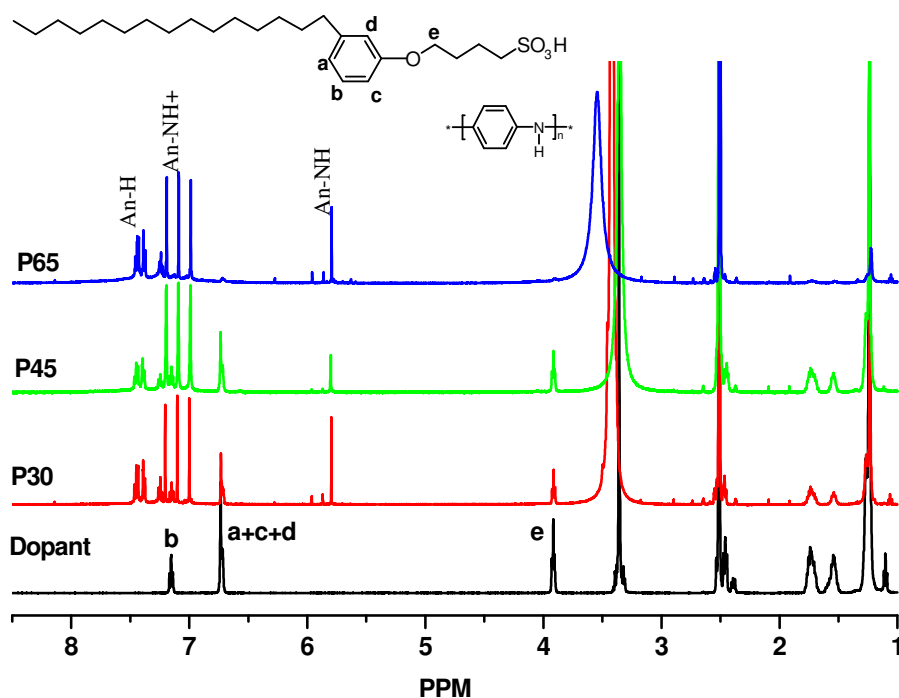


**Figure 5.12.**  $^1\text{H-NMR}$  spectra of polyaniline nanomaterials in  $d_6\text{-DMSO}$ .

The aromatic protons were appeared from 6.5 to 7.5 ppm and all three polymer samples possessed almost identical splitting patterns<sup>30,31</sup>. The peaks at 7.5-7.3 ppm region were assigned as protons of aromatic rings of polyaniline chains. The three equally intense peaks (triplet) at 6.9, 7.1 and 7.2 ppm are attributed to the free radical NH proton resonance due to the  $^{14}\text{N}$  with unit spin which makes the proton attached to it split into three lines<sup>31</sup>. The spectra of the samples also have peaks corresponding to the dopant molecule in addition to their peaks, which confirmed the strong binding of sulfonic acid dopant to the polymer structure. The ratio of the peak

integrals of the dopant (6.72/three protons) to polymer (7.39 and 7.45/four protons) indicated that the samples **P-30**, **P-45** and **P-65** have 34 %, 38 % and 8 % of dopants in the nanomaterials, respectively.

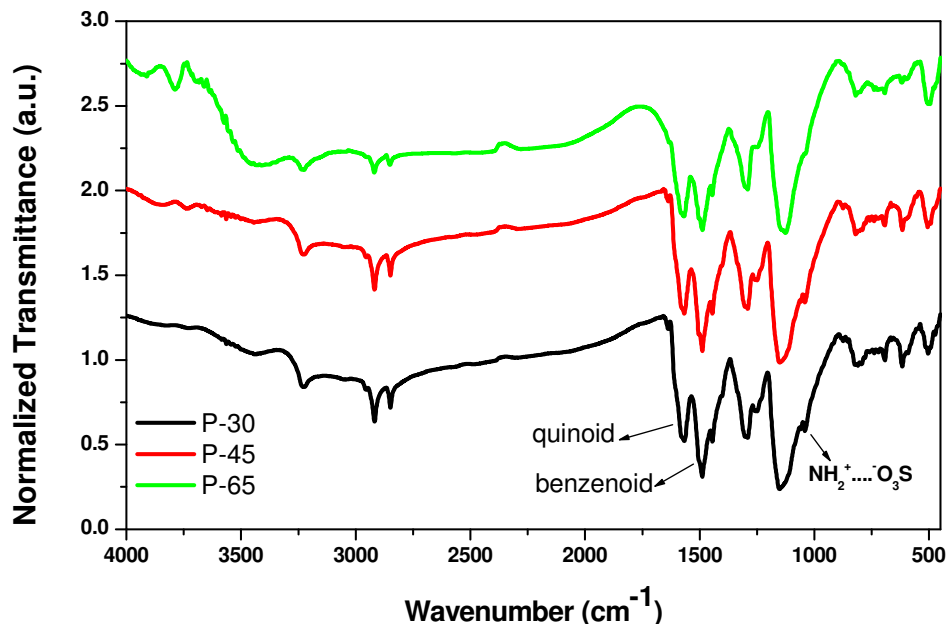


**Figure 5.13.** FT-IR spectra of polyaniline nanomaterials.

FT-IR analysis (see figure 5.13) of the polyaniline nano-materials showed two peaks at 3234 and 2920  $\text{cm}^{-1}$  corresponds to  $-\text{N-H}$  and  $-\text{C-H}$  vibrations, respectively<sup>32,33</sup>. The peaks 1575, 1495, 1310 and 815  $\text{cm}^{-1}$  were assigned to the quinoid ring  $\text{C}=\text{C}$ , benzenoid ring  $\text{C}=\text{C}$  stretching ring deformations,  $\text{C-N}$  stretching and  $\text{C-H}$  out-of-plane vibrations of 1, 4-disubstituted benzene ring, respectively<sup>32</sup>. The appearance of the peaks at 1300, ~ 630 and 1046  $\text{cm}^{-1}$  were attributed to symmetric, un-symmetric stretching vibrations of  $\text{O}=\text{S}=\text{O}$  and  $\text{S-O}$  groups and  $\text{NH}_2^+ \dots \text{SO}_3^-$  interactions between the polymers chain and the dopant<sup>34</sup>. The inherent viscosity of the polymer nanofibers (in PANI-EB form) was determined for 0.5 wt % solutions in NMP at 30 °C. The inherent viscosities of the polymers were obtained in the range of  $\eta_{\text{inh}} = 0.24\text{-}0.31$  dL/g. The viscosities of the samples indicate the formation of good molecular weight samples and the values are similar to the earlier reports for polyaniline materials<sup>35</sup>.

### 5.3.4. Optical and Solid-state Properties of Polyaniline Nanomaterials

The polyaniline nanostructures are water suspendable and the colloidal solution is stable for 5-7 hours at ambient conditions. UV-vis spectra of the nanostructures were recorded in water and are shown in figure 5.14. It is clear from the plots nanofiber samples that it contains all the characteristics peaks of doped polyaniline, the peaks at 310, 430 and 900 nm, which are assigned as the transitions from  $\pi$ - $\pi^*$  band, polaron band to  $\pi^*$  band,  $\pi$  band to polaron band, respectively<sup>36,37</sup>. All the samples showed a localized polaron peak at 900 nm characteristic of coiled nature of polymer chain conformation in these samples<sup>37</sup>. A possible reason for this coiled conformation is that the polymerization is taking place in ethanol solvent, which is not a good solvent for the charged polymer chains resulting the coiling of chains. Among the three cases the polaron peak of **P-65** is relatively less intense may be due to its poor morphology and lower degree of doping.

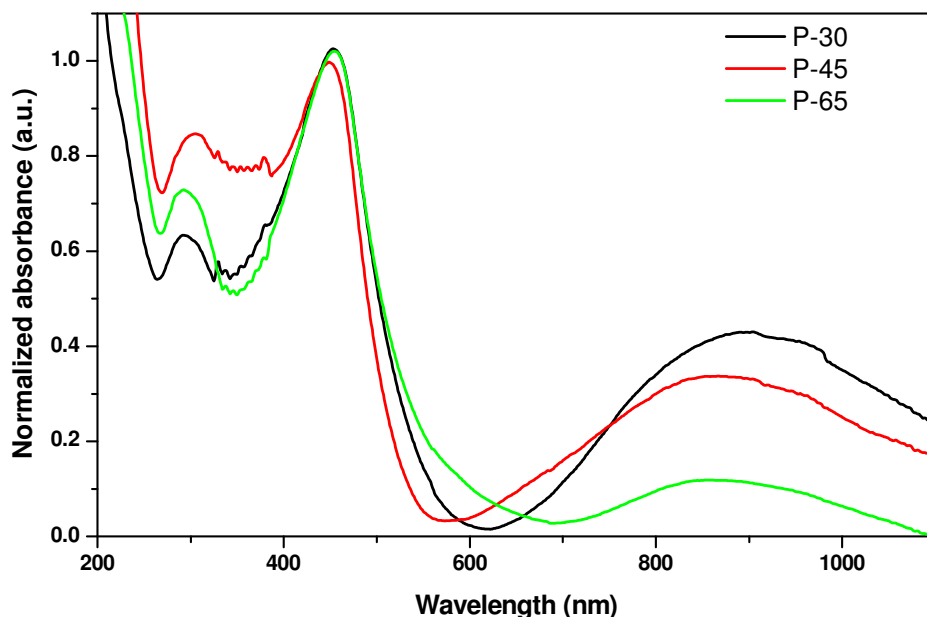


**Figure 5.14.** Absorption spectra of polyaniline nanomaterials.

The optical properties of the polyaniline nanostructures clearly demonstrated that the polymer chains are in coil-like conformation of emeraldine form and the morphology of the materials are inherent to the template selectivity in the nanomaterial synthesis.

Polyaniline nanostructures were subjected to powder X-ray diffraction studies for understanding their solid state properties. WXR D pattern of dopant gel and

polyaniline nanomaterials are shown in figure 5.15. The polyaniline nanomaterials have a sharp lower angle peaks at  $2\theta = 3.4^\circ$  (d-spacing = 25.6 Å) and at  $2\theta = 6.4^\circ$  (d-spacing = 13.7 Å) which are not observed in the dopant gel. These peaks are assigned to layered structural organization of polyaniline chains followed by the inter-digitations and crystallization of the dopant tails on the comb-shaped polymer chains.<sup>38-40</sup> Besides these peaks there are broad peaks around  $2\theta = 20^\circ$  (d=4.6 Å) and  $25^\circ$  (d = 3.5 Å) which is ascribed to the van der Waals distances between stacks of phenylene rings present in the polymer chain and between aliphatic chains of the dopant, respectively.

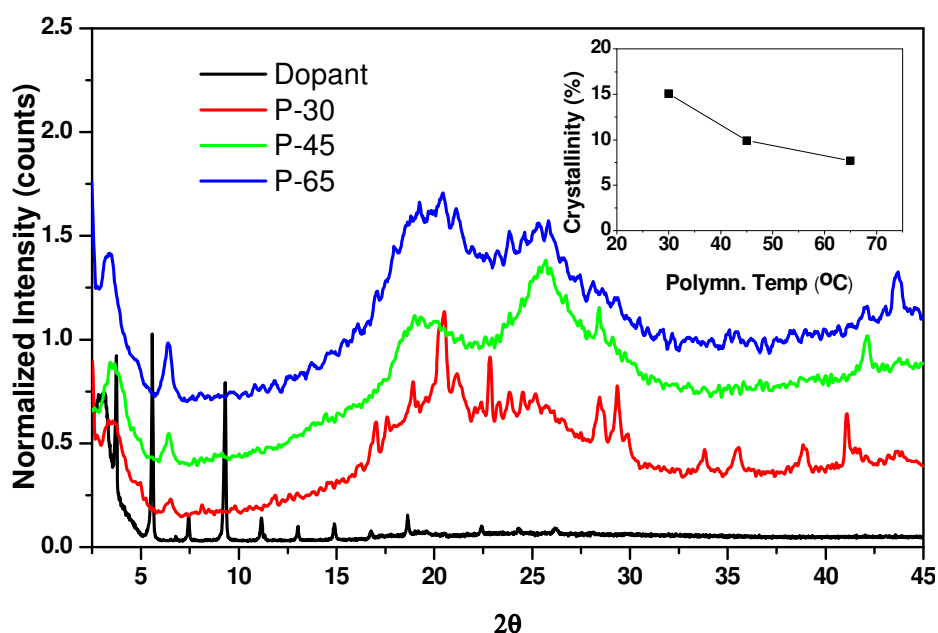


**Figure 5.15.** WXR D plots of polyaniline nanomaterials.

In all nanostructures the  $3.4^\circ$  Bragg peak have a d-spacing value in the range of 25.6 Å, which is comparable to the end to end molecular length of 27.1 Å of the dopant molecule. This suggests that the polyaniline-dopant complex exhibit a lamellar type structural organization in which stacks of polymer chains are separated by dopant sulfonate anions<sup>38</sup>. The second peak at  $6.4^\circ$  has a d-spacing of 13.7Å which may be coming from the second order diffraction of polyaniline-dopant lamellae. In **P-30** nanofibers the higher angle peaks are relatively very sharp and amorphous halo region is very much suppressed indicating more crystallinity in this sample. The percent crystallinity of the polymer samples were determined by deconvolution of the WXR D peaks and comparing crystalline peaks (sharp peaks) with amorphous broad regions<sup>40</sup>.

The percent crystallinity of the samples **P-30**, **P-45** and **P-65** were found to be 15.1, 9.9 and 7.7 % respectively (see figure 5.15, inset). This indicates that the gel-template stability and the morphology have prominent roles in solid state packing of the polymer chains. NMR analysis indicates that the samples **P-30** and **P-45** have 35-38 % of dopant molecules present in the nanomaterial whereas only 8 % in **P-65**. Therefore, the presence of large amount of dopant in **P-30** and **P-45** induce high self-organization and produced ordered and crystalline structures compared to **P-65**.

### 5.3.5. DSC Analysis of Dopant and Polyaniline Nanomaterials:

Polyaniline nanomaterials were subjected for differential scanning calorimetry (DSC) to study the thermal transitions and nature of supramolecular interaction between dopant and polyaniline polymer chains<sup>17,18</sup>.

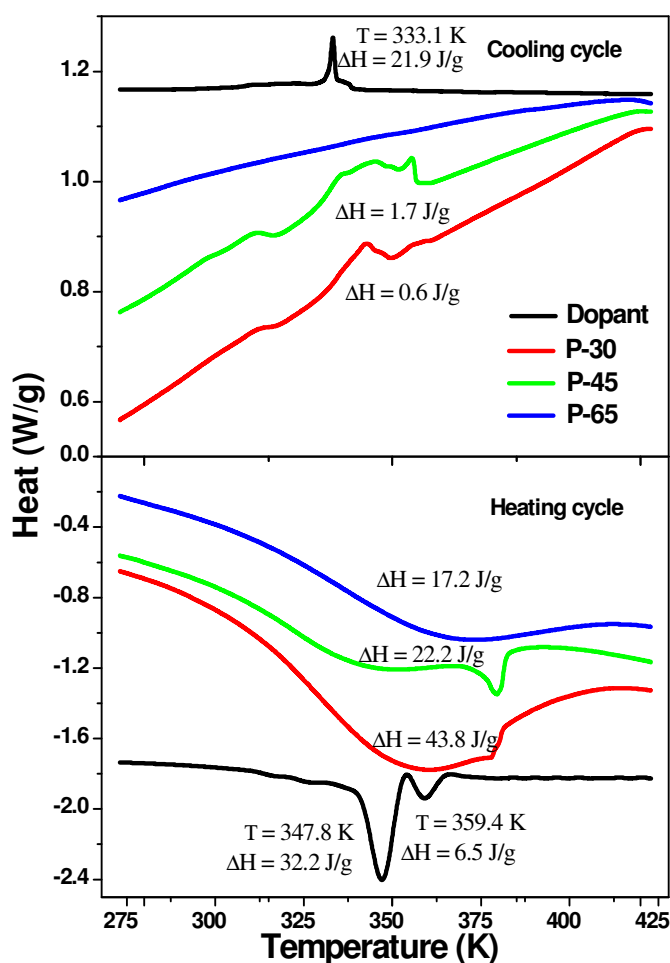


Figure 5.16. DSC thermograms of dopant and polyaniline nanomaterials.

Polyaniline samples were heated from 223 to 473 K (-50 to 200 °C) and cooled from 473 to 223 K at a rate of 10°/min to record the thermal transitions. The DSC plot of the dopant showed a sharp exothermic peak at 333 K ( $\Delta H = 21.9$  J/g) corresponding to crystallization upon cooling from the melt with a small shoulder peak. On subsequent heating two closely placed endothermic peaks [at 348 ( $\Delta H = 32.2$  J/g) and 359 K ( $\Delta H = 6.5$  J/g)] were observed corresponding to the transition from crystalline to melt. All the three samples showed multiple melting transitions in the first heating cycle. In the cooling cycle, the samples **P-30** and **P-45** showed a sharp crystallization peaks except **P-65**. In the subsequent second heating cycle, all the three samples failed to show any melting transitions. Therefore, all samples were subjected to annealing at 253 K (-20°C) for more than 48hs and then subjected to DSC analysis again for reproducible result. The heating/cooling cycles of annealed samples are shown in figure 5.16 along with dopant. The thermograms of annealed samples are almost identical to that of the first heating/cooling experiments; however, their enthalpies are significantly different. The samples showed broad endotherm in the region of 330- 400 K during heating with a sharp peak at 379 K corresponding to the melting of gel phase (in samples **P-30** and **P-45**). The enthalpies of melting transition for the annealed samples were obtained as 43.8, 22.2, and 17.2 J/g for **P-30**, **P-45** and **P-65** respectively. The more crystalline samples need higher energy for melting, therefore, the order of crystallinity in polyaniline samples are in the order of **P-30** > **P-45** > **P-65**. Upon cooling **P-30** and **P-45** showed crystallization peaks at 344 ( $\Delta H = 0.6$  J/g) and 312 K ( $\Delta H = 1.7$  J/g) whereas **P-65** failed to show any crystallization peaks. DSC analysis confirmed that the samples **P-30** and **P-45** which are synthesised using gel-state have more crystallinity than **P-65** which is prepared in sol-state. The WXR analysis (see figure 5.15) of the samples were also similar trend of high percent crystallinity for samples prepared in gel-state (**P-30** and **P-45**) compared to sol-state (**P-65**). It is reasonable to believe that in gel-state polymerization induce and retain the supramolecular interaction between the dopant molecules with polyaniline chain in the nano-fibrillar network structure for highly ordered and crystalline state. On the other hand, the samples prepared at sol-state (for **P-65**) is found amorphous due to the lack of dopant-polyaniline interactions.



### 5.3.6. Four Probe Conductivity Measurements of Polyaniline Nanomaterials

Generally the electrical properties of conducting polymers are strongly influenced by the effect of various type of ordered structures<sup>41,42</sup>. The DSC thermograms indicated that the samples are sensitive to thermal transitions between 300K to 450K. In the current system the polyaniline fibrils are arrested in dopant gel at lower temperature, become mobile at elevated temperatures and the electrical properties of the material is expected to change during this transition. In order to study the electrical behaviour temperature dependent four-probe measurements for compressed pellets in the range of 298 – 438 K were carried out and results are given in figure 5.17.

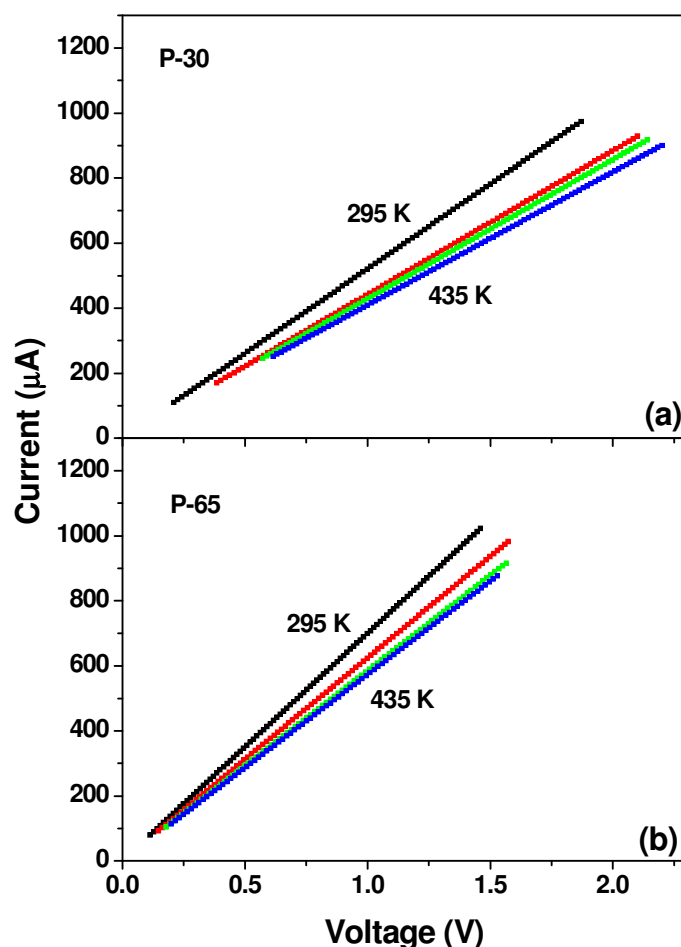


**Figure 5.17.** Current-Voltage (I-V) plots of polyaniline nanomaterials.

The linear trend in the current versus voltage (I-V) plots of the **P-30** and **P-65** (see figure 5.17a and 5.17b) clearly shows that the polyaniline nanomaterials are

following typical Ohmic behaviour<sup>43</sup>. The conductance versus temperature was plotted for all the three samples and shown in figure 5.18a. At room temperature (300K), the samples **P-30**, **P-45** and **P-65** showed conductance values of  $1.9 \times 10^{-2}$ ,  $7.2 \times 10^{-3}$ , and  $1.8 \times 10^{-5}$  S, respectively. The difference in conductance among the samples can be correlated to the difference in morphology, degree of doping and solid state properties.

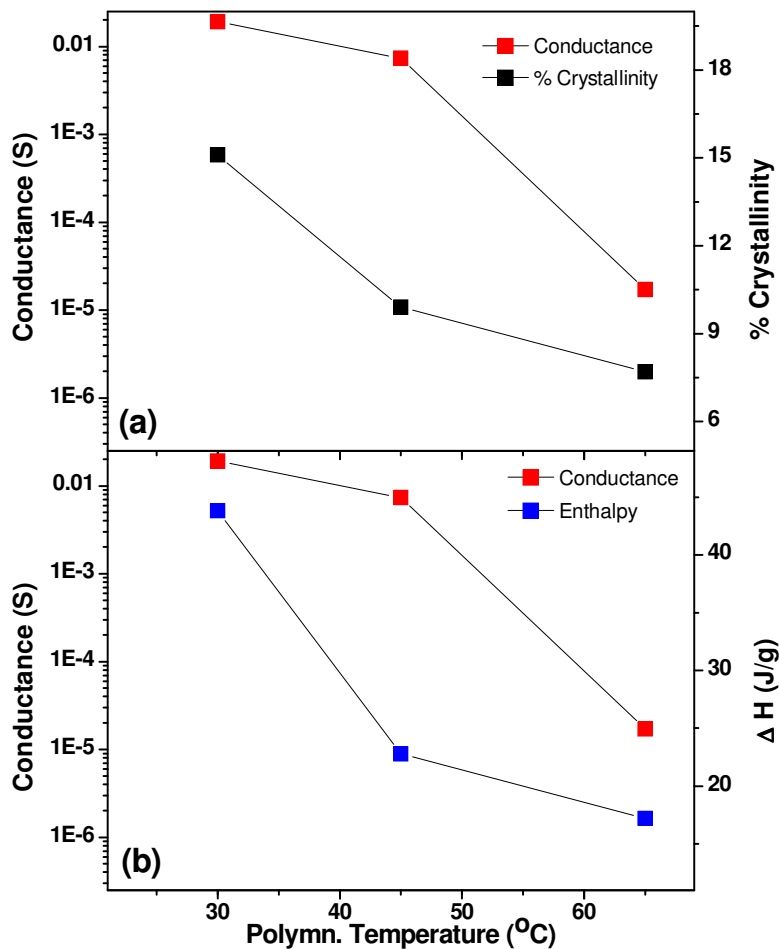


**Figure 5.18.** Plot showing variation of conductance with crystallinity and enthalpy of nanomaterials.

The room temperature conductance of the nanomaterials is correlated to the enthalpy values obtained by DSC and percent crystallinity by WXR (see figure 5.18b). The sample **P-30** showed a higher  $\Delta H = 43.8$  J/g (also % crystallinity) and has high conductivity whereas amorphous sample **P-65** (less  $\Delta H$  and % crystallinity) has three order less conductance than ordered structures (**P-30** and **P-45**). The temperature dependent conductance measurements revealed that there is a slight increase in the

conductivity of the samples upto 400 K, but a huge jump of two orders in magnitude was observed above 410 K (see figure 5.19). The conductance reaches the maximum value of 0.45 and 0.21 and for **P-30** and **P-45**, respectively. But the less ordered sample **P-65** still showed a less conductivity of  $3.3 \times 10^{-3}$  S even at 450K. It is interesting to note that the conductance increment occurs at a temperature just above melting temperature of dopant-polyaniline complex as obtained by DSC (380K). So it is reasonable to believe that upon heating the polymer fibrils becomes more flexible and better contact is established above 400 K and the expanded state in turn improve the conduction.

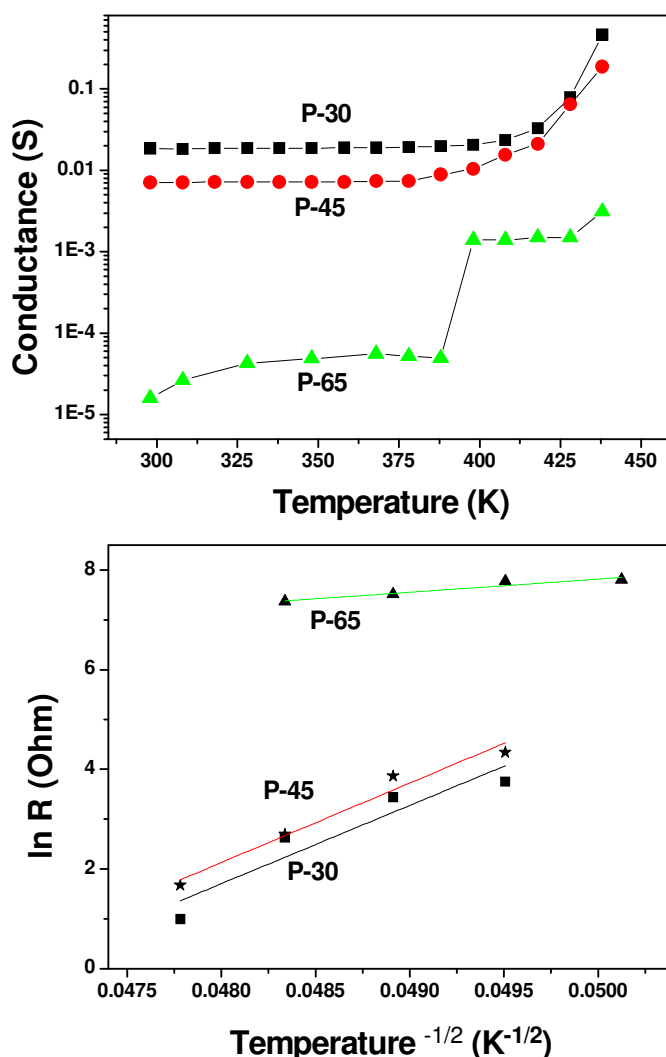


**Figure 5.19.** Conductance vs temperature and  $\ln R$  vs  $(T)^{-1/2}$  plots of nanomaterials.

In order to study the electronic transport behaviour of the material, the resistance of the material as function of temperature was measured. Over the temperature range (298-438 K), the nanomaterials exhibited semiconducting behaviour; i.e., the resistance decreased with increasing temperature<sup>43,44</sup>. In the insulating regime, the low-temperature resistivity  $\rho(T)$  of the conducting polymer follows the exponential temperature dependence of variable range hopping (VRH)<sup>44</sup>:

$$\rho(T) = \rho_0 \exp(T_0/T)^m$$

where the exponent  $m = 1/4, 1/3,$  and  $1/2$  for three dimensional (3D), two-dimensional (2D), and one dimensional (1D) hopping, respectively.  $T_0$  is the Mott characteristic temperature and can be obtained from the slope of  $\ln R(T)$  vs  $T^{-1/m}$  plot<sup>41,44</sup>. Since bulk conductivity of the nanofibres follow conductivity like one-dimensional semiconductors, the plot of  $\ln R$  versus  $T^{-1/2}$  is given in figure 5.19 for polyaniline nanomaterials. At temperatures below 400 K ( $T^{-1/2} > 0.049$ ) there is no considerable change in  $\ln R$  values and therefore the data above 410K ( $T^{-1/2} < 0.049$ ) are used for the Mott's plot. The plots showed a linear trend and followed VRH model. The  $T_0$  values for **P-30**, **P-45** and **P-65** were obtained as  $1.57 \times 10^3$ ,  $1.59 \times 10^3$ , and  $2.62 \times 10^2$  K respectively<sup>44</sup>. The ordered and crystalline samples showed almost one order difference in the Mott temperature compared to that of the amorphous one. The electrical conductance measurements revealed that the polyaniline nanomaterials exhibits linear current-voltage behaviour corresponding to electronic conductivity (Ohm's law) and the conductance showed a temperature dependent increment similar to a semi-conductor following the 3-D VRH model at elevated temperatures.

#### **5.4. Conclusion**

Self-assembled gel formed by a new renewable resource based amphiphilic sulfonic acid dopant was utilized as a template for polyaniline nanofibers. It is demonstrated that the gel template has a pivotal role in directing polyaniline chains to form nanofibers. SEM, AFM and TEM techniques have been successfully utilized to trace the nature and shape of polymerization templates to understand the mechanism of the nanomaterials formation. This novel gel template approach for polyaniline nanofibers has the following salient features (i) a novel gel forming amphiphilic sulfonic acid dopant was developed from renewable resource based 3-pentadecyl phenol, (ii) the dopant form self assembled opaque gels in highly polar organic solvents like aliphatic alcohols, chloroform, DMSO, etc, (iii) the gelation characteristics was studied by DSC and WXR, (iv) SEM, AFM and TEM analysis of dopant gels showed that the molecules are self-assembled into nanotubes, (v) the dopant molecules also self-assembled in the presence of aniline as gels with aniline molecule preferentially trapped inside the nanotubes (vi) this oxidation of gel-template produces polyaniline nanofibers, (vii) the polymerization at various temperatures clearly showed that the physical state and stability of the gel plays a major role in determining the morphology, (viii) the nanomaterials showed high solubility in polar solvents like water and dmsol that enabled us to characterize these materials by NMR,UV-vis, and FTIR, (ix) WXR and DSC analysis revealed that the samples synthesized at gel-state possessed highly crystalline compared that of sol-state samples, (x) the supramolecular interaction between dopant and polyaniline complex formed lamellae of interdigitated dopant molecules stacked in between polyaniline chains and improved the solid state properties and (xi) the temperature dependent conductance measurements showed a high conductivity of the gel-template synthesized samples and they followed 3-D VRH model at elevated temperature. In a nut shell, it is showed that the novel amphiphilic dopant derived from renewable resource is a good gelator and the gel assemblies are good template for the growth of highly ordered and soluble polyaniline nanofibers.

**5.5. References**

1. Li, D.; Huang, J.; Kaner, R. B. *Acc. Chem. Res.*, **2009**, *42*, 135-145
2. Wan, M. X. *Adv. Mater.* **2008**, *20*, 2926–2932
3. Zhang, D. H.; Wang, Y. Y. *Mater. Sci. Eng. B*, **2006**, *134*, 9.-19
4. Tran, H. D.; Li, D.; Kaner, R. B. *Adv. Mater.* **2009**, *21*, 1–13
5. Wan, M. X. *Macromol. Rapid. Commun.* **2009**, *30*, 963–975
6. Wei, Z.; Zhnag, Z.; Wan, M. *Langmuir*, **2002**, *18*, 917-921.
7. Zhang, Z.; Wei, Z.; Wan, M. *Macromolecules* **2002**, *35*, 5937-5942.
8. Carswell, A.D.W.; O'Rear, E.A.O.; Grady, B.P. *J. Am. Chem. Soc.*, **2003**, *125*, 14793-14800
9. Haung, K.; Wan, M.X. *Chem. Mater*, **2002**, *14*, 3486-3492
10. J. Han, G. Song, R. Guo, *Adv. Mater.* **2007**, *19*, 2993
11. Huang, L.; Wang, Z.; Wang, H.; Cheng, X.; Mitra, A.; Yan, Y. *J Mater. Chem*, **2002**, *12*, 388-391
12. J. Ryu, C. B. Park, *Angew. Chem. Int. Ed.* **2009**, *48*, 1–5.
13. Jung, J.H.; Lee, S.H.; Yoo, J. S.; Yoshida, K.; Shimizu, T.; Shinkai, S. *Chem. Eur. J.* **2003**, *9*, 5307 -5313.
14. Jia, Q.; Shimizu, T. *Chem. Commun.* **2005**, 4411–4413.
15. Shimizu, T. *J. Polym. Sci: Part A: Polym Chem.* **2008**, *46*, 2601–2611.
16. Shimizu, T. *J. Polym. Sci: Part A: Polym Chem.* **2006**, *44*, 5137–5152.
17. Jana, T.; Chatterjee, J.; Nandi, A. K. *Langmuir* **2002**, *18*, 5720.
18. Jana, T.; Roy, S.; Nandi, A. K. *Synth. Met.* **2003**, *132*, 257.
19. Kosonen, H.; Ruokolainen, J.; Knaapila, M.; Torkkeli, M.; Jokela, K.; Serimaa, R.; ten Brinke, G.; Bras, W.; Monkman, A. P.; Ikkala, O. *Macromolecules* **2000**, *33*, 8671.
20. L. Meng, Y. Lu, X. Wang, J. Zhang, Y. Duan, C. Li, *Macromolecules*, **2007**, *40*, 2981-2983
21. Li, G.; Zhang, Z.; *Macromolecules*, **2004**, *37*, 2683-2685
22. Tovar, J. D.; Rabatic, B. M.; Stupp, S. I. *Small.* **2007**, *3*, 2024 – 2028
23. John, G.; Jung, J.H.; Masuda, M.; Shimizu, T. *Langmuir*, **2004**, *20*, 2060-2065
24. Terech, P.; Weiss, R. G. *Chem. Rev.* **1997**, *97*, 3133-3159.
25. Estroff, L. A.; Hamilton, A. D. *Chem. Rev.* **2004**, *104*, 1201-1217.

26. A. Ajayaghosh, V. K. Praveen, *Acc. Chem. Res.* **2007**, *40*, 644–656
27. John, G.; Masuda, M.; Okada, Y.; Yase, K.; Shimizu, T. *Adv. Mater.* **2001**, *13*, 715–718.
28. Deepa, P.; Jayakannan, M. *J Polym. Sci: Part A: Poly. Chem.* **2007**, *45*, 2351–2366.
29. Rekha, N.; Asha, S. K. *J Polym Sci Polym Chem* **2009**, *47*, 2996–3009.
30. Zhou, C.; Han, J.; Song, G.; Guo, R. *J. Polym. Sci., Polym. Chem.* **2008**, *46*, 3563
31. Mu, S.; Yang, Y. *J. Phys. Chem. B*, **2008**, *112*, 11558
32. Zheng, W.; Angelopoulos, M.; Epstein, A. J.; MacDiarmid, A. G. *Macromolecules* **1997**, *30*, 7634–763
33. Kang, E. T.; Neoh, K. G.; Tan, K. L. *Prog. Polym. Sci.* **1998**, *23*, 211–324
34. Li, X.G.; Wang, H.Y.; Huang, M.R. *Macromolecules.* **2007**, *40*, 1489–1496
35. Erdem, E.; Karakısla, M.; Sacak, M. *Eur Poly J*, **2004**, *40*, 785–791
36. Xis, Y.; Wiesinger, J. M.; MacDiarmid, A. G. *Chem. Mater.* **1995**, *7*, 443–445
37. MacDiarmid, A. G.; Epstein, A. J.; *Synth. Met.* **1995**, *69*, 85–92.
38. Laska, J.; Djurado, D.; Lunzy, W. *Eur. Polym. J.* **2002**, *38*, 947–951.
39. Jana, T.; Nandi, A. K. *Langmuir* **2001**, *17*, 5768.
40. Lunzy, W.; Banka, E.; *Macromolecules* **2000**, *33*, 425.
41. Long, Y.; Zhang, L.; Ma, Y.; Chen, Z.; Wang, N.; Zhang, Z.; Wan, M. *Macromol. Rapid. Commun.* **2003**, *24*, 938–942
42. Long, Y.; Chen, Z.; Wang, N.; Ma, Y.; Zhang, Z.; Zhang L.; Wan, M.; *Appl. Phys. Lett.* **2003**, *83*, 1864–1865.
43. Long, Y.; Chen, Z.; Ma, Y.; Zhang, Z.; Jin, A.; Gu, C.; Zhang, L.; Wei, Z.; Wan, M. *Appl. Phys. Lett.* **2004**, *84*, 2205–2207.
44. Mativetsky, J. M.; Datars, W.R. *Physica B*, **2002**, *324*, 191–204

## ***Chapter-6***

---

### ***Functionalized Polyaniline Nanospheres: Vitamin-C sensing***



### 6.1. Introduction

A large number of methods are known for the synthesis of polyaniline nanostructures like fibres, tubes etc, but the synthesis of nanospheres has been noticed as a challenging task mainly because the nanofibrillar morphology appeared to be intrinsic to polyaniline while synthesized in water<sup>1-5</sup>. Unlike polyaniline nanofibers, the area of polyaniline nanospheres is restricted due to these synthetic limitations and almost the properties of nanospheres were not completely understood. The nanospheres are particularly interesting for optoelectronics and sensors due to their large surface area compared to that of nanofibers. It is also important to note that the nanospheres can be effectively solvated due to its globular nature which enhances the solubility in common solvents for structural characterization by spectroscopic techniques. There are very few examples reported for polyaniline nanospheres which include templates like polystyrene spheres, hydroxy alkyl cellulose and salicylic acid assisted polymerization, etc<sup>6-8</sup>. Also the synthesis and mechanism of nanospheres formation was not understood unlike their nanofiber counterparts.

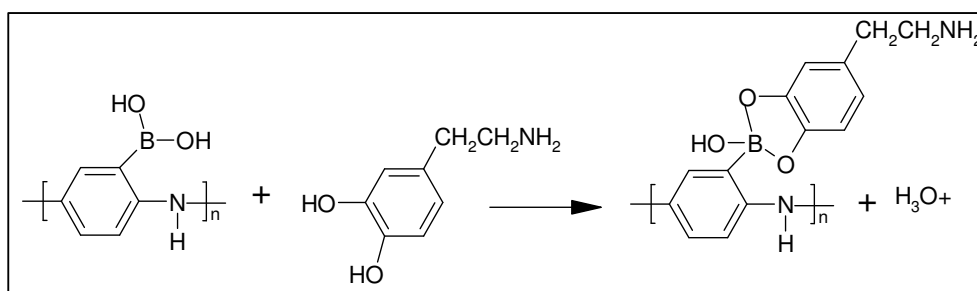


**Figure 6.1.** Self-doped poly (anilineboronic acid) as a sensor for dopamine.

Conducting polyaniline nanomaterials are highly sensitive to molecular interactions, which provide excellent signal transduction for molecular detection<sup>9</sup>. It has been extensively studied in chemical sensors but not that much study has been done in biosensors. The reason is that unsubstituted polyaniline is neither conductive nor electrochemically active in neutral solutions, which is a prerequisite for biosensor applications<sup>10</sup>. It is also limited both in specificity and in the selectivity of the detection. The development of self-doped polyaniline and polyelectrolyte-anion-doped polyaniline helped the use of polyanilines into the biosensor field due to the improved redox activity and conductivity in neutral pH solutions<sup>11,12</sup>. For example, self-doped poly (anilineboronic acid) showed good sensing towards bio-molecule like

dopamine (figure 6.1). However, compared to the parent polyaniline, the electrochemical activity, conductivity, and the chemical and mechanical stabilities of both self-doped polyaniline and bulky polyelectrolyte-doped polyaniline are greatly reduced due to steric effects<sup>13</sup>. So the development of polyaniline nanomaterials of lightly substituted monomers will increase the sensitivity of biosensors due to enhanced surface area available and specific functionalization. Additionally, polyaniline derivatives are known to have a lot of advantages over the parent polymer, such as improved solubility in most organic solvents, higher resistance against microbial and chemical degradation etc.<sup>3,12</sup>

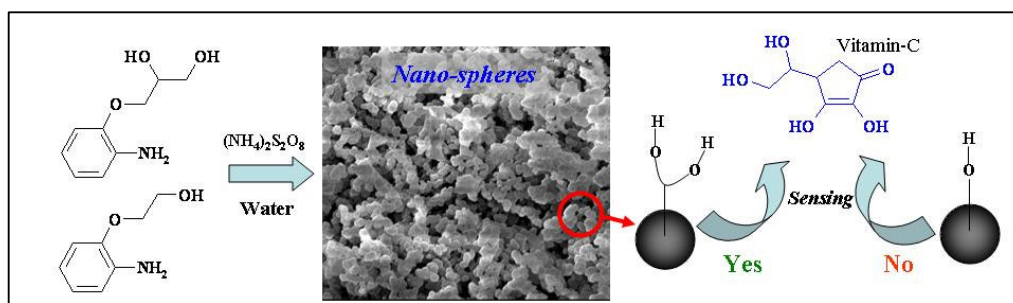


**Figure.6.2.** Hydroxyl Functionalized Polyaniline Nanospheres with Vitamin C sensing ability.

In this chapter, an alternate approach for nanospheres based on functionalized aniline monomer with hydroxyl groups was developed. This approach is very attractive mainly because the resultant nanomaterials bear functional groups at nanospheres surface which can be employed as tool for trapping various chemical and biological analyte for sensing applications. Though polyaniline (not nanomaterials) with functional groups such as alkyl, sulfonic acids, mesogenic groups and halide at the ortho-position in the aromatic ring were reported in the literature, so far polyaniline nanomaterials with active functional groups have not been explored<sup>14-16</sup>. Here, novel polyaniline nanospheres bearing mono and bis-hydroxyl functional groups were synthesised to study the molecular interactions at the nano-surfaces for vitamin-C sensing. Two new aniline monomers were synthesized with hydroxyl groups and polymerized via oxidative route to produce water soluble and uniform nanospheres. The structures of the monomers and polymers were characterized by NMR, FTIR techniques and the morphology of the nanomaterials was analyzed using SEM and TEM. FTIR and DLS were utilized to study the aggregation of monomers to produce nanospheres. The hydroxyl functionality improves solvent-particle

interactions and dissolves the polymer in various solvents like water and dimethylsulfoxide, which ease the structural characterization by NMR and other spectroscopic techniques. A controlled experiment with un-substituted aniline monomer (aniline hydrochloride) resulted in the formation of polyaniline nanofibers and confirming the importance of hydroxyl group in aniline monomer for producing nanospheres. To study the influence of nano-surface functionality on the sensing behaviour, interactions of vitamin-C with nanospheres having mono or bis hydroxyl groups (also without functional groups) were carried out in water. The primary idea of the work is to study and understand the molecular interactions at the nanomaterial surface and also emphasized to develop vitamin-C sensor. The studies reveal enhanced sensitivity in the nanospheres with bis-hydroxyl groups have compared to that of nanospheres with mono hydroxyl or nanofibers without any functional groups.

## 6.2. Experimental Section

**6.2.1. Materials:** 2-Amino phenol, aniline hydrochloride salt (AHC), 3-chloro-1, 2-propane-diol, 2-chloro ethanol, ammonium persulfate (APS) and vitamin C were purchased from Aldrich and used as such.

**6.2.2. Measurements:** NMR spectra of the compounds were recorded using 300-MHz Bruker NMR spectrophotometer. Infrared spectra of the polymers were recorded using a Perkin Elmer Spectrum one, FT-IR spectrophotometer in the range of 4000 to 400  $\text{cm}^{-1}$ . The purity of the compounds was determined by JEOL JSM600 fast atom bombardment (FAB) high-resolution mass spectrometry. For SEM measurements, polymer samples were subjected for thin gold coating using JOEL JFC-1200 fine coater. The probing side was inserted into JEOL JSM- 5600 LV scanning electron microscope for taking photographs. Wide angle X-ray diffractions of the finely powdered polymer samples were recorded by Philips Analytical diffractometer using CuK-alpha emission. The spectra were recorded in the range of  $2\theta = 0- 50$  and analyzed using X' Pert software. UV-Vis spectra of the PANI in water were recorded using Perkin Elmer Lambda-35 UV-VIS Spectrophotometer. All the polymers are dedoped using aq. ammonia, washed well with deionised water and dried. The pre-dried powder is dispersed in water under ultrasonic stirring to get a

solution with absorbance of 0.3 (O.D) (for sensing studies). Transmission electron microscope images were recorded using a FEI Tecnai 30G<sup>2</sup> S Twin HRTEM instrument at 100kV. For TEM measurements, the water suspension of nanospheres were prepared under ultrasonic stirring and deposited on Formvar coated copper grid. For dynamic light scattering (DLS) measurements, a Nano ZS Malvern instrument employing a 4mW He-Ne laser ( $\lambda=632.8\text{nm}$ ) equipped with a thermo stated sample chamber was used. For conductivity measurements, the polymer samples were pressed into a 10mm diameter disc and were measured by a standard four-probe method using a Keithley 6881 programmable current source and 2128A nanovoltmeter at 30°C. The resistivity of the samples was measured at five different positions and at least two pellets were measured for each sample: the average of 10 readings was used for conductivity calculations.

### 6.2.3. Synthesis of Monomers and Polymers

**Synthesis of 2-hydroxy-acetanilide (1):** 2-Aminophenol (11.0g, 0.1mol) was suspended in water (30 mL) by magnetic stirring. Acetic anhydride (12 ml, 0.13 mol) was added and the entire mixture was warmed to 70 °C for 3 h with constant stirring. It was cooled, the precipitate was filtered, washed with water and dried in a vacuum oven at 50 °C. The crude solid was further purified by re-crystallization from warm ethanol. Yield = 10.5 g (70%). <sup>1</sup>HNMR (DMSO-d<sub>6</sub>, 300 MHz)  $\delta$ : 2.11 ppm (s, 3H, COCH<sub>3</sub>), 6.85 ppm (m, 3H, Ar-H), 7.65 ppm (d, 1H, Ar-H), 9.31 ppm (b, 1H, -NH). FT-IR (KBr, cm<sup>-1</sup>) 3520, 3401, 2882, 1659, 1595, 1541, 1453, 1387, 1282, 1240, 1033, 761 and 668. FAB-MS (MW: 151.17): m/z = 152.32 (M+1).

**Synthesis of [2-(2, 3-dihydroxy-propoxy)]-acetanilide (2):** Sodium hydroxide (5.6 g, 0.14 mol) was dissolved in 50 ml ethanol+water mixture (1:1 v/v). 2-Hydroxy-acetanilide (10.6 g, 0.07 mol) was added to sodium hydroxide solution and refluxed for 1 h. It was cooled, and 3-chloro-1, 2-propanediol (15.5 g, 0.14 mol) was added and refluxed for 35 h. The slow evaporation of ethanol at atmospheric pressure resulted in the precipitation of the product as a white solid. The precipitate was filtered, washed with acetone and dried in a vacuum oven at 50 °C. The crude product was further purified by re-crystallization from hot ethanol. Yield = 11.8 g (70%):

$^1\text{H-NMR}$  ( $\text{DMSO-d}_6$ , 300 MHz)  $\delta$ : 2.1 ppm (s, 3H, aliphatic **H**), 3.8 ppm (t, 2H,  $-\text{OCH}_2$ ), 4.06 ppm (d, 2H,  $\text{OCH}_2$ ), 4.77 ppm (d, 1H,  $\text{OC}^*\text{H}$ ), 5.2 ppm (d, 1H,  $\text{OC}^*\text{H}$ ), 6.9 ppm (b, 1H, Ar-**H**), 7.01 ppm (b, 2H, Ar-**H**), 8.02 ppm (d, 1H, Ar-**H**), 9.08 ppm (s, 1H,  $-\text{NH}$ ); FT-IR (KBr,  $\text{cm}^{-1}$ ) 3351, 3272, 2944, 2881, 1654, 1539, 1460, 1255, 1050, 963, 784, 676 and 605. FAB-MS (MW: 225.25):  $m/z = 226.21(\text{M}+1)$ .

**Synthesis of [2-(2-hydroxy-ethoxy)]-acetanilide (3):** 2-Hydroxy-acetanilide (10.6 g, 0.07 mol) in sodium hydroxide (5.6 g, 0.14 mol) solution was reacted with 2-chloroethanol (11.3 g, 0.14 mol) as described for **2**. The product was further purified by silica gel column chromatography (50/50 ethyl acetate and hexane). Yield = 6.3 g (46%):  $^1\text{H-NMR}$  ( $\text{CDCl}_3$ , 300MHz):  $\delta$  2.1 ppm (s, 3H, aliphatic **H**), 3.879 ppm (t, 2H,  $\text{OCH}_2$ ), 4.05 ppm (t, 2H,  $\text{OCH}_2$ ), 6.94 ppm (t, 1H, Ar-**H**), 6.87 ppm (t, 1H, Ar-**H**) 6.82 ppm (d, 1H, Ar-**H**), 8.15 ppm (b, 2H, Ar-**H**,  $-\text{NH}$ ); FT-IR (KBr,  $\text{cm}^{-1}$ ) 3330, 2935, 2870, 1677, 1601, 1535, 1488, 1447, 1370, 1323, 1288, 1251, 1210, 1123, 1080, 1045, 909, 750, 602 and 543. FAB-MS (MW: 195.22):  $m/z = 196.20(\text{M}+1)$ .

**Synthesis of [2-(2, 3-dihydroxy-propoxy)] aniline hydrochloride (4):** **2** (1.5 g, 0.006 mol) was dissolved in ethanol (20 mL), conc. HCL (10 mL) was added and refluxed for 30 h under nitrogen atmosphere. It was cooled and ethanol was removed by rotary evaporated. Upon standing in a freezer, the viscous liquid was crystallized out. It was washed with acetone and dried in an oven at 60 °C. The crude solid was purified by re-crystallization from water. Yield = 0.97 g (80 % yield).  $^1\text{H-NMR}$ : ( $\text{D}_2\text{O}$ , 300MHz) : 3.8 ppm (b, 2H,  $\text{OCH}_2$ ), 3.96 ppm (b, 2H,  $\text{OCH}_2$ ), 4.15 ppm (b, 2H,  $\text{OCH}_2$ ), 7.01 ppm (t, 1H, Ar-**H**), 7.18 ppm (d, 1H, Ar-**H**), 7.37 ppm (m, 2H, Ar-**H**), 10.2 ppm (b, 2H,  $\text{NH}_3^+$ ).  $^{13}\text{C-NMR}$  ( $\text{D}_2\text{O}$ , 75MHz) $\delta$ : 39.5, 62.2, 69.8, 71.1, 113.1, 120.8, 123.9, 129.3, 151.7; FT-IR (KBr,  $\text{cm}^{-1}$ ) 3225, 2860, 2620, 2034, 1632, 1502, 1446, 1327, 1265, 1163, 1101, 1051, 979, 942, 846, 755, 646 and 506. FAB-MS (MW: 183.21):  $m/z = 184.43(\text{M}+1)$ .

**Synthesis of [2-(2-hydroxy-ethoxy)]-aniline hydrochloride (5):** **3** (3 g, 0.015 mol) was dissolved in ethanol and treated with conc. HCl as described for **4**. The crude solid was purified by re-crystallization from water. Yield = 1.5 g (65 % yield).  $^1\text{H-NMR}$  ( $\text{D}_2\text{O}$ , 300MHz)  $\delta$ : 3.75 ppm (t, 2H,  $\text{OCH}_2$ ), 4.1 ppm (t, 2H,  $\text{OCH}_2$ ), 7.01 ppm

(t, 1H, Ar-**H**), 7.18 ppm (d, 1H, Ar-**H**), 7.31 ppm (m, 1H, Ar-**H**), 7.39 ppm (m, 1H, Ar-**H**), 9.85 ppm (b, 2H,  $\text{NH}_3^+$ ).  $^{13}\text{C}$ NMR ( $\text{D}_2\text{O}$ , 75MHz): 839.5, 59.4, 70.7, 113.1, 120.8, 123.7, 129.1, 151.5; FT-IR (KBr,  $\text{cm}^{-1}$ ) 3348, 2866, 2612, 2010, 1641, 1542, 1502, 1455, 1321, 1296, 1265, 1190, 1128, 1066, 1044, 917, 895, 852, 761, 606, 550 and 503. FAB-MS (MW: 153.18):  $m/z = 154.33(\text{M}+1)$

**Synthesis of Poly [2-(2, 3-dihydroxy-propoxy)] aniline] (P-DH):** Monomer **4** (1.09 g, 0.005 mol) was dissolved in water (15 mL) and oxidized by ammonium persulfate (1.25 g, 0.0055 mol) in water (15 mL). The reaction mixture was kept for 24 h without disturbance at room temperature. The precipitate was centrifuged, washed several times with water and methanol. The isolated mass was dried in a vacuum oven at 55 °C for 40 h. Yield = 0.46g (43%).  $^1\text{H}$  NMR: ( $\text{DMSO-d}_6$ , 300MHz)  $\delta$ : 6.9 ppm (1H, Ar-**H**), 7.07 ppm (1H, Ar**H**), 7.24 ppm (1H, Ar**H**). FTIR (KBR,  $\text{cm}^{-1}$ ) 3414, 3197, 2934, 1572, 1485, 1414, 1336, 1268, 1182, 1101, 996, 829, 789, 674, 612, 584 and 504.

A similar procedure was adapted to synthesis **P-MH** from **5**. Yield = 45 %.  $^1\text{H}$ -NMR ( $\text{DMSO-d}_6$ , 300MHz)  $\delta$ : 6.95 ppm ( 1H, Ar-**H**), 7.12 ppm ( 1H, Ar-**H**), 7.3 ppm ( 1H, Ar-**H**). FT-IR ( $\text{cm}^{-1}$ ): 3202, 2935, 1574, 1485, 1266, 1195, 1112, 1035, 988, 899, 811, 610 and 586. Aniline hydrochloride was polymerized as described above to prepare **P-H**. Yield = 92%.FT-IR ( $\text{cm}^{-1}$ ); 3191, 1564, 1478, 1301, 1243, 1107, 881, 802, 703, 617, 588, 502. Insoluble for NMR characterization.

### 6.3. Results and Discussion

#### 6.3.1. Synthesis and Characterization

Two monomers consisting of hydroxyl functional groups in aniline at the ortho position were synthesized as shown in figure 6.3. Reactive amine group in 2-hydroxy aniline was protected by acetylating using acetic anhydride to yield 2-hydroxyacetanilide (**1**). **1** was reacted with 3-chloro-1, 2-dihydroxypropanediol and 2-chloroethanol under Williamson's etherification in ethanol/water to yield **2** or **3**. Subsequently, **2** and **3** were treated with conc. HCl at 60 °C to remove the acetyl protecting group and resulted in the formation of amine hydrochloride salts **4** and **5**, respectively<sup>16</sup>. The compounds **4** and **5** were purified by recrystallization from hot water to get pure white crystals. The <sup>1</sup>H-NMR of the product obtained in each step was given in figure 6.4 and protons were assigned alphabetically.

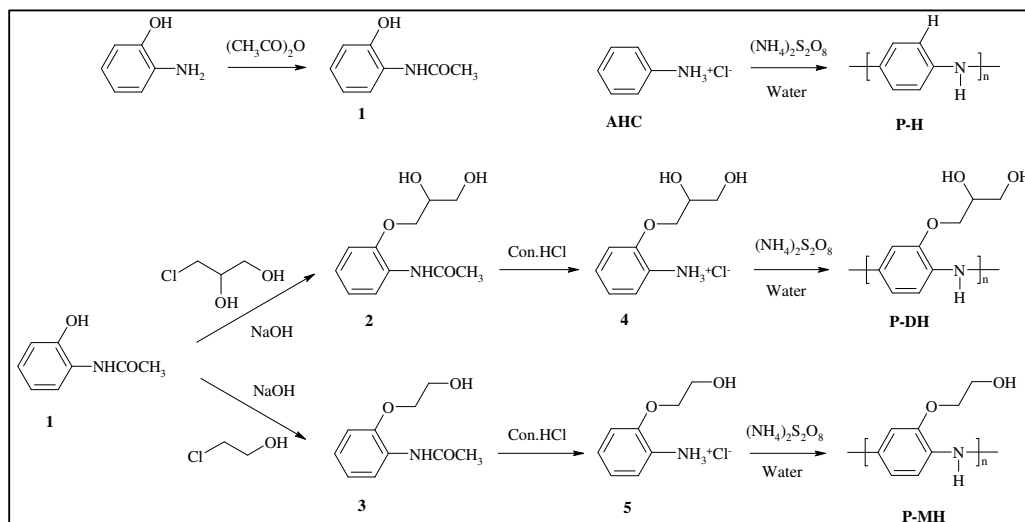


**Figure 6.3.** Synthesis of hydroxyl functionalized polyaniline nano-materials.

Typically, 1 g of the monomer **4** (or **5**) was dissolved in 15 ml double distilled water and oxidized with ammonium persulfate (0.36M) solution in water. The polymerization was continued for 24 h without disturbance at room temperature (30 °C). The room temperature polymerization was adopted for the nanomaterial synthesis from the novel hydroxyl functionalize monomers because the kinetics of polymerization is relatively high at 30 °C than 0-5 °C (usual temperature for conventional polymerization) and under these condition homogeneous nucleation favours for the formation of uniform nanostructures<sup>17</sup>.

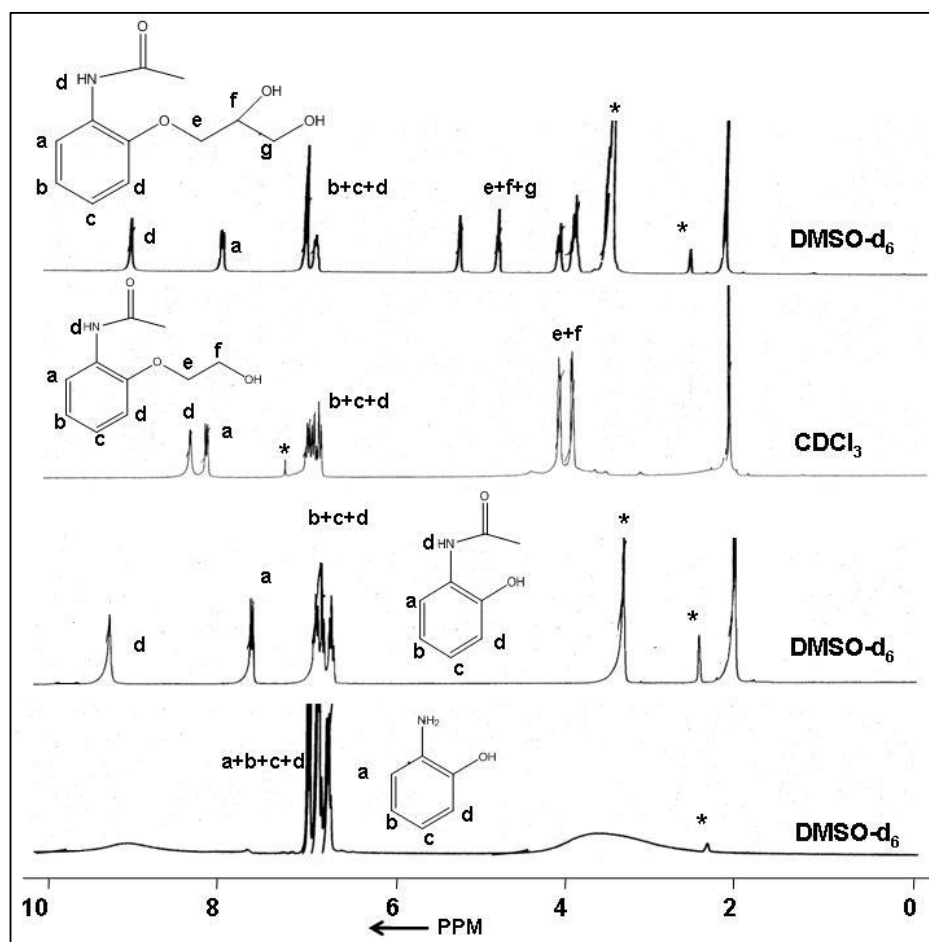


**Figure 6.4.**  $^1\text{H-NMR}$  spectra of intermediate compounds during monomer synthesis.

The product was filtered and washed with a large amount of water followed by methanol till the filtrate become colourless. Two polyaniline nanomaterials **P-DH** and **P-MH** (**DH** and **MH** refers di-hydroxyl and mono-hydroxyl) were prepared from monomers **4** and **5**, respectively (see figure 6.3). In order to study the influence of hydroxyl groups on the morphology and other physiochemical properties of polyaniline nanomaterials, a controlled polyaniline sample (**P-H**) was synthesized using aniline hydrochloride (AHC) as monomer under identical experimental conditions (see figure 6.3). Controlled polyaniline sample (**P-H**) was synthesized from AHC in water instead of conventional aniline in acid medium because the other two monomers **4** and **5** were amine-hydrochloride salt and polymerized under neutral conditions. This enabled to study the effect of hydroxyl substitution on the structure-



property relationship of all three polymers under identical conditions without the influence of external dopant like HCl.

The structures of the monomers and polymers were confirmed by  $^1\text{H-NMR}$ , FTIR and Mass spectra.  $^1\text{H-NMR}$  spectra of monomers are shown in figure 6.5 and various types of the protons in the structures are assigned alphabetically.

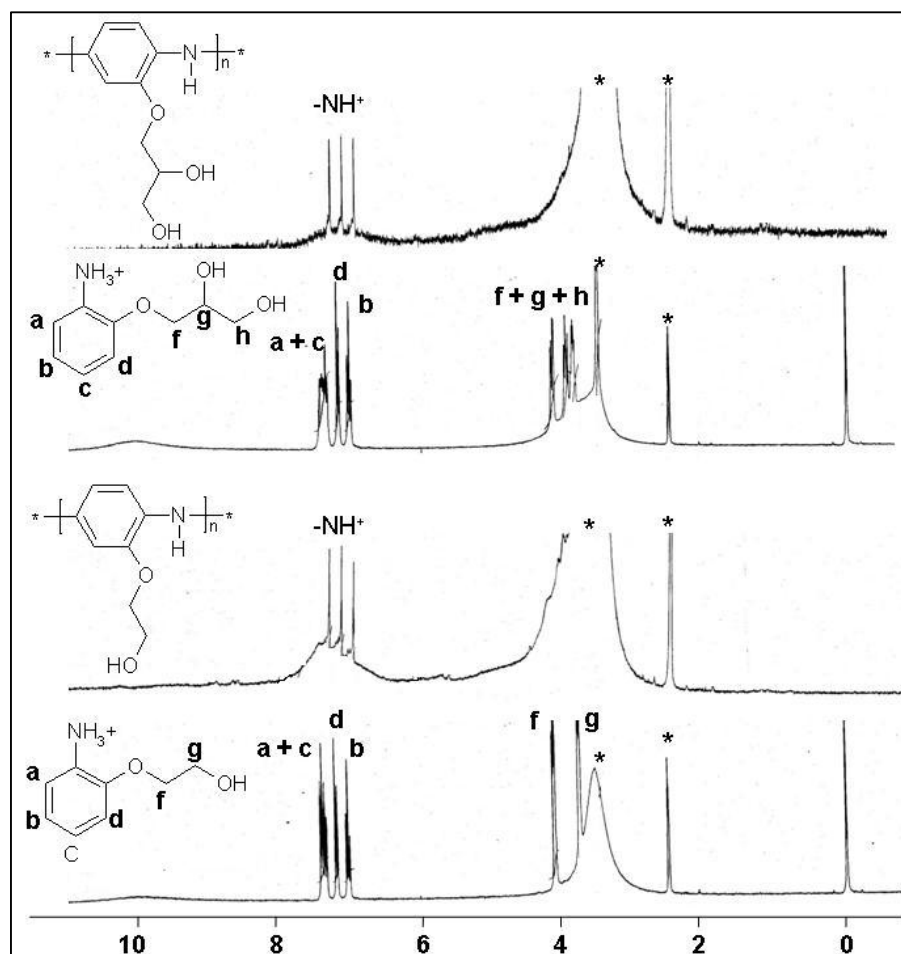


**Figure 6.5.**  $^1\text{H-NMR}$  spectra of the hydroxy monomers and the corresponding polyaniline nano-spheres.

Both the monomers showed the aliphatic protons of  $-\text{OCH}_2$  group in the 3-4 ppm region and aromatic protons in 6-9 ppm region. The monomers also showed a less intense broad peak  $\sim 10$  ppm, which is originating from ammonium ion ( $\text{NH}_3^+$ ) protons<sup>16</sup>. One of the limitations of conventional polyaniline is its poor solubility in common organic solvents, which hampered the structural characterization by NMR. Interestingly, the presence of hydroxyl groups in the polymers made these samples

soluble in highly polar solvents like DMSO (also DMF) that enabled us to record their NMR spectra. The NMR spectra of both polymers were recorded in DMSO-d<sub>6</sub> and shown in figure 6.5. The aromatic and -NH<sup>+</sup> protons in the polyaniline unit appear as peak at 6.8-7.4 ppm region<sup>18,19</sup>. The disappearances of p- (to amine group) aromatic proton and the absence of signal at 10.15 ppm corresponding to -NH<sub>3</sub><sup>+</sup> (visible in the monomer) in the polymer confirmed the formation of expected polymer structures<sup>16</sup>. The protons of the side chain methylene groups are expected to appear at 3.5-4.5 ppm, but these peaks are unable to distinguish since they are merged with solvent peaks (water in dms). The polymer **P-H** without hydroxyl functionalization (prepared from aniliniumhydrochloride) was not soluble in DMSO, which restrict its structural characterization by NMR.

The molecular weights of the **P-DH** and **P-MH** were determined by viscosity method in DMSO at 30 °C using Ubbelohde viscometer for 0.5 wt % polymer samples. The solubility of sample P-H was very low in DMSO, and therefore, only 0.3 wt % solution was used for the measurements. The inherent viscosities were obtained as 0.58, 0.45 and 0.66 dL/g for **P-DH**, **P-MH** and **P-H**, respectively (see table 6.1). The inherent viscosity values are matching with that of the polyaniline samples with literature reports which confirmed that the molecular weights obtained are very good for further analysis<sup>20</sup>.

**Table 1.6.1.** Yield, inherent viscosity, conductivity, dimensions and WXRd data of polyaniline nanomaterials.

Sample	Yield (%)	$\eta_{inh}^a$ (dL/g)	$\sigma$ (S/cm)	Diameter (nm) <sup>b</sup>	Peaks in WXRd <sup>c</sup>	
					Peak at(2 $\theta$ )	d-spacing(Å)
<b>P-DH</b>	43	0.58	$2.8 \times 10^{-3}$	Sp= 700±100nm	6.8,20.6,24.4	13.1,4.3,3.6
<b>P-MH</b>	45	0.45	$4.6 \times 10^{-3}$	Sp= 600±150nm	7.3, 24.4	12.7,3.6
<b>P-H</b>	92	0.66	$2.5 \times 10^{-1}$	Fib=50 nm	25.6, 29.7	3.1, 2.1

(a) Inherent viscosity measured at 30 °C using Ubbelohde viscometer.

(b) Average diameter is calculated based on SEM-images.

(c) Wide angle X-ray diffraction measurements were carried out at 30 °C.

The thermal properties of polyaniline nanomaterials were measured by means of thermogravimetric analysis (TGA). Typical TGA curves for nanomaterials are given in figure 6.6. All typical TGA curves have a typical three step weight loss behavior: the loss of water or solvent, dedoping and decomposition of dopant and decomposition of polyaniline chain. Thermal analysis showed that all the polyaniline nanomaterials are stable up to 250°C.

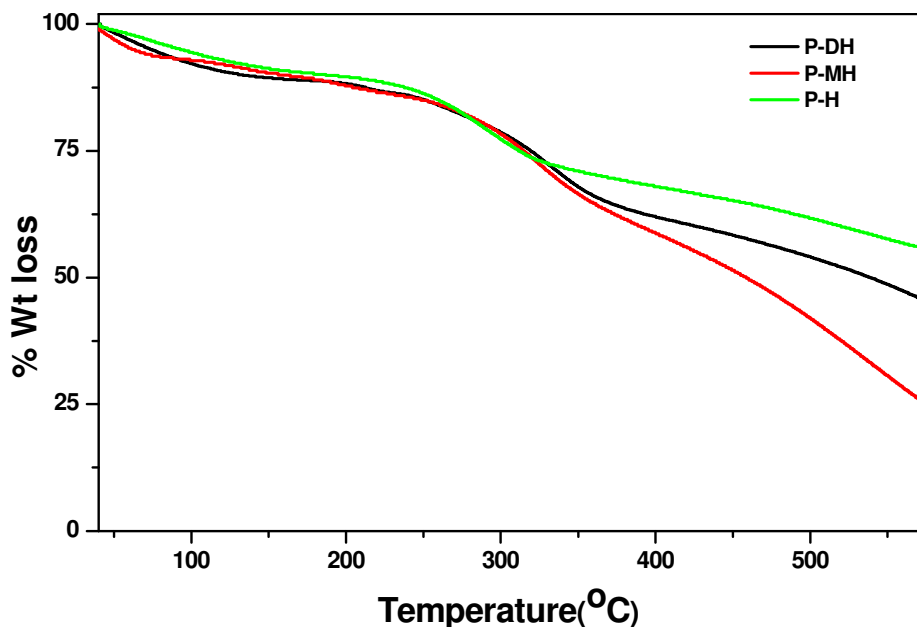
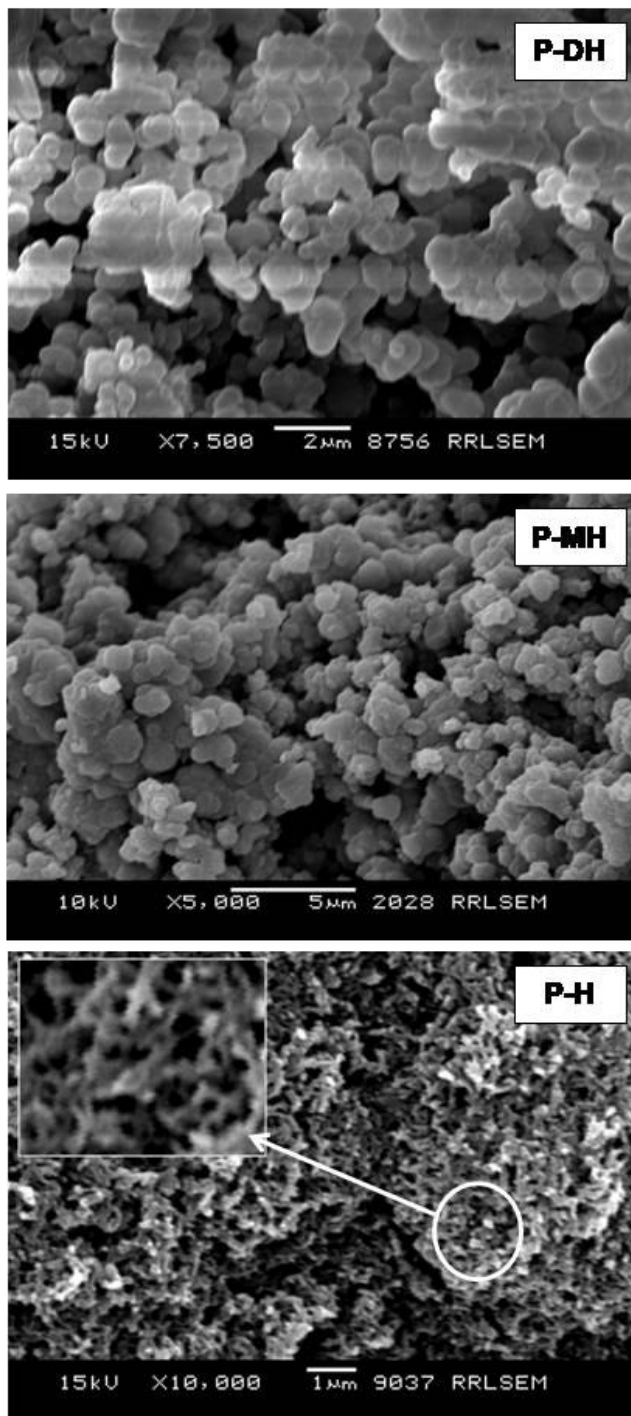


Figure 6.6. TGA plots of polyaniline nanomaterials.

### 6.3.2. Morphology of Nanomaterials by SEM and TEM

The morphologies of the polyaniline nanomaterials (**P-DH**, **P-MH** and **P-H**) by SEM are given in figure 6.7. The samples **P-DH** and **P-MH** were found with full of nanospheres and devoid of any nanofibers. **P-DH** contains spheres of diameter ranging from 600-800 nm and they are appeared as a cluster of spheres with a very uniform morphology. In the case of **P-MH** the diameters of nanospheres ranges from 450 – 750 nm and the spheres are more or less well-separated. **P-DH** morphology is not very uniform; it consists of two types of spheres one with average diameter ~400 nm and other bigger spheres with diameter around ~700nm. The sample **P-H** (without any hydroxyl functionalization), was found as thin nanofibers of diameter less than 50 nm and there is no trace amount of nanospheres. The samples **P-DH** and **P-MH** did

not show any traces of fibers, which indicate that the newly synthesized polymers has a tendency to self assemble to form spheres rather than fibres under similar aqueous polymerization conditions.



**Figure 6.7.** SEM images of polyaniline nanomaterials.

The TEM analysis of the samples has been carried out to check the internal features of nanospheres. For TEM analysis, the sample was dispersed in water under ultrasonic and a drop of the solution was evaporated on the Cu grid. The TEM image of **P-DH** (see figure 6.8) has confirmed the morphology of rigid nanospheres of diameter of 500 nm, which is matching with that of SEM images.

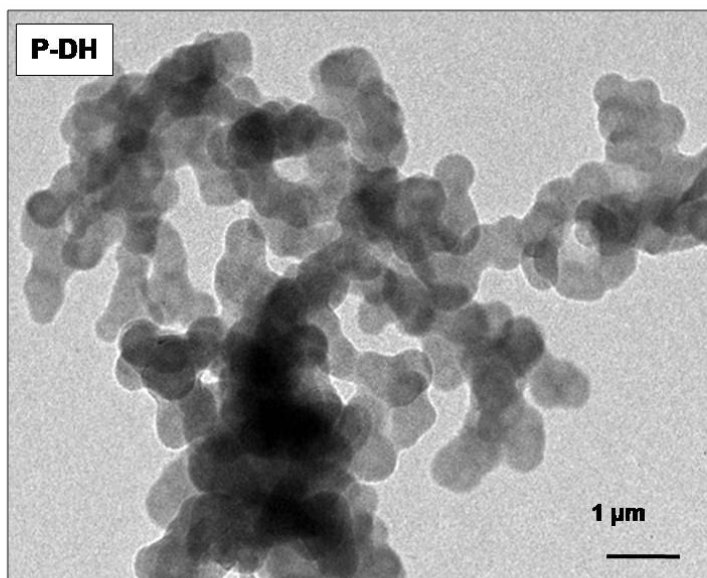


**Figure 6.8.** TEM images of polyaniline spheres (*P-DH*).

The morphology of the samples is clearly evident that the hydroxyl substitutions at aniline monomer drastically change the morphology of the resultant nanomaterials from fibre to nanospheres. The morphology of **P-H** is found as similar to that of polyaniline nanofibers produced from aniline in acidic solution (HCl)<sup>21</sup>. It suggests that the polymerization procedures adapted in the present investigation is in concordance with the literature reports in polyaniline nanomaterial synthesis. Therefore, the difference in the morphologies in samples **P-DH** (also **P-MH**) and **P-H** are directly related to difference in the polymerization mechanism of the hydroxyl functionalized monomers (**4** and **5**) with that of AHC. All the three monomers were subjected to polymerization under the identical conditions, and therefore, the difference in the nanomaterials morphology is the resultant of the difference in the monomer interactions at molecular level during the polymerization process.

### 6.3.3. Mechanism of Nanomaterials Formation

FTIR is a powerful tool to trace various hydrogen bonding interactions present in the molecular level<sup>22</sup>. In order to understand the hydrogen bonding interactions of monomers and resultant polyaniline nanomaterials, FTIR spectra of the samples were recorded and showed in figure 6.9.

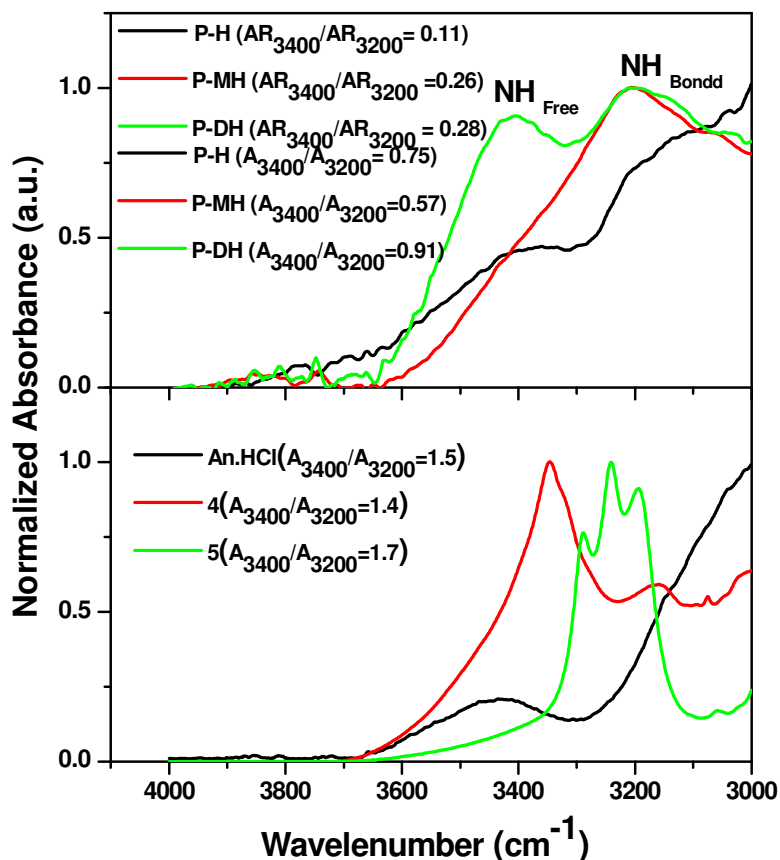


**Figure 6.9.** Expanded FTIR spectra of polyaniline nanomaterials and monomers. In the figure AR represents area of the peak and A represents absorption intensity.

The peaks corresponding to the hydrogen bonded and free N-H (or O-H) region is expanded for simplicity. The monomers (**4** and **5**) and polymers (**P-DH** and **P-MH**) have both N-H and O-H groups and these two stretching frequencies are very close and difficult to distinguish. However, the overall presence of free as well as hydrogen bonded N-H (or O-H) in the materials can be correlated based on their structural features. In all the samples there are two peaks present: (i) free N-H (or O-H) at higher wavenumber ( $3450\text{--}3300\text{ cm}^{-1}$ ) corresponding to anti-symmetric stretching and symmetric stretching respectively of free N-H (or O-H) groups and

(ii) a shoulder at lower wavenumber ( $3240\text{-}3100\text{ cm}^{-1}$ ) is stretching due to hydrogen bonded N-H (or O-H) groups<sup>22,23</sup>. The ratio of the intensity of these two peaks directly reflects on the availability of free versus hydrogen bonded protons with respect to their structure (see figure 6.9). The ratio of the  $A_{\text{Free}}/A_{\text{H-bonded}}$  ( $A$ = absorbance) was almost 5-6 times higher for hydroxyl functionalized monomer compared to that of AHC. It suggests that the presence of their free O-H and N-H groups in the monomers **4** and **5** experience a strong hydrogen bonding interactions, which may be the driving force for the nanospheres formation in the polymerization process.

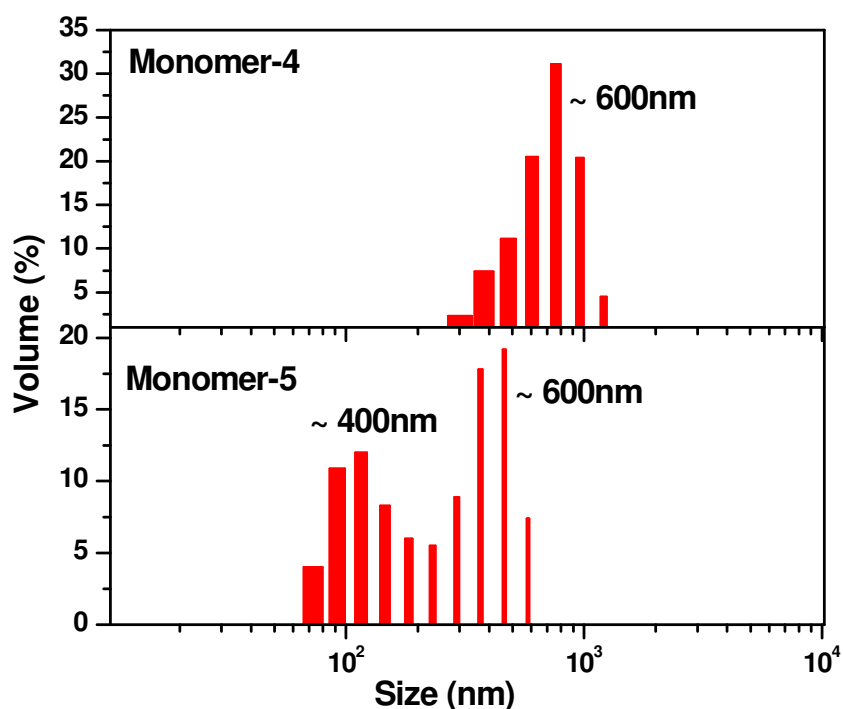


**Figure 6.10.** DLS histograms of monomers dissolved in water at  $30^{\circ}\text{C}$ .

Self-organization of molecules can be traced using dynamic light scattering (DLS) techniques in solution<sup>24</sup>. DLS histograms of the monomers **4** and **5** in water (0.35 M) were shown in figure 6.10. The histogram of AHC is almost features less with very weak and broad distribution and failed in DLS analysis. The DLS plots of monomers **4** and **5** showed good distribution characteristics with aggregates of average sizes 600 and 400 nm, respectively. It suggests that the hydroxyl functional monomers undergo self-organization in water (via hydrogen bonding as evident from FTIR analysis) to produce large size sub micron size aggregates. The formation of

these large aggregates is schematically shown in figure 6.11. The functionalized monomers **4** (also **5**) has a water loving hydrophilic hydroxyl head and hydrophobic aromatic ring and behave as an amphiphilic monomer. In water, the hydrophilic head tend to project outside and surround the aromatic ring to form a micelle<sup>25</sup>. The aggregation of such small monomer micelles produce a large sub-micron size aggregates, which selectively template for polyaniline nanospheres. Subsequent oxidation of these aggregated monomers by APS produces exclusively polyaniline nanospheres for hydroxyl functionalized monomers. On the other hand AHC did not have selective hydrophilic/hydrophobic part in the molecular structure and resulted in the formation of nanofibers.

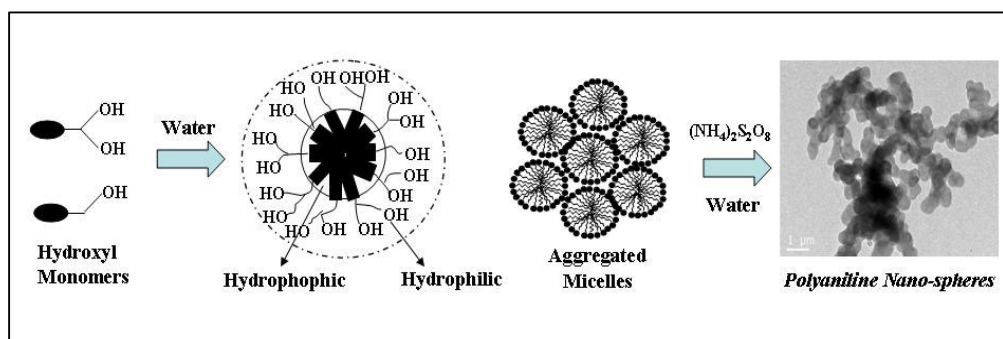


**Figure 6.11.** *Plausible Mechanism for the polyaniline nano-sphere formation.*

In polyaniline nanomaterials, two types of hydrogen bonding interactions are possible: (i) hydrogen bonding among the polymer chains within the nanospheres (or nanofibers) and (ii) free N-H or O-H groups available at the periphery of the nano-surface which may undergo inter-molecular hydrogen bonding at surfaces with another nanospheres (or fibers). All the samples expected to have these two types of hydrogen bonding, but their difference in relative intensities may reflect on their variation in structural differences. To trace the hydrogen bonding ability of nanomaterials, FTIR spectra of the polymers were recorded (doped stage) and shown along with monomers in figure 6.9. **P-DH** has bis-hydroxyl side chains and it was found to have more intense peak at  $3400\text{ cm}^{-1}$  ( $A_{\text{Free}}/A_{\text{H-Bonded}}$ ) compared to **P-MH** and **P-H** which indicating the availability of more free O-H protons at the nano-surfaces of **P-DH**. Additionally, the ratio of the peak area,  $AR_{\text{Free}}/AR_{\text{H-bonded}}$  ( $AR$ = area of the peak) were obtained by de-convolution method as 0.11, 0.27 and 0.28 for **P-H**, **P-MH** and **P-DH** respectively. It is also clear that the ratio  $AR_{\text{Free}}/AR_{\text{H-bonded}}$  is



2.5-3 times higher for hydroxyl polymers than **P-H** polymer. **P-H** is more planar (no substituent) and this will help the polymer backbone to undergo more  $\pi$ - $\pi$  interactions that will make the N-H groups very close to each other to form strong hydrogen bonds between amine groups.

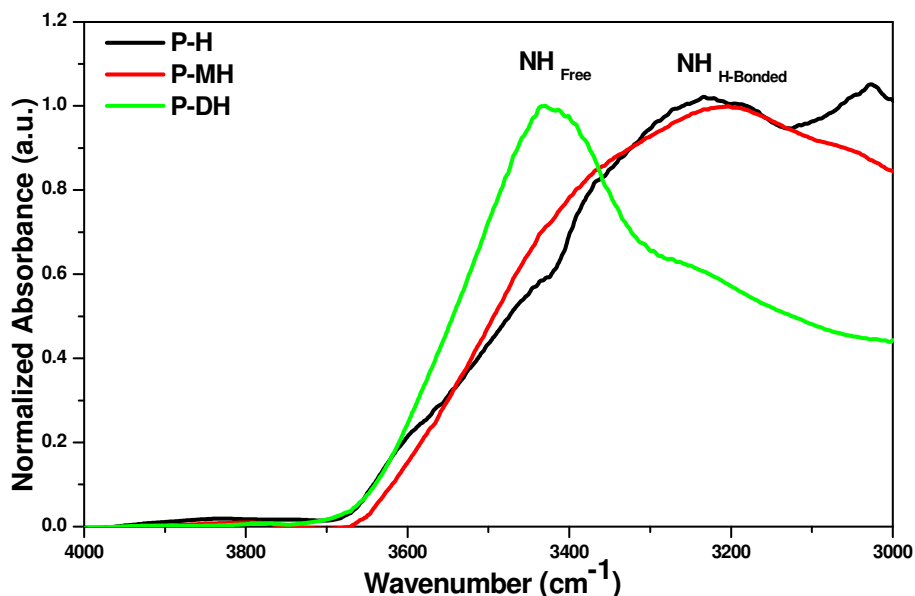


**Figure 6.12.** Expanded FTIR Spectra of the polyaniline nanomaterials (dedoped state).

The FTIR spectra of dedoped polymers are also recorded and the ratio of the absorbance and area at free and hydrogen bonded were compared (see figure 6.12). The dedoped sample was also following the similar trend that observed in the doped sample in both in their area as well as intensity, which confirmed that the hydrogen bonding nature of the nanomaterials are highly dependent on the structure rather than the doped/dedoped stage. Nevertheless, the FTIR clearly evident the availability of large number of free hydroxyl functional groups at the surfaces of **P-DH** nanospheres compared to that of **P-MH** nanospheres or **P-H** nanofibers. The ratio of the  $A_{\text{Free}}/A_{\text{H-bonded}}$  ( $A$ = absorbance) was almost 2-3 times higher for bis-hydroxyl functionalized **P-DH** compared to that of **P-MH** and **P-H**. It suggests that the presence of more number of free O-H and N-H groups in P-DH nanospheres surface than others, which may acts as a good handle for analyte molecules.

#### 6.3.4. Properties of Polyaniline Nanomaterials

To investigate the effect of hydroxyl functionality on the solid state crystalline characteristics of polyaniline, WXR patterns of the all three polymers **P-DH**, **P-MH**

and **P-H** were recorded (see figure 6.13). All the three samples showed the characteristic Bragg diffraction peaks at  $2\theta = 20^\circ$  and  $25^\circ$ , which is usually observed for polyaniline<sup>26,27</sup>. Both **P-MH** and **P-DH** have showed a sharp peak at lower angle at  $2\theta = 7.3^\circ$  (d-spacing of 12.7 Å) and  $2\theta = 6.8^\circ$  (d-spacing of 13.1 Å), respectively. The appearance of lower angle peak with high value of d-spacing in hydroxyl substituted polyaniline nanospheres confirmed that the occurrence of enhanced solid state ordering of polymer chains in the nanospheres compared to that of nanofibers<sup>28</sup>. In general, polymer chain has both amorphous and crystalline domains in the matrix and the percentage of the respective domains vary depending up on their backbone. HCl doped polyaniline back bone is highly rigid due to their linear structure and less flexible to chain folding to induce crystalline domain. Usually the solid state ordering in the polyaniline-dopant system is enhanced by the penetrating of the dopant molecules (like CSA and amphiphilic dopant) into the inter-lattice of polymer chains<sup>26</sup>. Interestingly, in the present case, the availability of free hydroxyl group in the **P-DH** and **P-MH** enhances the solid state ordering in the nanomaterials. So the X-ray diffraction study of polyaniline nanostructures suggests that in nanospheres the polyaniline exhibit a lamellar kind structural organization facilitated by side groups.

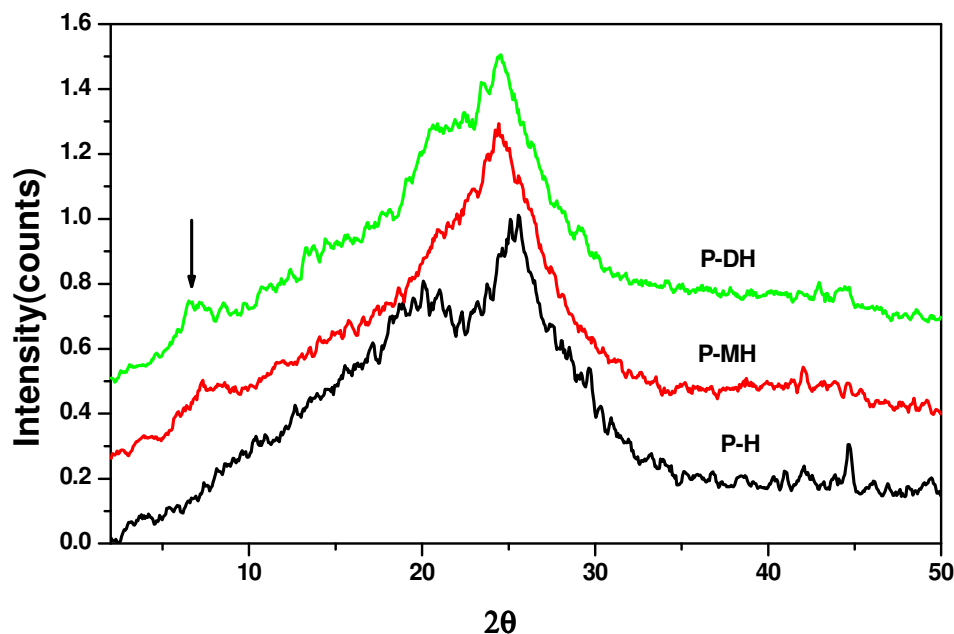
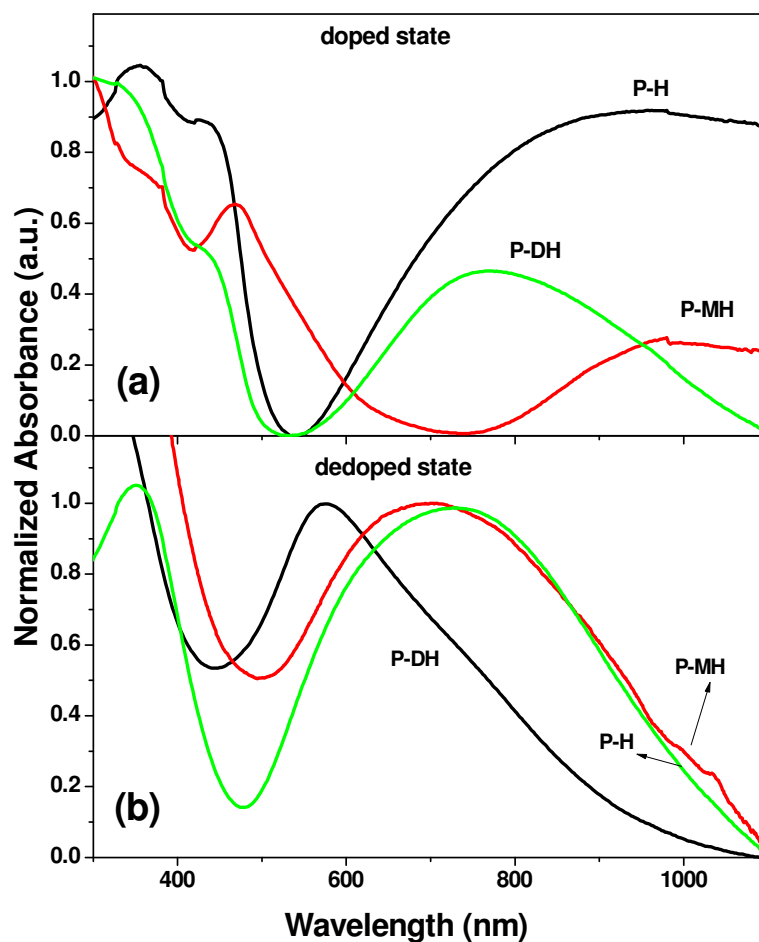


Figure 6.13. WXR D patterns of nano-materials.

The conductivity of the polyaniline nanomaterials was determined by four probe conductivity measurement for compressed pellets at room temperature<sup>29</sup>. **P-H** has showed conductivity in the range of  $2.5 \times 10^{-1}$  S/cm whereas other nanomaterials **P-DH** and **P-MH** showed a lower value in the conductivity and the values are obtained as  $2.6 \times 10^{-3}$   $4.8 \times 10^{-3}$  S/cm respectively. The conductivity of the **P-H** is one order lower than that of conventional doped systems ( $10^0$  S/cm), which may be due to the unavailability of free acid for doping in the reaction feed. The lower conductivity of the **P-DH** and **P-MH** is may be due to the non-planarity of the polymer backbone due to the steric effect induced by side chains<sup>30</sup>. However, it is very important to note that other factors like particle size and the nanomaterials shape (fibres versus sphere) may also influence on the conductivity values.



**Figure 6.14.** UV-Vis spectra of polyaniline nanomaterials (doped and dedoped state)

The polymer samples **P-DH** and **P-MH** were highly water dispersible owing to the hydrophilic nature of the polymer chain (**P-H** less soluble) resulting a green coloured solution. The absorption spectra of the polymers in water are shown in figure 6.14a. The absorption spectra of polymers are free from quinonid ring transition (at 650 nm), which confirmed their doped nature. All the three polymer samples showed three absorption maxima at approximately  $\lambda=300$ , 425, and  $>700$  nm, which are ascribed to the transitions from  $\pi$ - $\pi^*$  band, polaron band to  $\pi^*$  band,  $\pi$  band to polaron band, respectively, which is similar to doped polyaniline systems<sup>31</sup>. However, their positions and relative intensities are totally different. The polaron absorption band (approximately  $\lambda=950$  nm) at **P-MH** and **P-H** are having tail-like behaviour with respect to expanded chain confirmation whereas that of **P-DH** has peak characteristics corresponding to coil-like confirmation<sup>32</sup>. This suggests that in **P-DH**, the phenyl rings are more twisted due to the steric effects from side chain resulting a reduction in the extent of delocalization of electrons through polymer chain. Figure 6.14b shows the absorption spectra of dedoped nanomaterial samples in water. The samples **P-H** and **P-MH** shows an absorption typical of emeraldine base form with a quinoid peak at 650 nm, whereas nanospheres **P-DH** showed a blue shift to 590 nm in absorption indicating the presence of pernigraniline fraction in this sample<sup>33</sup>.

### 6.3.5. Vitamin C Sensing

The polyaniline nanomaterials have free and active hydroxyl groups at the nano-surfaces and it gives opportunities to study the molecular interaction at the polyaniline nanomaterial surfaces. Also these nanomaterials are highly dispersible in water even in dedoped state which gives the opportunities to investigate the interaction of nanomaterials with biomolecules like Vitamin C. Vitamin C (or L-Ascorbic acid) is prominent among the vitamins and important roles are its immune stimulating effect, as a powerful antioxidant, plays role in the synthesis of several important peptide hormones and neurotransmitters<sup>35</sup>. Vitamin C behaves as a weak vinylogous carboxylic acid and so capable of protonating polyaniline just like other protic dopants<sup>36</sup>. Additionally it contains four highly active hydroxyl groups and can selectively interact with nanomaterial surfaces by forming hydrogen bond with nanomaterials functionalities.

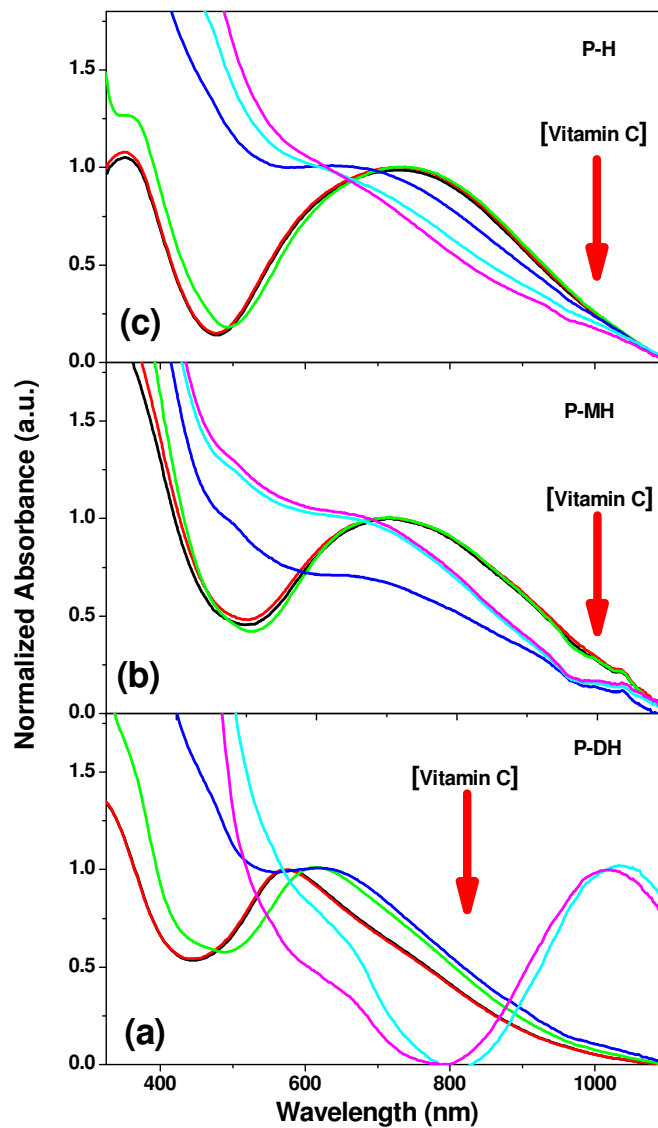


**Figure 6.15.** Normalized absorption spectra of nanomaterials. (a-c) the changes in absorption spectra of polyaniline nanomaterials in water upon addition of Vitamin C.

Recently, the successful sensing of Vitamin-C using un-substituted polyaniline as electrode materials has been reported<sup>37,38</sup>. The idea of the present study is not to demonstrate the efficiency of the new functionalized nano-material for vitamin-C sensor over the existing ones rather than as a tool to study the molecular interaction at the nano-surfaces. The three types of nanomaterials are chemically different: (i) nanofibers (**P-H**) with N-H groups over the surface (ii) nanospheres (**P-MH**) with N-H

and mono-hydroxy groups at the surface, (iii) nanospheres (**P-DH**) with bis-hydroxyl and N-H groups at the surface. Therefore, their interactions with vitamin-C are expected to be significantly different. Various types of possible molecular interactions between vitamin-C and nanospheres are schematically shown in figure 6.17.

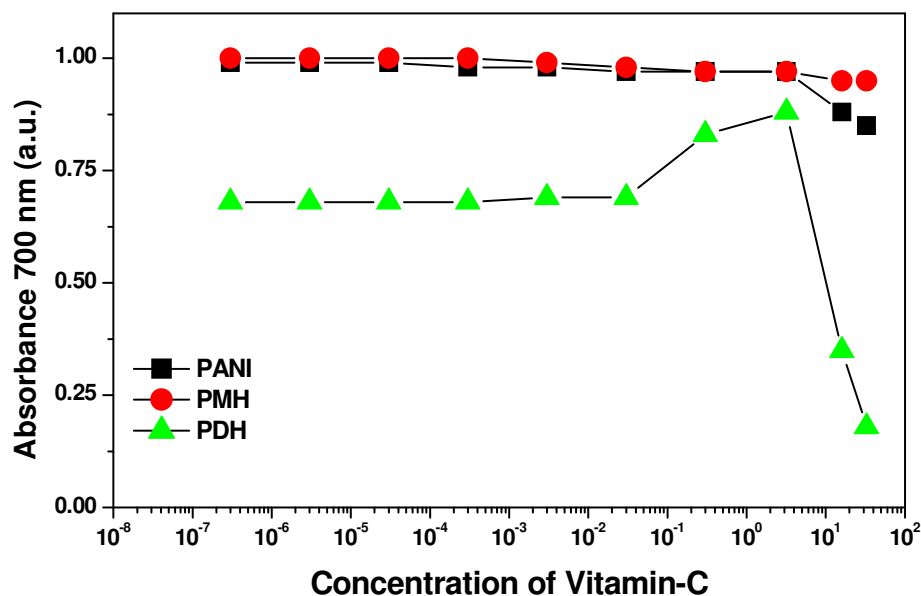


**Figure 6.16.** The changes in absorption at 700 nm of nanomaterials with respect to the concentration of Vitamin C.

To trace the molecular interactions, the dedoped sample is dispersed in water with absorbance of 0.3 (O.D) (see figure 6.15). The absorbance maxima of **P-DH** dedoped sample was obtained as 590 nm which was much lower than that of 710 nm of **P-MH** and **P-H**. This suggests that the **P-DH** chains contain a considerable form of pernigraniline base in dedoped stage whereas the other two samples were appeared in the emeraldine base form. These polyaniline nanomaterials solutions are doped with ascorbic acid solutions of concentration starting from  $10^{-8}$  to  $30 \times 10^{-3}$  M. The corresponding changes in absorption spectra are shown in figures 6.15a to 6.15c. In order to quantify the changes, the variation of absorbance at 700nm (disappearance of quinoid ring) was plotted versus the concentration of vitamin-C (see figure 6.16). The samples **P-H** and **P-MH** have showed almost similar behaviour towards vitamin-C and the addition of ascorbic acid did not show significant change in the absorbance at 700 nm in the entire composition range. On the other hand, the di-hydroxy functionalized polyaniline nanospheres (**P-DH**) showed effective molecular interactions towards vitamin C for more than  $1 \times 10^{-3}$  M concentration. It confirmed that

the functional groups at the nano-surfaces have high selectivity towards analyte (like vitamin-C). This may be a consequence of a higher oxidation state or of improved molecular interactions based on hydroxyl groups. The efficient tracing behaviour of **P-DH** sample towards vitamin-C can be understood from possible molecular interactions in figure 6.17.

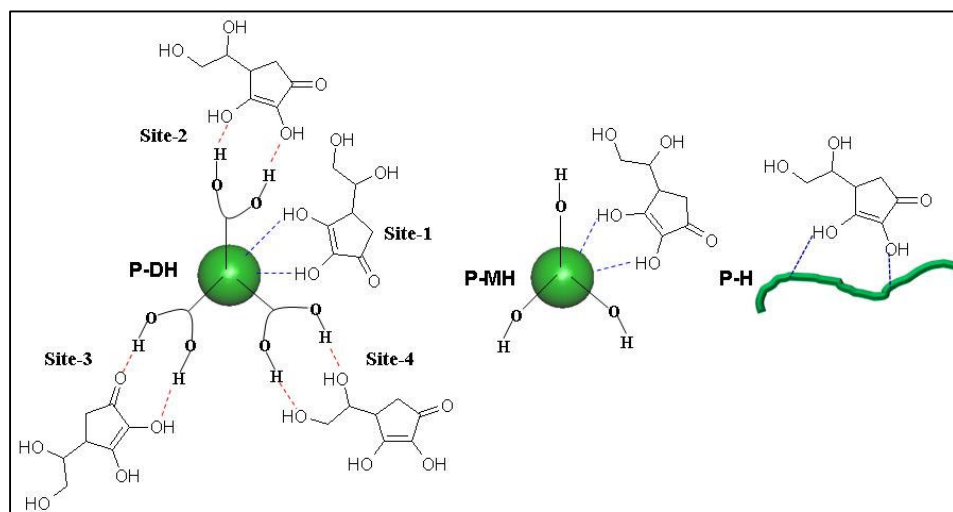


**Figure 6.17.** Schematic of various possible molecular interactions between Vitamin C and polyaniline nanomaterials.

The bis-hydroxyl functional group possesses very unique U-shaped hydrogen bonding socket for attracting vitamin-C molecules (sites 2 to 4), which are not available in **P-MH** (also for **P-H**). These increased hydrogen bonding interactions help the **P-DH** nanospheres to attract more number of vitamin molecules. This will in turn help the effective doping of polyaniline backbone of **P-DH** nanospheres than compared with other polyaniline nanomaterials. Therefore, the interaction of vitamin-C at the polyaniline nanomaterial is highly sensitive to the functional groups at nano-surfaces. Vitamin C (or ascorbic acid) is known to be highly ionisable in water (*ref*). In order to check the effect of pH changes during the doping process, firstly the pH of the dedoped polyaniline nanomaterials solution in water (0.3 O.D. solution) were measured and found that the pH as 7.05, 7.12, and 6.98 for **P-H**, **P-MH**, and **P-DH** respectively. It indicates that all the solutions are neutral besides the basic nature of polymer chain and it may be due to the low concentration of polymer samples (0.3 O.D.). To the dedoped sample solutions taken in separate vials added 15 mM Vitamin

C and checked the pH of the solution and found that the pH is reduced to 2.93, 2.98 and 3.14 for **P-H**, **P-MH** and **P-DH**, respectively. As expected, after the addition of Vitamin-C the solution become acidic and the difference in their pH values are with in the experimental error. Therefore, the difference in the sensing behaviour at the nano-surface is directly correlated to the functional groups at the surface rather than other external stimuli like pH. This unusual and interesting behaviour of hydroxy functionalized polyaniline nanomaterials may be very useful for the selective detection of other biologically important molecules like glutathione, dopamine etc. This study showed that the polyaniline nanomaterial, exclusively nanospheres, can be successfully functionalized using hydroxyl functional groups for tracing molecular interactions at the nano-surfaces with bio-molecules such as vitamin-C.



#### 6.4. Conclusion

In summary, two novel hydroxy functionalized polyaniline nanospheres to trace the molecular interaction at the nano-surfaces were designed and synthesised. It is shown that the di-hydroxy functionalized aniline monomers can be synthesized via tailor-made approach and polymerized to produce nanospheres with active hydrogen bonding sites at the surfaces. The approach demonstrated here is very unique and high novelty: (i) two new hydroxyl functionalized aniline molecules were synthesized for producing polyaniline nanospheres with active hydrogen bonding groups at the surfaces, (ii) the hydroxyl functional groups enhances the solubility of nanomaterials, which could be characterized by NMR spectroscopy, (iii) the mechanistic aspects of the polymerization was investigated by FTIR and DLS studies, (iv) the hydroxyl functionalized monomers undergo hydrogen bonded aggregation in water to form 400-600 nm aggregates and subsequent oxidations of these aggregates produce nanospheres rather than nanofibers (in the case of un-substituted monomer), (v) WXRd studies evident that enhanced hydrogen bonding interactions in the functionalized nanospheres with a appearance of new peak at 13.1 Å, (vi) vitamin-C was employed as a analyte to trace the molecular interactions at the polyaniline nanomaterials surface and (vii) the nanospheres with bis hydroxyl pendent at the surface showed selective interactions with vitamin-C and showed enhanced sensing properties. In a nut shell, the present investigations have proved the importance of surface functionalization right from the synthesis of polyaniline nanomaterials, exclusively nanospheres, using hydroxyl groups for studying the molecular interactions at the nano-surfaces with bio-molecules such as vitamin-C. These functionalized nanomaterials are novel and may find application in sensing other chemical and biological moieties.

**6.5. References**

1. Li, D.; Huang, J.; Kaner, R. B. *Acc. Chem. Res.*, **2009**, *42*, 135-145
2. Tran, H. D.; Li, D.; Kaner, R. B. *Adv. Mater.* **2009**, *21*, 1–13
3. Zhang, D. H.; Wang, Y. Y. *Mater. Sci. Eng. B*, **2006**, *134*, 9-19
4. Wan, M. X. *Adv. Mater.* **2008**, *20*, 2926–2932
5. MacDiarmid, A.G. *Angew. Chem., Int. Ed.* **2001**, *40*, 2581-259
6. Barthet, C.; Armes, S P.; Lascelles, S. F.; Luk, S. Y; Stanley, H. M. E. *Langmuir*, **1998**, *14*, 2032-2041
7. Riede, A.; Helmstedt, M .; Riede, V.; Stejskal, J. *Langmuir* **1998**, *14*, 6767-6771
8. Zhang, L.; Wan, M. X. *Adv. Funct. Mater.* **2003**, *13*, 815-820
9. Haung, J.; Virji, S.; Weiller, B. H.; Kaner, R. B. *Chem. Eur. J.* **2004**, *10*, 1314.
10. Ma, Y.; Ali, S. R.; Dodoo, A. S.; He. H. *J. Phys. Chem. B* **2006**, *110*, 16359-16365.
11. Kanungo, M.; Kumar, A.; Contractor, A. Q. *Anal. Chem.* **2003**, *75*, 5673-5679.
12. Ali, S. R.; Parajuli, R. R.; Ma, Y.; Balogun, Y.; He. H. *J. Phys. Chem. B* **2007**, *111*, 12275-12281
13. Feng, X.; Mao, C.; Yang, G.; Hou, W.; Zhu, J.J. *Langmuir* **2006**, *22*, 4384-4389.
14. Chen, S.A.; Hwang, G.W. *J. Am. Chem. Soc.* **1994**, *116*, 7939-7940
15. Kwon H.; Conklin J. A.; Makhinson M.; Kaner R. B. *Synth.Met*, **1997**, *84*, 95–96
16. Goto, H.; Akagi, K. *Macromolecules*; **2002**, *35*, 2545-2551
17. Li, D.; Kaner, R. B. *J. Am .Chem. Soc.* **2006**, *128*, 968-975
18. Zhou, C.; Han, J.; Song, G.; Guo, R. *J. Polym. Sci., Polym. Chem.* **2008**, *46*, 3563.
19. Mu, S.; Yang, Y. *J. Phys. Chem. B*, **2008**, *112* , 11558
20. Kim, B.J.; Oh, S.G.; Han, M.G.; Im, S.S. *Synth Met* ,**2001**,*122*, 297–304
21. Huang J.; Kaner R. B., *Angew. Chem., Int. Ed.*, **2004**, *43*, 5817–5821.

22. Zheng, W.; Angelopoulos, M.; Epstein, A. J.; MacDiarmid, A. G. *Macromolecules* **1997**, *30*, 7634-763
23. Zheng, W.; Angelopoulos, M.; Epstein, A. J.; MacDiarmid, A. G. *Macromolecules* **1997**, *30*, 2953-2955
24. Hassan, P. A.; Raghavan, S. R.; Kaler, E. W. *Langmuir*, **2002**, *18*, 2543-2548.
25. Hamley, I.W. Introduction to Soft Matter ,(2nd Edn.), Wiley, **2007**, 200-204
26. Jayakannan, M.; Annu, S.; Ramalekshmi, S. *J. Polym. Sci., Polym. Phys.* **2005**, *43*, 1321-1331.
27. Lunzy, W.; Banka, E. *Macromolecules*, **2000**, *33*, 425.
28. Winokur, M.J.; Guo, H.; Kaner R. B. *Synth Met.* **2001**, *119*, 403-404
29. Jana, T.; Roy, S.; Nandi, A. K. *Synth. Met.* **2003**, *132*, 257.
30. Zaidi, N.A.; Foreman, J.P.; Tzamalīs, G.; Monkman, S.C.; Monkman, A.P. *Adv. Funct. Mater.* **2004**, *14*, 479-486
31. Qiu, H.J.; Wan, M.X. *J. Polym. Sci., Part A: Polym. Chem.* **2001**, *39*, 3485-3497
32. Y. Xis.; J. M. Wiesinger.; A. G. MacDiarmid, *Chem. Mater.* **1995**, *7*, 443-445
33. Kang, E. T.; Neoh, K. G.; Tan, K. L. *Prog. Polym. Sci.* **1998**, *23*, 211-324
34. Bartlett, P. N.; Wallace. E. N. K.; *Phys. Chem. Chem. Phys.*, **2001**, *3*, 1491-1496
35. Bossi, A.; Castelletti, L.; Piletsky, S. A.; Turner, A. P. F.; Righetti, P. *Electrophoresis*, **2003**, *24*, 3356-3363
36. Hanstein, S.; Bonastre, A. M.; Nestler, U.; Bartlett, P.N.; *Sensors and Actuators B*, **2007**, *125*, 284-300
37. Connell, P.J.O.; Gormally, C.; Pravda, M.; Guilbault, G. G. *Anal. Chim. Acta.* **2001**, *431*, 239-247
38. Andreu, Y.; Marcos, S.; Castillo, J. R.; Galban, J. *Talanta*, **2005**, *65*, 1045-1051

***Chapter-7***

---

***Summary and Conclusions***

The thesis entitled “*Self-assembled Molecular Templates for Conducting Polyaniline Nanomaterials*” describes the design, synthesis, characterization and self-assembly of a series amphiphilic molecules as soft-templates for various types polyaniline nanostructures like fibres, tubes, spheres, rods and tapes. The major concept explored in the thesis is the role of molecular soft-templates on the morphology and other properties of polyaniline nanostructures.

A unique approach for high performance nano-structured conducting polyaniline developed from renewable resource raw material cardanol, which is an industrial waste and pollutant. Naturally available cardanol, which is an industrial waste from cashew nut industry, is utilized for producing well-defined polyaniline nanomaterials. A new amphiphilic molecule, [4-[4-hydroxy-2((Z)-pentadec-8-enyl) phenylazo]-benzenesulfonicacid (dopant 1), is designed and developed from cardanol. The micellar behaviour of this dopant was studied in detail by DLS, dye encapsulation, surface tension and ionic conductance methods. The surfactant dopant is found to form stable emulsion with aniline for wide composition range in water (1 to 1500 [aniline]/[dopant] mole ratio) to produce polyaniline nanomaterials. The SEM and TEM analysis of the nanomaterials reveals that the [aniline]/[dopant] ratio plays a major role in determining the type, shape and size of polyaniline nanostructures. The dopant-aniline templates were characterized by DLS, SEM and TEM studies. The dopant-aniline complex selectively exist in various forms such as salt, aggregated cylindrical micelles and layers in water depending upon the [aniline]/[dopant] ratio in the feed, which subsequently results in spheres, fibres and nanotubes. The amphiphilic dopant has in-built head to tail geometry and effectively penetrate in to the polyaniline chains to form highly organized nanofibers. The polyaniline nanofibers were soluble in various solvents and also hold high environmental and thermal stability up to 300 °C for various applications. This facile self-organized cylindrical micellar template approach was extended to reproducible large synthesis of polyaniline nanofibers up to 100 gram. These nanofibers showed high reversibility in morphology, optical and solid state properties in the repetitive doping/de-doping analysis and suitable for practical applications.

Further, the self-assembly property of azobenzene sulfonic acid dopant is utilized to for tuning various types of polyaniline nanomaterials such as fibres, rods,

spheres and tubes by soft templating in emulsion, dilute and interfacial routes. Upon adding aniline (or oxidant) to the micellar solution of dopant 1, the micelles self-organized to form micrometer sized cylindrical, layer-like, rod like or spherical assemblies depending upon their concentration or composition of different chemical constituents in the feed. The oxidation of these soft templates filled with monomer in water produced nanofibers, nanorods, nanotubes and nanospheres, respectively. The mechanistic details of the polyaniline nanomaterials formation was investigated by DLS and high TEM to trace the factors which control the morphology of the resultant materials. The amphiphilic nature of the dopant solubilises the nanomaterials in water and organic solvents that enabled us to characterize the polyaniline nanostructures by NMR, FTIR and UV-vis studies. The UV-vis studies of nanomaterials in water showed the chain conformational difference between various nanomaterials-the nanospheres possesses expanded confirmation and the fibres, rods and tubes were found to have coil-like confirmation. The wide angles X-ray diffraction studies confirmed the appearance of new peak at lower angle corresponding to the highly ordered polyaniline nanomaterials. The polyaniline nanomaterials doped with fluorescing azobenzene sulfonic acid dopant showed enhanced emission in water and the amount of the dopant in the nanomaterial as well as chain conformation plays a crucial role in luminescent intensity and quantum yields. Therefore, that precise control of soft template is very much essential for nanomaterials synthesis and various nanostructures were produced from same starting materials depending on how these constituents are self-organized and polymerized in water under normal conditions.

A custom designed surfactant-cum-dopant Z-4-(3-pentadec-8-enyl)phenoxy)-butane-1-sulfonicacid (dopant 2) from cardanol was developed and utilized as structure directing agent for polyaniline nanomaterials- nanofibers and nanotapes by emulsion and dispersion routes, respectively. The dopant forms micelle in water and its CMC was determined by multiple techniques such as dye encapsulation, surface tension and DLS methods. In emulsion route the cylindrical micellar soft template formed between dopant and aniline leads to the formation of nanofibers whereas in dispersion route the vesicular template of aniline+toluene produced nanotapes. The soft templates formed by dopant 2 were characterized by DLS and HR-TEM techniques. The polyaniline nanomaterials are highly soluble in water and polar solvents and enabled us the complete structural characterization. The WXRd studies

are utilized to study the solid-state ordering in polyaniline and confirmed the layered lamellar type packing of polymer chains in nanomaterials. This study established that the novel renewable resource amphiphilic dopant is a good candidate for the synthesis of high quality nanofibers and nanotapes by carefully choosing the amphiphilic dopant templates under emulsion and dispersion polymerizations in a single system.

A unique and novel approach for polyaniline nanofibers via self-assembled organogel templates based on new renewable resource amphiphilic dopant, 4-(3-pentadecylphenoxy)butane-1-sulfonic acid was developed. The gel template has a pivotal role in directing polyaniline chains to form nanofibers and also manipulating the number of properties such as conductivity, solubility, percent crystallinity and solid state ordering. SEM, AFM and TEM techniques have been successfully utilized to trace the nature and shape of polymerization templates to understand the mechanism of the nanomaterials formation. The polymerizations were carried out at various temperatures to establish the role of the physical state and stability of the organogel on the morphology of the resultant nanomaterials. The supramolecular interaction between dopant and polyaniline complex formed lamellae of interdigitated dopant molecules stacked in between polyaniline chains and improved the solid state properties. The temperature dependent conductance measurements showed a high conductivity of the gel-template synthesized samples and they followed 3-D VRH model at elevated temperature. This study showed that the novel amphiphilic dopant derived from renewable resource is a good gelator and the gel assemblies are good template for the growth of highly ordered and soluble polyaniline nanofibers.

To trace the molecular interactions at the nano-surfaces and sensing Vitamin C, novel polyaniline nanospheres bearing mono and bis-hydroxyl functional groups was developed. Two new aniline monomers were synthesized via tailor-made approach and polymerized to produce soluble and uniform polyaniline nanospheres. The structures of the monomers and polymers were characterized by NMR, FT-IR, Mass techniques and the morphology of the nano-materials was analyzed by SEM and TEM. The mechanistic aspects of the nanomaterials formations were analyzed by FTIR and dynamic light scattering techniques. Vitamin C was employed as an analyte to trace the molecular interaction at the nanosphere surface and study the influence of nano-surface functionalization on the sensing ability of bio-molecules. The bis-hydroxyl functionalized polyaniline nanospheres were found to show efficient

molecular interactions towards vitamin C whereas nanospheres with mono-hydroxyl group or un-substituted nanofibers failed as sensing materials. Hence, this study have proved the importance of surface functionalization of polyaniline nanomaterials, exclusively nanospheres, using bis-hydroxyl groups for improved molecular interactions at the nano-surfaces with bio-molecules such as vitamin-C.

The soft template approach based on tailor-made amphiphiles demonstrated a simple and facile method to fabricate a series of polyaniline nanostructures like fibres, tubes, rods, spheres and tapes. It was realized that the availability of pure, uniform diameter polyaniline nanomaterials in desirable quantities is a major difficulty in conducting nanomaterial research. Due to the ease of the synthetic method described in this thesis, sufficient polyaniline nanomaterial is now readily preparable. These nanomaterials possessed good optical, electrical and solid-state properties and so very much suitable for applications in microelectronics and sensor area. This approach fabricating nanostructures could be expanded to similar class of conducting polymers like polypyrrols and polythiophenes and may open new path ways for patterning conducting nanomaterials and understanding the mechanistic details of formation.



***List of Publications***

---

**Publications in International Journals**

1. **Anilkumar, P.;** Jayakannan, M. Self-Assembled Cylindrical and Vesicular Molecular Templates for Polyaniline Nanofibers and Nanotapes. *J. Phys. Chem. B.* **2009**, *113*, 11614-11624.
2. **Anilkumar, P.;** Jayakannan, M. Divergent Nanostructures from Identical Ingredients: Unique Amphiphilic Micelle Template for Polyaniline Nanofibers, Tubes, Rods, and Spheres. *Macromolecules*, **2008**, *41*, 7706-7715
3. **Anilkumar, P.;** Jayakannan, M. Hydroxyl-Functionalized Polyaniline Nanospheres: Tracing Molecular Interactions at the Nanosurface via Vitamin C Sensing. *Langmuir*, **2008**, *24*, 9754-9762
4. **Anilkumar, P.;** Jayakannan, M. A Single Molecular System Based Selective Micellar Templates for Polyaniline Nano-materials: Control of Shape, Size, Solid State Ordering and Expanded Chain to Coil-like Conformation. *Macromolecules*, **2007**, *40*, 7311-7319
5. **Anilkumar, P.;** Jayakannan, M. Fluorescent Tagged Probing Agent and Structure-Directing Amphiphilic Molecular Design for Polyaniline Nano-materials via Self-Assembly Process *J. Phys. Chem. C.* **2007**, *111*, 3591-3600.
6. **Anilkumar, P.;** Jayakannan, M. A Renewable Resource Molecular Design for Size-Controlled and Highly Ordered Polyaniline Nano-fibers. *Langmuir*, **2006**, *22*, 5952—5957
7. Jayakannan, M.; **Anilkumar, P.;** Sanju, A. Synthesis and Characterization of New Azo benzenesulfonic acid Doped Conducting Polyaniline. *Eur. Polym. J.* **2006**, *42*, 2623-2631
8. Jayakannan, M.; **Anilkumar, P.** Mechanistic Aspects of Ester–Carbonate Exchange in Polycarbonate/Cycloaliphatic Polyester with Model Reactions. *J Polym Sci: Part A: Polym Chem*, **2004**, *42*, 3996–4008
9. **Anilkumar, P.;** Jayakannan, M. Large-scale Synthesis of Polyaniline Nanofibers based on Renewable Resource Molecular Template. *J. Appl. Polym. Sci.* **2009** (ASAP article).
10. **Anilkumar, P.;** Jayakannan, M. Amphiphilic Dopant Organogel Nanotubular Template for Polyaniline Nanofibers (Manuscript submitted for publication).
11. **Anilkumar, P.;** Jayakannan, M. Tracing emission properties of azobenzene molecules confined at nanomaterial surface (Manuscript under preparation).

**Publications in International Conference Proceedings**

12. **Anilkumar, P.;** Jayakannan, M. Hydroxyl Functionalized Polyaniline Nanospheres for Sensing Bio-analytes, *MACRO 2009*, Chennai, India, Mar 9-11, **2009**.
13. Jinish Antony, M; **Anilkumar, P;** Jayakannan, M. Renewable Resource Approach for Conducting Polymer Nanomaterials, *MACRO 2009*, Chennai, India, Mar 9-11, **2009**.
14. **Anilkumar, P.;** Jayakannan, M. Micellar Template for Conducting Polyaniline Nano-architectures, *RSC-CRSI 2009*, Pune, India, Feb 6-8, **2009**.
15. **Anilkumar, P.;** Jayakannan, M. A Renewable Resource Amphiphilic Molecular Approach for Controlling The Size ,Shape and Conformation of Conducting Polyaniline Nanomaterials, *DST-JSPS 2008*, Thiruvananthapuram, India, Jan 20-22, **2008**.
16. **Anilkumar, P.;** Jayakannan, M. Conducting Polyaniline Nano-Materials: Tuning of Size, Shape and Conformation, *ICAMC-2007*, Thiruvananthapuram, India, Oct. 24-26, **2007**. (**Selected for Best Poster Award**)
17. **Anilkumar, P.;** Jayakannan, M. Self-Assembly Approach For Controlled Synthesis Of Conducting Polyaniline Nano-Materials. *IUMRS-ICAM 2007*, Bangalore, India. Oct 8-13, **2007**.
18. **Anilkumar, P.;** Jayakannan, M.; A Facile Renewable Resource Strategy for Size-Controlled and Highly Ordered Polyaniline Nano-Fibers. *MACRO 2006*, Pune, India, Dec 17-20, **2006**.
19. **Anilkumar, P.;** Jayakannan, M. A Unique Structure Directing and Renewable Resource Amphiphilic Dopant for Polyaniline Nano-fibers. *EMSI 2006*, Thiruvananthapuram, India, Apr. 15-17, **2006**.
20. **Anilkumar, P.;** Jayakannan, M. Transesterification reaction in polycarbonate / cycloaliphatic polyester .*MACRO 2004*, Thiruvananthapuram, India, Dec. 15-17, **2004**.